DISSERTATION

GLIAL INFLAMMATION AS A KEY REGULATOR AND THERAPEUTIC TARGET FOR PRION DISEASE

Submitted by

Arielle Hay

Department of Microbiology, Immunology and Pathology

In partial fulfillment of the requirements

For the Degree of Doctor of Philosophy

Colorado State University

Fort Collins, Colorado

Summer 2023

Doctoral Committee:

Advisor: Mark Zabel
Co-Advisor: Julie Moreno

Ronald Tjalkens
Kelly Santangelo
Soham Chanda

ABSTRACT

GLIAL INFLAMMATION AS A KEY REGULATOR AND THERAPEUTIC TARGET FOR PRION DISEASE

Prion diseases are lethal neurodegenerative diseases characterized by the misfolding of the cellular prion protein, PrP^{C}, into the infectious PrP^{Sc}. PrP^{Sc} accumulation in the brain contributes to the activation of microglia and the subsequent increase in reactive astrocytes, which together contribute to neuroinflammation. PrP^{Sc} aggregation triggers and leads to the dysregulation of a variety of cellular stress pathways, including the oxidative stress response, unfolded protein response, ubiquitin-proteosome system, autophagy and lysosomal degradation. Most critically, PrP^{Sc} contributes to neuronal toxicity and death, but the mechanism behind this is poorly understood. Prion diseases affect humans and a variety of mammalian species, with no available treatments. The majority of therapeutics developed to combat these diseases have targeted the prion protein itself. As these have been unsuccessful, it is time to turn our attention to treatments that target the cellular pathways and neuroinflammation caused by PrP^{Sc} accumulation in the brain. The overarching goal of this work is to identify glial-induced inflammation as a candidate for therapeutic intervention of prion diseases. We assessed the use of mesenchymal stromal cells (MSCs), which are potent regulators of inflammatory signaling and glial polarization, in cell culture and animal models of prion disease. Additionally, we investigate the role of a key inflammatory signaling pathway, Nuclear Factor-Kappa B (NF-κB) in microglial response to prion infection. Our findings both characterize contributions of specific glial cells to prion-induced inflammation, as well as uncovering novel targets for the treatment of prion diseases.

First, we assessed the therapeutic potential of adipose-derived mesenchymal stromal cells (AdMSCs) in a cell culture model of glial prion infection. MSCs are known for their ability to migrate to sites of inflammation and produce immunomodulators. We evaluated the ability of cultured AdMSCs to respond to molecular factors present in brain homogenates from prion-infected animals. We found that these cells upregulate anti-inflammatory genes in response to both specific inflammatory cytokines and crude prion brain homogenates. Moreover, AdMSCs migrate towards prion brain homogenates in an *in vitro* model. Co-culturing AdMSCs with prion-treated BV2 cells or infected primary mixed glial cultures resulted in a significant decrease in markers of inflammation and disease-associated microglia and reactive astrocyte markers. These findings were independent of PrP^{Sc}, as AdMSCs had no effect on prion accumulation in mixed glial cultures. Collectively, these findings highlight AdMSCs as an intriguing candidate for modulating glial-induced inflammation in prion disease.

Next, we evaluated AdMSCs in a mouse model of prion disease. Prior to delivery into prion-infected mice, AdMSCs were stimulated with TNFα, which we show increases their upregulation of anti-inflammatory molecules and growth factors. Stimulated AdMSCs were delivered intranasally to prion-infected mice every two weeks beginning from early in infection (10 weeks post-infection (wpi)) and ending late in infection (20 wpi). A cohort of mice was euthanized at various stages in infection, at 14 wpi, 16 wpi and 18 wpi. We show that AdMSCs are able to migrate throughout the brain when delivered intranasally, with the most cells being found in the hippocampus and thalamus. Although AdMSCs were not successful in improving behavior or increasing survival in prion-infected mice, they did induce changes in prion pathology at early time points in disease. A decrease was seen in inflammatory cytokines and markers of glial activation. No changes were seen in PrP^{Sc} accumulation or neuronal loss

compared to untreated controls. However, at both 16- and 18 wpi, we identified significant changes in both glial numbers as well as morphology, indicating that AdMSCs attenuate reactivity in microglia and astrocytes. Together, these findings highlight AdMSCs as potent regulators of prion-induced glial inflammation, and warrants further investigation to optimize these cells as a treatment for prion disease.

In addition to assessing therapeutics that decrease inflammation and reprogram glial cells to a homeostatic phenotype, we wanted to better characterize specific inflammatory pathways and understand how these were being regulated in glial cells in response to prion infection. NF-κB-related genes have long been identified in the brains of animal models with prion disease, but studies that have investigated its role in prion pathogenesis have focused on neurons and astrocytes. Microglia are critical innate immune regulators in the brain, and interact closely with both neurons and astrocytes to regulate inflammation and cell survival. Therefore, we saw an immediate need to characterize NF-κB signaling in microglia, and its contribution to prion-induced neuroinflammation. IKβ kinase (IKK) is a complex that responds to cell stressors and is critical for NF-κB signaling to occur. We utilized a primary mixed glial model containing wild-type (WT) astrocytes and IKK KO microglia. Upon infecting these mixed glial cultures with prions, we saw a drastic decrease in NF-κB-related genes compared to cultures containing WT astrocytes and WT microglia. Despite this, cultures containing IKK KO microglia still contribute neurotoxic signals that induce neuronal cell death. Moreover, we found that cultures with IKK KO microglia showed significantly more PrP^{Sc} accumulation, suggesting that these cells may have impaired autophagy. This work implicates microglial NF-κB-signaling and IKK as a potent inducer of inflammation and regulator of autophagy in prion disease.

DEDICATION

This work is dedicated to my mom, who has always been my biggest support and has been reading my work since the very beginning. In her words, my scientific writing is much better than my fiction.

TABLE OF CONTENTS

Chapter 1:

Introduction

What are prions?

Prion diseases may just be the black sheep of infectious diseases. Unlike bacterial or viral infection, the disease agent arises from the host itself in the form of the cellular prion protein (PrP^C). PrP^C can be coerced to misfold from an alpha-helical form to a form rich in beta-sheets, which acts as a catalyst to induce the misfolding and aggregation of more host PrP^C.[1] The misfolded, infectious form of the protein is denoted PrP^{Sc}. The "protein only hypothesis" states that PrP^{Sc} is able to bind PrP^C and induce conformational changes, leading to an autocatalytic reaction that leads to exponential production of PrP^{Sc}.[2] The initial misfolding can be sporadic, due to a genetic mutation in the protein, or, most intriguingly, due to acquired infection by PrP^{Sc}.[3] PrP^C is expressed ubiquitously in tissue, but has the highest expression in the brain, particularly in astrocytes and neurons,[4] and PrP^{Sc} aggregation disrupts homeostasis in these cells and leads to fatal neurodegeneration. Prion diseases are also called transmissible spongiform encephalopathies (TSEs), as the main hallmark of disease, apart from abundant protein aggregation in the brain, is the sponge-like appearance of brain tissue, referred to as vacuolization.[5]

First, we must talk a bit about the structural biology of PrP before we can get into the how this misfolded protein causes disease. PrP is expressed in all mammalian cells. It is a glycoprotein that is anchored to the surface of the cell via a glycosylphosphatidylinositol (GPI) anchor.[6] The secondary structure of PrP is conserved between many species, namely mammals.[3] The human prion protein is composed of 209 residues and two N-linked glycosylation sites.[7] The native form of the protein is divided into an N-terminal and C-terminal domain. The disordered

N-terminal domain ranges residues 23-125, while the C-terminal domain ranges residues 126-231. The majority is composed of 3 α-helices, ranging residues 144-154, 175-193 and 200-219. These are denoted α1, α2 and α3, respectively. It also contains two antiparallel β-strands that span residue 127-132 and 161-164, denoted β1 and β*2* (Figure 1.1). [6,8]

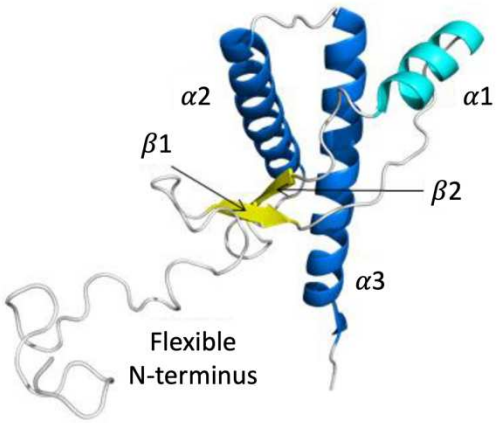

Figure 1.1 General structure of mammalian PrP^{C}. Adapted from Cheng and Daggert, 2014.

PrP^{Sc} replicates itself and forms oligomers, which may lead to fibrillization. The role of fibrils in prion pathogenesis remains controversial. Early studies suggest that the aggregation of fibrils can lead to neurodegenerative disease, hypothesized to be caused by a toxic gain-of-function. However, more recent studies have determined that fibrils in themselves are not infectious. There is mounting evidence that oligomers are the predominant cause of neurotoxicity.[9] Additionally, residues 106 - 126, adjacent to the β1 region, can form a β-sheet rich structure that is neurotoxic and alone can be converted to the amyloid fibrils.[10,11]

The intra- and extracellular deposits of these macromolecular structures are the defining characteristic of prion disease.[2] The misfolded proteins aggregate to form fibrils that continue to lengthen and clump together. Fibril formation may actually be a mechanism evolved to protect against the toxic effects of oligomerization.[12] and deposits visible plaques in the brain.[13] Protein

aggregation and fibrillization takes place well before the onset of the disease. By the time the disease can be clinically recognized, brain regions rich in PrP^{Sc} are already undergoing neurodegeneration.[2]

Prion diseases have been around for a long time. Scrapie, a prion disease that effects sheep, is the earliest described prion disease, first reported in the 16th century.[14] Or was it? Analysis of ancient Chinese texts suggest that this disease may have been affecting sheep in China up to 2000 years earlier,[15] but it was first identified by the English in the 16th century. Human prion diseases have only been reported in the last century, and diseases like chronic wasting disease in cervids was first reported in the 1960s.[16]

Now, I must speak about the disease that sparked my interest in the prion field as a naïve sophomore in college. Outbreaks of prion diseases have been known to occur, including variant Creutzfeldt-Jakob disease (the human form of "mad cow disease"), and the first human prion disease identified - kuru. Kuru was first described in 1959, and its similarities to scrapie were identified in 1965.[13] Kuru affected the Fore people living in a remote area of Papua New Guinea. It is postulated that this disease began as an individual case of sporadic Creutzfeldt-Jakob (CJD), and was then spread throughout the population through cannibalism.[13] All prion diseases do not affect the same brain structures, and therefore show different symptoms. Kuru prions specifically target the cerebellum. Ataxia develops, along with tremors of the head, trunk and legs that worsen as the disease progresses until walking and movement are no longer possible. Unlike other prion diseases, individuals cognition remains intact until just before death,[13] when they begin to display decreased mental behavior and dementia.[17]

There are a variety of causes of prion diseases. They may be hereditary, such as familial CJD and Gerstmann-Straussler-Scheinker Syndrome (GSS). They can be transmitted through

contact with infectious prions, such as iatrogenic CJD and kuru. They can also be the result of spontaneous prion conversion, such as sporadic CJD. Not all variants of PrP are equally susceptible to disease. Heterozygosity for methionine and valine at residue 129 is a common polymorphism seen throughout the world. It gives some protection against a variety of prion diseases, including those heritable, acquired, and occurring sporadically. It is hypothesized that this variant was selected for during human evolution. There is evidence that heterozygosity at this residue limits interactions between homologous proteins that may be critical in the conversion of PrP^{C} into PrP^{Sc}, as well as oligomerization and fibrillation.[18] Heterozygosity of polymorphism 129 is seen in the majority of survivors of the kuru epidemic, indicating that this genotype is protective.[19]

A single substitution of glycine for valine at residue 127 (denoted V127) in the human prion protein has also been shown to prevent prion infection.[18] This mutation, the topic of my undergraduate thesis, sparked my interest in prion pathogenicity and potential therapeutics. This human variant was discovered by Mead et al. in 2009 and is unique to the Fore population in Papua New Guinea. No individuals with the V127 polymorphism were found to have clinical signs of neurodegenerative disease, suggesting that it is protective against kuru and was selected for during the outbreak.[20] Additionally, there is a higher frequency of the V127 polymorphism in those homozygous at codon 129 in individuals born before 1960 (before cannibalism was outlawed in Papua New Guinea and the kuru epidemic came to a halt).[21]

Being a relatively new field (the term "prion" was first coined by Stanley Prusiner in a paper published in Science in 1982),[22] there are still much uncharted territory when it comes to how the central nervous system responds to prion infection, and what pathways to target to best inhibit disease progression. To this day, prion diseases remain invariably fatal.

The importance of developing therapeutics for human prion diseases

Although human prion diseases such as CJD can develop spontaneously and only affect approximately one in a million people worldwide,[23,24] the infectious nature of prions have led to outbreaks of CJD. These were the result of prions being transmitted iatrogenically [25] or through the consumption of infected beef. [26] The outbreak of variant CJD in the UK in the 1980s and 90s through consumption of cattle with prion disease ('mad cow disease') highlights a critical need for treatments. Because the infectious agent, PrP^{Sc}, can cross the species barrier, future outbreaks could occur. Luckily, there is not convincing evidence that diseases like scrapie in sheep can cross the species barrier into humans, despite being around for hundreds (or thousands?) of years.[14] Between it is considered safe to handle and has been thoroughly characterized, mouse-adapted scrapie is the most commonly used experimental model for prion studies.

Although proper hospital sterilization techniques and USDA regulations have limited the risk of acquiring prion disease through these routes, there is growing fear that chronic wasting disease (CWD) - a rampant prion disease in cervid populations throughout the United States, Canada, Scandinavia and South Korea - will cross the species barrier to infect humans. There is mounting evidence that CWD could transmit to humans, including recent findings showing that humanized mice infected with CWD prions succumb to disease.[27] Other mouse models have not confirmed this, and transmission studies in non-human primates have been inconclusive.[28] Interestingly, a recent case study reported a patient who developed CJD and had recently been consuming supplements containing deer antler velvet and bovine colostrum, but this could not be directly attributed to the development of disease.[29] Although findings from these studies are conflicting and inconclusive, and the zoonotic potential of CWD remains a point of contention in

the prion field, the potential of transmissibility indicates an immediate need for prion disease treatments in order to prevent future outbreaks.

Different strains, different diseases

Understanding strain differences is not critical to understanding my research, but I would be remised if I failed to mention prion strains, as this is a huge focus of research in the Zabel laboratory[30] and in the prion field as a whole.[31] Moreover, it emphasizes why we are interested in developing therapeutics that act upon cellular pathways, such as glial inflammation, as opposed to developing antibodies to target PrP^{Sc}. This is because when PrP^{C} misfolds into PrP^{Sc} and aggregates, the secondary, tertiary and quaternary structures, as well as histological and clinical manifestations of disease, can be different, even with the same primary structure! The most intriguing example of this is the "hyper" and "drowsy" prion strains, derived from natural prion disease in minks and studied using hamsters in the laboratory. The same primary structure in hamsters leads to very different tissue tropism in the brain, different biochemical properties, and, as the name suggests, differences in behavior. Moreover, these prion strains are not transmissible to mice, indicating a species barrier. Similarly, single point mutations in humans can lead to genetic disease, and polymorphisms can lead to different manifestations of the same disease.[31-33] In case you didn't think things were already complicated enough, this adds a new level of difficulty in developing therapeutics for prion diseases.

PrP is critical for infection, but not survival

There is, in fact, one way to survive prion infection, and that is by not expressing the prion protein. Prion knock-out (PrP KO) mouse models have some developmental and

behavioral differences compared to wild-type mice, including alterations in circadian rhythms, neural stem cell differentiation, synaptic plasticity, peripheral nerve myelination, and olfaction.[34] However, none of these differences appear to have any effects on survival or general day-to-day life of these animal models.[35-37] Regardless of the method of infection, PrP KO mice are completely resistant to prion disease.[36] PrP expression in neurons is known to be critical for neurodegeneration to occur upon prion infection, as neuron-specific PrP KO animals do not succumb to disease.[38] Importantly, behavioral and clinical signs of prion disease are not the result of a loss of function of PrP^{C}, as removal of PrP from neurons in adulthood had no obvious effects.[39]

Cells of the brain

Neurodegenerative diseases are characterized by the degeneration of neurons. Neurons are critical for sending signals throughout the central nervous system to regulate autonomic behaviors, motor movement, and cognition. Neurons make up almost half of cells within the brain,[40] and when enough are killed with neurodegeneration, it leads to loss of memory and motor functions, and eventually paralysis and death. Although critical, neurons cannot function without the involvement of three other key cell types in the brain - oligodendrocytes, astrocytes and microglia. Oligodendrocytes compose the myelin sheath that wraps around the neuron's axon, allowing for rapid transmission of action potentials through a process called saltatory conduction. Loss of myelin is associated with neuronal dysfunction, such as in multiple sclerosis, but there is little evidence that oligodendrocytes can be infected with PrP^{Sc} or have any significant involvement in prion disease[41] and have been largely ignored in the field of prion disease.

Astrocytes are also principal regulators of neuronal function and play a large role in prion pathogenesis. These cells regulate communications between neurons and the brain's blood vessels and maintain the blood brain barrier, which is composed of vascular endothelial cells, tight junctions, basement membranes, smooth muscle cells and astrocytes themselves.[42] Astrocytes are critical in maintaining homeostasis of neurons by regulating potassium and glutamate levels and neurotransmitters.[43,44] Astrocytes also regulate the survival and function of neurons, and can induce pruning of neuronal synapses by increasing complement component 1q (C1q) production on synapses. This binds to the complement component 3a (C3a) receptor on microglia, which prune the synapses via the classical compliment cascade. This can be further triggered by activation of astrocytes and increased production of astrocytic C3, which can induce further phagocytosis of neuronal synapses by microglia. Further neuronal damage can initiate a positive feedback loop and, when left unchecked, lead to neuronal loss.[42,45]

The phenotypes of glial cells fluctuate depending on the environment of the brain. Injury and inflammation in the brain can induce astrocytes to shift from a homeostatic phenotype to a "reactive" phenotype. This is characterized by an increase in the size of their cytoskeleton, increased expression of glial fibrillary acidic protein (GFAP), upregulation of many genes, particularly those involved in inflammatory pathways, extension of their processes, and formation of glial scars. When astrocytes become reactive, they release factors that increase permeability of the blood brain barrier and allow immune cells from the periphery to infiltrate.[42]

Astrocytes demonstrate few morphological and phenotypical change in response to insult and injury in the absence of microglia. Classic studies have demonstrated that factors secreted by microglia, such as interleukin 1α (IL1α) and tumor necrosis factor alpha (TNFα), induce astrocyte reactivity, and in the absence of microglia, astrocytes remain relatively unresponsive to

environmental changes and do not reach full states of activation.[45,46] Once triggered by microglia, astrocytes are subject to morphological and phenotypic changes, the most thoroughly described being in response to microglial activation by lipopolysaccharide (LPS), inducing "A1" reactive astrocytes that produce unknown neurotoxic factors.[45,47] This state is specific to LPS, but shares many hallmarks of astrocytes in the prion-infected brain.[48-50] More generally, this group of reactive astrocytes are referred to as neurotoxic astrocytes. Although the exact neurotoxic factors they secrete remain unknown, they can also induce a positive feedback loop by producing inflammatory cytokines such as C-C motif chemokine ligand 2 (CCL2) and complement proteins to promote activation and increased migration of microglia.[42,51]

Although they only account for 10-20% of all cells in the brain,[42,52] microglia are the first line of defense and arguably have the largest effect on the inflammatory state in the brain. Toll-like receptors (TLRs), namely TLR4, respond to pathogen-associated molecular patterns (PAMPs) such as LPS, and activation of microglia increases TLR4 expression.[42,53] In response, they secrete soluble factors such as cytokines, chemokines, nitric oxide (NO), and reactive oxygen species (ROS) and migrate to sites of insult. These can act upon astrocytes or directly upon neurons, triggering oxidative stress and even cell death.[51,52] States of microglia are slightly better defined than those of astrocytes, and generally mimic those of macrophages, and were previously categorized as M1 and M2 activation states. There has recently been a push to change this to disease-associated microglia (DAM) and homeostatic microglia. This terminology is currently up for debate and has both pros and cons (for example, there are various phenotypes of microglia in the terminal prion brain, similar to both M1 and M2, both being considered "DAM"). Therefore, moving forward I will use this terminology interchangeably depending on the context.

Regardless of the denotations DAM and homeostatic, or M1 and M2, these are an oversimplification, and different insults and diseases induce varied phenotypes. Generally speaking, "classical activation" refers to M1 microglia, which are induced by interferon gamma (IFNγ) or LPS, and show increased expression of surface markers CD16, CD32 and CD86. M1 microglia upregulate NF-κB-related genes (described later on) and produce IL1α and IL1β, TNFα, interleukin 6 (IL6) and NO.[51,52,54] These cells undergo morphological changes, with a rounder, amoeboid shape and decreased process length, in conjuncture with increased phagocytosis, cytokine release, antigen presentation and proliferation.[55] This morphology is associated with increased neuronal death, whereas M2 microglia are neuroprotective.[56] M2 microglia were formerly called "resting" microglia, but this term is out of date as these cells are quite active. This phenotype can be induced by interleukin 4 (IL4) or interleukin 13 (IL13), referred to as "alternative activation." These cells have increased expression of CD206, and secrete factors involved in neuroprotection and tissue repair, namely arginase-1 (Arg1) and insulin-like growth factor 1 (Igf1).[52] These cells are involved in scavenging and phagocytosis of misfolded proteins and cell debris, and appear ramified, with increased process number and length for constant surveillance of their environment.[55] A third state is referred to as "acquired deactivation," is induced by interleukin 10 (IL10) and transforming growth factor beta (TGFβ), and includes microglia with characteristics of both phenotypes as they return from an activation state to a scavenging state.[42,52,57] A microglial cell will likely change activation states multiple times throughout its life, as they are able to live to be more than four years old. Their activation states also influence neighboring astrocytes. As M1 microglia secrete factors that shift astrocytes toward an A1 phenotype, M2 microglia produce anti-inflammatories such as IL10 and TGFβ that shift astrocytes toward an A2 phenotype.[42]

Importantly, the molecular milieu produced by M1 microglia negatively regulates that of M2 microglia, and vice versa, supporting a tightly regulated process, potential for phenotype switching, and resulting in an environment in the brain for one state of activation over another.[52,56]

An astro-nomical number of astrocytes

Understanding inflammation and the contributing roles of astrocytes and microglia is critical for early diagnostics and development of robust therapeutics for prion disease. The number of both microglia and astrocytes are significantly increased in both humans and animal models, and this is present long before onset of clinical signs.[48,58,59] Intriguingly, mouse studies have demonstrated that translation of neuronal proteins remains relatively consistent throughout the course of disease, whereas translation in both astrocytes and microglia changes drastically.[60]

S100 calcium-binding protein β (S100β), a general astrocyte marker, has been cited as a reliable biomarker of CJD and scrapie when detected in cerebrospinal fluid and serum in humans and animals, respectively.[61-63] S100β, in combination with the complement protein C3, is a marker for reactive astrocytes in prion and other neurodegenerative diseases, [45] as is lipocalin 2 (LCN2) in combination with C3.[64] LCN2 is a protein secreted by astrocytes in inflammatory conditions that contributes to apoptosis and morphological changes.[65] Guanidine-binding protein 2 (GBP2) is another markers of neurotoxic astrocytes that are highly abundant in the brains of prion infected animals and CJD patients. [45,49] Although still poorly understood, these reactive astrocytes are known to secrete toxic mediators, such as saturated lipids, that contribute to neuronal cell death. [45,47,49,66,67]

Recently, astrocyte-derived saturated lipids from Apolipoprotein E (APOE) and Apolipoprotein J (APOJ) have been shown to induce neuronal cell death *in vitro* and in an *in vivo* model of acute axonal injury.[66] Interestingly, APOE has been shown to be upregulated in prion mouse models,[50] particularly in microglia.[68] However, knockout of this protein was not protective, and resulted in decreased incubation time and increased inflammatory cytokines, increased markers of A1 astrocytes, increased markers of both DAM and homeostatic microglia, and neuronal loss. Additionally, microglia show an impaired ability to clear PrP^{Sc} and damaged neurons.[68] Although this does not completely exclude the potential involvement of astrocyte-derived saturated lipids in prion pathogenesis, it does suggest that there may be other neurotoxic factors, as knockout of APOE would be expected to restore health in infected animals.

Transitioning from a "resting" astrocyte to a neurotoxic astrocyte requires microglia-derived C1qα, IL1α and TNFα.[45] Logically, abolishment of these signals, here referred to as triple knock-out, should prevent or at least decrease neurodegeneration in the context of prion disease. However, removal of these inflammatory proteins, although successful in abolishing C3+ astrocytes, also accelerated disease in mouse models.[49] No changes were detected in vacuolization, PrP^{Sc}, GFAP (marker of astrocytes) or ionized calcium-binding adaptor molecule 1 (Iba1) (marker of microglia). However, homeostatic microglia, marked by expression of transmembrane protein 119 (TMEM119) and purinergic receptor P2Y12 (P2RY12),[69,70] were significantly decreased in the prion-infected triple knock-out mice.[49] This suggests that, as microglia are critical for astrocyte activation, reactive astrocytes may indeed be critical in regulating microglia phenotypes as well, and that this process is important for combatting prion infection.

Both astrocytes and neurons can be infected with PrP^{Sc},[38] and astrocytes demonstrate the ability to transfer PrP^{Sc} between each other and to neurons.[71] Astrocytes more readily take up PrP^{Sc} than neurons. It is unknown whether this is a due to increased susceptibility, or as a mechanism to protect the neurons. Despite this, neuronal expression of PrP^{C} is required for disease to be fatal. When PrP^{C} is expressed solely in astrocytes, there is significant PrP^{Sc} accumulation, but no microgliosis, astrogliosis, vacuolization, or neuronal loss, and mice do not develop signs of clinical disease. When PrP^{C} is restricted to neurons, mice develop all the classic signs of prion disease, but have less gliosis and live significantly longer than wild-type animals. This suggests that astrocytes becoming infected and further disseminating prions can accelerate disease and promote inflammation, but that they are not required for disease to occur.[38]

Microglia follow a similar pattern of dispersal throughout the brain as PrP^{Sc}, [72,73] likely due to their role in phagocytosis. Astrocytes, however, show a much different pattern of activation that is not consistent with PrP^{Sc} deposition, and different regions of the brain display different astrocyte morphology. This is particularly apparent in the hippocampus and thalamus. There are multiple strains of mouse-adapted scrapie that have been developed for research purposes, the most common in the United States being 22L, RML and ME7, which show different PrP^{Sc} deposition, but similar gliosis.[48] Intriguingly, in 22L-infected mice, an a greater increase in microglia is seen in the thalamus compared to the hippocampus, but a greater increase in astrocytes is seen in the hippocampus compared to the thalamus.[73] This suggests that these cell types are working somewhat independently of one another. We have made similar observations in RML-infected mice (see Chapter 3). These observations are based solely on GFAP and Iba1 expression of astrocytes and microglia, respectively, and does not delve into the molecular profiles of these cells.

A healthy mouse contains seven distinct types of astrocytes, with different levels of protein expression and distribution throughout the brain, based on single-cell profiling.[74] The profiles of astrocytes in response to prion disease have only begun to be interrogated. Although more phenotypes are being uncovered, A1 and A2 astrocytes are still the best characterized. Interestingly, translational profiling of cells in the prion-infected brain showed an increase in both A1 and A2 astrocytes as disease progressed, despite A2 being generally associated with homeostatic function and maintenance of neuronal health. This suggests that a subset of astrocytes may be contributing to preventing neurodegeneration, even in the late stages of disease.[60]

DAM! Look at all those microglia

The role of microglia in prion disease remains controversial, as studies show that they are critical, expendable, and everything in between. Ultimately, this depends on the mechanism used to decrease or eliminate microglia, as well as the time point at which this is done.

Single-cell analysis shows that microglia decrease their homeostatic signature (characteristic of M2 microglia) and developed a disease-associated signature (characteristic of M1 microglia) over the course of disease.[60] Specifically, the homeostatic markers TMEM119 and P2RY12 decrease. P2RY12 expression is associated with ramified microglia, containing small cell bodies and long, thin processes. Changes in microglia are first detectable in the thalamus at preclinical stages, and cell morphology shifts from being ramified to activated or amoeboid. This is particularly apparent in the loss of P2RY12+ and TMEM119+ microglia in the thalamus,[69] while Iba1+ microglia increase in number and appear more amoeboid with thick processes in both the thalamus and hippocampus (see Chapter 3).[69,75]

Microglial contribution to neuronal toxicity was first described in prion disease in 1998 by Giese et al. They co-cultured primary microglia and neurons infected with PrP^{Sc}, and ascertained that having microglia present in the culture was critical for PrP^{Sc}-induced neurotoxicity. This was corroborated using three different scrapie mouse models, for each of which PrP^{Sc} accumulation correlated strongly with microglial activation, which preceded neuronal cell death.[76] Compared to other cell types in the brain, microglia express much less PrP, but can still become infected, replicate, and spread PrP^{Sc}, and it has been suggested that their ability to migrate may help in dissemination.[77] Microglia from the bone marrow can infiltrate the brain upon prion infection, suggesting a huge role in prion migration and a potential route of transmission from peripheral infections.[78] However, other studies suggest that few peripheral immune cells make it to the brain upon prion infection.[79]

Microglia appear to be effective in phagocytosis and clearance of apoptotic neurons and cellular debris, but unfortunately are inefficient in phagocytosing PrP^{Sc}.[80] Proteins involved in the complement cascade, namely C1q and C3, and the receptor C3 receptor on microglia, have been shown to be involved in phagocytosis and over-pruning of synapses in a mouse model of Alzheimer's disease, and inhibition of these proteins leads to improved neuronal health.[81] However, the same has yet to be shown for prion disease.

Microglia recognize misfolded PrP, particularly $PrP_{106\text{-}126}$, a peptide that is known to mimic the neurotoxic effects of PrP^{Sc}.[11] $PrP_{106\text{-}126}$ induces the production of nitrite, inducible nitric oxide synthase (iNOS), ROS, IL1β and IL6. Microglial-derived IL6 has been shown to induce neuronal cell death.[82] Phagocytosis of $PrP_{106\text{-}126}$ by BV2 microglia increases mRNA for TNFα and iNOS, markers of classically activated or M1 microglia, and decreases mRNA for Arg1 and mannose-receptor c-type 1 (Mrc1), markers of alternatively activated or M2 microglia,

and appears to have little effect on mRNA for suppressor of cytokine signaling 3 (SOCS3) and interleukin 4 receptor alpha (IL4Rα), markers of acquired deactivation.[57]

PrP^{Sc} activates microglia and polarizes them toward a classically activated phenotype. However, the anti-inflammatory cytokines TGFβ, IL10 and IL13, are upregulated in the brain at late stages of prion disease,[83] as are markers of alternative activation and acquired deactivation.[60,84] Because these activation types are not being induced by microglia upon prion infection, this suggests that crosstalk between cells is responsible for producing factors that polarize microglia from a DAM state to a homeostatic phenotype, likely in an attempt to attenuate inflammation. In fact, some studies have shown that knockout of IL10 in mice lead to increased susceptibility to disease,[83] suggesting cytokines, particularly those responsible for acquired deactivation, are critical in dampening prion-induced inflammation.

Interestingly, some experiments have suggested that one of the functions of PrP may be the activation state of microglia, as knock-down of PrP has been shown to decrease markers of classically and alternatively activated microglia.[85,86] However, these experiments were performed in an immortalized cell line, BV2 cells, and should be repeated using primary microglia, or ideally *in vivo* models.

So, are microglia protective to neurons? Or are they contributing to neurodegeneration? To help answer this question, we need to discuss what happens when you remove or decrease microglia during the course of prion infection. This has been the section I have least looked forward to writing because there are many studies that have attempted this, and they all seem to have conflicting results. Therefore, we will review them in chronological order, and then discuss any patterns in the overall findings.

Microglial proliferation and survival requires continual stimulation by the tyrosine kinase macrophage colony stimulating factor receptor (CSF1R).[87] CSF1R is activated by colony stimulating factor 1 (CSF1) and interleukin 34 (IL34), which are produced by astrocytes and neurons. CSFR1 stimulation induces expression of PU.1 and C/EBPα, which drive renewal, differentiation and survival of microglia.[88] Both PU.1 and C/EBPα are increased in the brains of CJD patients. The function of CSF1R can be inhibited by the drug GW2580.[75] Infected mice that received this drug showed decrease, but not ablation, of microglial, a decrease in PU.1 and C/EBPα, and a modest increase in markers of M2 microglia. Moreover, these mice had improved neuronal health and increased survival compared to vehicle-treated mice.[75] A second study used CSF1R signaling to modify microglial numbers. Stimulation with stereotaxically injected CSF1 or IL34 was used to increase the function of CSF1R and increase microglial proliferation, and GW2580 was used to inhibit the receptor and decrease microglial numbers.[89] Conversely to the previous study, increases microglia was associated with improved neurogenesis and neuronal development in the hippocampus. Microglial-derived TGFβ was determined to be responsible for this, as neurogenesis was decreased when TGFβ was inhibited.[89] Another study knocked out IL34 in tga20 mice, which decreased microglial numbers. They observed shorter incubation times with prions and an increase in PrP^{Sc}. They saw similar effects when they ablated microglia from mouse ex vivo organoid cultures, in addition to more neuronal loss, decreased TNFα and IL1β mRNA, and increased CCL2 and CCL5 mRNA.[90]

Another study used PLX5622, another inhibitor of CSF1R, was used to decrease the number of cortical microglia by as many as 90%, and was associated with decreased survival, both when the drug was administered at 14 days post infection (dpi), or at preclinical stages of disease (80 dpi). Although microglia were decreased, mice showed increased vacuolization,

astrogliosis, and, importantly, similarly distributed but significantly increased PrP^{Sc}, suggesting an important role for microglia in clearance of prion aggregates. These results were consistent amongst three different mouse-adapted scrapie models.[91] Similar to the previous study, key inflammatory cytokines such as TNFα and IL1α were decreased in PLX5622-treated mice,[91] suggesting that microglia may be a large source of these inflammatory mediators, and suggesting that elimination of inflammation may not be completely protective.

Now that we have studies that contradict the effects of microglia in survival of prion-infected animals, let's discuss a study that contradicts the role of microglia in reduction of PrP^{Sc}. Once again, this group targeted CSF1R, but they deleted an enhancer of the receptor that prevents microglial development but allows mice to develop normally. These mice are referred to as *Csf1r*$^{\Delta FIRE}$, and it results in complete knock-out of microglia.[92] *Csf1r*$^{\Delta FIRE}$ mice succumbed to disease more rapidly, solidifying a role for microglia in neuroprotection. Similar to the previous experiments, TNFα mRNA was significantly decreased, further identifying this as a microglia-derived cytokine. The brains of *Csf1r*$^{\Delta FIRE}$ mice showed significantly more vacuoles, but neuronal counts in the CA1 region of the hippocampus were unchanged. No differences were seen in PrP^{Sc} through immunohistochemical staining, western blotting, or seeding activity of PrP^{Sc}.[92] These animals showed decreased GFAP+ astrocytes in the hippocampus compared to wild-type controls, although total brain mRNA for GFAP was the same. Additionally, mRNA for GBP2 was decreased,[92] a gene associated with reactive astrogliosis.[49] Interestingly, an increase in reactive astrocytes was observed in the superior colliculus, as more C3+/LCN2+/GFAP+ astrocytes were detected via immunofluorescence. GFAP+ astrocytes appeared to have enhanced phagocytosis in the absence of microglia, as these cells showed increased uptake of neuronal synapses. Astrocytes also showed increased unfolded protein response (UPR) early in disease,

associated with an increase in phosphorylated PERK and eIF2α (reviewed later on).[92] The overall findings of this study corroborate the role of microglia in neuroprotection against prions, and also highlight their regulatory role in astrogliosis, as astrocytes appear to compensate for microglia by increasing phagocytosis and UPR functions, with deleterious effects.[64,92]

A recent study showed the effects of intermittent treatment of PLX5622, (an inhibitor of CSFR1 used in a previously mentioned study) on microglial proliferation throughout prion disease to identify when these cells are most beneficial. Oral administration of this drug can decrease microglia by inducing caspase-3-mediated apoptosis, resulting in up to a 90% decrease in microglial numbers in 7 days. Race et al. ablated microglia 7 days *prior* to infection with prions. Treatments were continued on to 7 dpi, 77 dpi, or 112 dpi (mean survival is ~150 dpi) showed a significant reduction in Iba1 cells, but no changes in PrP^{Sc} seeding activity. Early treatment with PLX5622 (prior to inoculation) did not change susceptibility to prion infection.[87] It is established that microglial morphology and function changes with age, characterized by increased inflammatory mediator production and decreased phagocytic abilities.[93] Consistent administration of PLX5622 is necessary to maintain decreased CNS microglia, and cells return rapidly after dosing ends. These new microglia are similar to those present in young mice. Therefore, Race et al. hypothesized that reintroduction of healthy microglia may be beneficial in attenuating prion disease. Beginning at 80 dpi, mice were treated for one week with PLX5622, either once, two times with two weeks between treatments, or three times with two weeks between treatments. Regardless of when or how frequently the drug was administered, mice succumbed to disease at the same time, and no significant changes in Iba1+ cells were observed. Uninfected mice, however, showed a decrease in Iba1+ cells with treatment, suggesting that the drug was working, but is ineffective in reducing microglia at last stages of disease.[87] Finally, to

further interrogate the role of microglia in potentially decreasing PrP^{Sc} accumulation, they utilized another model of mice, called tga20 mice, that express PrP at 6 to 10-fold normal expression and succumb to disease more rapidly than WT mice, but have less than 10% the amount of PrP^{Sc}. These mice were treated with PLX5622 beginning at 14 dpi and for the duration of the study and showed significant reduction in Iba1+ cells. Tga20 mice treated with PLX5622 showed a slight, but significant, decrease in survival time compared to untreated tga20 mice,[87] whereas this survival time difference was much greater in this group's previous study using WT mice that show significant PrP^{Sc} accumulation.[91] Together, this data suggests that microglia do not show a significant role in prion pathogenesis early in disease, but that they show benefits at later time points in disease, and that one of these benefits may be the clearance of PrP^{Sc} itself.

Altogether, what do these experiments tell us? Having a balance of microglia is important, and this can be hard to achieve. Whether or not microglia improve survival may be dependent on the drug or transgenic model used. However, overall, it appears that microglia are beneficial to the host in prion infection. Although classically activated phenotypes may be responsible for production of inflammatory cytokines that may promote astrogliosis and neurotoxicity,[75,89] the alternatively activated and acquired deactivated phenotypes appear to be neuroprotective and mediate astrocyte reactivity.[89] Phagocytosis of PrP^{Sc} may be important later in the course of disease.[87,91] Moreover, in the absence of microglia, astrocytes compensate by increasing dysregulated phagocytosis and UPR activities, which contribute to neurodegeneration.[64,92]

Mechanisms of neurotoxicity

One of the difficulties in designing therapeutics for prion diseases is that the actual mechanism of neurotoxicity has not been fully elucidated. It has long been hypothesized that prions themselves, particularly oligomeric species, are the neurotoxic agent. However, a recent study using highly purified prions isolated from mice with RML-scrapie has shown that these are not toxic to primary neuronal cultures, whereas raw RML brain homogenates are highly toxic. Moreover, highly purified prions, when resuspended in brain homogenate from uninfected mice, do not show toxicity in neurons.[94] This suggests that the infectious agent may not be the prion itself, but something produced in the replication process, or by cells as a response to the prion. Additionally, there is a distinction between infectivity and neurotoxicity, as animal models show two distinct phases of disease – rapid accumulation of misfolded prions, followed by a gradual development of neurological changes that are inversely related to expression of PrP^{C}.[72,95]

It has been well established that prion-induced neuronal cell death occurs in prion disease,[96] however, the cellular response of the neuron leading up to this is poorly understood. Some of the difficulties in understanding neurotoxicity arise from a lack of understanding of the physiological role of the cellular prion protein (PrP^{C}), how it interacts with PrP^{Sc}, and the location and mechanism of misfolding. *In vitro* models may be the best to elucidate neurotoxicity, but many of these have caveats. Few immortalized cell lines are infectable with PrP^{Sc}, and those that are do not undergo apoptosis. Ex vivo organoid slices and organoids derived from pluripotent stem cells can also be used to study neurotoxicity,[97] but these require multi-week incubation with PrP^{Sc} to become infected, which makes it difficult to parse out the effects of prion infectivity from neurotoxicity, as these are two distinct phases of disease.[72,95,98] Primary cultures of neurons demonstrate similar issues - not displaying neurotoxicity,[99] or

difficulty in separation of infectivity and toxicity.[100] A co-culture model with primary neurons and astrocytes was recently described that allows for rapid transmission of PrP^{Sc}, allowing seeding events to occur within minutes of infection.[98] Other cell types, particularly glial cells, may be critical to recapitulate the neurotoxicity seen in the prion-infected brain, and many models in particular lack microglia,[94,97,98] which I have hopefully convinced you are critical in understanding prion diseases.

Despite the lack of perfect *in vitro* models, we can still uncover important information from primary neuronal and organoid cultures. Having the same primary structure makes differentiating between PrP^{C} and PrP^{Sc} difficult. The easiest way to differentiate the β-sheet rich PrP^{Sc} from the predominantly α-helical PrP^{C} is using proteinase K (PK), as PrP^{Sc} is PK resistant. This is commonly used in western blots for cell lysates and brain homogenates, but can be too damaging to primary cell cultures. The development of PrP^{Sc}-specific antibodies have allowed for detection of PrP^{Sc} (Figure 1.2) in delicate primary neuronal cultures without damage induced by PK degradation.[99,101] Moreover, PK-sensitive PrP^{Sc} may include oligomeric species that are neurotoxic.[98] Therefore, PK degradation, although a helpful tool in identifying infectious PrP, may be detrimental in studies of neurotoxicity.

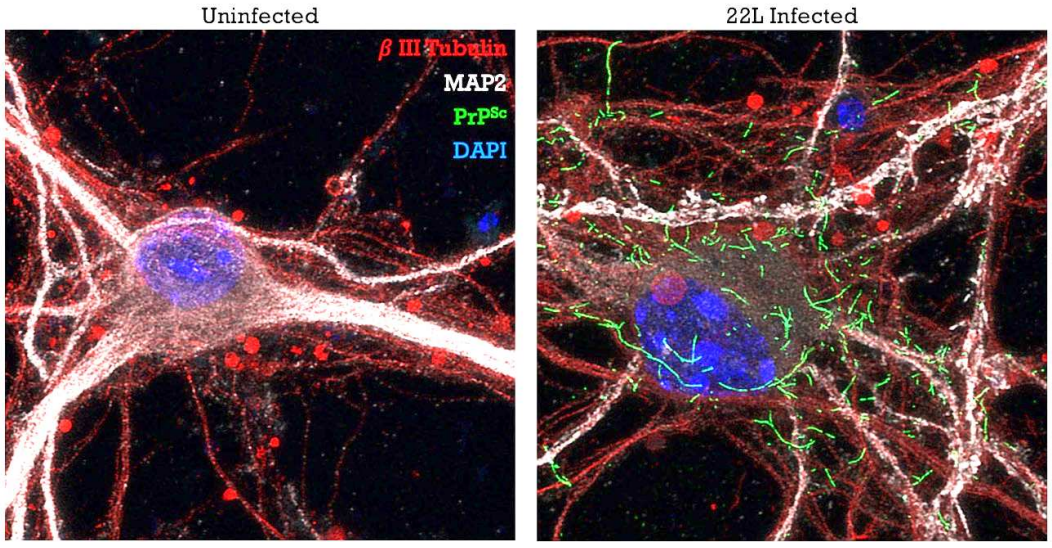

Figure 1.2. PrP^{Sc}-specific antibody in infected primary thalamic neurons. Neuronal markers MAP2 (white) and β III tubulin (red), PrP^{Sc} (green) and DAPI (blue). Imaged by Arielle Hay, unpublished.

Knockout of PrP does not induce neurotoxicity in infected cultures, suggesting that loss-of-function is not involved in neuropathology. However, studies modifying PrP suggest that there may be a toxic gain-of-function. PrP is normally attached to the surface of the cell via a GPI anchor, which may be critical for its normal function. Animal models without this anchor show distinct neuropathology and increased infectivity.[102,103]

One of the first signs of prion disease on a cellular level is synaptic degeneration, and PrP^{Sc} is often found around sites of synapses. Both *in vitro* and *in vivo* studies have shown swelling of neuronal dendrites and retraction of their spines, which are critical sites of synaptic contact. This is most apparent in excitatory, not inhibitory, synapses, and seems independent of PK treatment, suggesting that all forms of PrP^{Sc} may contribute to dendritic spine abnormalities. Dendritic spines are highly involved in synaptic plasticity important for learning and memory,[98] and this dysregulation is likely associated with some of the behavioral changes associated with prion diseases. Synaptic degeneration may occur from the binding of PrP^{Sc} to cell surface PrP^{C}, which may act as a ligand and signal transducer, respectively, to generate toxic downstream events. Another hypothesis is that the tight binding of PrP^{C} to PrP^{Sc} localizes PrP^{Sc} to the cell surface, where it interacts with other membrane proteins and the lipid bilayer, potentially inducing changes in receptor and ion channel activities. Binding of PrP^{Sc} to PrP^{C} on the cell surface may also immediately convert the native protein to the infectious form.[98]

Although the function of PrP remains unclear, there is evidence that PrP^{C} interacts with N-methyl-D-aspartate (NMDA)-type glutamate receptor subunits and modifies their function. NMDA receptors are involved in regulating the actin cytoskeleton of dendritic spines. PrP^{Sc} may activate NMDA glutamate receptors, as associated Ca^{2+} influx can be observed in primary

cultures shortly after PrP^{Sc} infection. Glutamate excitotoxicity is seen in prion infection, and glutamate receptor antagonists have been shown to be protective against dendritic spine loss in infected neuronal cultures and animal models,[104,105] as have peptides that stabilize actin cytoskeletons.[98] The involvement of glutamate receptors is consistent with the observation that excitatory neurons are more susceptible to prion-induced degradation.[98]

Mitogen-activated protein kinases (MAPKs) respond to intra- and extracellular signals. p38 MAPK is particularly important for signal transduction and synaptic plasticity in the central nervous system, and its dysregulation has been cited in multiple neurodegenerative diseases. This includes the involvement of excitotoxicity in prion disease.[98,104] Treatment with PrP^{Sc} causes an increase in phosphorylation of p38 in dendritic spines, and blockage of this signaling with pharmacological inhibitors reverses spine degradation.[98,104]

Another large area of research into neurotoxicity of prions has focused on changing the primary structure of PrP, particularly the N-terminal domain. As mentioned, $PrP_{106-126}$ can mimic the toxic effects of PrP^{Sc} and form fibrils. Deletion of the N-terminal domain (residues 23-125) induce motor defects and cerebellar degeneration in mice, leading to death within 3 months.[106] Deletion of 21 amino acids from the central region of the protein (residues 105-125) induces death within a week of birth.[107] Glutamate excitotoxicity and ion channel abnormalities were shown to lead to neurodegeneration in this model.[98,108] Intriguingly, similar dysregulation of ion channel currents were observed in cellular models with point mutations associated with genetic prion disease, such as P101L, the murine analogue for the P102L mutation seen in GSS.[109] Co-expression of normal PrP alleviates the neurotoxic effects of these N-terminal modification models in a dose-dependent manner, suggesting that these deleterious effects are due to a divergence from PrP cellular function. Likewise, antibodies that bind to the first α-helical region

(α1) of PrP induce changes in ion currents and dendrite degradation in primary neurons. This is reliant on the N-terminal domain, as removal of residue 23-31 of the N-terminus prevents this degradation.[98] Together, these data suggest a toxic gain-of-function, particularly involving the N-terminal region and its normal, regulatory interactions with the C-terminal domain. This may lead to synaptic dysregulation, glutamate excitotoxicity, and related dendrite spine degeneration. Additionally, these results suggest that any antibody developed for therapeutic purposes against PrP^{Sc} should avoid targeting the N-terminal region.

NF-κB signaling in prion pathogenesis

Nuclear factor-κB (NF-κB) refers to a group of innate immune transcription factors that respond to insult, inflammation and injury. These proteins include NF-κB1 (or p50), NF-κB2 (or p52), RelA (or p65), RelB and c-Rel, which form homo- and heterodimers that bind to and transcribe a DNA element called κB enhancer. Under normal conditions, NF-κB remains sequestered in the cytoplasm, inhibited from translocating to the nucleus by IκB and related proteins. The IκB kinase complex (IKK) is composed of the catalytic subunits Iκκα and Iκκβ, and a regulatory subunit, Iκκγ. IKK can be activated by a variety of stimuli such as cytokines (particularly TNFα and IL1β), growth factors, PAMPs and DAMPs (see Figure 1.3). In the context of prion disease, activated of IKK predominantly occurs through TLRs and nucleotide-binding oligomerization-domain protein-like receptors (NLRs) such as NLR family pyrin domain containing 3 (NLRP3) (described later).[110,111]

Once activated, IKK phosphorylates IκBα, leading to IκBα being ubiquitinated and degraded by the proteosome. Uninhibited, NF-κB can translocate to the nucleus to upregulate a huge number of NF-κB related genes. These include cytokines (TNFα, IL1α and IL1β, and IL-6),

chemokines (CCL2, CCL4 and CCL5), adhesion molecules, enzymes (cyclooxygenase-2 (COX2) and iNOS), and regulators of apoptosis.[111-113] NF-κB signaling is also tightly regulated with autophagy and mitophagy, and the IKK complex can stimulate autophagy (described later), even in the absence of NF-κB.[114] In the brain, NF-κB contributes to signaling events that promote either synaptic plasticity, or induce neuronal apoptosis.[115] As inflammation, autophagy and apoptosis are all key factors in prion pathogenesis, investigation of the role of NF-κB and related proteins is essential.

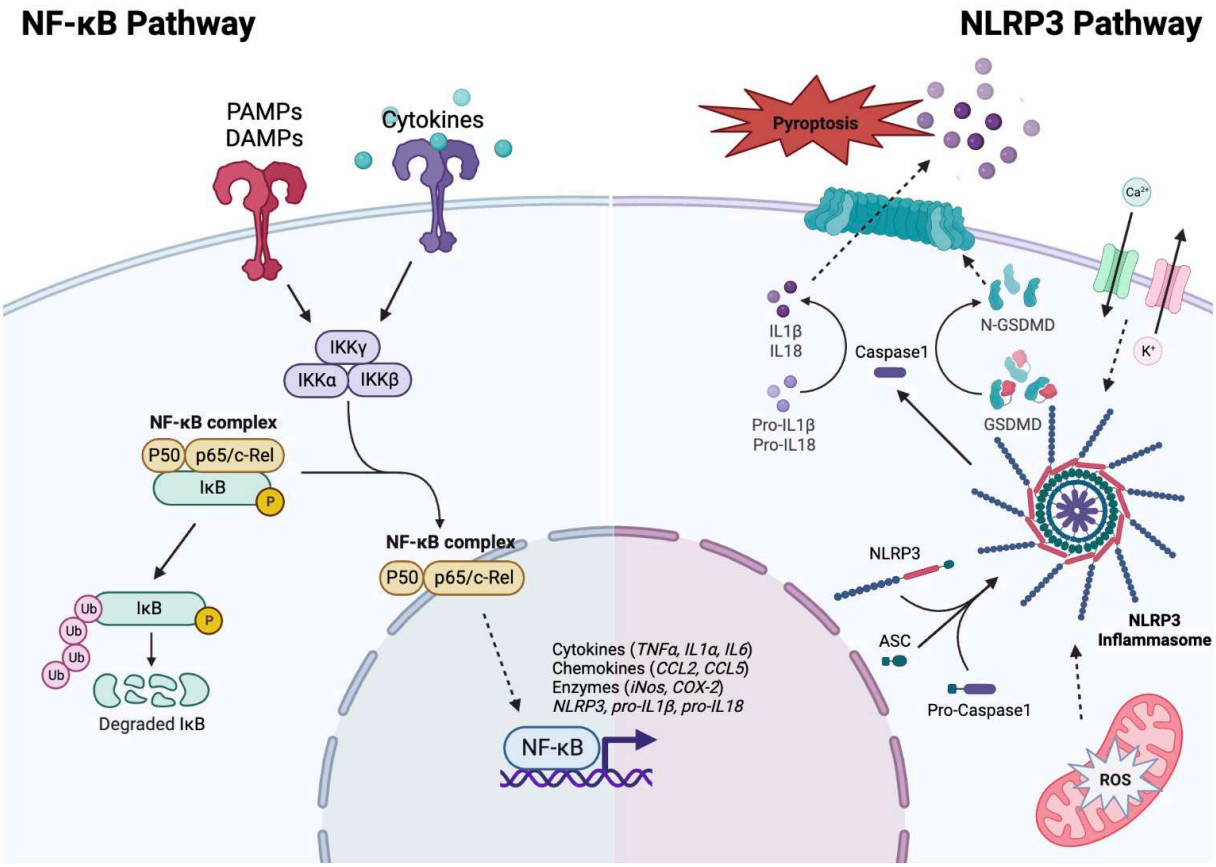

Figure 1.3. Interconnection of the NF-κB and NLRP3 Inflammasome Pathways. Graphic created with BioRender.com.

A non-canonical pathway is also involved in the activation of NF-κB, but this is a function of the adaptive immune system,[112] and is therefore outside the scope of this dissertation, as prions do not trigger an adaptive immune response.

The connection of the NF-κB pathway in prion pathogenesis was first made in 1999 by Kim et al. when the observation was made that NF-κB activity was significantly increased in the hippocampus and thalamus of scrapie-infected mice, in addition to cytokines that are both known to induce the NF-κB pathway, and those that are known to be upregulated by NF-κB.[116] The synthetic prion peptide $PrP_{106-126}$ has demonstrated the ability to induce NF-κB in human microglia, accompanied by an increase in iNOS and TNFα.[117] Despite this, few studies have attempted to elucidate the role of NF-κB in prion pathogenesis. Time and time again researchers have described NF-κB-related genes upregulated in the brains of prion-infected animals.[48,50,84,118] Why, then, has this pathway been generally ignored as a potential therapeutic target, or utilized as a biomarker for human prion diseases?

It is likely that a study from the Aguzzi lab conducted in 2008 has stymied any further attempts to investigate the role of this pathway in disease. This study utilized the *CreLox* system to target cells of the CNS neuroectodermal lineage under control of the *Nestin* promoter. *Nestin-Cre* mice were crossed with *loxP*-flanked IKKβ or IKKγ mice, generating a line of mice that effectively did not express NF-κB in astrocytes, neurons and oligodendrocytes. When infected with prion disease, no significant changes in survival or disease pathogenesis were observed in these mice compared to controls. This led the researchers to conclude that NF-κB signaling does not contribute significantly to disease outcome.[119]

There is a major caveat to this conclusion – it does not take into account the role of microglial NF-κB signaling, as these cells are derived from a separate lineage – the peripheral

mesoderm or myeloid tissue – as opposed to the ectoderm.[120] Although this has not been formerly characterized in prion disease, our data suggest that microglia-specific NF-κB signaling has a significant effect on both the inflammatory state of glial cells, as well as downstream pathways such as autophagy (see Chapter 4, data unpublished). Although they make up a small percentage of the overall cell population, astrocytes show limited response to inflammation in the absence of microglia.[45,46] It has been shown that, even in cell culture models, the presence of even a few microglia can elicit large changes in the phenotype of astrocytes.[121] Therefore, by not removing IKKβ or IKKγ from microglia, it is inappropriate to conclude that this signaling pathway has a limited role in prion pathogenesis, as microglia would have continued to respond to prions, damage-associated molecular patterns (DAMPs) and cytokines to induce NF-κB signaling and related downstream pathways.

The role of microglia-specific NF-κB signaling has been investigated by Srivastava et al. in an in vitro model of prion-treated microglia. Both the BV2 microglial cell line as well as primary microglia were treated for 18 hours with 22L mouse-adapted scrapie purified from terminally ill mice or infected cells. They observed an increase in NF-κB-associated cytokines IL6 and TNFα, as well as nitrite and iNOS, in addition to degradation of Iκβα, indicative of NF-κB activation.[122] Together, these data suggest an immediate response of microglia to the prion protein itself, as well as suggesting potential downstream effects, as microglia-derived cytokines such as TNFα are strong inducers of astrocyte reactivity.[45,46] Data from our laboratory has demonstrated an increase in the NF-κB-related genes CCL2, CCL5 and IL1β in primary mixed glial cultures (containing both astrocytes and microglia) that have been infected for two weeks with 22L mouse-adapted scrapie (see Chapter 2).[123]

Interestingly, it is suggested that PrP itself may be critical in regulation of the NF-κB pathway by enhancing response to TNFα.[124] As many prion therapeutics target PrP (reviewed later), this highlights a potential downstream effect that may allow for a decrease in inflammation. Overall, the NF-κB pathway should not be dismissed as either a biomarker for disease or a therapeutic target.

The NLRP3 inflammasome

Some genes transcribed by NF-κB include *NLRP3*, *pro-IL1β* and *pro-IL18*, genes for key proteins in the innate immune NLRP3 inflammasome, which responds to a variety of signals including cellular damage. The first signal, priming, is well characterized and includes TLR binding of PAMPs and DAMPs, or binding of cytokines such as IL1β via IL1R and TNFα via TNFR, resulting in NF-κB activation and transcription, as described above. The second signal, referred to as activation, remains poorly understood. Various extracellular stimuli, generally referred to as NLRP3 agonists, are able to induce assembly of the NLRP3 inflammasome. These agonists do not bind directly to NLRP3, but instead induce cellular or mitochondrial damage or changes in intracellular calcium and potassium levels. For example, NLRP3 can be triggered by extracellular ATP, mitochondrial DNA, or mitochondrial-derived ROS. It is hypothesized that NLRP3 responds to a common cellular event triggered by these agonists as opposed to binding individually to these structurally diverse stimuli. The NLRP3 inflammasome refers to a large multimeric protein complex composed of individual monomers of NLRP3 and the adaptor protein apoptosis-associated speck-like protein containing a CARD (ASC, also known as PYCARD), which recruit pro-Caspase1, which cleaves itself to form Caspase-1. Caspase-1 cleaves pro-IL1β and pro-IL18, releasing the inflammatory cytokines IL1β and IL18. Caspase-1

also cleaves gasdermin D (GSDMD), a protein that oligomerizes and forms a pore in the cell membrane that releases IL1β and IL18, and induces pyroptosis by disrupting the cells osmotic potential (Figure 1.3). [125,126]

Arguably even less characterized in prion disease than the NF-κB pathway is the NLRP3 inflammasome pathway. This pathway can be activated by NF-κB, as well as by agonists of NLRP3 itself. NLRP3-related genes, *NLRP3*, *Pycard* (which encodes ASC), *Caspase1* and *IL1β* are all upregulated in infected mouse microglia.[110] The neurotoxic peptide $PrP_{106-126}$ can induce NLRP3 activation when phagocytosed by both primary and BV2 microglia.[57,127,128] Likewise, PrP fibrils induce NF-κB, and IL1β can be released from macrophages and microglia in vitro, but this is significantly decreased in the absence of NLRP3, ASC or Caspase1.[129] Cell-based models of prion disease have shown an intriguing role for NLRP3 in inflammation and neurotoxicity, but animal models have not demonstrated this.

Previous studies have dismissed this pathway as having any significant implications in prion pathogenesis. mRNA analysis of infected wild-type mice showed that *Pycard* and *Caspase1* increased only slightly, and *NLRP3* and *IL1β* transcript levels remained unchanged at terminal prion disease.[110] This contradicts the findings of another study, in which analysis of three mouse-adapted scrapie strains all showed significant upregulation of *IL1β* at terminal disease.[48] The Aguzzi group generated NLRP3 knockout (KO) or ASC KO mice and infected them with prions. They showed no significant differences in the time-course or pathogenesis of disease, as determined by survival, spongiosis, astrocyte and microglial numbers, and PrP^{Sc} accumulation. Additionally, no significant changes were seen in IL1β in the prion-infected KO mice, [110] suggesting another source of this cytokine besides the NLRP3 inflammasome (hmm…perhaps an inflammatory pathway that has been previously mentioned…NF-κB?)

Although the NLRP3 inflammasome may not have a significant role in prion pathogenesis to change survival or obvious disease phenotypes, it may contribute to other pathways, such as autophagy, mitophagy, and pyroptosis, and of course NF-κB, which may have implications in prion disease. An interesting study by Lai and colleagues found that inhibition of autophagy in microglia increased the processing and release of IL1β, and that autophagy is increased by inhibition of the NLRP3 inflammasome. TIR-domain-containing adaptor inducing interferon β (TRIF) and TLR4 were both found to be important for the autophagy of $PrP_{106\text{-}126,}$ as their knock-down by siRNA lead to a decrease in autophagy. They suggested that TLR4 binds $PrP_{106\text{-}126,}$ and recruits TRIF to promote autophagy. Caspase1 was found to cleave TRIF and halt autophagy, suggesting a mechanism by which the NLRP3 inflammasome inhibits autophagy of the neurotoxic prion peptide.[130]

Oxidative stress

Cellular stress caused by misfolded proteins and associated inflammation leads to an increase in ROS. This has been described in the brains of CJD patient and prior to clinical signs in animal models, and leads to DNA damage and increased glial numbers, particularly microglia.[131-134] NO and iNOS are also increased in prion disease.[135] Knockout of proteins involved in repair of oxidative DNA damage leads to increased nuclear and mitochondrial DNA damage, decreased astrocyte numbers, and shortened survival time.[134] The source of ROS is predominantly microglia, and the majority of ROS is produced by the NADPH oxidase 2 enzyme (NOX2), an electron transporter that produces ROS upon phagocytosis to kill pathogens. Knockout of NOX2 slowed presentation of clinical and behavioral signs and increased survival time in animal models.[136] Together, these findings support the role of microglia in production of

ROS, and highlight the importance of repair mechanisms for DNA damage induced by oxidative stress in prion disease.

The Keap1-Nrf2 pathway is a key regulator in oxidative stress response. Under healthy conditions, nuclear factor erythroid 2-related factor 2 (Nrf2) remains bound to kelch-like ECH-associated protein 1 (Keap1), where it is ubiquitinated and degraded by the proteosome. Upon sensing ROS and electrophiles, Keap1 releases Nrf2 to be translocated to the nucleus. Here, Nrf2 binds to antioxidant response elements (ARE) to initiate the transcription of antioxidant and detoxifying genes.[137]

Nrf2 is increased in the brains of CJD patients, indicating that this cellular stress pathway is increased to combat prion pathogenesis.[135] Nrf2 knockout animals undergo neurodegeneration, accompanied by increased cytokines and astrogliosis, indicating this pathway as a key regulator in maintaining neuronal health.[111]

The Keap1-Nrf2 and NF-κB pathways negatively regulate one another through multiple mechanisms. The Nrf2 target gene heme oxygenase-1 (HO-1), which is upregulated in prion mouse models, negatively regulates NF-κB-mediated transcription of adhesion molecules. Keap1 is a negative regulator of IKKβ, inducing stabilization of IκBα, and effectively preventing NF-κB translocation. The p65 subunit of NF-κB has multiple mechanisms to negatively regulate ARE-mediated gene expression (Figure 1.4). The autophagy protein, p62, is an Nrf2 target gene and is important in regulating the fine balance between Keap1-Nrf2 and NF-κB pathways,[111] and will be described in the next section.

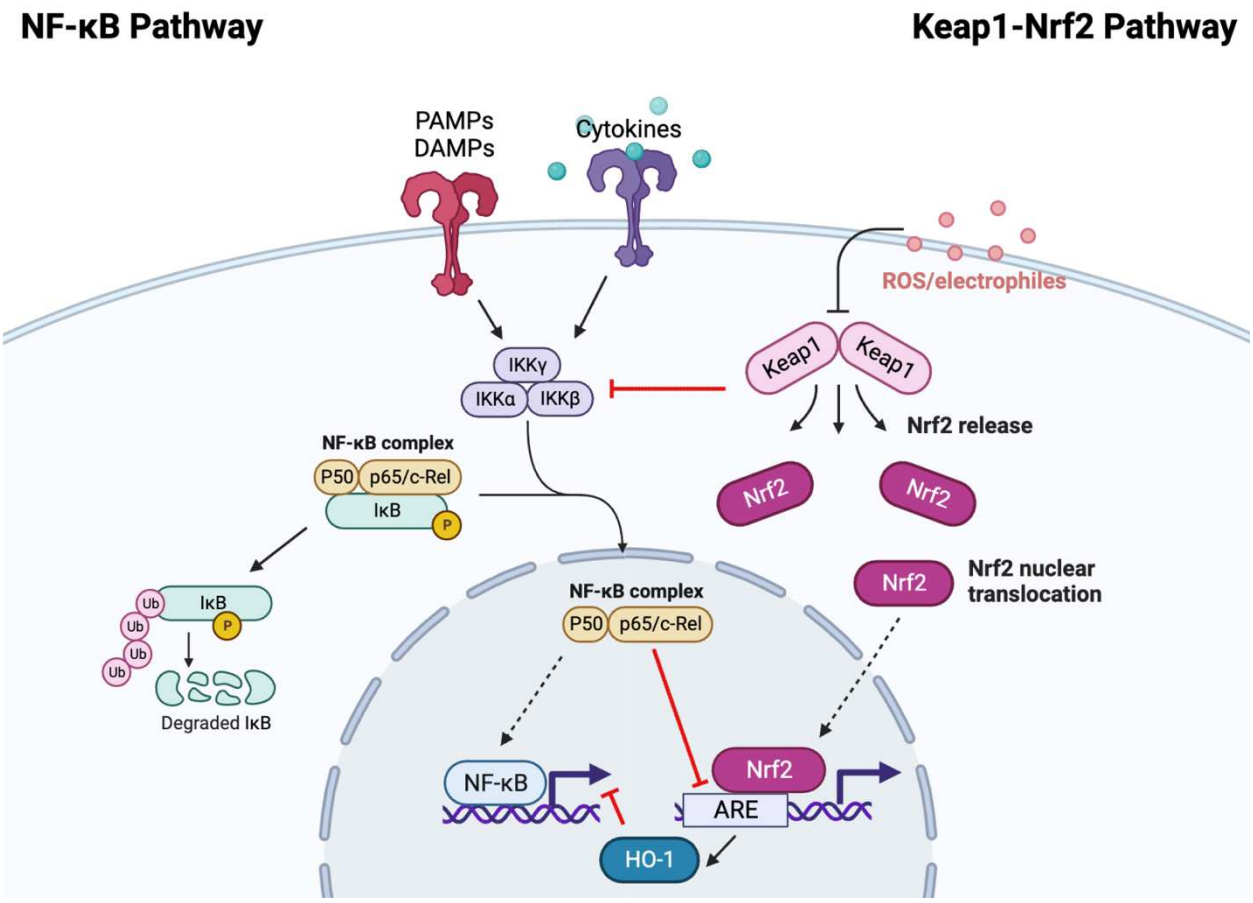

Figure 1.4. The NF-κB and Keap1-Nrf2 pathway negatively regulate one another. Graphic created with BioRender.com.

Clearance of protein aggregates

Cells have multiple pathways in place for responding to misfolded proteins. However, the number of normal cell processes that are dysregulated by the accumulation of misfolded PrP is perverse and often baffling. This is likely due to the sheer volume of misfolded proteins, and the structurally favorable β-sheet-rich PrP^{Sc}, which is highly resistant to degradation. The ubiquitin-proteosome system (UPS) is responsible for polyubiquitinating redundant or misfolded proteins, leading to their degradation by the 20S proteosome. Ultimately, PrP^{Sc} aggregates stabilize the closed conformation of the substrate entry channel of the proteosome, preventing its function and

leading to an increase of detectable proteosome substrates in the brain, such as p27, p53 and IκBα.[138,139]

A key protein that is a regulator between the NF-κB pathway, Keap1/Nrf2 pathway, the UPS, apoptosis and autophagy is p62. This is a scaffold protein that modulates enzyme function, and contains binding regions for several different proteins, including LC3, Keap1, ubiquitin, TRAF6 and RIP1 (involved in NF-κB signaling), and others.[140,141] Interestingly, p62 itself is an Nrf2 target gene. After translation it undergoes various modifications, and its phosphorylated form binds ubiquitinated cargo, such as protein aggregates. It is then phosphorylated by mTORC1, which allows it to competitively bind to Keap1, initiating its release from Nrf2 and allowing transcription of Nrf2 target genes (such as p62). The p62-Keap1-ubiquitinated cargo complex is then degraded by the autophagosome (Figure 1.5). Of note, phosphorylated p62 can also competitively bind Keap1 in the absence of ubiquitinated cargo, making this protein a strong initiator of Nrf2 and oxidative stress response.[141]

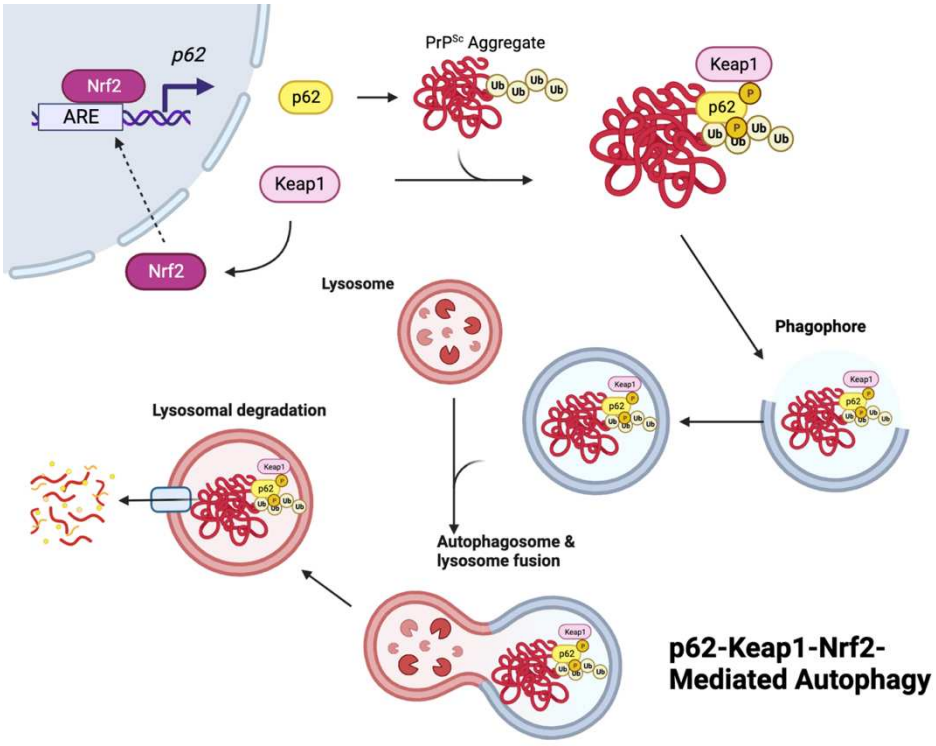

Figure 1.5. p62-Keap1-Nrf2-mediated autophagy. Graphic created with BioRender.com.

Selective autophagy requires the sequestering function of p62. Protein aggregates bind to chaperone proteins and are ubiquitinated by UPS proteins. The ubiquitinated aggregates become bound to and surrounded by p62, which forms dimers and oligomers. LC3II is recruited, which binds to and surrounds p62 to form an autophagosome. This then fuses with the lysosome, which undergoes acidification to degrade proteins. Two major indicators of autophagy function are LC3II, and p62, as fluctuations or buildup in these proteins may suggest that autophagy is dyregulated.[140] Analysis of prion-infected cell lines show that PrP^{Sc} aggregates undergo ubiquitination and p62-LC3II-mediated autophagy. However, both LC3II and p62 accumulation are seen in animal models of prion disease, suggesting that this pathway is not functioning to its full capacity.[142]

Newly synthesized PrP aggregates are trafficked from the endoplasmic reticulum (ER) to the lysosome via the autophagy pathway.[143] However, at some point during prion disease, autophagy can become impaired. Treating a mouse model of GSS with rapamycin, an autophagy-inducing drug, increased survival, improved motor function, and decreased PrP^{Sc} aggregation. Interestingly, apoptosis was increased via rapamycin-induced autophagy in these mice, but it was specific to astrocytes, not neurons.[144] Together, these data highlight an important role for autophagy in misfolded protein clearance in prion disease, and suggest that impairment occurs in this pathway during the natural course of disease and contributes to neurodegeneration.

As mentioned previously, autophagy both regulates and is regulated by the NF-κB pathway and apoptosis. Not only is p62 upregulated by Nrf2, but it is also upregulated by NF-κB.[145] Stress signals that activate the IKK complex, important for NF-κB activation, can initiate

autophagy even in the absence of downstream NF-κB signaling, and knockout of IKK actually leads to impaired autophagy.[114]

Autophagy is also important for clearance of damaged organelles within the cell. A significant portion of ROS are derived from mitochondria, which are highly affected by prion disease and other neurological disorders. $PrP_{106-126}$ has been shown to cause rapid mitochondrial depolarization in immortalized human neuronal cells, resulting in increased caspase activation and downstream apoptosis.[135] This peptide has recently been shown to impair selective autophagy of mitochondria (mitophagy) in infected cell lines[146]. Although this pathway has only begun to be investigated in prion disease, PINK1/Parkin mediated mitophagy is well characterized in other neurodegenerative diseases, and even viral infection[147,148]. Ultimately, stress resulting from PrP^{Sc} accumulation in the cell leads to increased production of ROS and decreased production of ATP by the mitochondria, and mitophagy of damaged mitochondria is important for regulating oxidative stress.

The unfolded protein response

Inability to remove PrP^{Sc} via the UPS leads to changes in translation of proteins induced by the unfolded protein response (UPR). This pathway halts translation by the endoplasmic reticulum (ER) to prevent further proteins from entering into the system. Although there are multiple pathways within the UPR, here we will review the PERK-eIF2α pathway, as this has implications in prion disease. PERK is a protein located on the membrane of the ER where, in a healthy cell, it is bound to the chaperone BiP. BiP is recruited away from PERK to misfolded proteins such as PrP^{Sc}. As BiP attempts (unsuccessfully) to retain the native conformation of PrP^{Sc}, PERK dimerizes with a second PERK protein, and both become phosphorylated.

Phosphor-PERK (p-PERK) acts as a kinase to phosphorylate eIF2α (p-eIF2α), which attenuates synthesis of proteins by preventing the initial step of translation. This is a temporary mechanism, as protein synthesis is critical for cell survival. Therefore, p-eIF2α also induces the protein ATF4, which induces the expression of CHOP, which induces GADD34 expression, and can initiate apoptosis. GADD34 dephosphorylates p-eIF2α to re-initiate translation (Figure 1.6).[149]

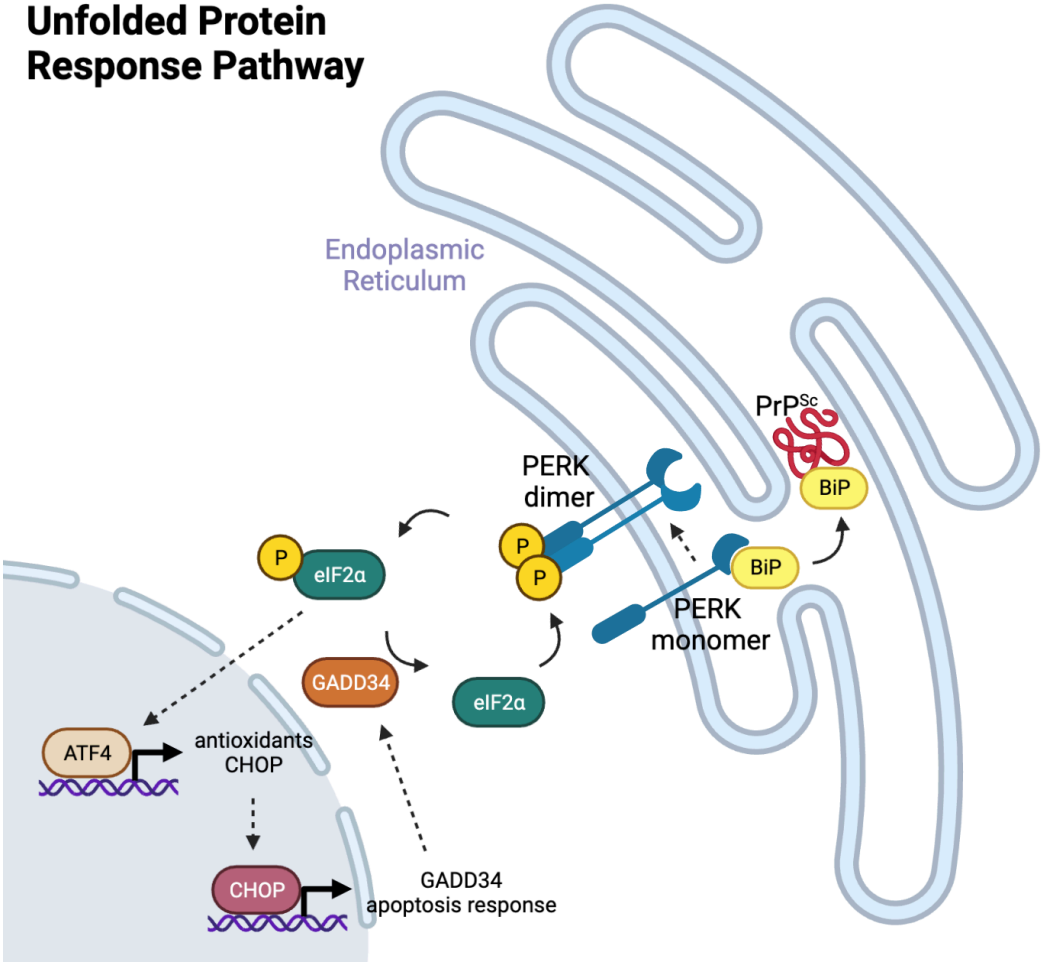

Figure 1.6. The unfolded protein response pathway. Graphic created with BioRender.com.

The UPR is highly dysregulated in prion disease. Both p-PERK and p-eIF2α are increased in the brains of prion-infected animals, as are levels of ATF4 and CHOP, but this is not associated with any changes in GADD34. Global translation rates, however, are decreased, and

changes in markers of the UPR coincide with synaptic dysfunction, clinical signs and neuronal death. Together, these data suggest that the PERK- eIF2α UPR pathway is being turned on around the time of clinical manifestations of prion disease and is not being turned off. Pharmacological intervention to prevent eIF2α phosphorylation, or initiate its dephosphorylation, were able to circumvent neuronal death.[150,151]

Interestingly, different cell types have different UPR responses in prion disease. In neurons, there is an increase in p-PERK, but it is not associated with downstream p-eIF2α or paused translation.[152] Astrocytes, however, appear to be culpable for UPR dysfunction leading to neuronal cell death. UPR-reactive astrocytes have significant changes in their secretome, increased expression of C3 and LCN2, and fail to promote synaptogenesis in neurons. Introduction of astrocyte-specific GADD34 increases survival time and improves neuronal health in prion infected mice.[64]

The lysosome itself and the endolysosomal pathway are additional sources of dysfunction, and the UPR may exacerbate this further. Impairment of the lysosome has also been cited in prion disease,[153] and may account for the development of vacuoles in the brain. Attempts to degrade prions in the endolysosomal pathway are impaired by prion-induced degradation of PIKfyve, a kinase critical for the maturation of the endolysosome. Degradation of PIKfyve can occur through UPR impairment, as pharmacological targeting of this pathway[151] lead to an increase in PIKfyve. Overexpression of proteins that support PIKfyve function restores lysosomal function and prevents vacuolization. The leading hypothesis is that a sustained UPR leads to downstream PIKfyve degradation and associated impaired endolysosomal maturation. Instead of developing functional lysosomes, vacuoles form, and, in neurons, this leads to synaptic dysfunction, introducing yet another potential source of neurotoxicity.[5]

Apoptosis

Ultimately, too much cellular damage and inability to clear misfolded proteins may leads to cell death, although as described earlier, the exact cause of cell death, particularly in neurons, is poorly understood and may include many contributing factors. In fact, it is not evident what type of cell death is occurring in prion-infected neurons. Initially it was assumed that it was apoptosis,[96] but this was prior to the discovery of multiple forms of programmed cell death, such as pyroptosis and even ferroptosis. Observations of cell death in animal models can be inconclusive,[150] and some forms of cell death have yet to be explored. For example, due to the controversial role of NLRP3 signaling in prion disease, pyroptosis is not (currently) known to be a contributor to cell death. Here, I will briefly describe the apoptotic pathway, as this seems to be assumed as the major pathway prion-infected neurons undergo.

Extrinsic signaling through TNF receptor 1 (TNFR1), TLRs and death receptors can trigger apoptosis, which activate caspase 8, which activates caspase 3/7 and leads to apoptosis. TNFR1 and TLRs likewise can activate the NF-κB pathway, which produces anti-apoptotic and cell survival signals, allowing for tight regulation of this pathway. Intrinsic stress signals are sensed by the mitochondria and trigger the oligomerization of the proteins Bax and Bak. The Bax/Bak dimer form pores on the membrane of the mitochondria and allow the release of cytochrome c. Cytochrome c induces the formation of the apoptosome, which activates caspase 9, which in turn activates caspase 3/7, leading to apoptosis. There are many proteins that can inhibit steps in this pathway, the best-known example being Bcl2, which is upregulated by NF-κB and inhibits the Bax/Bak complex.[154,155] For research purposes, common markers of apoptosis are caspase 3/7, which is upstream of apoptosis, and the loss of plasma membrane

integrity, an early stage of apoptosis, and finally release of cellular DNA, indicative of the end stages of cell death.[156]

Available treatments for human prion diseases

As the title of this dissertation implies, I want to convince you that (despite all the many cellular pathways implicated in prion disease) glial inflammation, particularly involving the NF-κB pathway, is poorly studied and a promising therapeutic target. Now, I will discuss some of the failed therapeutics before we get into the good stuff.

To sum up this section and save you some time, there are no available treatments for human – or any other – prion diseases. All attempts to treat prion diseases to this day have been unsuccessful, and these diseases remain 100% fatal to both humans and animals alike. Currently, people diagnosed with CJD and other prion diseases are given drugs to treat dementia, and antidepressants and sedatives to treat the psychological symptoms.[157]

Current anti-prion pharmacological interventions either stabilize specific conformations of PrP^{C}, non-specifically stabilizing PrP^{C}, or preventing PrP^{Sc} aggregation. Developing a successful drug for prion disease requires it to have one of the listed functions, but also be non-toxic, not interact with other proteins, have good bioavailability and be able to cross the blood brain barrier (BBB). Of the compounds used to treat prion disease in animal models, few have met these criteria to make it into clinical trials.

Anle138b is a compound that shows efficacy against both PrP^{Sc} and α-synuclein (which aggregates in Parkinson's disease) in animal models. Anle138b recently underwent Phase 1 trials in healthy individuals and was found to be non-toxic, and may be considered to treat Parkinson's and perhaps prion disease.[157] However, assessment of this drug in mouse models of genetic prion

disease was inconclusive, as even the control animal models did not develop disease.[158] The dearth of sufficient animal models for prion disease introduces yet another difficulty in developing therapeutics.

A classic example of a failed therapeutic is IND24 and similar compounds developed in Stanley Prusiner's lab. These compounds were able to extend the lives of scrapie-infected mice from ~120 days to over 450 days. However, this was dependent on the strain of scrapie used, as some strains showed few changes after drug treatment in infected cell culture models. Histological analysis revealed decreased astrogliosis, and unique patterns of PrP^{Sc} deposits in different brain regions, depending on the compound used. The disappointment arose when these compounds were tested in humanized mice infected with CJD and no extension of survival was observed,[159] preventing any further translational studies with these compounds.

Strain differences present a difficulty in developing PrP-targeting therapies for prion diseases, as the same, or very similar, amino acid sequences in the prion protein can present with different PrP^{Sc} structures, tissue tropism, and even behavioral and clinical symptoms.[31-33] However, many cellular pathways are similarly dysregulated in animal models, regardless of the prion strain. For example, a thorough profiling of three mouse-adapted scrapie strains identified predominant PrP^{Sc} in different cell types, and detection of PrP^{Sc} aggregates at different timepoints in different brain regions. Despite this, all three strains showed comparable increase in astrocyte and microglial numbers throughout the course of disease, in addition to similar upregulation of inflammatory cytokines and chemokines.[48] Together, these data suggest that although targeting of PrP^{Sc} accumulation may need to be strain specific, inflammatory pathways are more universal and may provide a larger target for treatment of prion diseases.

Some FDA-approved non-steroidal anti-inflammatory drugs (NSAIDs) have been assessed in prion-infected cell or mouse models. Celecoxib, a COX2 inhibitor, was able to prevent prion-induced microglia activation and release of COX2, PGE2 and nitric oxide. A derivative of this drug that is used for cancer treatment, AR-12, was shown to decrease PrP^{Sc} accumulation in cell culture models and promote autophagy. Imatinib showed similar effects as AR-12, but when it was put into a mouse model it was unable to effectively cross the BBB.[157] The drug GSK2606414, which selectively inhibits PERK in the UPR pathway, is effective in preventing neuronal loss and clinical signs in animal models, but unfortunately shows toxicity to the pancreas.[151]

The antimalarial drug quinacrine is able to cross the BBB, and made it to phase 2 clinical trials in CJD patients, before it was discontinued for inducing liver dysfunction. Notably, there is evidence that prions develop drug resistance, which has been observed with quinacrine. Another drug that made it into clinical trials was FLU, an NMDA receptor antagonist that showed promise in decreasing excitotoxicity and dendritic degradation in neurons. Although this drug was sufficient in crossing the BBB and well tolerated by patients, it had no effect in CJD patients. The antibiotic doxycycline was also shown to be effective in cell and animal models in decreasing PrP^{Sc}, but showed no efficacy when introduced into patients. Recently, the anti-PrP^{C} monoclonal antibody PRN100 was put into clinical trial in 6 CJD patients. This drug was well tolerated and able to penetrate the BBB, but the sample size was too small to determine its efficacy.[157]

Targeting oxidative stress may be beneficial for prion disease. Cannabidiol (CBD), a non-psychoactive drug derived from *Cannabis*, showed inhibition of PrP^{Sc} accumulation in mouse and sheep, although through an unknown mechanism, as it does not affect trafficking or pre-

existing deposits of PrP^{Sc}.[157] Our laboratory has demonstrated the ability of CBD to increase uptake of ROS and prevent protein aggregation in a *C. elegans* model of Alzheimer's disease by acting upon the Nrf2 pathway (Skn-1 in *C. elegans*) (unpublished work). It is possible that CBD could alleviate prion disease through a similar mechanism. Cell culture models have also shown that curcumin, derived from turmeric, effectively decreases ROS and promotes autophagy.[157]

Treatments with anti-inflammatories such as prednisone acetate has been shown to be beneficial in mice inoculated intraperitoneally with scrapie, and extended survival by more than 200 days, but was ineffective in mice inoculated intracranially. Treatment with ibuprofen in mice had severe side effects.[79] Together, these data present a need for a safe, effective treatment that can cross the BBB.

Both the JAK-STAT and NF-κB pathways are activated in prion-infected mouse models, and over 50% of the proinflammatory genes that are upregulated are NF-κB-related.[79] Therefore, targeting this pathway may be a promising avenue for developing therapeutics. Knockout of individual inflammatory genes such as *TNFα* and *IL6*, and receptors such as *CCR2* and *CCR5* have not affected prion pathogenesis, and knockout of *CCL2* and *IL10* have had conflicting results, by both extending or shortening survival time, depending on the animal model used.[79] Together, these data suggest that removal of a single protein may be less effective than targeting an entire pathway.

However, as I have hopefully conveyed to you, many of the cellular pathways that are implicated in prion disease are intertwined with one another. For example, inhibiting a pathway such as NF-κB will likely have many downstream effects on other pathways such as autophagy and oxidative stress. This leads nicely into the next – and final – section of this literature review.

Mesenchymal stromal cells

The unique anti-inflammatory and glial-modulating properties of mesenchymal stromal cells highlight them as a therapeutic avenue for prion diseases. This treatment modality is able to modulate multiple pathways and mechanisms of pathogenesis. These cells do not inhibit one specific protein or pathway in the brain, but instead respond to their environment by secreting immunological modulators that have been known to act on a variety of pathways implicated in inflammation. These include NF-κB, NLRP3 signaling, and Nrf2 signaling, as well as adapting the phenotypes of specific cells that contribute to this inflammation, namely microglia and astrocytes.[123,160-164]

Mesenchymal stromal cells (MSCs), formally known as mesenchymal stem cells, were first described by Friedenstein et al. in 1974 when they were identified in bone marrow.[165] Since then, their popularity in regenerative medicine has skyrocketed. MSCs are adult multipotent stem cells that are most commonly derived from bone marrow, compact bone, adipose tissue and the umbilical cord.[160,166] These cells can differentiate into a variety of cell types, including adipocytes, chondrocytes and osteocytes,[167] but have also been reported to differentiate into neurons and astrocytes.[166,168] MSCs demonstrate potent migratory ability when delivered intranasally, intravenously, or intracranially into animal models, as they contain a variety of chemokine receptors that initiate chemotactic migration toward lesions and sites of increased inflammation.[169-172] Through paracrine signaling and the release of extracellular vesicles, MSCs secrete anti-inflammatory cytokines and chemokines, growth factors, and microRNAs (miRNAs). These cells are particularly appealing for diseases of the CNS, as they are able to regulate inflammation in glial cells through paracrine signaling of immune modulators. They produce growth factors that promote myelination, axon repair and neurogenesis, and produce

miRNAs and proteins such as Bcl2 that promote cell survival. MSCs have been used to treat spinal cord injury, cerebral ischemia, and a variety of neurodegenerative diseases.[166]

In protein-misfolding neurodegenerative diseases such as Parkinson's disease (PD) and Alzheimer's disease (AD), MSCs have demonstrated the ability to improve clinical and behavioral signs, decrease levels of TNFα and IL1β, and increase markers of M2 microglia in animal models.[166] Intriguingly, these cells can also reduce protein aggregates. MSCs increased IL4 production from microglia and promoted their clearance of amyloid-β (Aβ) in an AD model.[173] The secretome was isolated from MSCs that were exposed to AD mouse brain homogenates in vitro, and delivered intranasally into this mouse model, showing improved memory, and decreased gliosis and Aβ.[174] Multiple studies with MSCs have been shown their ability to polarize microglia and astrocytes to an M2 and A2 phenotype, respectively. MSCs have been implicated in improved autophagy, decreased ROS, and have even been shown to deliver healthy mitochondria to rescue dying neurons in AD models. Multiple clinical trials are currently recruiting to test the benefits of these cells in early stages of AD, including one in China in which patients are inhaling exosomes from adipose-derived MSCs (AdMSCs).[168]

In PD models, MSCs have demonstrated the ability to regulate autophagy, cleave and inhibit the spread of α-synuclein, decrease neuronal loss, and of course modulate inflammation.[175,176] In fact, bone marrow-derived MSCs have been stereotaxically transplanted into the sublateral ventricular zone of seven PD patients, three of whom showed great improvement and had no negative side effects or tumor formation.[176]

It should be noted that many treatments that have shown benefits for AD and PD have not been successful in prion disease. The use of MSCs for treatment in prion disease has only begun to be investigated. Work from the Horiuchi lab has set a foundation for MSCs in prion disease.

They initially investigated immortalized human MSCs derived from bone marrow that stably expressed the marker β-galactosidase. These cells were transplanted stereotaxically into the left hippocampus of scrapie-infected mice at 120 dpi. By staining for β-galactosidase, they found these cells still present in the brain 3 weeks post-transplantation, many of which had migrated to the right hippocampus, where their location correlated with prion deposition. They also assessed intravenous delivery of these cells, and found the cells had infiltrated the cortex, hippocampus, thalamus and cerebellum. MSCs extended survival time and expressed the growth factors VEGF and BDNF, and the neurotrophic factor NT3, and even demonstrated the ability to differentiate into astrocytes and neurons.[177] These promising results initiated further investigation. MSCs derived from compact bone were isolated from the tibia and femur of mice and transplanted through stereotaxic injection into the hippocampus of prion-infected mice at 120 dpi. These cells were shown to modestly extend survival, and although they did not demonstrate changes in vacuolization or PrP^{Sc}, they did increase microglial numbers in the hippocampus at 3 weeks post-transplantation. Hippocampal mRNA demonstrated an increase in *IL1β*, *TNFα*, and *CD68*, a microglial marker of phagocytic activity. They also saw increased expression of *CD206*, *Ym-1*, *Retnla* and *IL10*, markers of homeostatic microglia. They did not see any changes in nerve growth factor or BDNF.[160] Together, these studies suggest that both source and delivery method of MSCs have a significant impact on the pathological outcomes, but that MSCs demonstrate promise in modulating glial inflammation that may be beneficial for survival in prion disease.

Our laboratory is working toward optimizing the use of MSCs as a treatment for prion diseases. We are utilizing AdMSCs, which demonstrate an increased production of anti-inflammatory molecules and growth factors compared to MSCs derived from bone marrow.[166] Moreover, these cells have increased therapeutic potential, as they can be excised from patients

through a minimally invasive lipectomy,[178] compared to isolation from bone marrow, or compact bone which requires the removal of entire bones.[160] Additionally, delivery of autologous cells will eliminate some threat of rejection by the immune system. Finally, we are employing the method of intranasal delivery, as this is much less invasive than stereotaxic injection. The following two chapters detail our findings in an in vitro and *in vivo* model of prion disease.

Chapter 2:

Adipose-Derived Mesenchymal Stromal Cells Decrease Prion-Induced Glial Inflammation In Vitro

Published in Scientific Reports, December 2022

Summary

Prion diseases are characterized by the cellular prion protein, PrP^{C}, misfolding and aggregating into the infectious prion protein, PrP^{Sc}, which leads to neurodegeneration and death. An early sign of disease is inflammation in the brain and the shift of resting glial cells to reactive astrocytes and activated microglia. Few therapeutics target this stage of disease. Mesenchymal stromal cells produce anti-inflammatory molecules when exposed to inflammatory signals and damaged tissue. Here, we show that adipose-derived mesenchymal stromal cells (AdMSCs) migrate toward prion-infected brain homogenate and produce the anti-inflammatory molecules transforming growth factor β (TGFβ) and tumor necrosis factor-stimulated gene 6 (TSG-6). In an in vitro model of prion exposure of both primary mixed glia and BV2 microglial cell line, co-culturing with AdMSCs led to a significant decrease in inflammatory cytokine mRNA and markers of reactive astrocytes and activated microglia. This protection against in vitro prion-associated inflammatory responses is independent of PrP^{Sc} replication. These data support a role for AdMSCs as a beneficial therapeutic for decreasing the early onset of glial inflammation and reprogramming glial cells to a protective phenotype.

Introduction

Prion diseases are rare protein-misfolding neurodegenerative diseases (PMNDs) that can be genetic, sporadic, or acquired through infection. This family of diseases result from the native conformation of the cellular prion protein (PrP^{C}) misfolding to the infectious form, denoted PrP-scrapie (PrP^{Sc}) [22,179]. PrP^{C} is expressed ubiquitously in tissue, but is highly expressed in neurons [180]. Once PrP^{C} changes conformation to the beta-sheet rich PrP^{Sc}, the protein has the propensity to form amyloid fibrils and aggregates, which disrupt homeostasis in the brain [1,181,182].

An early sign of disease is neuroinflammation caused by reactive astrocytes and the activation of microglia. This is due to the accumulation of PrP^{Sc} and results in oxidative stress, disruption of neural signaling, and glial scarring [183]. The combination of these symptoms leads to cellular dysfunction of neurons, including synaptic dysfunction and the loss of synaptic proteins, which leads to neuronal death [5,38,72,150,184]. As there are limited sources of neurogenesis in the brain, this leads to irreversible neuronal loss and ultimately neurodegeneration. However, there is evidence that PrP^{Sc} itself is not neurotoxic [72,150,182], and that other cellular stress pathways, including the inflammation of glial cells, play a major role in disease pathogenesis [64,75,150]. Astrocytes function to promote homeostasis in the brain, including maintenance of the blood brain barrier, uptake of neurotransmitters, and response to infection [47,185]. It is well established that astrocyte numbers and inflammatory phenotypes increase in the prion-diseased brain, and that this is an early sign of infection, well before clinical signs appear [49,50,59,73,186]. Therefore, a critical window exists in the treatment of prion diseases and other PMNDs – the initial inflammation stage, prior to the irreversible loss of neurons.

Astrocytes communicate not only with neurons, but also with microglia, considered to be the resident macrophages of the brain. Together these cells respond to PrP^{Sc} aggregation by

producing proinflammatory cytokines and chemokines, as well as neurotoxic signals that can contribute to neuronal death. Both astrocytes and microglia can be infected by PrP^{Sc} and disseminate infectious prions to neurons [38,71]. Interestingly, significant transcriptional changes are seen in glial cells in the prion-infected brain, but few are seen in neurons [60], further demonstrating role of glia in disease pathogenesis.

Significant cross-talk occurs between microglia and astrocytes after insult to the brain. Further elucidating how these cells respond and interact with one another in the context of prion disease is critical to developing therapeutics to alleviate prion-induced neuroinflammation. Microglia show an increased capacity to phagocytose during prion disease and are able to clear PrP^{Sc} at early stages of disease, but this declines as disease progresses [80,90]. In addition, microglia respond to PrP^{Sc} accumulation by secreting tumor necrosis factor alpha (TNFα), interleukin 1 alpha (IL-1α) and complement component 1, subcomponent q (C1q), which induce the development of A1 astrocytes, marked by proteins such as S100β and the complement protein C3 [45,49,50]. Unlike resting astrocytes, which promote the formation of neuronal synapses, reactive A1 astrocytes are unable to maintain synapses and secrete unknown neurotoxic signals, resulting in the dysfunction and death of neurons [45]. Reactive astrocytes in turn further activate and induce an M1 phenotype in microglia through the secretion of pro-inflammatory cytokines such as CCL2 [51], resulting in increased cytokine production by microglia and migration to sites of inflammation [56]. The complete knock out of TNFα, IL-1α and C1q in mice has been shown to be sufficient in preventing A1 astrocyte development in prion infected mice, but these mice showed a significant decrease in survival time compared to wild-type (WT) mice [49]. This suggests that A1 astrocytes play a multifaceted role in prion disease through their production of inflammatory cytokines and clearance of infected neurons. Similarly, decreasing microglia midpoint in disease

may be beneficial in extending survival and decreasing inflammation of prion-infected mice [75], but ablation of microglia during early-, mid- or late-disease increased astrogliosis and disease progression and decreased survival [50,91]. Together, these findings show that both activated microglia and reactive astrocytes are critical in curtailing disease, but that they can become detrimental to the host if left unchecked. Although further investigation is necessary to determine the time-point in disease that modulating gliosis would be beneficial, we propose that the ideal treatment for prion-induced inflammation is a reduction in A1 astrocytes and M1 microglia without eliminating these cells altogether.

A key to developing a successful therapy for prion disease is to use a multi-target approach to treat clinical signs and neuropathology. Here, we introduce a novel approach to decrease neuroinflammation in glial cells through the use of mesenchymal stromal cells (MSCs). MSCs can be derived from the bone marrow, umbilical cord, and adipose tissue, and can be expanded easily in culture [187]. Adipose-derived mesenchymal stromal cells (AdMSCs) can be taken from patients in a minimally invasive lipectomy to remove small amounts of adipose tissue [178]. AdMSCs have been shown both in vitro and *in vivo* to be able to secrete mediators such as anti-inflammatory cytokines and chemokines, neurotropic factors and growth factors in response to inflammatory conditions [171,188,189]. The capacity of AdMSCs to modulate inflammation in a paracrine manner has been well established in a variety of neurological disorders [188,189], including mouse models of PMNDs such as Alzheimer's and Parkinson's diseases [190,191]. AdMSCs are recruited to sites of inflammation and injury through signaling mechanisms involving chemokines, cytokines and growth factors [172].

Currently there are only a few compounds that have been shown to reduce signs of prion disease in mouse models, many of which have been determined to have toxic effects in the brain or elsewhere [151,192-194].

AdMSCs are a suitable alternative, given their ability to adapt in response to the cytokine milieu in their environment, and migrate to regions with high cytokine gradients. Here, we demonstrate the capacity of AdMSC to regulate inflammatory signaling from glial cells with in vitro prion infection.

Materials and Methods

Animal care and ethics statement

Mice were euthanized by deeply anaesthetizing with isoflurane followed by decapitation. All mice were bred and maintained at Lab Animal Resources, accredited by the Association for Assessment and Accreditation of Lab Animal Care International, in accordance with protocols approved by the Institutional Animal Care and Use Committee at Colorado State University.

Brain homogenates

C57Bl/6 (Jackson Laboratory) mice were intracranially inoculated with 30ml of 1% 22L, Rocky Mountain Laboratories (RML), or normal brain homogenate (NBH). Mice were monitored for weight loss and clinical signs of prion disease and euthanized after showing signs of terminal illness. 20% brains homogenates in phosphate-buffered saline (PBS) were made using beads and a tissue homogenizer (Benchmark Bead Blaster 24) and stored at -80C. Brain homogenates were aliquoted and treated with UV light for 30 minutes to sterilized before being used for cell culture.

Isolating and maintaining AdMSCs

Female and male C57Bl/6 mice were euthanized and the abdominal adipose tissue was dissected, placed in HyClone Hank's Buffered Saline Solution containing 25% Trypsin (HyClone, 0.25%) and cut into small chunks. Adipose tissue was dissociated by incubating with a mixture of 200U/ml Dnase-I (Roche) and 400U/ml Stemxyme (Worthington Biochemical Corporation) in DMEM/F12 media (Caisson Labs) at 37C for 1 hour. The tissues were centrifuged at 4C for 5 minutes at 1000 x g to pellet stromal vascular fraction. The pellet was washed once with sterile phosphate-buffered saline (PBS) and centrifuged at 1000 x g. The pellet was resuspended in 1 ml of AdMSC media (low glucose DMEM containing L-glutamine and supplemented with essential and non-essential amino acids, 15% heat-inactivated FBS, and PSN). The AdMSC cell resuspension was filtered through a 40 mm cell strainer (Fisher) to remove any non-dissociated tissue. Cells were plated onto 10 cm dishes and grown in AdMSC media – low glucose DMEM containing L-glutamine (Cytiva) and supplemented with essential and non-essential amino acids (Gibco) containing 15% heat-inactivated fetal bovine serum (FBS) (Peak Serum) and 1% penicillin/streptomycin/neomycin (PSN) (Sigma). 72 hours later, cells were passaged at a 1:3 ratio and again every 3-4 days. For all experimentation, cells were used at passage 2 or 3.

Flow cytometry

AdMSCs at passage 3 were washed three times with sterile PBS. Cells were incubated with 3 ml of Cellstripper (Corning) for up to 15 minutes, tapping on plate every 5 minutes to dislodge cells. Cells were scraped and pooled then centrifuged for 5 mins at 1000 x g at 4C. Cells were resuspended in FACS buffer (1% hiFBS and 1mM EDTA in sterile PBS) and centrifuged at 1000 x g for an additional 3 minutes. The cell pellet was resuspended in FACS buffer and aliquoted

into 1.5ml tubes. The cells were incubated for 30 minutes on ice with following antibodies: Mouse IgG FITC (1:2000, Bio-Rad), CD34-FITC (1:1000, Bio-Rad), CD44-FITC (1:1000 or 1:1000, Bio-Rad), CD45-FITC (1:1000, Bio-Rad), CD73-FITC (1:2000, BioLegend), CD90-FITC (1:100, Abcam), CD105 (1:100, Bio-Rad, made in rat, with anti-rat 488 secondary, 1:500). Cells were centrifuged at 500 x g for 30 seconds on a tabletop centrifuge and washed three times with FACS buffer. On the final wash, cells were transferred into library tubes with 500 ml FACS buffer and placed on ice. Live/dead stain (Sytox AADvance, Invitrogen) was added at 1:100 dilution to all samples excluding reference controls. 10,000 live cells per sample were analyzed using the Cytek^{TM} 4-laser Aurora Cytometer and data was processed in FlowJo, gating on single cells, live cells, then FITC-positive and FITC-negative cells.

AdMSC Stimulation and Migration Assays

AdMSCs at passage 3 were plated at 100,000 cells/well in 6-well plates. The following day, cells were stimulated with either cytokines or brain homogenate. Cytokine-treated cells received media containing 10 ng/ml TNFα or 200 ng/ml IFNγ (R&D Systems) for 1, 4, 8, 12 or 24 hours, following RNA isolation. Cells treated with brain homogenate were treated with media containing 0.1% normal or 22L brain homogenate for the same time course before RNA isolation. Control cells received media only. AdMSCs at passage 2 were stimulated for 24 hours with media containing 10 ng/ml TNFα. Cells were washed and incubated in serum-free media for 4 hours. 1% RML or NBH were plated in serum-free media in a 24-well plate. 24-well inserts with a pore size of 8 micrometers (Greiner Bio-One) containing 25,000 serum-starved AdMSCs per insert were added to corresponding wells. Cells were incubated for 16 hours at 37C, washed, then a cotton swab was used to gently remove cells from the top chamber of the insert. Cells

were incubated for 1 hour in crystal violet solution (0.2% crystal violet, 11% formaldehyde, 2% ethanol, 2% paraformaldehyde in H2O) and washed thoroughly with PBS. Four random areas were selected from each insert and cells were imaged and counted with a 10x objective on an inverted microscope (Laxco) using SeBaView software.

Isolating and prion infection of mixed glia and BV2 cells

Zero to two-day old C57Bl/6 pups were euthanized and brains were extracted. Cerebellum was separated from cortex, meninges and midbrain were removed and discarded, and the brains were placed in MEM/EBSS containing 2x PSN on ice. Cortical tissue was used for mixed glial cultures [195,196]. Media was removed and replaced with prewarmed dissociation media (MEM/EBSS, 2x penicillin-streptomycin-neomycin (PSN) and 1.5U/ml Dispase (Gibco) and triturated with a Sigmacote (Sigma) coated glass pipet. The mixture was transferred to a beaker containing a stir bar and stirred gently for 10 minutes. Tissue was allowed to settle and supernatant was removed and transferred to a tube on ice. Dnase-I (4000U/ml, Roche) was added to dissociation media and tissue was resuspended and stirred for an additional 10 minutes. Extractions were repeated by adding fresh dissociation media (without Dnase-I) 2 to 4 additional times, depending on the amount of tissue, until only fibrous tissue remained in the bottom of the beaker. The tube containing cell supernatant was centrifuged for 10 minutes at 1000 x g at 4C, media was aspirated from cell pellet and replaced with glial growth medium (MEM/EBSS, 10% FBS and 1% PSN). Mixed glia were plated at 1,000,000 cells per 10 cm dish. 24 hours later, media was replaced. Media was changed weekly. Mixed glia and AdMSC cultures were plated at 100,000 cells per well in 6-well plates and infected with 0.1% normal or 22L brain homogenate once cells were 80-90% confluent. Media was removed 72 hours later and cells were washed

twice with PBS prior to fresh media being added. Media was changed weekly on infected cells. BV2 cells were maintained in High Glucose DMEM containing 10% FBS and 1% Pen-Strep and split weekly.

Immunofluorescence to characterize AdMSCs

Cells were fixed with cold 4% paraformaldehyde for 10 minutes and permeabilized with 0.1% Triton-X for 5 minutes, and incubated in blocked in PBS containing 10% normal goat or donkey serum for 1 hour at room temperature (RT). Antibodies in 5% serum were incubated at 4C overnight. AdMSC markers include Oct3/4 (1:100, Abcam) and vimentin (1:100, Sigma Aldrich); prion-specific antibodies include Bar224 (1:100, Cayman Chemicals) and Sha31 (Cayman Chemicals). Following the overnight incubation, cells were washed and incubated with 488- or 555-conjugated anti-rabbit, anti-mouse and anti-chicken secondary antibodies (1:500, Southern Biotech) were incubated in the dark at RT for 1 hour. Slides were incubated in Hoechst stain (ThermoFisher, 1:2000 dilution) for three minutes then mounted with ProLong Gold Antifade media (ThermoFisher) and cover slipped (Globe Scientific, #1).

Co-culture of prion-infected mixed glia and BV2 cells with AdMSCs

For RNA assays, mixed glia were plated in glial growth medium (MEM/EBSS, 10% fetal bovine serum (FBS) and PSN) on 6-well dishes at 100,000 cells per well. Once confluent, cells were treated with media containing 0.1% NBH or 22L brain homogenate. 72 hours later, media was removed, cells were washed twice with PBS, and fresh media was added. Four days later, media was changed to AdMSC media (low glucose DMEM containing L-glutamine and supplemented with essential and non-essential amino acids, 15% heat-inactivated FBS, and

PSN). 6-well inserts with a pore size of 0.4 micrometers (Greiner Bio-One) containing 100,000 AdMSCs per insert were added to corresponding wells. Co-cultures were grown for one week before inserts were removed and glial RNA was isolated. For immunofluorescence, mixed glia were seeded on 24-well plates containing glass coverslips at 5,000 cells per well. 72 hours later, cells were treated with media containing 0.1% NBH or 22L. Four days later, media was changed to AdMSC media. 24-well inserts with a pore size of 0.4 micrometers containing 10,000 AdMSCs-insert were added to corresponding wells. Co-cultures were grown for one or two weeks with a full media change every week before inserts were removed and glial RNA was isolated.

BV2 microglia were plated at 50,000 cells per well and infected 24 hours later with 0.1% NBH or RML. AdMSCs at passage 1 were stimulated 24-hours prior to co-culturing by treatment with media containing 10ng/ml TNFα for 24 hours. After 24 hours, media was removed, cells were washed three times with PBS, and stimulated AdMSCs were trypsinized and added to inserts above the infected glia at 6 dpi. BV2 cells were co-cultured with AdMSCs for 24 hours before RNA was isolated from the BV2 cells.

Semi-quantitative real time PCR analysis

RNA was extracted from cell culture 6cm dishes using cell scaping, QIAshredder and Rneasy extraction kits, in accordance with manufacturer's protocol, including a Dnase digestion step with the Rnase free Dnase kit (Qiagen, Valencia, CA). Purity and concentration were determined using a ND-1000 spectrophotometer (NanoDrop Technologies, Wilmington, DE). Following isolation and purification, 25ng of RNA was reverse transcribed using the iScript Reverse Transcriptase kit (BioRad, Hercules CA). The cDNA was amplified within 24 hours of reverse

transcription using iQ SYBR Green Supermix (BioRad, Hercules CA). The corresponding validated primer sequences were used for each gene at 10mM. The expression data was analyzed using the 2-ΔΔCT method normalized to *b-actin* or *GAPDH* expression and the fold difference was compared to control (normal brain homogenate treated) samples (10.1006/meth.2001.1262). Validated primer sequences are as follows:

(TSG-6) 5'- GCTACAACCCACATGCAAAGGA-3' (forward), 5'-CCGTACTTGAGCCGAATGTGC-3' (reverse); (TGFβ1) 5' – CTTCAATACGTCAGACATTCGGG – 3' (forward), 5' -GTAACGCCAGGAATTGTTGCT - 3' (reverse); (IL1β) 5' – GCAGCAGCACATCAACAAG – 3' (forward), 5' – CACGGGAAAGACACAGGTAG – 3' (reverse); (TNFα) 5'- CCGATGGGTTGTACCTTGTC – 3' (forward), 5'- AGATAGCAAATCGGCTGACG – 3' (reverse); (CCL2) 5'-TTAAAAACCTGGATCGGAACCAA – 3' (forward), 5'-GCATTAGCTTCAGATTTACGGGT – 3' (reverse); (CCL5) 5'-GCTGCTTTGCCTACCTCTCC – 3' (forward), 5' – TCGAGTGACAAACACGACTGC – 3' (reverse); (C3) 5'-GAGCGAAGAGACCATCGTACT – 3' (forward), 5' – TCTTTAGGAAGTCTTGCACAGTG – 3' (reverse); (S100β) 5' – CGAGAGGGTGACAAGCACAAG – 3' (forward), 5' – CTTCCTGCTCCTTGATTTCCTCCA – 3' (reverse); (TMEM119) 5' – TCACCCAGAGCTGGTTCCATA – 3' (forward), 5'-GAGTGACACAGAGTAGGCCA – 3' (reverse); (Arg-1) 5' – CGTAGACCCTGGGGAACACTAT – 3' (forward), 5' – ^{TCCATCACCTTGCCAATCCC} – 3' (reverse); (IL-6) 5' -CTGCAAGAGACTTCCATCCAG – 3' (forward), 5 ' – AGTGGTATAGACAGGTCTGTTGG – 3' (reverse); (CD16) 5' – TTTGGACACCCAGATGTTTCAG – 3' (forward), 5'- GTCTTCCTTGAGCACCTGGATC – 3' (reverse); (NLRP3) 5' – CCTGGGGGACTTTGGAATCA -3' (forward), 5'-

GACAACACGCGGATGTGAGA – 3’ (reverse); (β-actin) 5’- GCTGTGCTATGTTGCTCTAG – 3’ (forward), 5’ – CGCTCGTTGCCAATAGTG – 3’ (reverse);
(GAPDH) 5’ – AGGAGAGTGTTTCCTCGTCC – 3’ (forward), 5’ – CCGTTGAATTTGCCGTGAGT – 3’ (reverse).

Immunoblotting

Cell lysates were isolated using the protein lysis buffer (50mM Tris, 150mM NaCl, 2mM EDTA, 1mM MgCl2, 100mM NaF, 10% glycerol, 1% Triton X-100, 1% Na deoxycholate, 0.1% SDS and 125mM sucrose) supplemented with Phos-STOP and protease inhibitors (Roche). A BCA Protein Assay kit (Thermo Scientific) was used to quantify protein concentration of lysates, and 250 mg – 500mg protein was digested with 20 mg/ml proteinase K (PK) (Roche) for PrP^{Sc} blots for 1 hour at 37C. Digestion was terminated with X amount of PMSF and lysates were spun at 40,000 x g for 1 hour at 4C before being loaded on a gel. For PrP^{C} blots, 20 mg of samples were used. Samples were run using 4-20% acrylamide SDS page gels (BioRad) and then transferred onto PVDF blotting paper (MilliPore). Primary antibody Bar-224 (Cayman Chemical Company) was used at 1:1,000 dilution for PrP^{Sc} blots dilution and 1:5,000 dilution for PrP^{C} blots. HRP-conjugated secondary antibodies were used at a concentration of 1:5,000 (Vector Laboratories). For PrP^{C} blots, loading control GAPDH was ran at a 1:5,000 dilution (MilliPore), with HPR-conjugated secondary at 1:5,000 dilution (Southern Biotech). The protein antibody complex was visualized using SuperSignal West Pico PLUS Chemiluminescent Substrate (Thermo Scientific) and visualized with the BioRad ChemiDoc MP.

Scrapie Cell Assay

Protocol adapted from Bian et al. 2010 [197]. Primary glial cells at passage 1 were plated in 24-well plates at 25,000 cells/well and infected with 0.1% 22L or normal brain homogenate for 72 hours, as described above. 7 days post-infection they were co-cultured with 25,000 AdMSCs on passage 3, as described above. 7 days later, AdMSC inserts were removed and plates were trypsinized and 20,000 cells were transferred to each well of a 96-well ELISpot plate (Millipore). Liquid was removed from the plates via a bottom vacuum and plates were thoroughly dried at 50°C. Plates were treated with cell lysis buffer (50 mM Tris-HCl, 150mM NaCl, 0.5% IGEPAL-CA630, 0.5% Sodium Deoxycholate in H2O pH= 7.6) containing 5ug/ml PK (Sigma Aldrich) and incubated for 90 min at 37°C on a shaker. The digestion was terminated with 2mM phenylmethylsulphonyl fluoride (PMSF, Thermo Fisher) at room temperature incubation on a shaker for 20 minutes. The vacuum was applied and plates were incubated with 3M Guanidinium Thiocyanate (Research Products International) in 10mM Tris-HCl (Sigma) (pH 8.0) for exactly 10 min at room temperature on a shaker. Digestion was terminated with vacuum and application of 150 ml PBS to each well. Plates were washed thoroughly, then plate was blocked for 1 hour at room temperature with 5% Superblock (Pierce, Rockford, IL) on a shaker. The vacuum was applied and plates were incubated overnight at 4C with primary antibody, Sha31 (Cayman Chemical Company), diluted 1:5000 in TBST (Tris-Buffered Saline with Triton-X). Plates were washed with TBST and incubated for 1 hour at room temperature with secondary antibody, AP-α-Mouse IgG (Southern Biotechnology Associates, Birmingham, AL), diluted 1: 5000 in TBST. Plates were washed thoroughly and dried overnight. NBT/BCIP tablet (Roche) in ultrapure water was added to plates and incubated in the dark for 30 minutes. Plates were washed and dried overnight at 4C. Plates were scanned with a ImmunoSpot S6-V analyzer (Cellular Technology

Ltd, Shaker Heights, OH), and determined spot numbers using ImmunoSpot5 software (Cellular Technology Ltd, Shaker Heights, OH).

Enzyme-Linked Immunosorbent Assay

AdMSCs at passage 3 were treated with media containing 10 ng/ml TNFα for 24 hours. Media was then removed and cells were washed three times with PBS to remove any residual TNFα. 24 hours later, media was removed and an ELISA was used to identify TNFα in the media. ELISAs were performed as per manufacturer's instructions (R&D Biosystems).

Results

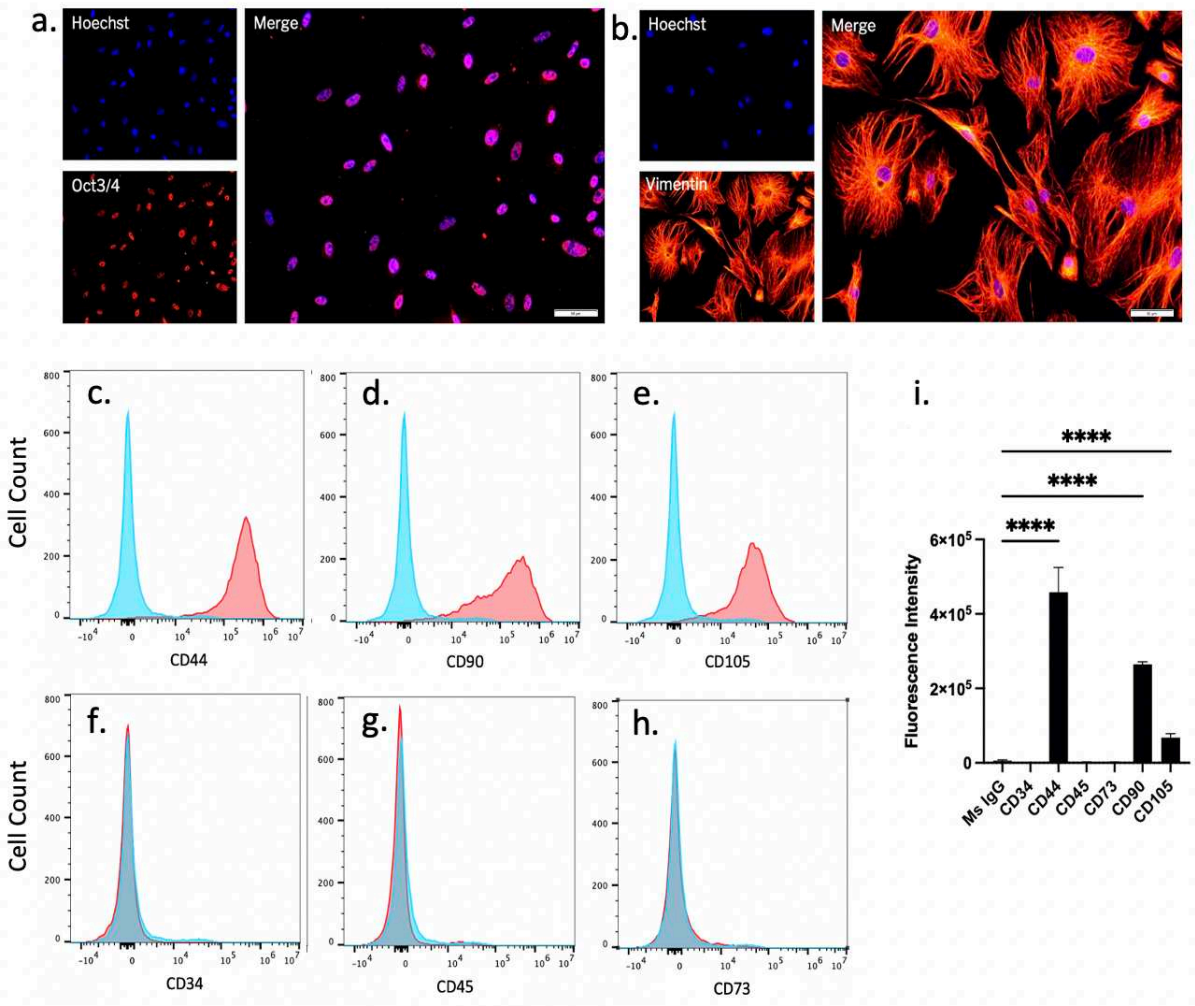

Figure 2.1. Characterization of adipose-derived mesenchymal stromal cells isolated from mouse visceral fat and expanded in culture. AdMSCs express the **(a)** undifferentiated cell marker Oct3/4 and **(b)** the structural protein Vimentin. AdMSCs express **(c)** CD44, **(d)** CD90 and © CD105 but not **(f)** CD34, **(g)** CD45 or **(h)** CD73 (red histograms) compared to IgG control (blue histograms). **(i)** Fluorescent intensities of AdMSC profile quantified in FlowJo. Scale bar = 50mm. Representative histograms from three biological replicates with 10,000 events each. Two-way ANOVA and post-hoc Tukey test, error bars = SEM, **** $p < 0.0001$

Characterization of adipose-derived mesenchymal stromal cells isolated from mouse visceral fat and expanded in culture

Adipose-derived mesenchymal stromal cells (AdMSCs) were isolated from the abdominal adipose tissue of C57Bl/6 mice and expanded to passage 3 before characterization. AdMSCs express the undifferentiated cell marker Oct3/4 and the structural marker Vimentin, as shown by immunofluorescence (Figure 2.1a). Consistent with adipose-derived mesenchymal stromal cells [198], these cells express membrane markers CD44 (97.1%), CD90 (74.2%) and stem cell marker CD105 (68.9%) and do not express hematopoietic stem cell markers CD34 (>0.1%) or CD45 (3.0%), nor do they express significant CD73 (2.1%), as shown by flow cytometry (Figure 2.1b and 2.1c). It should be noted that expression of markers was not uniform across all cells, suggesting that this is a heterologous population.

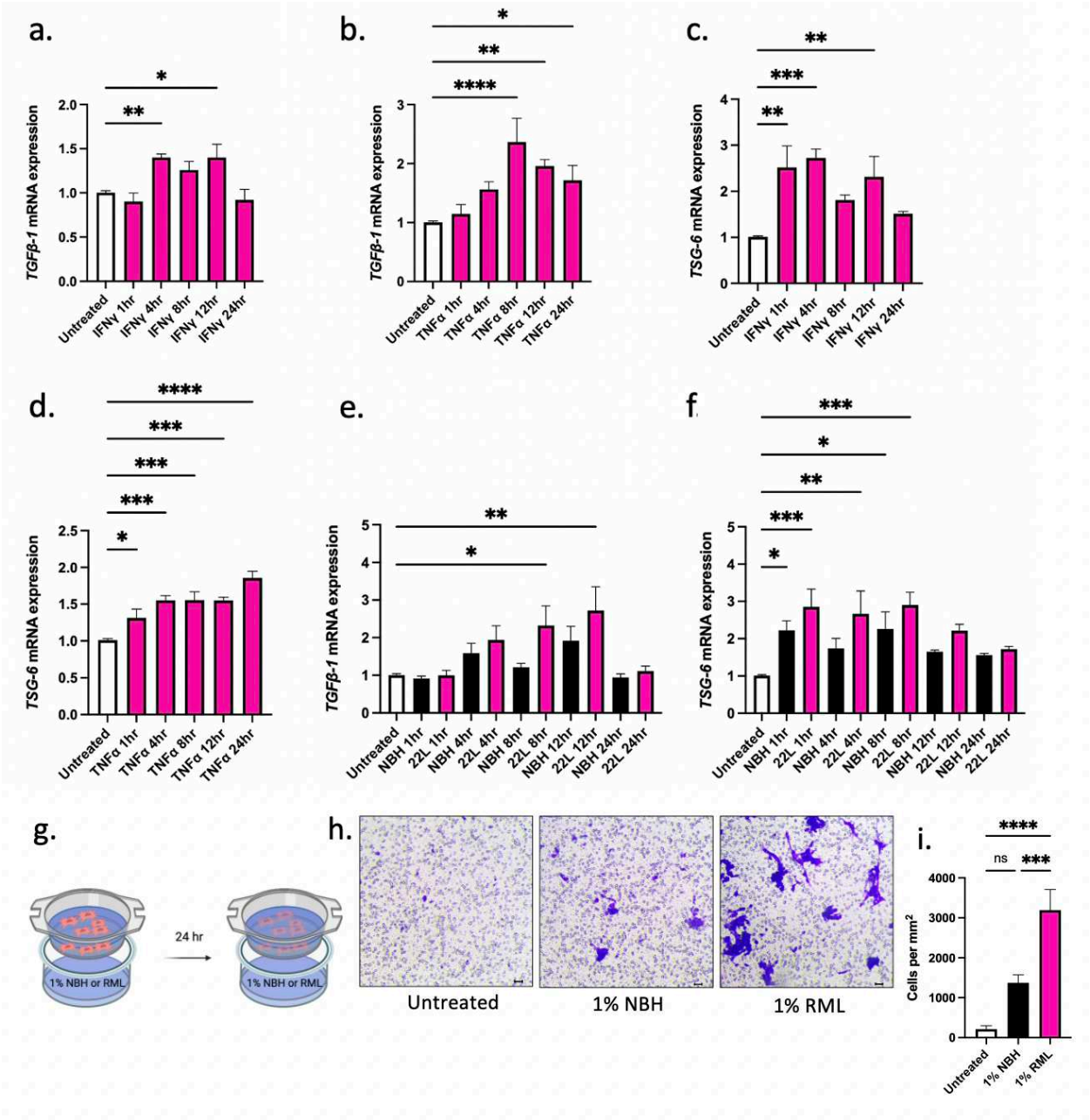

Figure 2.2. AdMSCs produce anti-inflammatory molecules in response to inflammatory cytokines and prion-infected brain homogenate. Exposing AdMSCs to IFN-γ or TNFα increases **(a, b)** *TGFβ-1* and **(c, d)** *TSG-6* mRNA. Exposing AdMSCs to 22L prion-infected but not normal brain homogenate (NBH) increases © *TGFβ-1*. Both NBH and 22L brain homogenate increase **(f)** *TSG-6* mRNA. Two biological replicates, each with three technical replicates, all analyses normalized to *b-actin*. **(g-i)** TNFα stimulated AdMSCs migrate toward RML prion brain homogenate after 24-hour exposure. Cell counts were taken from four randomly selected fields of view at 10x magnification. Scale bar = 10 μm. Three biological replicates each with three technical replicates. One-way ANOVA and post-hoc Tukey test, error bars = SEM, * $p < 0.05$, ** $p < 0.01$, *** $p < 0.001$, **** $p < 0.0001$, ns = not significant. Graphic created with BioRender.com

AdMSCs produce anti-inflammatory molecules in response to inflammatory cytokines and prion-infected brain homogenate

To stimulate the upregulation of anti-inflammatory genes, AdMSCs were treated with 10 ng/ml TNFα or 200 ng/ml IFNγ [199]. To determine if AdMSCs upregulate genes when exposed to the cytokine milieu of the prion-infected brain, AdMSCs were exposed to normal or 22L brain homogenates. Cytokines or brain homogenates were diluted in media and incubated for 1, 4, 8, 12 or 24 hours before RNA was collected.

AdMSCs increase expression of the anti-inflammatory cytokine *TGFβ-1* mRNA when exposed to the cytokines IFNγ and TNFα. Treatment with IFNγ triggered the production of *TGFβ-1* mRNA after 8 and 12 hours ($p<0.01$). Treatment with TNFα produced a maximum increase in *TGFβ-1* mRNA after 8 hours ($p<0.001$) and *TGFβ-1* mRNA was sustained at 12 and 24 hours ($p <0.01$). Additionally, mRNA for the secreted protein, tumor necrosis factor-stimulated gene 6 (TSG-6), was produced by AdMSCs when exposed to IFNγ and TNFα (Figure 2.2a-d). Treatment with IFNγ triggered the production of *TSG-6* mRNA after 1, 4 and 12 hours ($p <0.05$; $p <0.01$; $p <0.05$). A more dramatic increase in *TSG-6* mRNA was seen after treating AdMSCs with TNFα, which resulted in an increase after 4 hours ($p <0.001$) that was sustained until 24 hours ($p <0.0001$).

Treatment with brain homogenates from 22L-infected mice was sufficient to stimulate *TGFβ-1* mRNA production in AdMSCs after 8 hours ($p <0.05$). This increase was maintained at 12 hours ($p <0.01$), but at 24 hours had returned to baseline, showing no significant change in mRNA compared to untreated control cells (Figure 2.2e-f). *TSG-6* mRNA showed an increase in cells treated with 22L brain homogenates after only 1 hour ($p <0.01$), and this was sustained after 4 and 8 hours ($p<0.01$) before returning to baseline at 12 hours. For statistical analysis, two

biological replicates were used, each with three technical replicates. All analyses were normalized to *b-actin* mRNA expression. One-way ANOVA with post-hoc Tukey test were performed with a p value of 0.05.

It has been reported that pre-treating MSCs with TNFα can improve their ability to migrate to sites of inflammation [200,201]. The ability of AdMSCs to migrate to sites of prion-induced inflammation was assessed in vitro using a cell migration assay. AdMSCs were stimulated for 24 hours with TNFα and plated in inserts above media containing vehicle-only or 1% normal or RML-scrapie brain homogenate (Figure 2.2g). Cells were incubated for 24 hours and the cells on the upper side of the insert were removed. Cells on the bottom of the insert were stained and four randomly selected fields of view were imaged and counted at 10x magnification (Figure 2.2h). No statistical difference was seen in cell counts between cells exposed to vehicle (mean = 7.267) and NBH (mean = 65.18) ($p=0.0852$). Significantly more cells migrated toward RML brain homogenate (mean=146.6) compared to both vehicle ($p<0.0001$) and NBH ($p=0.0007$) (Figure 2.2i). The experiment was repeated with AdMSCs derived from three different animals, each using three inserts per treatment group. A One-way ANOVA with post-hoc Tukey test were performed with a p value of 0.05.

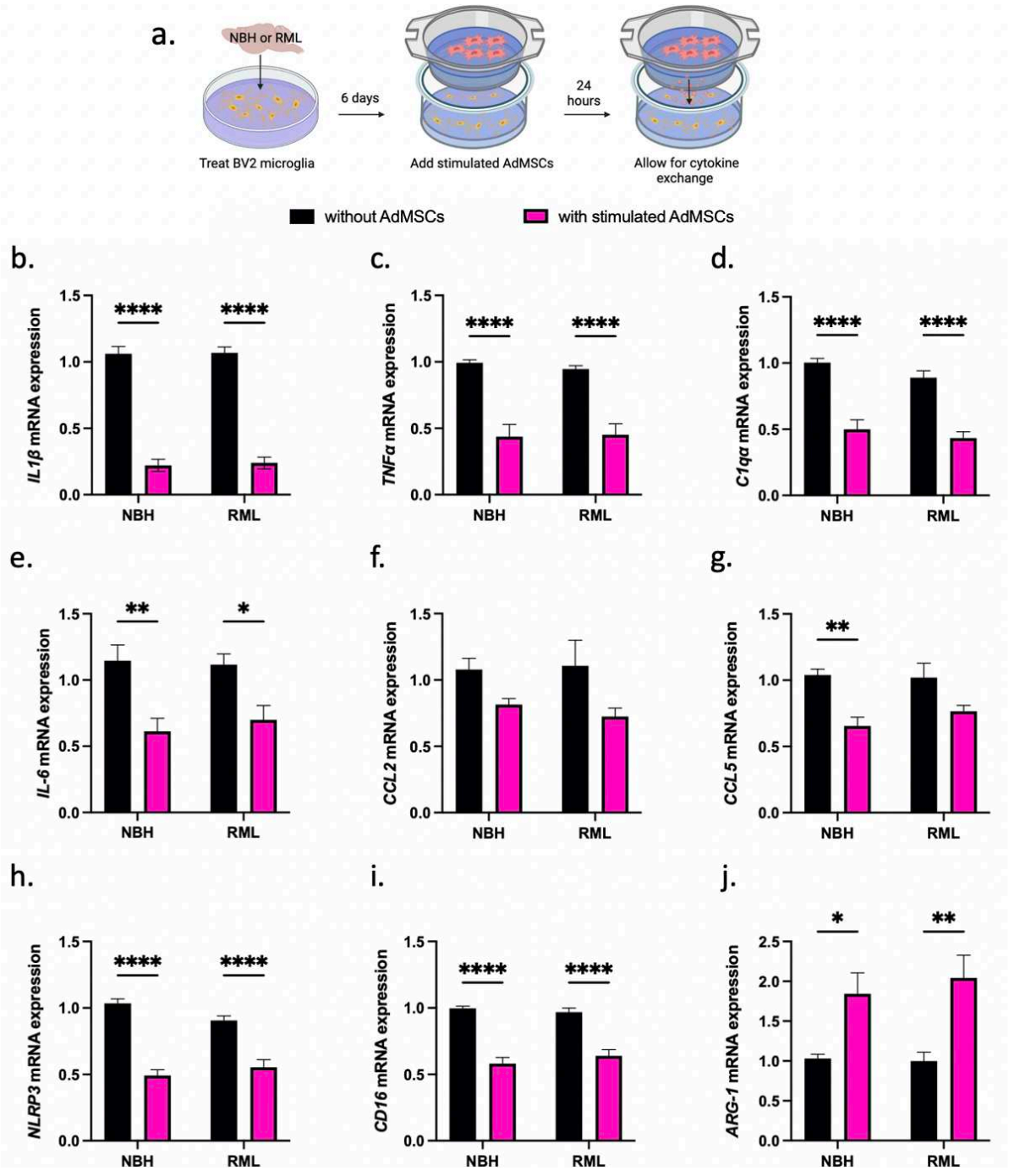

Figure 2.3. Stimulated AdMSCs decrease inflammatory phenotypes in BV2 microglia. (a) BV2 microglia were exposed to RML prion brain homogenate or normal brain homogenate (NBH) for 6 days, then co-cultured for 24 hours with TNFα-stimulated AdMSCs. This resulted in a decrease in inflammatory cytokines **(b)** IL1β, **(c)** TNFα, **(d)** C1qα, and © IL-6. No significant change was seen in **(f)** CCL2 and a decrease was seen only in the NBH treatment for **(g)** CCL5. A decrease was seen in mRNA for the **(h)** NLRP3 inflammasome and for M1 marker **(i)** CD16. An increase was seen for the M2 marker **(j)** Arg-1. Three biological replicates, with three technical replicates, all analyses normalized to *β-actin*. Two-way ANOVA and post-hoc Tukey test, error bars = SEM, *p < 0.05, ** p< 0.01, *** p< 0.001, **** p< 0.0001. Graphic created with BioRender.com.

Stimulated AdMSCs decrease inflammatory phenotypes in BV2 microglia

To determine whether AdMSCs influence microglia-derived inflammatory molecules and markers of polarized glia, the BV2 murine microglia cell line was utilized. BV2 cells were plated at 50,000 cells per well and treated the following day with 0.1% normal brain homogenate (NBH) or RML brain homogenate. We have demonstrated that stimulating AdMSCs with TNFα causes an increase in production of the anti-inflammatory genes *TGFb-1* and *TSG-6* (Figure 2.2b and d). Therefore, to increase the anti-inflammatory effects of AdMSCs, we pre-treated with 10 ng/ml TNFα for 24 hours prior to co-culturing with BV2 cells. At 6 dpi, BV2 cells were co-cultured with AdMSCs for 24 hours before media and RNA isolation from the BV2 cells (Figure 2.3a). It should be noted that after stimulation and washing with PBS, TNFα is not significantly detectable by ELISA in AdMSC media (Supplemental Figure 1), and therefore it can be concluded that none of the results are the effect of residual TNFα in the media.

AdMSCs induced a drastic decrease in markers of inflammation in BV2 cells. A significant decrease was seen in *IL1β* for both NBH-treated and RML-treated BV2 cells ($p<0.0001$) (Figure 2.3b). Intriguingly, mRNA for the genes *TNFα* and *C1qα* were decreased in both NBH-and RML-treated BV2 cells ($p<0.0001$) (Figure 2.3c and d). These genes are critical for microglia-derived molecules that polarize astrocytes to the A1 reactive phenotype [45]. Additionally, a significant decrease was seen in *IL-6* mRNA for both NBH-treated ($p=0.0044$) and RML-treated BV2 cells ($p=0.0337$) (Figure 2.3e). No significant decrease was seen in mRNA for the inflammatory cytokines *CCL2* in RML-treated BV2 cells co-cultured with AdMSCs (Figure 2.3f). A decrease was seen in *CCL5* mRNA, but was significant in the NBH-treated glia ($p = 0.0030$), and not the RML-treated glia ($p=0.0753$) (Figure 2.3g). A decrease was seen in mRNA for the NLRP3 inflammasome in both NBH-treated and RML-treated BV2 cells

(p<0.0001) (Figure 2.3h). Additionally, culturing with AdMSCs led to a decrease in the marker for M1 microglia *CD-16* was in both NBH- and RML-treated BV2 cells (p<0.0001) (Figure 2.3i). mRNA for *Arg-1*, a marker for M2 microglia, was increased for both NBH-treated (p=0.0378) and RML-treated BV2 cells (p=0.0051) (Figure 2.3j). It should be noted that AdMSCs that were not stimulated with TNFα were sufficient to decrease expression of some inflammatory genes in infected BV2 cells, but did not show as robust of an effect against many genes compared to pre-treated/stimulated AdMSCs (Supplemental Figure 2). Three biological replicates were used, each with three technical replicates. All analyses were normalized to *β-actin* and fold changes were assessed using a Two-way ANOVA and Tukey test with a p value of 0.05.

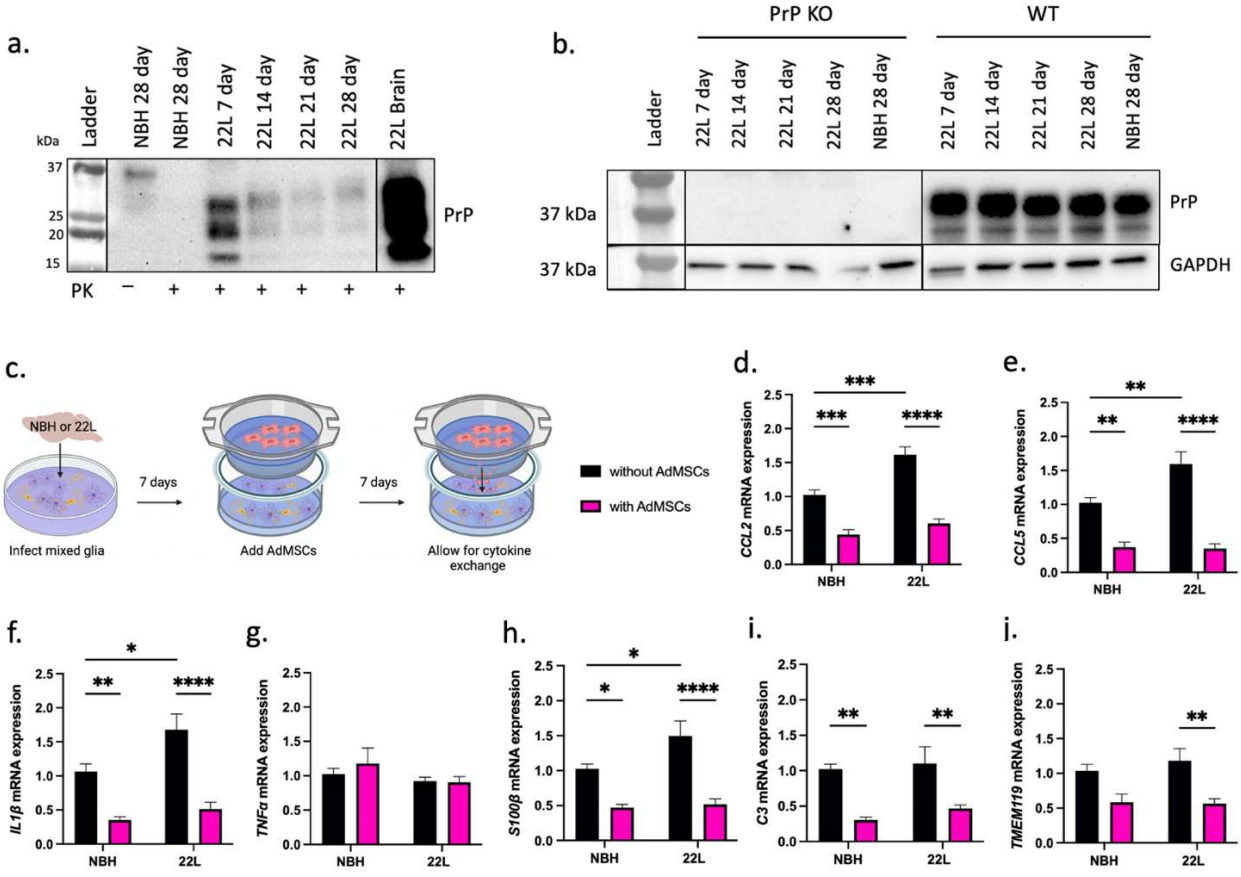

Figure 2.4. Co-culture with AdMSCs decreases mRNA for inflammatory genes in infected glia.
Wild-type mixed glia can be infected by being exposed to 0.1% 22L brain homogenates (diluted in media) and maintain infection. PK treatment of glia to remove PrP^{C} signal demonstrates that PrP^{Sc} remains in 22L-treated, but not NBH treated glia. An example of a terminal 22L brain (20% brain homogenate in PBS) used to infect these cells is in right-most lane (full exposure blot in Supplemental Data Figure 4). **(b)** Total PrP signal (no PK digestion) demonstrates that PrP knock-out glia cannot be infected with 22L prions and maintain infection, indicating that signal or changes in gene expression is not due to residual brain homogenate on cells. Infected wild-type glia show continuous expression of PrP^{C}. Blots are cropped and stitched together to remove empty lanes. **(c)** Mixed glial cultures were exposed to normal (NBH) or 22L-prion infected brain homogenates and incubated for 7 days, then co-cultured with or without AdMSCs for an additional 7 days. A decrease was seen in mRNA for inflammatory markers **(d)** CCL2, © CCL5, and **(f)** IL1β, but not **(g)** TNFα. Reactive astrocyte markers **(h)** S100β and **(i)** C3, and the microglia-specific marker **(j)** TMEM119 also decreased. Four biological replicates, with three technical replicates, all analyses normalized to *GAPDH*. Two-way ANOVA and post-hoc Tukey test, error bars = SEM, * $p< 0.05$, ** $p< 0.01$, *** $p< 0.001$, **** $p< 0.0001$. Graphic created with BioRender.com.

Co-culture with AdMSCs decreases mRNA for inflammatory genes in infected glia

Although microglia play a unique and critical role in the prion infected brain [69], elucidating the effects AdMSCs have on both astrocytes and microglia, and the cross-talk between these cell types, is essential. To best model the prion-infected brain in vitro, primary mixed glial cultures were utilized. These cultures are derived from cortices of C57Bl/6 mice at zero to two days old and contain both astrocytes and microglia [196]. Confirmational western blot analysis shows that exposure of glial cultures to 22L brain homogenate for 3 days is sufficient for infection, as detectable PrP^{Sc} accumulation can be seen at 7-, 14-, 21- and 28-days post-infection (dpi) (Figure 2.4a). PrP knock-out glia were infected for 7 to 28 days and no residual PrP^{C} was detected in these cells, while PrP^{C} remained consistent in infected glia throughout this time-course (Figure 2.4b). Together, these data show that glia can be infected and maintain infection for at least 28 days, and that there is no residual PrP remaining in the media. Glia at passage 1 were plated at 100,000 cells per well. 24 hours later, glial cultures were infected with media containing 0.1% 22L brain homogenate or NBH. At 3 dpi, cells were washed twice with PBS and new media was added. At 7 dpi, a co-culture system was established by adding 100,000 AdMSCs (passage 3) to inserts. Glia were co-cultured with AdMSCs for 7 days (Figure 2.3c) before RNA and protein samples were isolated from the glia.

A significant increase in *CCL2*, *CCL5, IL1β* and *S100β* mRNA was seen in glial cells infected with 22L compared to NBH (Figure 2.4d, e, f, h, $p<0.001$; $p<0.01$; $p<0.05$; $p<0.05$, respectively). After co-culturing for 7 days with AdMSCs, a decrease in *CCL2* mRNA was seen in both NBH-treated ($p<0.001$) and 22L-infected cells ($p<0.0001$) (Figure 2.4d). *CCL5* mRNA decreased in NBH-treated and 22L-infected glia co-cultured with AdMSCs ($p<0.01$; $p<0.0001$) (Figure 2.4e). Likewise, co-culturing with AdMSCs decreased *IL1β* mRNA in NBH-treated and 22L-infected glia ($p<0.01$; $p<0.0001$) (Figure 2.4f). No significant changes were seen in *TNFα* mRNA expression (Figure 2.4g).

Both overall astrocyte number and the number of C3+ reactive astrocytes increase in the prion-infected brain [49,61]. Here, we show that co-culturing with AdMSCs decreased both the pan-astrocyte marker *S100β* in NBH and 22L-treated glia ($p<0.5$; $p<0.0001$) (Figure 2.4h) and C3 in NBH and 22L-treated glia ($p<0.01$; $p<0.01$) (Figure 2.4i). The number of microglia is also known to increase in prion infection although analysis of TMEM119, a marker for a subset of microglia,[202] did not recapitulate this in our cell model. Co-culturing with AdMSCs did however decrease the amount of *TMEM119* mRNA in 22L-infected glia ($p<0.01$) (Figure 2.4j).

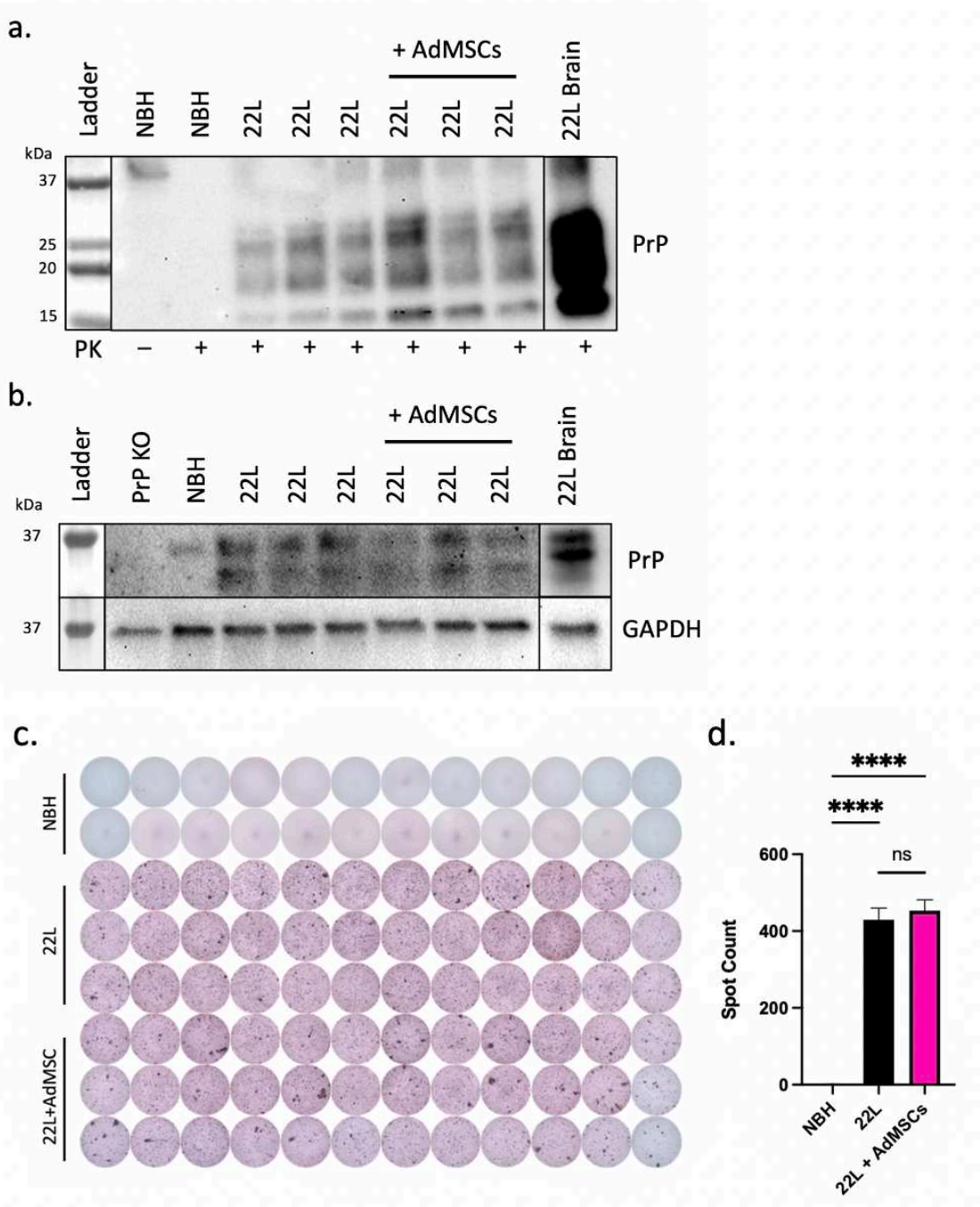

Figure 2.5. Protection against glial inflammation is independent of PrP^{Sc}. Infected mixed glial cells were cocultured with AdMSCs and western blot was used to analyze **(a)** PrP^{Sc} and **(b)** PrP^{C}. 22L-infected brain homogenate positive control (lower exposure) in right-most lanes. **(c)** Scrapie cell assay was used to analyze PrP^{Sc} spot counts. Representative image from three separate experiments. **(d)** Spot counts analyzed with One-way ANOVA and post-hoc Tukey test, error bars = SEM, **** $p < 0.0001$, ns = not significant.

Protection against glial inflammation is independent of PrP^{Sc}

Co-culture systems were set up as described above. After 7 days of infection and an additional 7 days of co-culturing with AdMSCs, cell lysates were taken from glial cells and analyzed for PrP^{Sc} expression using western blot. No significant differences were seen between amounts of PrP^{Sc} from infected cells co-cultured with AdMSCs to those without (Figure 2.5a). Similar findings were seen by scrapie cell assay (Figure 2.5b and c). This suggests that although AdMSCs have a significant impact on the cytokine expression of glial cells, they do not have any direct or indirect effects on the accumulation of PrP^{Sc} in these glial cells.

Discussion

Profiling of the prion-infected brain has revealed an upregulation of multiple inflammatory cytokines and chemokines, including IL1β, TNFα, and CCL2-CCL6 [48,79], with significant changes in gene expression and glial cell activation beginning as early as 70 days post infection (dpi) in infected C57Bl/6 mice [72,84]. At this time-point there is a shift in the number and profile of astrocytes, demonstrated by an increase in GFAP+ cells, as well as markers specific to the reactive A1 phenotype, namely S100β and C3 ([45,49]. This astrocyte reactivity and inflammatory profile is induced by secreted factors derived from activated microglia, TNFα, C1qα, IL1α and IL1β [45]. This initiates a positive feedback loop, as reactive astrocytes produce chemokines such as CCL2, which induces an M1 phenotype in microglia [51]. Contrary to the homeostatic, neuroprotective role that A2 astrocytes and M2 microglia play in the brain, A1 astrocytes have neurotoxic effects [45] and M1 microglia produce inflammatory cytokines such as TNFα, IL1β and nitric oxide and have increased migratory abilities [51].

Decreasing the number of microglia in the brain lengthens survival in prion-infected mice, but ablation of microglia altogether has proven to be detrimental [75,91]. Moreover, the removal of A1 astrocytes leads to an acceleration in disease and a decrease in activation of microglia [49]. Therefore, to properly treat early inflammation in prion disease, a fine balance must be established to decrease the number of activated glia without eliminating them all together. A1 astrocytes retain a neurotoxic phenotype in vitro, even after the removal of inflammatory cytokines. However, treatment with TGFb-1 or FGF are sufficient to revert A1 astrocytes back to a non-reactive phenotype [45].Thus, not only is it critical to decrease soluble factors that are contributing to glial activation and neuronal death, but also introduce anti-inflammatory factors that can restore glia to their protective phenotype.

We have demonstrated that adipose-derived mesenchymal stromal cells (AdMSCs) can be isolated from the peritoneal visceral fat of mice and expanded in culture (Figure 2.1). These cells respond to inflammatory cytokines and prion-infected brain homogenate by increasing production of anti-inflammatory genes such as TGFb-1 and TSG-6 (Figure 2.2), both of which have separately demonstrated an ability to decrease A1 astrogliosis [45,161]. TSG-6 secreted from mesenchymal stromal cells (MSCs) was recently shown to decrease LPS-induced NF-κB activation in astrocytes [161]. Moreover, MSC-derived TSG-6 can inhibit LPS-induced M1 polarization of microglia and promote M2 polarization [203]. We hypothesized that AdMSCs would show similar effects in a cell model of prion-induced glial inflammation. We infected primary cell cultures containing both astrocytes and microglia with brain homogenates from 22L-infected mice and co-cultured with AdMSCs. We saw a dramatic reduction in mRNA from the inflammatory cytokines CCL2, CCL5 and IL-1β, but not TNFα (Figure 2.3d-j). Additionally, culturing with AdMSCs directly affected the phenotype of both astrocytes and microglia,

contributing to a decrease in S100β, C3 and TMEM119, markers which are associated with prion and other neurodegenerative diseases [45,49,202,204].

To further elucidate the mechanism underlying the protective capacity of AdMSCs on prion-infected glia, AdMSCs were stimulated prior to co-culturing with BV2 microglia. Our data and others [170,199,205] show that stimulating MSCs with cytokines increases their production of small anti-inflammatory molecules. We have demonstrated their ability to upregulate mRNA for TGFb-1 and TSG-6 in response to TNFα, with the highest expression between 8 and 24 hours (Figure 2.2a-d). Therefore, we stimulated AdMSCs with TNFα 24 hours prior to being plated in co-culture inserts in order to maximize their production of inflammatory modulators. Co-culturing stimulated AdMSCs with infected BV2 microglia for as little as 24 hours was successful in decreasing a variety of inflammatory markers in these cells, including IL-1b, IL-6 and TNFα, but not CCL2 and CCL5 (Figure 2.4b-i). These findings are consistent with what has been reported for cross-talk between microglia and astrocytes, as microglia secrete TNFα to induce the A1 phenotype in astrocytes [45,49], and astrocytes secrete CCL2 to polarize microglia to an M1 state [51].

Culturing infected mixed glia with AdMSCs decreased the microglia-specific marker TMEM119 (Figure 2.3j), but significant changes in M1 and M2 microglia were difficult to characterize in this culture system, likely due to a limited number of microglia present. It has been reported that MSCs can change the phenotype of microglia from the activated and inflammatory M1 phenotype to the neuroprotective M2 phenotype [160,203,206,207]. It has been reported that prion-infected microglia show an increase in M1 markers [50,51], but the role of M1 and M2 microglia is only beginning to be elucidated in prion pathogenesis [50,93]. Our BV2/AdMSC co-culture systems demonstrated a decrease in M1 gene CD16 (Figure 2.4i), as

well as an increase in Arg-1 (Figure 2.4j), an M2 gene involved in restoration and repair [56], suggesting that AdMSCs influence polarization of microglia in the context of prion infection.

Although the study at hand cannot sufficiently differentiate between the inflammatory pathways that AdMSCs may be acting upon to dampen inflammation in in vitro prion infection, the effects of these cells on specific molecules can begin to hint at which pathways may be involved. There is evidence that NF-κB signaling is an early indicator of prion infection in vitro and *in vivo* [82,84,122]. This signaling can result in a vast number of secreted cytokines and chemokines, many of which are demonstrated here to be decreased in infected glial cells exposed to AdMSCs. This includes but is not limited to TNFα, IL1β, IL-6, CCL2 and CCL5. It has been reported that interference with NF-κB signaling in prion disease is neuroprotective [82,208]. Because these molecules are also implemented in other signaling pathways, this study alone is not sufficient in determining that AdMSCs have an effect on prion-induced NF-κB signaling. However, it has been established that mesenchymal stromal cells can decrease NF-κB in astrocytes activated by LPS exposure [161,203]. A second pathway that has been implicated in in vitro models of prion disease is the NLRP3 inflammasome, which has been reported as the primary source of microglia derived IL1β in prion infection [128]. Although the role of the NLRP3 inflammasome in mouse models of prion disease remains controversial [110], it has been established as a marker of prion-induced inflammation in primary microglia and BV2 cells [128,130]. Co-culturing prion-infected primary mixed glia and BV2 cells with AdMSCs resulted in a significant decrease in IL1β, a key cytokine produced by - but not limited to - the NLRP3 inflammasome pathway. Further evidence that AdMSCs are acting upon this pathway was the significant decrease in mRNA for NLRP3 in AdMSC-treated BV2 cells (Figure 2.4h). AdMSCs have differing effects on the transcriptional profile of prion-infected BV2 microglia compared to

primary mixed glial cells (composed of predominantly astrocytes). Changes in genes associated with reactive astrocytes and inducing astrogliosis suggests that AdMSCs cause synergistic dampening of inflammation and adapting the profile of both reactive astrocytes and activated microglia.

MSCs have shown the capacity to not only decrease inflammatory signaling, but to decrease protein aggregates. AdMSCs and AdMSC-derived exosomes have membrane-bound nephrilysin, an enzyme that degrades protein aggregates such as amyloid-b. A decrease in amyloid-b has been demonstrated in both cell [209] and mouse models of Alzheimer's disease after tail injection of MSC cells or exosomes [210,211]. Although it shares similarities, prion disease is characterized by a unique subset of glial cells compared to those seen in other neurodegenerative diseases [50,77,82]. To determine if similar effects could be seen in prion disease, co-culture systems of infected glia and AdMSCs were analyzed for abundance of PrP^{Sc} using both western blot and scrapie cell assay. AdMSCs did not show an ability to decrease PrP^{Sc} in the context of persistent infection in glial cells. This demonstrates that the protective capacity of AdMSCs in prion infection is independent of PrP^{Sc}. This is consistent with previous studies, which did not report any changes in PrP^{Sc} deposition after intervening in gliosis in prion-infected mice, despite observations of increased survival and improved clinical and behavioral signs [75,160,208].

The therapeutic advantages of mesenchymal stromal cells (MSCs) have been well established, particularly their ability to regulate inflammation by secreting anti-inflammatory small molecules and promote angiogenesis and neurogenesis [171,188,189]. The secretome of these cells includes anti-inflammatory cytokines and chemokines, growth factors, microRNA and messenger RNAs [212]. Intriguingly, these cells can be taken autologously from patients via a relatively non-invasive procedure [178]. The capacity of MSCs to modulate inflammation in a

paracrine manner has been well established in a variety of neurological disorders [188,189], including neurodegenerative diseases such as Alzheimer's and Parkinson's [176,190,191]. Here, we have shown that MSCs derived from adipose tissue are effective in decreasing inflammation in an in vitro model of prion-induced gliosis. Our in vitro data suggests that AdMSCs will be successful in decreasing inflammation, but not in the clearance of PrP^{Sc}. This poses a limitation to AdMSCs alone as a potential treatment for prion disease. However, it suggests that AdMSCs may be advantageous in combatting inflammation, especially if combined with another therapeutic that can decrease PrP^{Sc} in the brain.

Supplemental Data

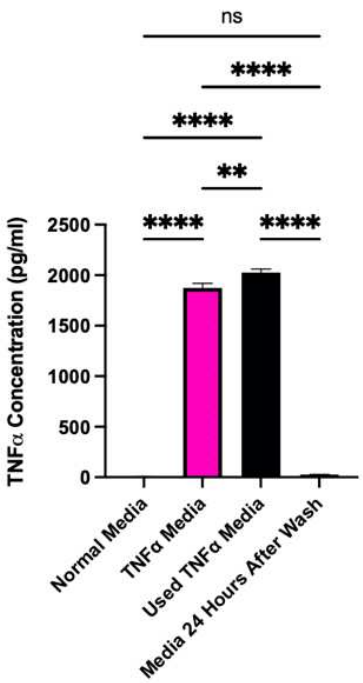

Supplemental Figure 2.1. TNFα is significantly detectable by ELISA in media from AdMSCs that have been stimulated for 24 hours with TNFα, but not after thorough washing and media change. One-Way ANOVA and Tukey test, p<0.05, error bars = SEM. * p< 0.05, ** p< 0.01, *** p< 0.001, **** p< 0.0001, ns = not significant.

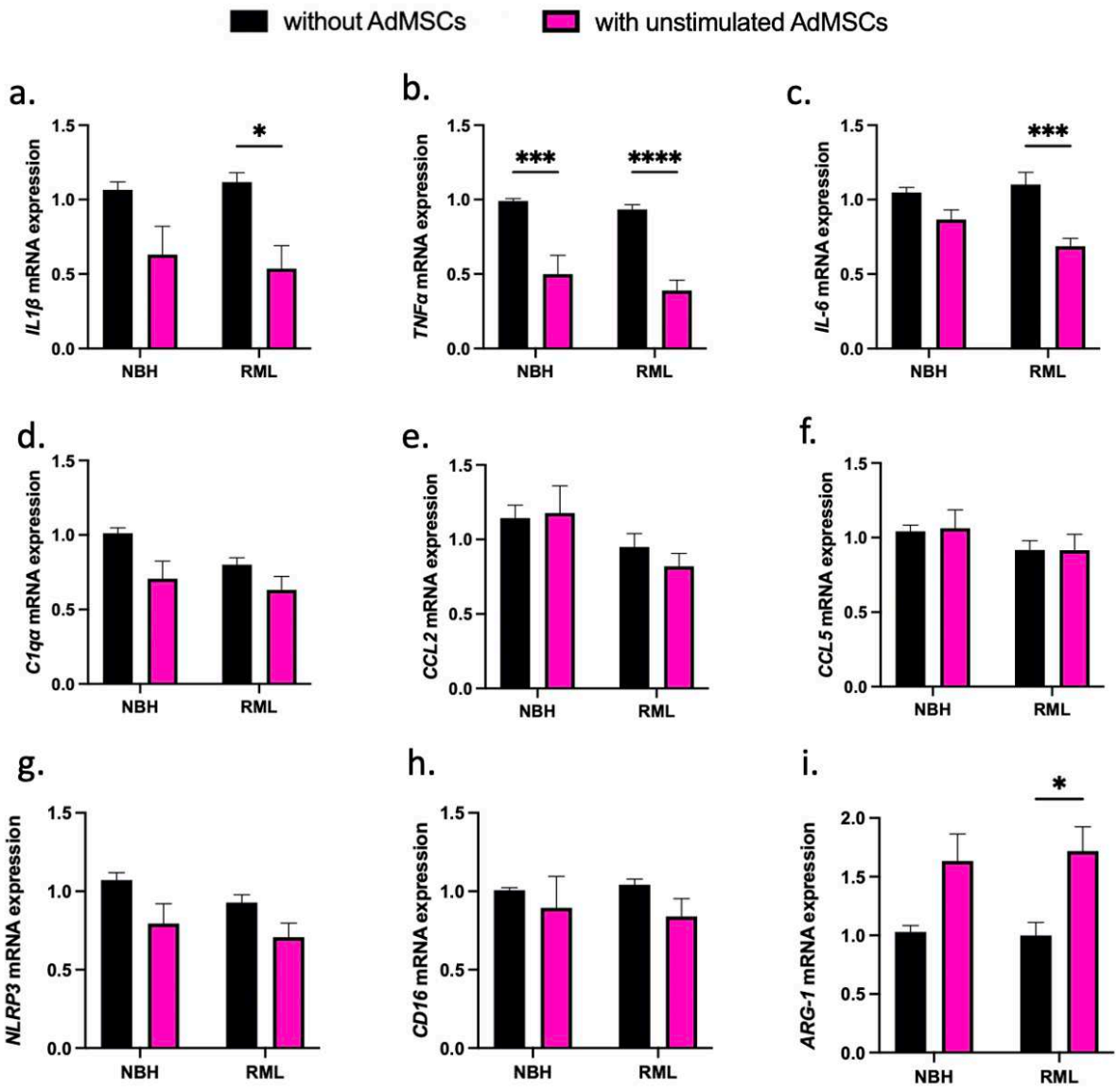

Supplemental Figure 2. BV2 microglia were infected with 0.1% RML brain homogenate or normal brain homogenate (NBH) for 6 days, then incubated for 24 hours with unstimulated AdMSCs. This resulted in a decrease in **(a)** IL1β, **(b)** TNFα and **(c)** IL-6 mRNA, but not **(d)** C1qα, **(e)** CCL2, **(f)** CCL5, **(g)** NLRP3, or **(h)** CD16. **(i)** An increase was seen in the M2 marker Arg-1. Three biological replicates, each with three technical replicates, all analyses normalized to *b-actin*. Two-way ANOVA and Tukey test, p<0.05, error bars = SEM. * < 0.05, ** < 0.01, *** < 0.001, **** < 0.0001

Chapter 3:

Intranasally Delivered Mesenchymal Stromal Cells Decrease Glial Inflammation Early in Prion Disease

Published in Frontiers in Neuroscience, May 2023

Summary

Mesenchymal stromal cells (MSCs) are an intriguing avenue for the treatment of neurological disorders due to their ability to migrate to sites of neuroinflammation and respond to paracrine signaling in those sites by secreting cytokines, growth factors, and other neuromodulators. We potentiated this ability by stimulating MSCs with inflammatory molecules, improving their migratory and secretory properties. We investigated the use of intranasally delivered adipose-derived MSCs (AdMSCs) in combating prion disease in a mouse model. Prion disease is a rare, lethal neurodegenerative disease that results from the misfolding and aggregation of the prion protein. Early signs of this disease include neuroinflammation, activation of microglia, and development of reactive astrocytes. Later stages of disease include development of vacuoles, neuronal loss, abundant aggregated prions, and astrogliosis. We demonstrate the ability of AdMSCs to upregulate anti-inflammatory genes and growth factors when stimulated with tumor necrosis factor alpha (TNFα) or prion-infected brain homogenates. We stimulated AdMSCs with TNFα and performed biweekly intranasal deliveries of AdMSCs on mice that had been intracranially inoculated with mouse-adapted prions. At early stages in disease, animals treated with AdMSCs showed decreased vacuolization throughout the brain. Expression of genes associated with Nuclear Factor-kappa B (NF-κB) and Nod-Like Receptor

family pyrin domain containing 3 (NLRP3) inflammasome signaling were decreased in the hippocampus. AdMSC treatment promoted a quiescent state in hippocampal microglia by inducing changes in both number and morphology. Animals that received AdMSCs showed a decrease in both overall and reactive astrocyte number, and morphological changes indicative of homeostatic astrocytes. Although this treatment did not prolong survival or rescue neurons, it demonstrates the benefits of MSCs in combatting neuroinflammation and astrogliosis.

Introduction

Prion diseases are fatal neurodegenerative diseases characterized by the misfolding and aggregation of the prion protein (PrP), due to either a genetic mutation in the protein, or a spontaneous or acquired source of misfolded PrP (denoted PrP^{Sc}).[22] According to the CDC, each year approximately 1.5 per one million people in the United States develop classic Creutzfeldt-Jakob Disease (CJD), the most common spontaneous prion disease (CDC 2021). Individuals with CJD undergo rapid loss of memory and motor function, which ultimately lead to death. There are currently no available treatments for CJD or any other prion diseases, because after clinical signs occur, PrP^{Sc} accumulation and neurodegeneration are irreversible.

An early sign of prion disease, prior to detectable PrP^{Sc} in the brain or behavioral changes, is astrogliosis. In animal models, astrocyte numbers increase throughout the brain prior to signs of neurodegeneration. This is accompanied by an increase in microglia numbers, as well as inflammatory cytokines and chemokines.[50,72,79] There is evidence that PrP^{Sc} aggregates are not the only source of neurotoxicity, and that neuroinflammation may be contributing to neuronal

loss and degeneration.[38,45,64,76,82] An ideal treatment should therefore target both early inflammation as well as protein aggregation.

Here, we investigate the therapeutic potential of adipose-derived mesenchymal stromal cells (AdMSCs) in decreasing glial inflammation in a mouse model of prion disease. These cells can be easily isolated from adipose tissue, expanded in culture, and injected into animals or patients with little immunogenic effects.[166,213] They follow chemokine gradients to migrate to sites of inflammation, where they respond by secreting anti-inflammatory cytokines, chemokines, and growth factors.[166,169,172,200] We recently demonstrated the therapeutic ability of AdMSCs in decreasing glial inflammation in a cell-culture model of prion disease through a reduction of genes associated with signaling pathways such as pro-inflammatory transcription factor, Nuclear Factor-kappa B (NF-κB) and the Nod-Like Receptor family pyrin domain containing 3 (NLRP3) inflammasome.[123] MSCs also decrease markers of reactive astrocytes and M1 activated microglia,[123,160-162,203] cell types which are highly abundant in prion infection. Mesenchymal stromal cells (MSCs) have been used in mouse models of neurodegenerative diseases such as Alzheimer's and Parkinson's.[168,176,191,214] MSCs derived from bone marrow and compact bone have been used to decrease inflammation in prion-diseased mice when delivered intracranially through stereotaxic surgery.[160,177] Although this was successful in increasing the lifespan of these animals, it poses some limitations when translated to the clinic, as acquiring MSCs from the bone and injecting them stereotaxically into the brain are very invasive procedures.

In this study, we investigate the effectiveness of intranasal delivery of MSCs from adipose tissue into mice with prion disease. We delivered cytokine-stimulated AdMSCs derived from prion knockout (PrP KO) mice every two weeks beginning at 10 weeks post-infection (wpi)

and ending at 20 wpi. We assessed both behavioral and clinical signs of disease, neuronal loss and vacuolization, development of inflammation, and astrogliosis as disease progressed.

Materials and Methods

Animal care and ethics statement

All mice were bred and maintained at Colorado State's Lab Animal Resources, accredited by the Association for Assessment and Accreditation of Lab Animal Care International. This was done in accordance with protocols approved by the Institutional Animal Care and Use Committee at Colorado State University.

Brain preparations

C57Bl/6 (Jackson Laboratory) mice were anaesthetized with isoflurane prior to intracranial inoculation with 30µl of 1% Rocky Mountain Laboratories (RML) strains of mouse-adapted prions, or normal brain homogenate (NBH). Mice were subjected to intranasal delivery of AdMSCs and behavioral assays, as described below. Mice were euthanized for time-course study at 14, 16, and 18 wpi, three days after intranasal delivery was performed, while the remaining mice were taken to terminal disease. Mice were monitored for weight loss and clinical signs of prion disease and euthanized by deep isoflurane anaesthetization followed by decapitation after showing signs of terminal illness. NBH mice were sacrificed after all prion-infected mice had been euthanized. The right hemisphere was fixed in 10% neutral-buffered formalin. The left hemisphere was removed and olfactory bulbs, hippocampus, thalamus and cerebellum were removed and stored in RNAlater (Qiagen) at -80C prior to RNA analysis. The remainder of the

left hemisphere was used to make 20% brain homogenates in phosphate-buffered saline (PBS) using beads and a tissue homogenizer (Benchmark Bead Blaster 24) and stored at -80C prior to western blot analysis.

Isolating and maintaining AdMSCs

AdMSCs were isolated as described previously.[123] Adult TALEN PrP knock-out (KO) C57Bl/6 mice[215] were euthanized and abdominal adipose tissue was removed and placed in Hank's Buffered Saline Solution containing 25% Trypsin (HyClone, 0.25%). Adipose tissue was dissociated by incubating with a mixture of 200 U/ml DNase-I (Roche) and 400 U/ml Stemxyme (Worthington Biochemical Corporation) in DMEM/F12 media (Caisson Labs) at 37° C for 1.5 hours. The tissues were triturated and centrifuged at 4° C for 5 minutes at 1000 x g to pellet the stromal vascular fraction. The pellet was washed once with sterile PBS and centrifuged at 1000 x g. The pellet was resuspended in 1 ml of AdMSC media (low glucose DMEM containing L-glutamine and supplemented with essential and non-essential amino acids (Gibco), 15% heat-inactivated fetal bovine serum (FBS) (Peak Serum), and penicillin/streptomycin/neomycin (PSN) (Sigma)). Resuspension was filtered through a 40 μm cell strainer (Fisher) to remove any non-dissociated tissue. Cells were plated in 10 cm dishes and grown in AdMSC media at 37° C with 5% CO2. 72 hours later, cells were passaged at a 1:3 ratio and again every 3-4 days.

Stimulating AdMSCs for mRNA transcript analysis

AdMSCs were plated at 100,000 cells per well in 6 cm plates at passage 3. The following day, media was removed and replaced with media containing 10 ng/ml tumor necrosis factor alpha (TNFα), 100 ng/ml interferon gamma (IFNγ), or normal media as a negative control. 24-hours later, cells were washed twice with sterile PBS and cell lysates were obtained using RLT

buffer (Qiagen) containing β-mercaptoethanol (Sigma-Aldrich) and filtered through a QiaShredder column (Qiagen). RNA isolation and qRT-PCR protocol is described below.

Intranasal delivery of AdMSCs

PrP KO AdMSCs at passage 3 were stimulated with 10ng/ml TNFα 24 hours prior to intranasal delivery. Cells were washed three times with sterile PBS and trypsinized with 0.25% Trypsin, resuspended in AdMSC media, then spun at 4C for 5 minutes at 1000 x g. Cells were washed thoroughly with PBS, spun an additional time, counted on a hemocytometer, and resuspended in PBS at $1x10^6$ cells per 18 µl. Mice were anaesthetized with isoflurane and treated with 100U hyaluronidase (United States Biochemical Corporation) in PBS, with 3µl delivered to each nostril, 3 times per nostril, for a total of 18 µl, 1 hour prior to intranasal AdMSC delivery. 3 µl AdMSC cell suspension was then delivered to each nostril, 3 times per nostril, for a total of 18 µl, or $1x10^6$ cells per animal. Control mice were given PBS containing no AdMSCs. Mice were monitored for 10 minutes after regaining consciousness to ensure no adverse side effects. AdMSC treatments were performed at 10, 12, 14, 16, 18 and 20 weeks post infection (wpi). This experiment was repeated twice. The first cohort contained all female mice, 12 NBH mice and 24 of RML-infected (16 received AdMSCs and 12 received PBS), all of which were taken to terminal stages of disease. The second cohort contained both male and female mice, 7 NBH mice and 40 RML mice (24 received AdMSCs and 16 received PBS). 10 mice (6 AdMSC and 4 PBS) were euthanized at 14, 16, and 18 wpi.

Clinical and behavioral assays

Ability of mice to build nests was evaluated by placing three fresh napkins weekly in the cage. 24 hours later, the position of the napkins was evaluated on a score of 0 to 5, with 0 being untouched, dirty and marked with urine, and 5 being positioned into a compact nest that provided full shelter to the mice. Nests were evaluated beginning at 10 wpi until euthanasia. For burrowing assessment, female mice were separated into individual cages containing a 6-inch section PVC pipe that was closed off at one end and filled with 120 grams of food pellets. Mice were given 30 minutes to "burrow" into the PVC pipe by removing the pellets. Mice were returned to their home cage and the remaining pellets in the PVC pipe were weighed. Burrowing was performed on mice every other week beginning at week 13 and ending at week 21. Clinical signs and weight were evaluated beginning at 17 wpi and continuing until mice were euthanized. Mice were evaluated weekly and scored from 0 (no signs) to 2 (severe signs) on the following signs of RML prion disease: tail rigidity, hyperactivity, ataxia, extensor reflex, tremors, righting reflex, kyphosis and poor grooming. Mice were additionally monitored for severe weight loss. Clinical signs and weight were monitored twice a week beginning at 20 wpi. When mice reached a total score of 10 for any combination of signs they were euthanized. Mice inoculated with normal brain homogenate (NBH) were used as a control for all behavioral assays and clinical signs.

Immunohistochemistry

Fixed brain hemispheres were embedded in paraffin and sliced and mounted on slides at 5μm using the HM325 microtome (Thermo Scientific). Tissue was deparaffinized and rehydrated and underwent antigen retrieval in 0.01M sodium citrate buffer for 20 minutes at

95°C. Endoperoxidases were inactivated by incubating tissue in 0.3% hydrogen peroxide. Tissue was blocked in Tris A (Tris-buffered saline (TBS) and Triton-X (Sigma-Aldrich)) containing 2% bovine serum albumin (BSA, Sigma-Aldrich) and 10% horse serum (Corning) for 1 hour at room temperature. Primary antibodies were made in Tris A/2% BSA and incubated overnight in a humidity chamber at 4° C. The following primary antibodies were used: Iba1 (Abcam) at 1:400 dilution and GFAP (Dako) at 1:400 dilution. Tissue was washed with Tris A/2% BSA and incubated with biotinylated secondary antibody at 1:250 (Vector Laboratories) for 1 hour, washed, and incubated with ABC complex (Vector Laboratories) for 1 hour as per manufacturer's instructions, washed, and incubated with DAB (Vector Laboratories) until color change was observed (time dependent on antibody used). Tissue was washed with TBS and counterstained with hematoxylin (Epredia) and bluing reagent (Cancer Diagnostics, Inc). Tissue was dehydrated and coverslips (Globe, #1) were mounted with media (Epredia) and dried overnight or longer before imaging with the Olympus VS120 Scanning Microscope. Representative 40x images were taken using the Olympus BX53. Cell counts were performed using the Olympus cellSens software (v 1.18). Outliers were identified and removed using a ROUT outlier test and a Welch's T-test was used to compare treated and untreated groups using Prism (v 9.1.0).

Immunofluorescence quantification and skeletonization

Tissue was deparaffinized, rehydrated, sodium citate treated, and blocked in Tris A/BSA and incubated with primary antibody overnight, as described above. The following primary antibodies were used: Iba1 (Abcam) at 1:50 dilution, GFAP (Dako) at 1:100 dilution, S100β (Abcam) at 1:750 dilution and C3 (Abcam) at 1:250. Tissue was washed with TBS and incubated

for 1 hour in the dark with Alexa Fluor-488, -555 or -647 (Invitrogen) secondary antibodies at 1:500 dilution and 2% normal donkey serum (Jackson ImmunoResearch). Slides were washed and incubated in Hoechst at 1:2000 dilution in PBS for 3 minutes. Slides were coverslipped with Prolong Gold Antifade mounting media (Thermo Scientific) and kept in the dark at room temperature for 24 hours, then in 4°C prior to imaging. GFAP slides were imaged on an Olympus BX60 fluorescent scope with a DP23 camera. For skeletonization experiments, four to five regions between the dentate gyrus and CA1-CA3 region of the hippocampus were imaged at 40x for each animal. All other slides were imaged with an Olympus BX63 fluorescence microscope equipped with a motorized stage and Hamamatsu ORCA-flash 4.0 LT CCD camera and an Olympus Xline apochromat 20X (0.8 N.A.) air objective. Exposures for each stain were set for the same period of time within each channel. Regions of interest (ROI) were selected with Olympus cellSens software to identify S100β^{+} astrocytes within the hippocampus using adaptive thresholding and then converted into individual ROIs. Mean gray intensity of C3 was determined within each S100β^{+} cell ROI. Skeletonization of astrocytes and microglia was performed using IMARIS 9.9.1. Using the calculate soma model, new starting points were detected using the largest diameter of 9.5 um, and seed points using the thinnest diameter of 0.570 um. Astrocytes were analyzed in channel 555 with a manual starting point threshold at 33.3, and seed point threshold at 43.1. Microglia were analyzed in channel 647 with automatic starting point threshold and seed point thresholds. These numbers were adjusted for each image to eliminate background. Seed points around starting points were removed using a sphere region diameter of 19.0 um. Disconnected segments were removed with an automatic absolute intensity threshold for both astrocytes and microglia. The dendrite diameter threshold was set at 4.51 for astrocytes and 4.91 for microglia. A max gap length of 11.4 um was used. After filaments were traced,

processes that did not correspond to fluorescent staining were manually removed. Data generated by IMARIS was analyzed in Prism (v 9.1.0). Outliers were identified and removed using a ROUT outlier test and a Welch's T-test was used to compare treated and untreated groups.

Hematoxylin and eosin staining

Slides were deparaffinized and rehydrated before being treated with hematoxylin and bluing reagent. Tissue was counterstained with eosin (Epredia). Slides were dehydrated and coverslips (Globe, #1) were mounted with media. Slides were imaged with the Olympus VS120 Scanning Microscope. Vacuoles were scored for each brain region (frontal cortex, hippocampus, thalamus and cerebellum) on a scale of 0 (no pathology) to 5 (significant pathology) by three pathologists who were blinded to the treatment groups.[216-218] Both quantity and size of vacuoles were considered during scoring. An average of the three scores was taken for each brain region. Pyknotic neurons were counted manually within the CA1 region of the hippocampus.

Immunoblotting

20% brain homogenates were analyzed with a BCA Protein Assay Kit (Thermo Scientific) to quantify protein concentration. 100 μg of protein was digested with a final volume of 20 μg /ml proteinase K (PK) (Roche) for PrP^{Sc} blots for 1 hour at 37°C. Digestion was terminated with 2mM PMSF (Thermo Fisher) and samples were suspended in loading buffer (Bio-Rad) containing β-mercaptoethanol (Sigma-Aldrich) before being loaded on a gel. For PrP^{C} blots, 25 μg of sample was used with no PK digestion. Samples were run on a 4-20% acrylamide SDS page gels (Bio-Rad) and transferred to PVDF blotting paper (MilliPore). Primary antibody Bar-224 (Cayman Chemical Company) was used at 1:10,000 dilution. HRP-conjugated secondary antibodies were used at a concentration of 1:5,000 (Vector Laboratories). After imaging, PrP^{C}

blots were stripped and loading control GAPDH was ran at a 1:10,000 dilution (MilliPore), with HPR-conjugated secondary antibody at 1:5,000 dilution (Southern Biotech). Western blots were visualized using SuperSignal West Pico PLUS Chemiluminescent Substrate (Thermo Scientific) and visualized with the BioRad ChemiDoc MP.

Live animal imaging and intranasal delivery assessment

48 CD-1 mice (Charles River) were inoculated intracranially with 1% RML, as described above. PrP KO AdMSCs were isolated and expanded as described above, stimulated for 24 hours with 10ng/ml TNFα, then labeled with DiD Vybrant Cell-Labeling Solution (Invitrogen) [219,220], following manufacturer's protocol, or mock-labeled with PBS. Cells were intranasally delivered to the CD-1 mice at 18 weeks post-infection, as described above. 24 mice received unlabeled cells, the remaining 24 received labeled cells. Mice were imaged with a Xenogen IVIS Imaging System at 24, 48, 72 hours, 7 days and 14 days post-delivery. At each timepoint, brains were extracted from 4 mice receiving both labeled AdMSCs and 4 mice receiving unlabeled AdMSCs. Brains were fixed for 60 seconds in 10% neutral buffered formalin (NBF) and then imaged with the Xenogen IVIS with an excitation filter of 640 and an emission filter of 680. Maximum radiance efficiency was measured for both animals and brains by creating a region of interest (ROI). The same size ROI was used to analyze each animal or brain for each image.

This study was repeated in a cohort of 12 RML-infected female CD-1 mice that did not undergo live-animal imaging, to prevent any loss of signal from the DiD-labeled AdMSCs. 10 mice received DiD-labeled AdMSCs, and the remaining 2 received mock-labeled AdMSCs. 6 mice were euthanized at 48 hours post-delivery (one control and 5 DiD-labeled), and the remaining 6 were euthanized at 7 days post-delivery, and brains were bisected sagitally,

hemispheres were placed side-by-side in OCT Freezing Medium (Sakura Finetek) and immediately frozen on dry ice. Brains were cut sagitally using a Microm HM 525 Cryostat in 10μm-thick sections. Each slide received 3 sets of sections (each consisting of both hemispheres), with 50μm separation between each set. 10 slides were made for each brain, spanning approximately 1500μm from the most medial section to the most lateral section. The first (most medial), middle and last (most lateral) slides were selected, washed with PBS, incubated in Hoechst at 1:2000 dilution in PBS for 3 minutes, and coverslipped with Prolong Gold Antifade mounting media (Thermo Scientific) and kept in the dark at room temperature for 24 hours, then in 4°C prior to imaging. Slides were imaged with an Olympus BX63 fluorescence microscope equipped with a motorized stage and Hamamatsu ORCA-flash 4.0 LT CCD camera and an Olympus Xline apochromat 20X (0.8 N.A.) air objective. DiD (Cy5) exposure time was selected based on control slides. For each brain, the cortex, hippocampus, thalamus and cerebellum were analyzed and presence of DiD+ cells were recorded. Representative images for each brain region showing significant cell migration were taken at 20x.

Slides from brains that showed significant DiD+ cells in the hippocampus were selected and blocked in Tris A/BSA and incubated overnight, as described above. The following primary antibodies were used: Oct3/4 (Abcam) at 1:100 dilution, Vimentin (Abcam) at 1:100 dilution. Tissue was washed with TBS and secondary antibody at 1:500 (Southern Biotech) containing 2% serum was incubated at 1:500 dilution in the dark for 1 hour at room temperature. Slides were washed, counterstained with Hoechst, and coverslipped. Hippocampi were imaged at 20x to identify DiD+ cells that also expressed Oct3/4 and Vimentin, indicative of AdMSCs. Mean gray intensity of DiD in Oct3/4+ cells was measured, as described above, using representative images of hippocampus and thalamus for animals that received mock- and labeled AdMSCs. To

determine cytological staining of Oct3/4, Vimentin and DiD in AdMSCs, PrP KO AdMSCs were labeled with DiD, as described above, and plated at 20,000 cells per well in chamber slides (Thermo Scientific) and incubated for 48 hours, as described above. Cells were washed, fixed with 4% PFA for 10 minutes, incubated with 10% normal donkey serum, and stained, as described above. Representative images were taken at 40x.

Reverse transcriptase quantitative PCR analysis

RNA was extracted from cells or hippocampal tissue using QIAshredder and RNeasy extraction kits, in accordance with manufacturer's protocol, including a DNase digestion step with the RNase free DNase kit (Qiagen, Valencia, CA). Purity and concentration were determined using a ND-1000 spectrophotometer (NanoDrop Technologies, Wilmington, DE). 25-50ng RNA was reverse transcribed using the iScript Reverse Transcriptase kit (BioRad, Hercules CA). The cDNA was amplified within 24 hours of reverse transcription using iQ SYBR Green Supermix (BioRad, Hercules CA). The corresponding validated primer sequences were used for each gene at 10mM. The expression data was analyzed using the $2^{-\Delta\Delta CT}$ method and normalized to expression of reference gene *β-actin.*[221] All RT-PCR was done following MIQE guidelines. Validated primer sequences are listed in Table 3.1.

Statistical analysis

For all analyses, outliers were identified and removed using a ROUT outlier test (Q=1%). Cleaned data for two groups was measured using a Welch's T-test. For three or more groups, cleaned data was analyzed using a One-way ANOVA with Tukey's post-hoc analysis. A p-value of 0.05 was used for all analyses. All figures present mean +/- standard error of the mean (SEM). All data analysis and generation of graphs was done with Prism (v 9.1.0).

Results

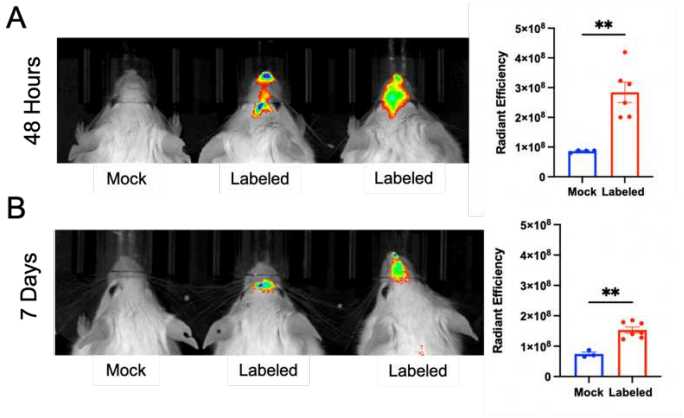
A
48 Hours
Mock
Labeled
Labeled
Radiant Efficiency
**
Mock Labeled
B
7 Days
Mock
Labeled
Labeled
Radiant Efficiency
**
Mock Labeled

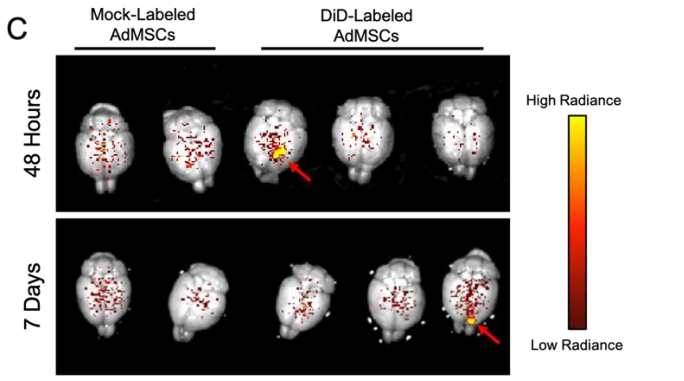
C
Mock-Labeled AdMSCs
DiD-Labeled AdMSCs
48 Hours
7 Days
High Radiance
Low Radiance

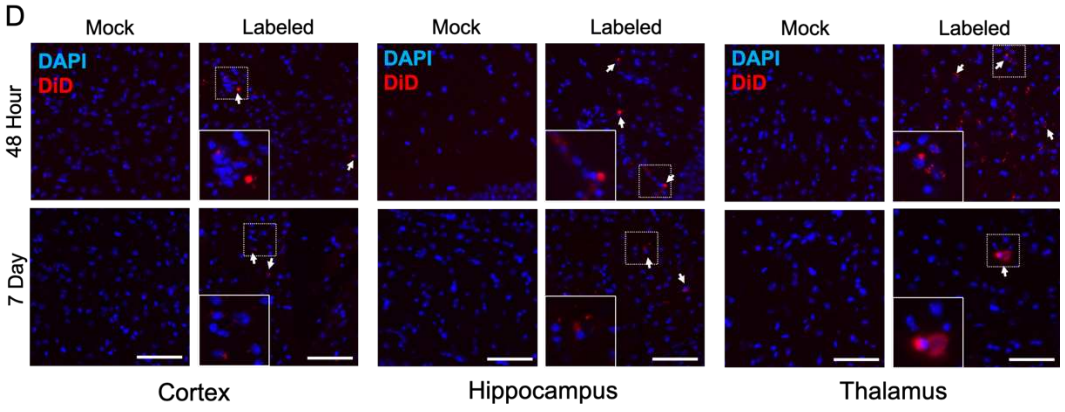
D
Mock
Labeled
Mock
Labeled
Mock
Labeled
48 Hour
7 Day
DAPI
DiD
Cortex
Hippocampus
Thalamus

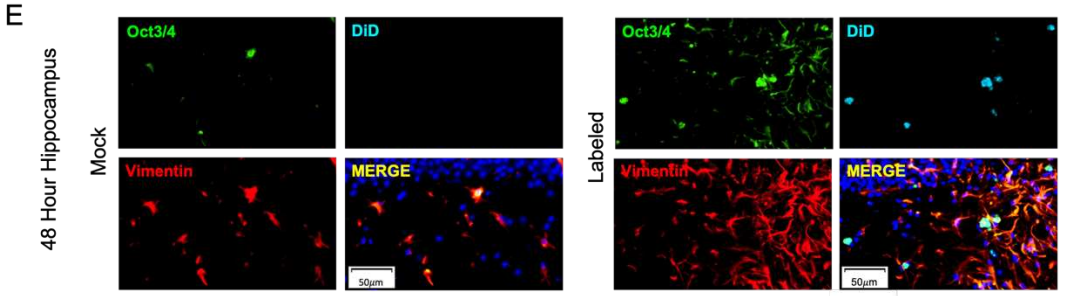
E
48 Hour Hippocampus
Mock
Labeled
Oct3/4
DiD
Vimentin
MERGE
50μm

Figure 3.1. Fluorescently-labeled AdMSCs migrate deep into the olfactory system and into the brains of prion-infected mice. AdMSCs were stimulated for 24 hours with TNFα, labeled with DiD lipophilic dye and delivered intranasally into mice with RML exposure at 18 weeks post infection (wpi). Control mice received unlabeled AdMSCs. Live animal imaging was performed (A) 48 hours and (B) 7 days post-delivery. Both time points showed significant maximum radiance from cells in the olfactory region, determined using a T-test with Welch's corrections, **p<0.01, error bars = SEM. (C) At each timepoint, brains were removed and imaged. Areas of labeled cells were visible in some brains at 48 hours and 7 days post-delivery (shown by red arrows). Radiance scale used for degree of fluorescent dye positivity in brains. (D) Representative images of DiD+ cells in the cortex, hippocampus and thalamus at 48 hours and 7 days post-delivery, compared to brains from animals that received mock-labeled AdMSCs. Arrows indicate DiD+ cells. Cell nuclei are stained with DAPI. Scale bar = 50 μm. (E) Hippocampus of animals that received mock-labeled or DiD-labeled AdMSCs at 48 hours post-delivery. Tissue was co-stained for AdMSC markers Vimentin and Oct3/4, which co-localizes with DiD staining. 20x representative images, scale bar = 50 μm.

Fluorescently-labeled AdMSCs migrate deep into the olfactory system and into the brain of prion-infected mice

We have shown previously that AdMSCs isolated from the abdominal adipose tissue of C57Bl/6 mice contain a heterologous population of cells with characteristics of mesenchymal stem cells. Additionally, these cells can migrate in an in vitro model toward the prion-infected brain.[123,160] PrP KO AdMSCs were stimulated for 24 hours with tumor necrosis factor alpha (TNFα) to promote migration to the prion-infected brain [170,200,201] and labeled with fluorescent lipophilic dye (DiD) or mock-labeled with PBS and intranasally delivered into RML-infected CD-1 mice at 18 wpi. Live mice were imaged with the Xenogen IVIS Imaging System at 24, 48, 72 hours, 7 days and 14 days post-delivery and brains were extracted and imaged at each of these timepoints. Analysis of the maximum radiance showed significantly more fluorescence signal from mice receiving the labeled AdMSCs at 24 hours ($p<0.01$; data not shown), 48 hours (Figure 3.1A; $p<0.01$), 72 hours ($p<0.001$; data not shown) and 7 days (Figure 3.1B; $p<0.01$), but no significant difference were seen between groups at 14 days (data not shown). When brains were dissected out and imaged with the Xenogen IVIS, no significant differences in maximum radiance of whole brains were seen between mock- and labeled AdMSC-treated groups. However, specific sites of fluorescently labeled cells can be observed (Figure 3.1C, shown by

red arrows) in some of the brains that received labeled AdMSCs. Of the brains that received labeled AdMSCs, regions of fluorescence were seen in two of four brains at 24 hours, one of four brains at 48 hours, and one of four brains at 7 days. No regions of fluorescence were seen at 72 hours or 14 days post-delivery (data not shown), nor were they seen in mice that received mock-labeled AdMSCs.

A cohort of 12 CD-1 mice at 18wpi were given stimulated intranasally-delivered DiD- or mock-labeled PrP KO AdMSCs, following an identical protocol as above. At 48 hours and 7 days post-delivery, mice were euthanized and brains were immediately frozen on dry ice. Brain sections were assessed for DiD+ cells in the cortex, hippocampus, thalamus and cerebellum. DiD+ cells were found in almost all animals in the cortex, hippocampus, and thalamus (Figure 3.1D), and in less than half of animals in the cerebellum at both 48 hours and 7 days post-delivery (Table 3.2). No DiD+ cells were found in brains from mice that received mock-labeled AdMSCs. Brains from mice at 48 hours post-delivery that showed significant DiD+ cells in the hippocampus were stained with the stem cell marker Oct3/4 and the structural marker Vimentin, both of which label AdMSCs.[123,198] Note that there are no markers specific to AdMSCs that are not expressed in other cell types in the brain. Oct3/4 can also be expressed in pluripotent cells, and Vimentin is also expressed in astrocytes. All DiD+ cells analyzed were Oct3/4+ and the majority were Vimentin+ (Figure 3.1E). This staining pattern is recapitulated when AdMSCs are labeled and grown in vitro (Supplemental Figure 3.1A). Quantification of DiD in Oct3/4+ cells in the hippocampus and thalamus demonstrated significantly more fluorescent intensity in animals that received labeled AdMSCs (Supplemental Figure 3.1B). Together, these data suggest that AdMSCs delivered intranasally can migrate throughout the brain and remain there for a minimum of 7 days.

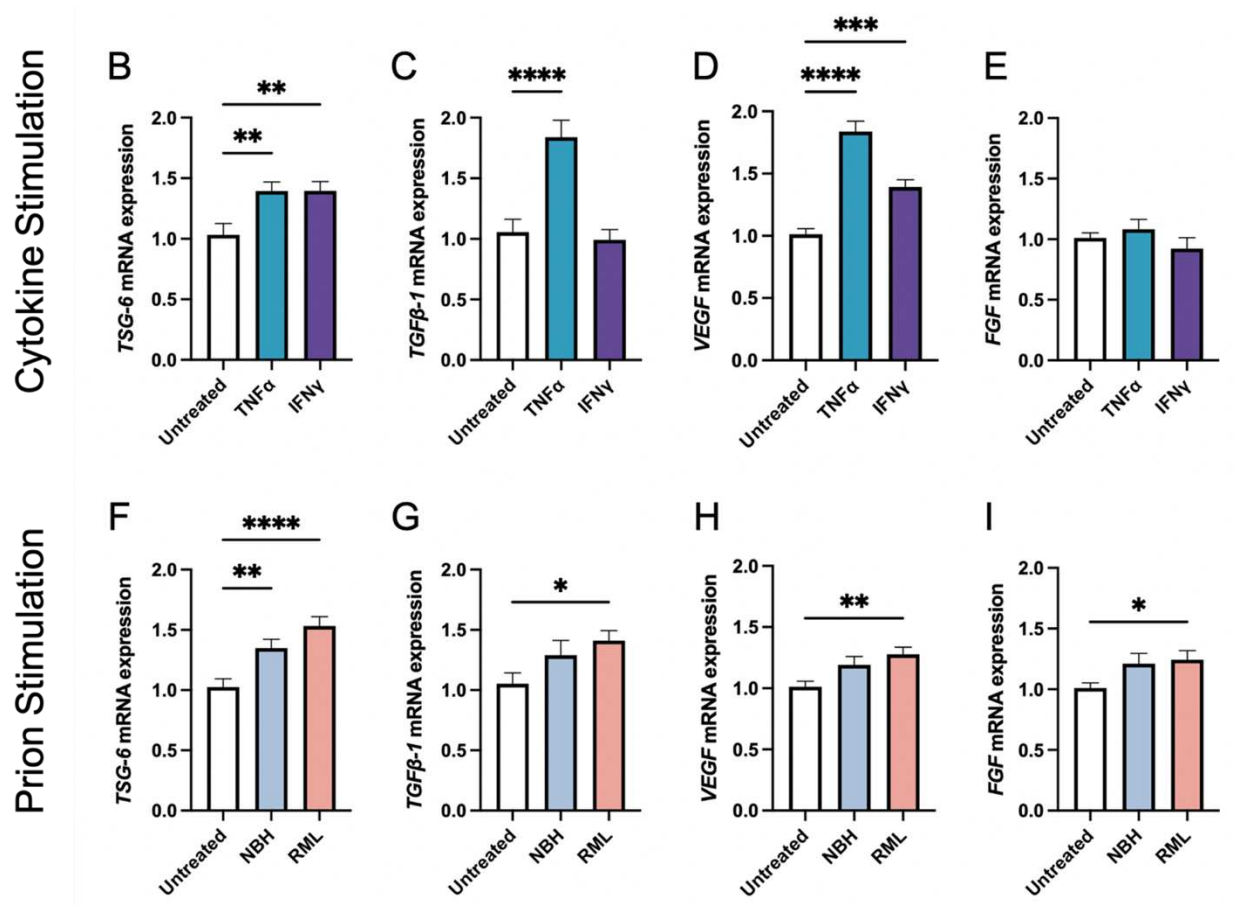

Figure 3.2. Stimulating AdMSCs with inflammatory cytokines and prion-infected brain homogenate for 24 hours increases production of anti-inflammatory molecules and growth factors. AdMSCs were incubated for 24-hours in media containing TNFα or IFNγ. These AdMSCs showed significant increase in mRNA expression levels for (A) *TSG-6*, (B) *TGFβ-1*, and (C) *VEGF*, but no changes in (D) *FGF.* AdMSCs were incubated for 24-hours in media containing NBH or RML-infected brain homogenates. In AdMSCs exposed to RML, a significant increase was seen in (E) *TSG-6*, (F) *TGFβ-1*, (G) *VEGF*, and (H) *FGF* mRNA. One-way ANOVA with post-hoc Tukey's test, *p<0.05, **p<0.01, ***p<0.001, ****p<0.0001, error bars = SEM. Combined data from four separate experiments, each with three technical replicates.

Stimulating AdMSCs with inflammatory cytokines and prion-infected brain homogenate for 24 hours increases production of anti-inflammatory molecules and growth factors

Our laboratory and others have demonstrated that stimulating MSCs with inflammatory molecules increases secretion of anti-inflammatory molecules and growth factors.[123,170,199] Here,

we demonstrate that stimulating AdMSCs for 24 hours with TNFα or interferon gamma (IFNγ) induces a 36%-fold increase of TNF-stimulated gene 6 (*TSG-6*) mRNA (Figure 3.2A; $p<0.01$). Stimulation with TNFα, but not IFNγ, causes a 78%-fold increase in transforming growth factor beta-1 (*TGFβ-1*) mRNA (Figure 3.2B; $p<0.0001$).[123] Stimulation with TNFα induced an 83%-fold increase, and stimulation with IFNγ induced a 38%-fold increase in vascular endothelial growth factor (*VEGF*) mRNA (Figure 3.2C; $p<0.0001$, $p<0.001$, respectively), but no changes were seen in fibroblast growth factor (*FGF*) mRNA (Figure 3.2D).

We also demonstrate that culturing AdMSCs in media containing 0.1% Rocky Mountain Laboratories (RML) strain mouse-adapted scrapie brain homogenate elicits a similar upregulation of genes for anti-inflammatory molecules and growth factors, suggesting that AdMSCs respond to factors in the prion-infected brain, such as damage-associated molecular patterns (DAMPs) and the cytokine milieu.[222,223] After 24 hours in media containing normal brain homogenate (NBH) or RML, AdMSCs increased expression of *TSG-6* mRNA by 32% and 51%-fold change from baseline, respectively (Figure 3.2E; $p<0.01$, $p<0.0001$, respectively). Treatment with RML, but not NBH, increased mRNA for *TGFβ-1* by 35%-fold (Figure 3.2F; $p<0.05$), *VEGF* by 27%-fold (Figure 3.2G; $p<0.01$), and *FGF* by 23%-fold(Figure 3.2H; $p<0.05$).

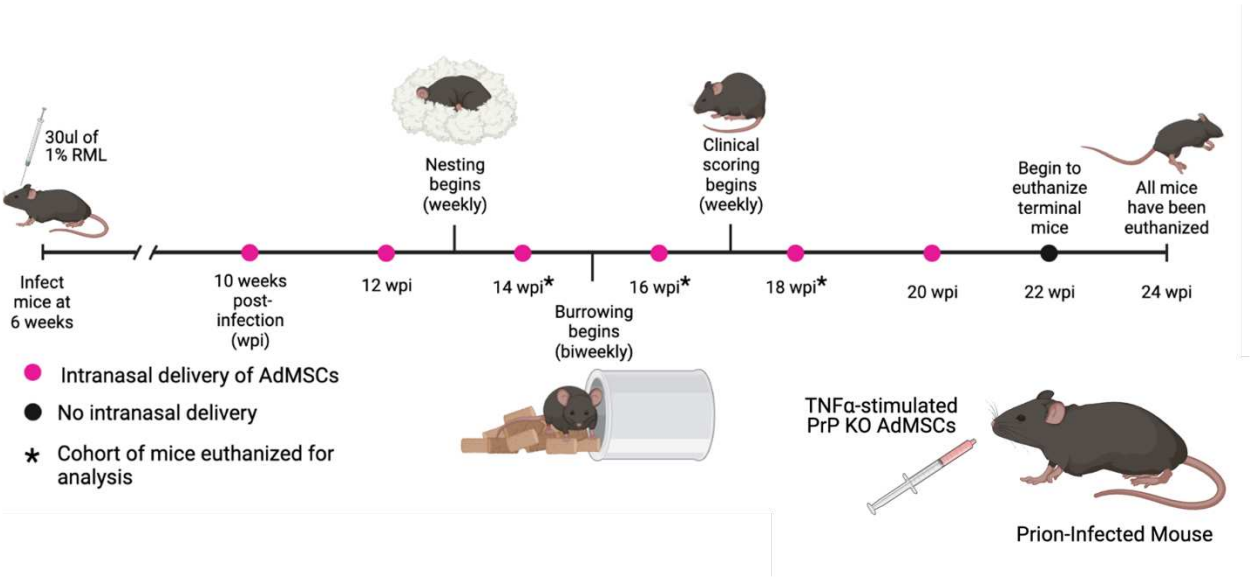

Figure 3.3. Prion-infected mice were treated with stimulated AdMSCs every two weeks. RML-infected mice received intranasal delivery of TNFα-stimulated PrP KO AdMSCs biweekly from 10 weeks post infection (wpi) to 20 wpi. Hippocampal-specific behavioral analyses, nesting and burrowing, were performed beginning at 13 wpi. Clinical signs were analyzed weekly beginning at 17 wpi until mice were euthanized. No changes in behavioral signs, clinical signs, or survival were observed between AdMSC-treated mice and PBS-treated controls (see Supplemental Figure 2). Graphic created with BioRender.com.

Prion-infected mice were treated with stimulated AdMSCs every two weeks

Mice received 30 µl of 1% RML mouse-adapted scrapie brain homogenate or NBH inoculated intracranially at 6 weeks of age. RML-infected mice received an intranasal delivery of $1x10^6$ PrP KO AdMSCs or vehicle (PBS) every two weeks beginning at 10 weeks post-infection (wpi) and continuing to 20 wpi (Figure 3.3). PrP KO AdMSCs were used instead of wild-type to eliminate any possibility of these cells becoming infected and further disseminating PrP^{Sc}, as expression of PrP is critical for cells to be infectable.[36,76] Prior to each intranasal delivery, AdMSCs were incubated in media containing 10ng/ml TNFα for 24 hours. We have demonstrated here (Figure 3.2) and previously that this induces increased expression of anti-inflammatory molecules and growth factors. After 24 hours, cells are sufficiently washed and TNFα is no longer detectable in the media,[123] eliminating any concern that it may be transferred into the brain when AdMSCs are intranasally delivered.

Hippocampal-associated behavioral analysis was used to monitor early signs of disease. Nesting began at 10 wpi, but data is only shown from 13 wpi to 22 wpi. A decline in nesting behavior was observed for the AdMSC-treated mice at 17 wpi ($p<0.01$). At 18 wpi, both AdMSC-treated and mock-treated animals showed decline in nesting behavior ($p<0.001$), and this was observed until mice were euthanized ($p<0.0001$). Meanwhile, NBH mice maintained perfect nests from 18 wpi until the termination of the study at 23 weeks (Supplemental Figure 3.2A). Burrowing began at 13 wpi and was repeated the following two weeks to allow for a "training period" for the mice, before being performed every two weeks. Decline in burrowing was seen for mock-treated ($p<0.001$) and AdMSC-treated mice ($p<0.05$) beginning at 17 wpi and continuing until burrowing was discontinued after 21 wpi ($p<0.0001$). NBH mice maintained healthy burrowing behavior through 21 weeks (Supplemental Figure 3.2B).

Early signs of clinical scores began for both mock- and AdMSC-treated mice at 17 wpi, but signs were not statistically significant compared to NBH mice until 21 wpi ($p<0.0001$) (Supplemental Figure 3.2C). Mice were euthanized when they showed a clinical score of 10, and all mice had been euthanized before 25 wpi. No changes in survival were seen between the mock- and AdMSC-treated mice, with a mean survival of 163 days for both (Supplemental Figure 3.2D). NBH mice remained healthy and were euthanized after all RML-infected mice had been euthanized. To determine the effects of intranasally-delivered AdMSCs throughout disease progression, a cohort of mice was sacrificed at 14 wpi (after 3 treatments), 16 wpi (after 4 treatments), and 18 wpi (after 5 treatments). The remainder of the mice received 6 treatments total and were euthanized when they showed significant clinical signs.

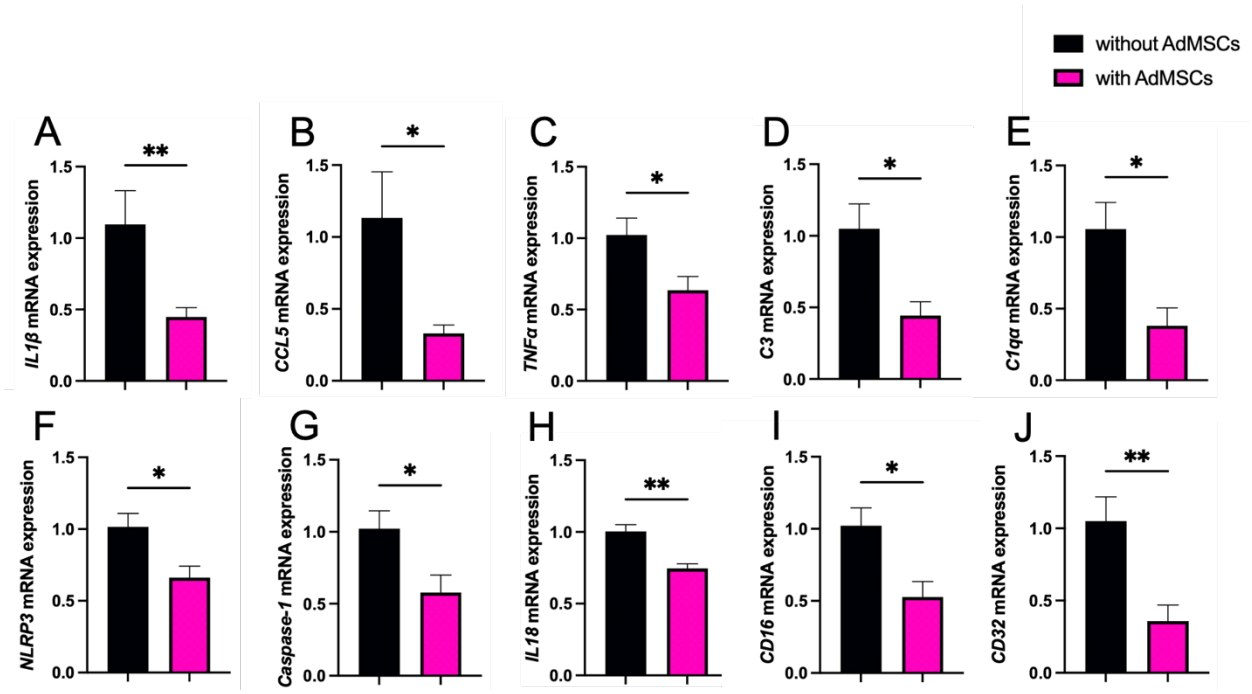

Figure 3.4. AdMSC treatment decreases inflammatory cytokine transcripts in the hippocampus at 16 weeks post infection (wpi). Hippocampal mRNA expression was decreased in animals treated with AdMSCs for (A) *IL1β*, (B) *CCL5*, (C) *TNFα*, (D) *C3*, (E) *C1qa*, (F) *NLRP3*, (G) *Caspase-1*, (H) *IL18*, (I) *CD16*, and (J) *CD32.* Hippocampi were analyzed from 10 animals, 6 AdMSC-treated and 4 PBS-treated controls. T-test with Welch's corrections, *p<0.05, **p<0.01, error bars = SEM.

AdMSC treatment decreases inflammatory cytokine transcripts in the hippocampus at 16 weeks post-infection (wpi)

mRNA levels of genes associated with prion disease were measured in hippocampi from mice at 16 wpi and 18 wpi. At 16 wpi, AdMSC treatment led to significant decreases in inflammatory genes and markers of astrogliosis. A 68.4%-fold decrease was seen in the inflammatory molecule interleukin 1 beta (*IL1β*) (Figure 3.4A; p<0.01), an 80.5%-fold decrease in chemokine ligand 5 (*CCL5*) (Figure 3.4B; p< 0.05), and a 38.8%-fold decrease in *TNFα* (Figure 3.4C; p<0.05). AdMSC treatment caused a 60.7%-fold decrease for complement component 3 (*C3*) (Figure 3.4D; p< 0.05), and a 67.5%-fold decrease in mRNA for the complement C1q subcomponent subunit A (*C1qa*) (Figure 3.4E; p<0.05), both of which are

known contributors to the development of neurotoxic reactive astrocytes.[45,49] AdMSCs induced changes in genes associated with the NLRP3 inflammasome pathway. A 35.3%-fold decrease was seen in mRNA for *NLRP3* with AdMSC treatment (Figure 3.4F; $p<0.05$). mRNA for *Caspase 1*, which is recruited and activated by the NLRP3 inflammasome, decreased by 44.3%-fold upon treatment (Figure 3.4G; $p< 0.05$). Recruitment of Caspase-1 by NLRP3 processes inactive pro-interleukin 18 (pro-IL18) and pro-IL1β to the active forms, IL18 and IL1β.[126] As it decreased for *IL1β*, mRNA for IL18 decreased by 25.7%-fold in AdMSC treated hippocampi (Figure 3.4H; $p<0.01$). Additionally, a 49.6%-fold decrease was shown in *CD16* (Fc gamma III receptor) (Figure 3.4I; $p< 0.05$) and a 69.2%-fold decrease for *CD32* (Fc gamma II receptor) (Figure 3.4J; $p<0.01$), two genes associated with M1 microglia.

No changes were seen in mRNA for interleukin 6 (*IL6*), chemokine ligand 2 (*CCL2*), inducible nitric oxide synthase (*iNos*) or *NF-κB1*, or in markers of M2 microglia, arginase-1 (*Arg-1*) or insulin-like growth factor (*Igf-1*) (Supplemental Figure 3.3). Additionally, no significant changes were seen in any of the genes analyzed in the hippocampi of mice at 18 wpi (Supplemental Figure 3.4).

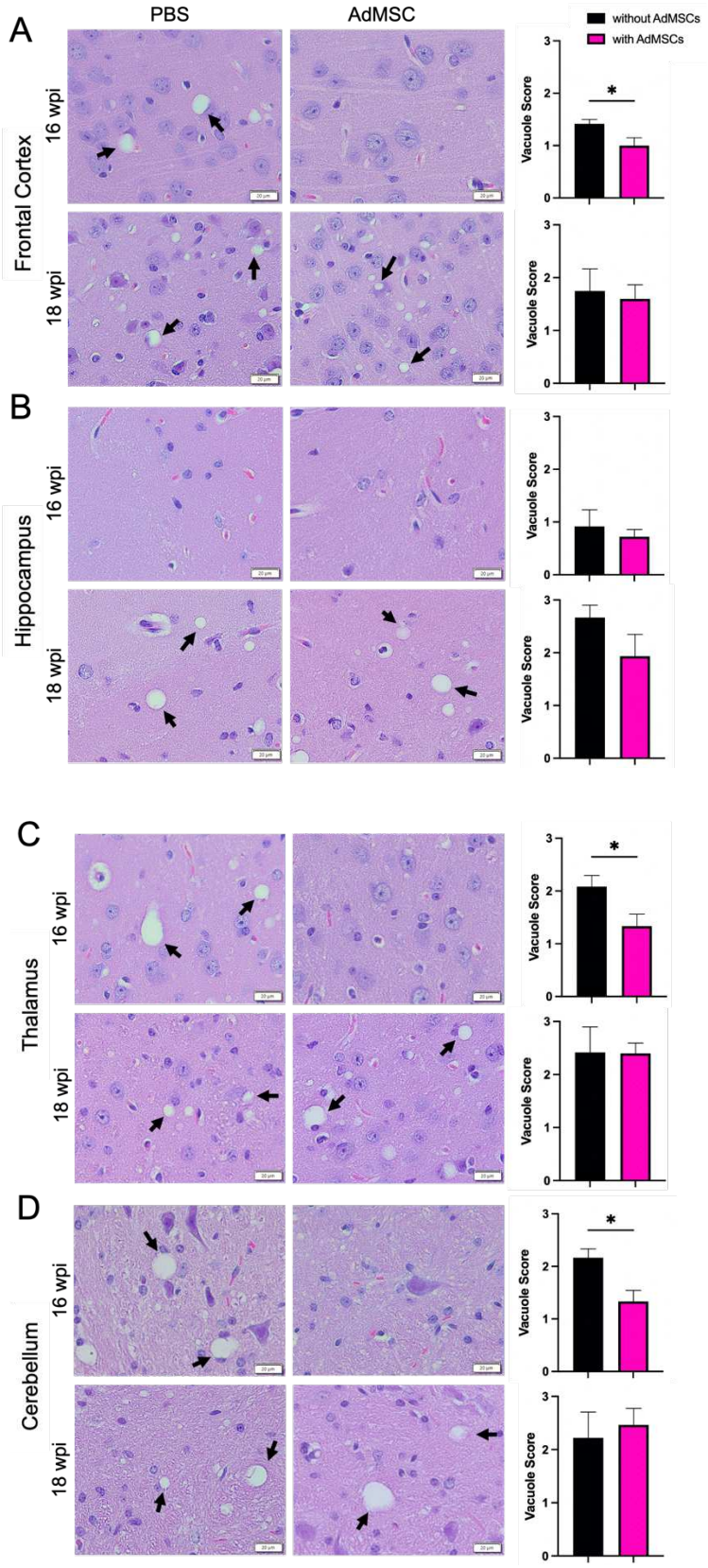
A
PBS
AdMSC
without AdMSCs
with AdMSCs
Frontal Cortex
16 wpi
18 wpi
Vacuole Score
*
B
Hippocampus
C
Thalamus
D
Cerebellum

Figure 3.5. Less vacuolization throughout the brain of AdMSC-treated mice at 16 weeks post infection (wpi). Vacuoles in the (A) frontal cortex, (B) hippocampus, (C) thalamus and (D) cerebellum were scored on a scale of 0-5 based on size and number. An average of three scores for each brain region was calculated for each animal. 16 wpi AdMSC-treated mice had decreased vacuoles in all brain regions except for the hippocampus. No differences in vacuolization were detected between treatment groups for 18 wpi animals. H&E stained brains were analyzed from 10 animals per timepoint, 6 AdMSC-treated and 4 PBS-treated controls. T-test with Welch's corrections, *$p<0.05$, error bars = SEM. 40x representative images, scale bar = 20 μm.

Less vacuolization throughout the brains of AdMSC-treated mice at 16 wpi

Fixed tissue was stained with hematoxylin and eosin and images of the frontal cortex, hippocampus, thalamus and cerebellum were taken. Three pathologists who were blinded to the treatment groups scored each brain region from 0 (no vacuolization) to 5 (severe vacuolization) based on size and number of vacuoles.[216-218] Significant vacuolization can be seen in the brains of terminal prion-infected mice in these brain regions, compared to healthy mice from age-matched mice that received NBH brain inoculum (Supplemental Figure 3.5; $p<0.0001$). At 16 wpi, brains with AdMSC treatment showed significantly less vacuolization in the frontal cortex (PBS mean = 1.41, SD = 0.167; AdMSC mean = 1.00, SD = 0.365), thalamus (PBS mean = 2.08, SD = 0.419; AdMSC mean = 1.33, SD = 0.558) and cerebellum (PBS mean = 2.17, SD = 0.333; AdMSC mean = 1.33, SD = 0.471) (Figure 3.5A-D; $p<0.05$). Interestingly, no differences were seen in vacuole severity in the hippocampus at this timepoint (PBS mean = 0.917, SD = 0.631; AdMSC mean = 0.722, SD = 0.328). No differences were seen in vacuolization at 18 wpi (Figure 3.5A-D), nor were there significant changes in vacuoles at 14wpi, prior to development of clinical signs or at terminal disease (data not shown).

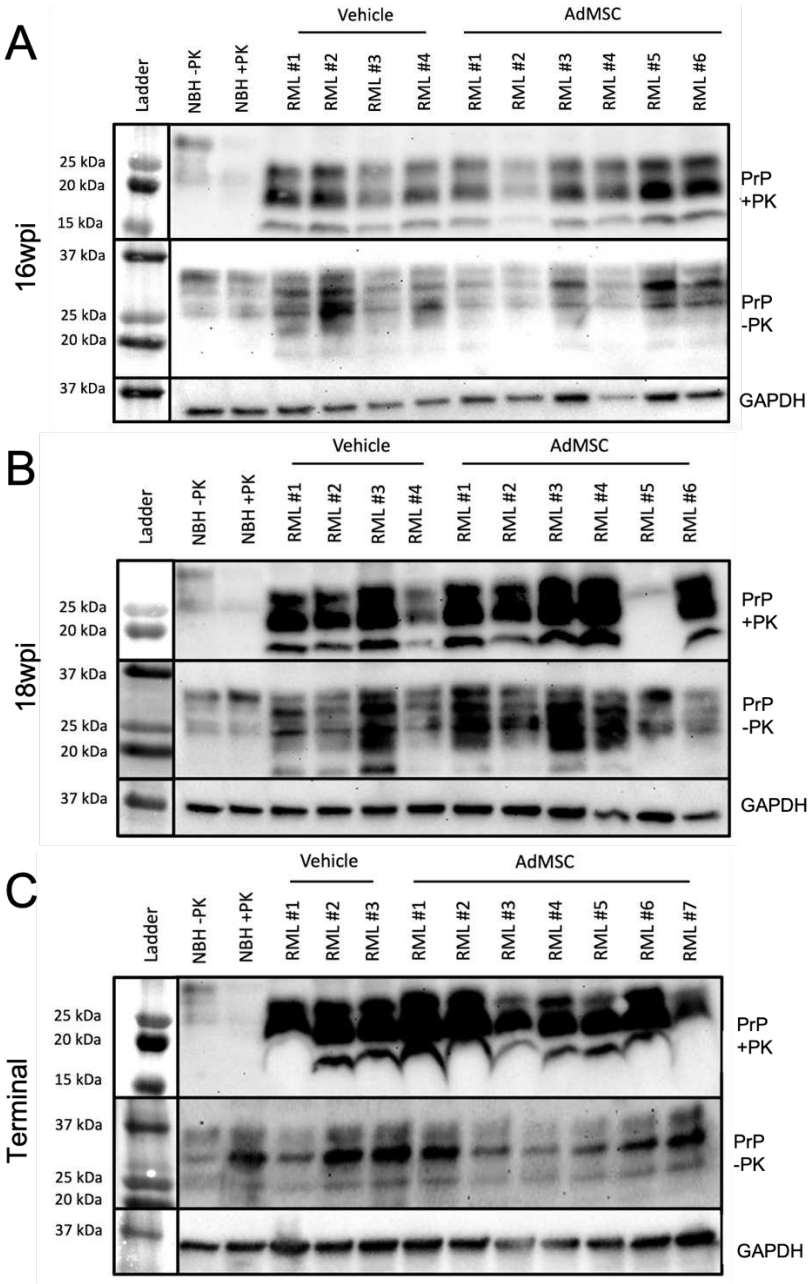

Figure 3.6. AdMSC treatment does not induce detectable changes in PrP^{Sc}. Western blots were used to compare both PrP^{Sc} (PK-resistant PrP) and total PrP (not PK-treated) between vehicle and AdMSC-treated mice at (A) 16wpi, (B) 18wpi and (C) terminal stages of disease with no detectable differences between treatments (see Supplemental Figure 6 for quantification). GAPDH is used as loading control. Brain homogenates were analyzed from 10 animals per timepoint, 6 AdMSC-treated and 4 PBS-treated controls (for terminal mice, 7 AdMSC-treated and 3 PBS-treated controls).

AdMSC treatment does not induce detectable changes in PrP^{Sc}

Brains from mice at 16 wpi, 18 wpi, and terminal stage disease were homogenized and analyzed via western blot to detect both total PrP and the disease-associated proteinase-K (PK) resistant infectious PrP (PrP^{Sc}). Equivalent amounts of protein were loaded and band intensity was analyzed in ImageJ. A Rout's test was used to identify outliers. One animal in the 18 wpi cohort (labeled RML #5) showed significantly lower PrP^{Sc} (but comparable PrP^{C}) to the rest of its cohort. This animal likely did not receive a full dose of RML brain homogenate when inoculated, and was therefore removed from all histological data analyses. Band intensity from all other brain samples was compared between treated and untreated groups (Supplemental Figure 3.6). Normal brain homogenate (NBH) with and without PK was used as a negative control. AdMSC treatment did not induce changes in either total PrP or PrP^{Sc} in 16 wpi (Figure 3.6A), 18 wpi (Figure 3.6B) or terminal brain homogenates (Figure 3.6C).

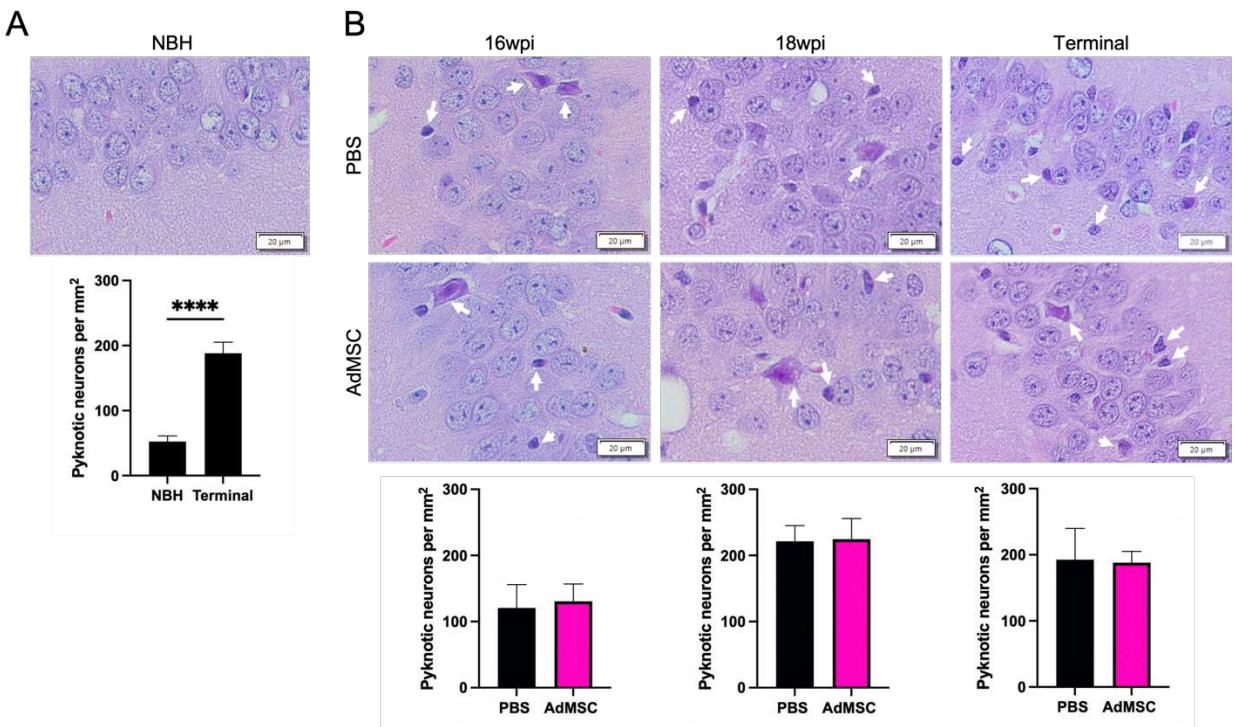

Figure 3.7. Death of hippocampal neurons is not prevented by AdMSC treatment. Swollen and pyknotic neurons in the CA1 region of the hippocampus were compared. (A) Significantly more pyknotic neurons were seen in terminally-infected mice when compared to age-matched NBH mice. (B) No changes were seen between AdMSC-treated and control mice at 16 wpi, 18 wpi or terminal stages of infection. Hippocampi were analyzed from 10 animals per timepoint, 6 AdMSC-treated and 4 PBS-treated controls. T-test with Welch's corrections, ****p<0.0001, error bars = SEM. IHC: 20x, IF: 40x representative images, scale bar = 20 μm.

Death of hippocampal neurons is not prevented by AdMSC treatment

Pyknotic neurons were assessed in tissue stained with hematoxylin and eosin. Specifically, both swollen/apoptotic and shrunken neurons were manually counted in the CA1 region of the hippocampus.[150,224,225] Significantly more neuronal death was seen in terminal mice regardless of treatment compared to NBH mice (Figure 3.7A; p<0.0001). AdMSC treatment did not induce changes in the number of pyknotic neurons at 16 wpi, 18 wpi or terminal stages of disease (Figure 3.7B).

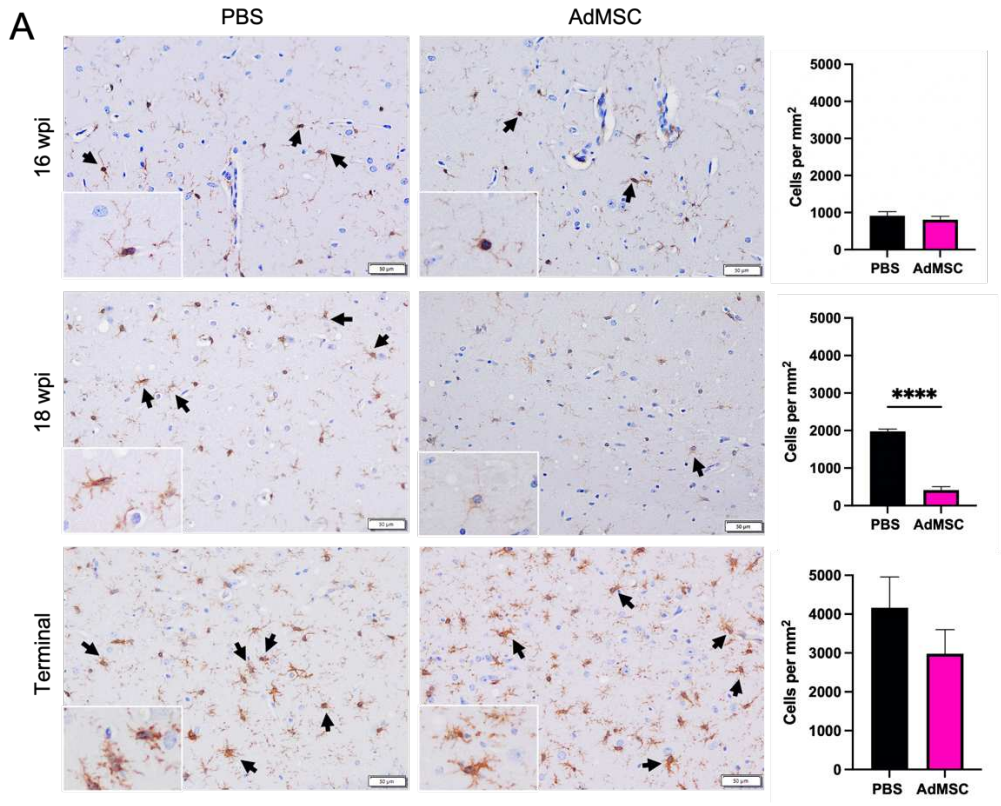

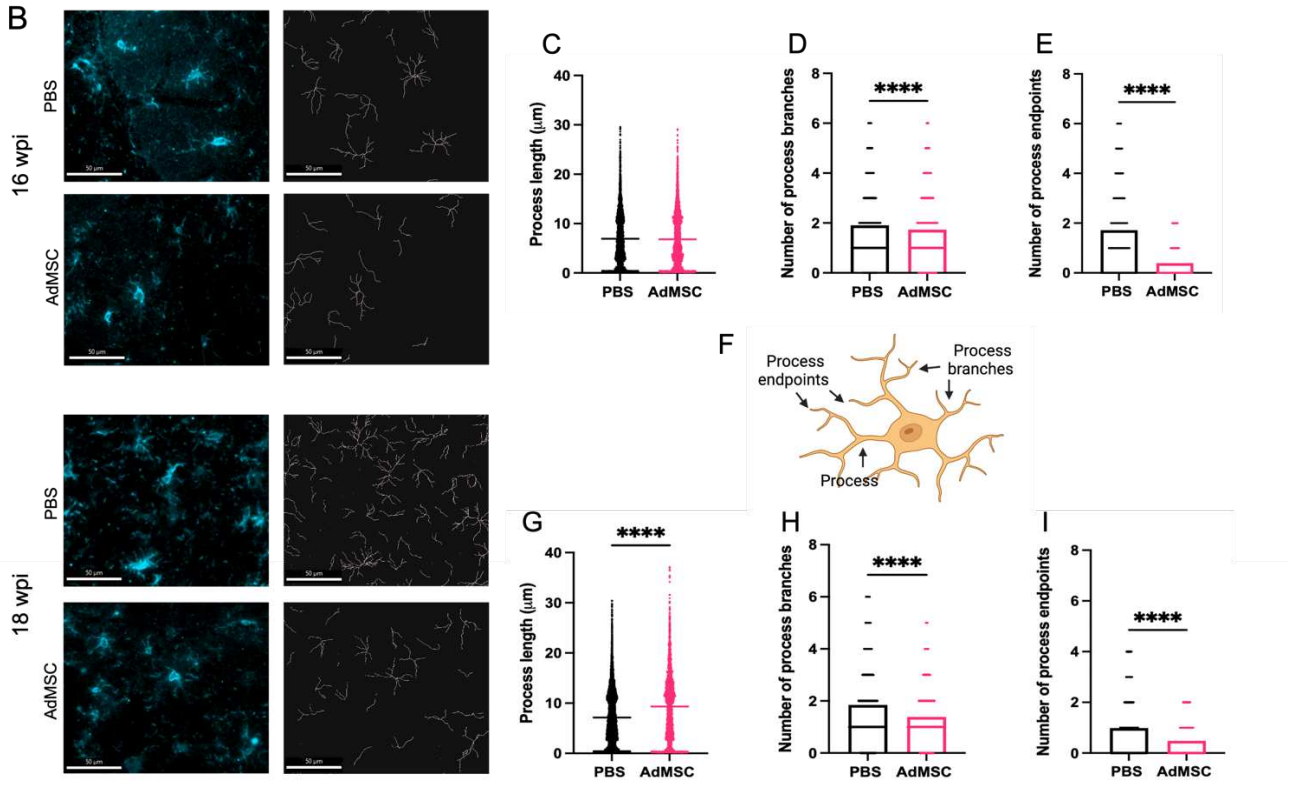

Figure 3.8. AdMSC treatment promotes ramified microglia in the hippocampus. (A) Counts of Iba1+ cells were performed in the hippocampus. (B) Skeletons of Iba1+ hippocampal cells were analyzed with IMARIS for mice at 16 weeks post infection (wpi) and 18 wpi. AdMSC-treated animals at 16 wpi had no change in process length, but (D) fewer process branches and (E) fewer process endpoints. (F) Illustration depicting processes, process branches, and process endpoints in microglial cell. AdMSC-treated animals at 18 wpi had (G) longer processes, and (H) fewer branches and (I) fewer endpoints. Hippocampi were analyzed from 10 animals per timepoint, 6 AdMSC-treated and 4 PBS-treated controls. T-test with Welch's corrections, ****$p<0.0001$, error bars = SEM. IHC: 20x, IF: 40x representative images, scale bar = 50 µm. Graphic created with BioRender.com.

AdMSC treatment promotes ramified microglia in the hippocampus

The marker Iba1 was used to stain and count microglia throughout the brain. Surprisingly, no changes were seen in microglia number at 16 wpi in treated mice. At this time point microglia remained sparse in the hippocampus. At 18 wpi, however, AdMSC-treated mice showed a significant decrease in microglia number in the hippocampus compared to PBS-treated controls (Figure 3.8A; $p<0.0001$). No differences were seen between treated and untreated mice in number of microglia in terminal mice, or between treatment groups in the frontal cortex,

thalamus or cerebellum (representative images of thalamic microglia are available in Supplemental Figure 7).

Morphology of hippocampal microglia was analyzed using IMARIS software (Figure 3.8B) to identify process length, number of process branches, and number of process endpoints for each cell (see Figure 3.8F for examples). Differences in microglia morphology were less visibly apparent in mice at 16 wpi. However, quantification with IMARIS demonstrated that although process length was equivalent between AdMSC-treated animals and controls, the number of process branches was significantly lower in AdMSC-treated microglia (PBS mean = 1.91, AdMSC mean =1.73, $p<0.0001$). This was also associated with fewer process endpoints (PBS mean = 1.72, AdMSC mean =0.39, $p<0.0001$). At 18 wpi, microglia from AdMSC-treated mice had longer processes (PBS mean = 7.16 μm, AdMSC mean =9.33 μm, $p<0.0001$), fewer process branches (PBS mean = 1.85, AdMSC mean =1.39, $p<0.0001$), and fewer process endpoints (PBS mean = 0.98, AdMSC mean =0.48, $p<0.0001$) (Figure 3.8C-I). Together, these data suggest that AdMSCs are inducing a phenotypic change in hippocampal microglia, promoting ramified, homeostatic microglia as opposed to activated, amoeboid microglia.[55]

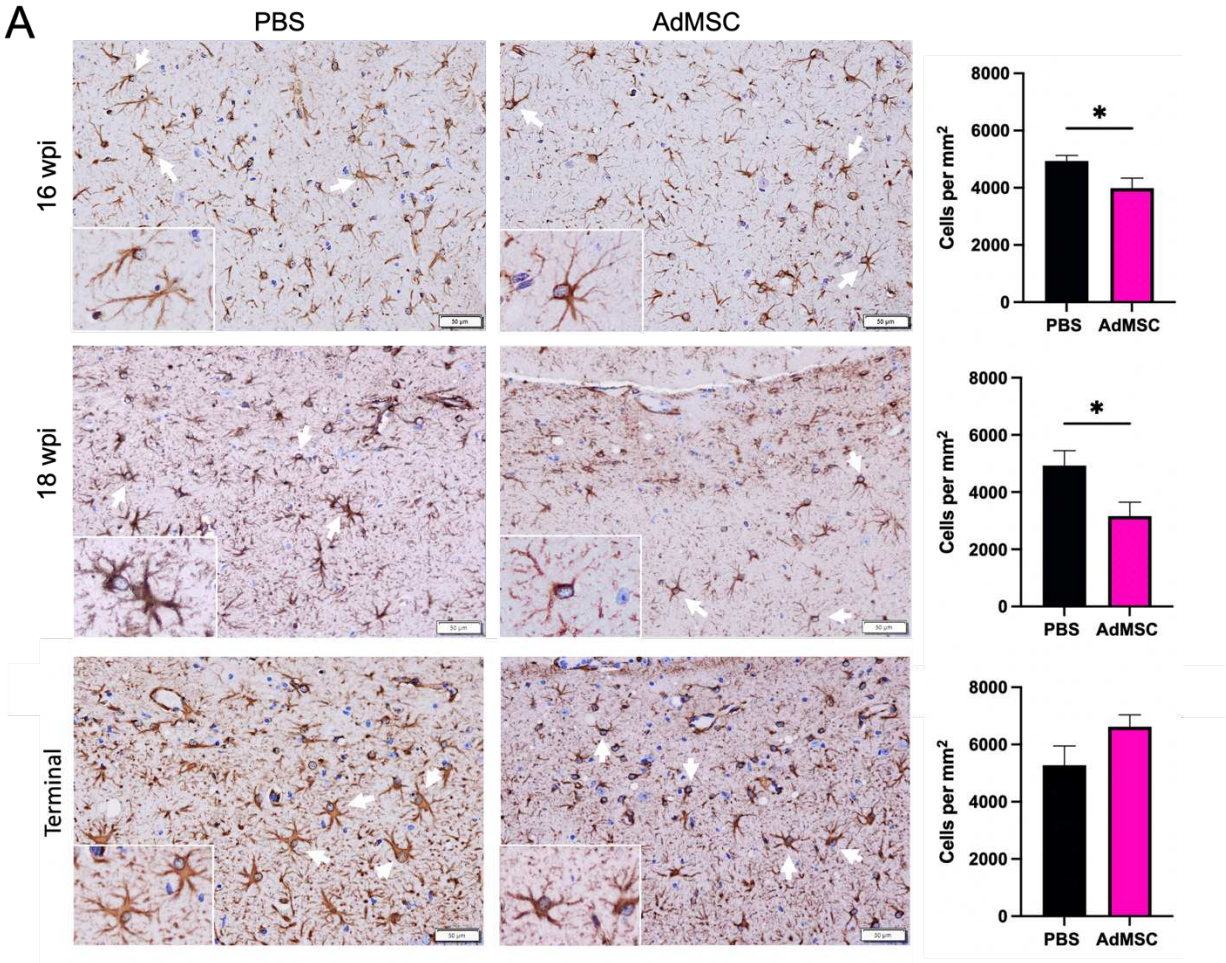
A
PBS
AdMSC
16 wpi
18 wpi
Terminal
Cells per mm²
8000
6000
4000
2000
0
*
PBS
AdMSC

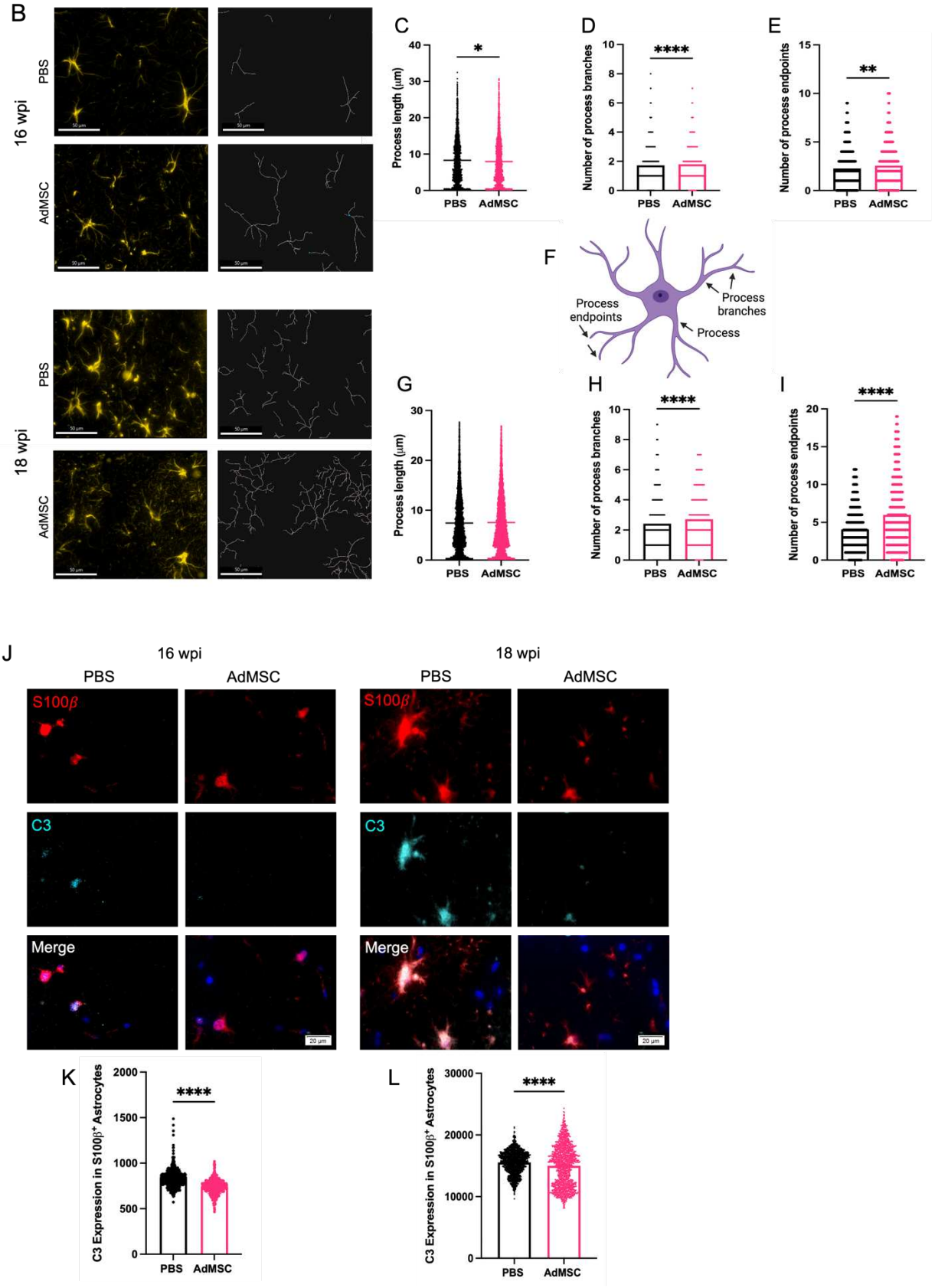
B
16 wpi
PBS
AdMSC
18 wpi
PBS
AdMSC
C
Process length (μm)
*
PBS
AdMSC
D
Number of process branches
****
PBS
AdMSC
E
Number of process endpoints
**
PBS
AdMSC
F
Process endpoints
Process branches
Process
G
Process length (μm)
PBS
AdMSC
H
Number of process branches
****
PBS
AdMSC
I
Number of process endpoints
****
PBS
AdMSC
J
16 wpi
18 wpi
PBS
AdMSC
PBS
AdMSC
S100β
C3
Merge
S100β
C3
Merge
K
C3 Expression in S100β+ Astrocytes
****
PBS
AdMSC
L
C3 Expression in S100β+ Astrocytes
****
PBS
AdMSC

Figure 3.9. The pan-astrocyte marker glial fibrillary acidic protein (GFAP) was used to stain and count astrocytes throughout the brain. In mice that received intranasal delivery of AdMSCs, significantly fewer astrocytes were seen in the hippocampus at both 16 wpi and 18 wpi (Figure 3.9A; $p<0.05$), but no differences were seen in terminal mice. No differences were seen between treated and untreated mice in number of GFAP+ astrocytes in the frontal cortex, thalamus or cerebellum (representative images of thalamic astrocytes are available in Supplemental Figure 3.8).

Morphology of hippocampal GFAP+ astrocytes was analyzed using IMARIS software (Figure 3.9B) to identify process length, number of process branches, and number of process endpoints for each cell (see Figure 3.9F for examples). At 16 wpi, astrocytes from AdMSC-treated mice had slightly shorter processes (PBS mean = 8.30 μm, AdMSC mean =7.95 μm, $p<0.05$), more process branches (PBS mean =1.724, AdMSC mean =1.793, $p<0.0001$), and more process endpoints (PBS mean =2.276, AdMSC mean =2.565, $p<0.01$). At 18 wpi there was no difference in process length between treatment groups. AdMSC-treated mice had significantly more astrocyte process branches (PBS mean =2.42, AdMSC mean =2.71, $p<0.0001$), and process endpoints (PBS mean =4.05, AdMSC mean =5.99, $p<0.0001$) (Figure 3.9C-I). Together, these data suggest that AdMSCs are inducing a phenotypic change in hippocampal astrocytes, promoting a homeostatic, neuroprotective phenotype.

Colocalization of S100β and the complement protein C3 is a marker for a subset of reactive neurotoxic astrocytes in a variety of neurodegenerative diseases.[45] The mean fluorescence intensity of C3 in S100β+ cells was quantified in the hippocampus of mice at 16 wpi and 18 wpi. At both timepoints, significantly less C3 was identified in animals that had been treated with AdMSCs (Figure 3.9J-L; $p<0.0001$), suggesting that AdMSCs are decreasing the number of reactive astrocytes in the hippocampus.

Discussion

Mesenchymal stromal cells (MSCs) can migrate toward prion-infected brain homogenate *in vitro*.[123,160] In this study, the therapeutic capacity of intranasal delivery of AdMSCs was investigated in mice inoculated with mouse-adapted scrapie prions. We labeled AdMSCs with a fluorescent, lipophilic dye called DiD and intranasally delivered them into mice with RML scrapie at 18 wpi. We removed the brains from a cohort of mice at 48 hours and 7 days and found areas of DiD+ cells in approximately one out of four brains (Figure 3.1). Assessment of sagittal brain sections identified DiD+ cells in the cortex, hippocampus, thalamus and cerebellum of animals at both 48 hours and 7 days post-delivery, suggesting that AdMSCs delivered intranasally can migrate throughout the brain and remain for at least 7 days (Table 3.2). DiD+ cells assessed in the hippocampus of mice at 48 hours post-delivery were also positive for Oct3/4 and Vimentin, two markers of AdMSCs.[123]

MSCs are known to respond to an inflammatory environment by producing anti-inflammatory and protective factors. To mimic the inflammatory environment of the prion-infected brain, AdMSCs were incubated in media containing either inflammatory cytokines TNFα or IFNγ, or brain homogenate from terminally-infected mice with RML-scrapie for 24 hours. Both cytokines and RML brain homogenates resulted in an upregulation in *TSG-6, TGFβ1, VEGF* and *FGF* (Figure 3.2). TSG-6 is an immunomodulator produced by MSCs and has been linked to decreasing NF-κB and other inflammatory signaling in glia, and reprogramming M1 microglia to an M2 phenotype.[161,163,203] TGFβ1 promotes neurogenesis by promoting quiescent microglia in mouse models of prion disease.[89,226] VEGF promotes angiogenesis and tissue repair and decreases inflammatory cytokines in the brain,[227] and FGF downregulates NF-κB signaling in microglia and decreases astrogliosis in models of traumatic

brain injury.[228,229] Together, this data suggests that stimulation of AdMSCs with inflammatory cytokines such as TNFα increases their production of protective molecules. The exact factors that AdMSCs are responding to in crude brain homogenate from RML-infected animals is unclear, although we hypothesize it is a combination of DAMPs and inflammatory cytokines.[170,199,222,223] Our data suggests that, when delivered intranasally, stimulated AdMSCs will migrate to the brain of prion-infected mice and secrete protective, anti-inflammatory factors. They can remain in the brain for at least 7 days, and during this time will continue producing protective factors in response to the cytokine milieu in the prion-infected brain.

Intranasal delivery of AdMSCs was performed every other week on RML-infected mice, beginning at 10 wpi and ending at 20 wpi (Figure 3.3). Prior to delivery, AdMSCs were stimulated for 24 hours with TNFα to increase production of anti-inflammatory genes,[123] and to promote homing to inflammatory tissue.[170,200,201] mRNA analysis of the hippocampus in mice at 16 wpi and 18 wpi was performed (after 4 or 5 AdMSC deliveries, respectively). Mice at 16 wpi that received AdMSCs demonstrated a significant decrease in the inflammatory cytokines *IL1β, CCL5* and *TNFα,* as well in the complement proteins *C3* and *C1qa* which are associated with reactive astrocytes and phagocytic microglia.[45,49,81] AdMSC treatment decreased mRNA transcript levels for genes associated with the NLRP3 inflammasome, *NLRP3, Caspase-1* and *IL-18*, which have been implemented in *in vitro* models of prion infection.[128,130] *CD16* and *CD32,* two markers of M1 microglia, were also decreased at 16 wpi in AdMSC-treated hippocampi, however no changes were seen in markers for M2 microglia (Figure 3.4). Interestingly, no significant changes were seen in mRNA transcript levels in the brains of mice at 18 wpi, despite cellular changes being apparent at this timepoint (Figures 3.8 and 3.9), suggesting that AdMSCs only regulated mRNA expression for these genes early in disease (Supplemental Figure 3.4).

Astrogliosis, neuronal loss, and the development of spongiform tissue throughout the brain are hallmarks of prion diseases, and though poorly understood, the development of vacuoles is indirectly attributed to neuronal death.[230] Both size and quantity of vacuoles were assessed to score spongiform development in the frontal cortex, hippocampus, thalamus and cerebellum. Interestingly, a significant decrease in vacuolization was only seen in the frontal cortex, thalamus and cerebellum of AdMSC-treated mice at 16 wpi, not in the hippocampus (Figure 3.5). Changes in mRNA expression and astrocyte and microglia morphology (described below) were seen in the hippocampus at this time point, suggesting that inflammation and astrogliosis may be separate from the development of vacuoles. It was recently reported that prion-induced depletion of the phosphoinositide kinase PIKfyve causes vacuolation in prion-infected cells, neurons and brains.[5] Heterogeneous PIKfyve depletion during prion infection and AdMSC treatment may uncouple these prion disease processes, or the timing of them.

The number of microglia was assessed throughout the brain using Iba1 staining. Significantly fewer microglia were seen in the hippocampus of mice treated with AdMSCs at 18 wpi (Figure 3.8). The visual appearance of these microglia suggests a homeostatic quiescent phenotype,[231] with longer and fewer processes, whereas the microglia of vehicle-treated mice have more and shorter processes and appear amoeboid, indicative of an activated phenotype.[52,232] Skeletonization of Iba1+ microglia in the hippocampus demonstrated a significant decrease in process branch number and process endpoint number with AdMSC treatment at both 16 and 18 wpi, in addition to significantly longer processes in microglia at 18 wpi (Figure 3.8). Together, these data suggest that intranasally-delivered AdMSCs polarize microglia towards a ramified, neuroprotective phenotype. The ability of AdMSCs to reprogram microglia has been demonstrated by our lab in vitro using BV2 microglia.[123] Additionally, it has been shown with

intracranially-delivered bone marrow-derived or compact bone-derived MSCs in the context of prion disease and other neuroinflammatory diseases.[160,177,203] Interestingly, a decrease in markers of M1 microglia, *CD16* and CD32, was only observed in mice treated with AdMSCs at 16 wpi (Figure 3.4), but not at 18wpi (Supplemental Figure 3.4), and no changes are seen in *Arg-1* or *Igf-1* mRNA (Supplemental Figure 3.3), two markers of M2 microglia. These observations suggest that although AdMSCs promote polarization of microglia toward a homeostatic state, it is not characteristic of the classic M2 phenotype. Further investigation is required to fully characterize these microglia.

The pan-astrocyte marker GFAP was used to quantify astrocyte numbers throughout the brain. A decrease in GFAP+ astrocytes was seen in the hippocampus of AdMSC-treated mice at 16 wpi and 18 wpi (Figure 3.9). At both timepoints, GFAP+ astrocytes from AdMSC-treated animals appear star-like with more branches, indicative of homeostatic astrocytes. Astrocytes from vehicle controls appear amoeboid, suggesting that they are activated, characteristic of hippocampal astrocytes in prion-infected mice.[73] Skeletonization analyses of these cells revealed significantly more process branches and terminal endpoints in those from AdMSC-treated animals, indicative of a less reactive phenotype. AdMSC treatment decreased C3 expression in S100β+ astrocytes, further suggesting that AdMSCs limit astrogliosis in the hippocampus. Neurotoxic, formerly called A1, astrocytes upregulate C3 in prion diseases and other neuroinflammatory and neurodegenerative diseases.[45,49]

Early stages of prion pathogenesis include astrogliosis and the activation of microglia and associated inflammation, followed by detectable accumulation of PrP^{Sc}, synaptic dysfunction and neuronal cell death.[64,72,150,182] The neurotoxic agent in prion disease has not been fully elucidated. PrP^{Sc} itself does not kill neurons in standard 2D cell culture models, suggesting that involvement

of other cell types is critical for neurotoxicity.[97] *In vivo* studies that modulate expression and phenotypes of microglia and astrocytes demonstrate that these cells play a dual role, contributing to both attenuation of disease as well as neurotoxicity.[49,75,91,92] We have demonstrated that AdMSCs can modulate transcript expression of markers of astrogliosis and inflammation early in prion disease, dampen activation of microglia and alleviate neurotoxic morphology in astrocytes in the hippocampus of prion-infected mice. However, we found no evidence that AdMSCs prevent neuronal loss in the hippocampus (Figure 3.7), which was consistent with behavioral assessments, clinical scores and survival (Supplemental Figure 3.2).

Our in vitro analysis of AdMSCs suggest that they decrease astrogliosis but have no effect on PrP^{Sc} accumulation in glial cells.[123] Analysis of brain homogenate via western blot demonstrated similar findings, as there were no changes in either PK-resistant PrP^{Sc} or total PrP (Figure 3.6). These findings suggest that AdMSCs have no effects on PrP^{Sc} accumulation when delivered intranasally. The requirement of PrP^{C} expression in neurons for neuronal death to occur [38,39,76] suggests that targeting PrP^{Sc} may be critical to prevent neurodegeneration. Although AdMSCs demonstrated effective attenuation of reactive astrocytes and reprogramming of microglia, the burden of prion aggregation was ultimately overpowering.

Bi-weekly administration of AdMSCs beginning at 10 weeks after prion infection may not be frequent or early enough to halt irreversible neuronal loss. We showed that intranasally-delivered AdMSCs are detectable in the brain using our imaging methods at 7 days, but not after 14 days (Figure 3.1). Prion-induced neurodegeneration is rapid, with animal models succumbing to disease within weeks after development of behavioral and clinical signs. Moreover, once animals reached late stages of disease, undergoing anesthesia required for intranasal delivery became too stressful and potentially lethal, so treatments were stopped after 20 wpi. Effective AdMSC

therapy for prion disease may require prophylactic and more frequent treatment to prevent the astrocyte induced inflammation that precedes, and may trigger, later pathologic processes and signs of prion diseases. Intranasally-delivered AdMSCs do not decrease PrP^{Sc} accumulation directly or indirectly, nor do they prevent hippocampal neuronal loss or vacuole development at late stages of disease. Together, these findings suggest that intranasal delivery of AdMSCs alone may not be an effective therapeutic to prevent prion-induced neurodegeneration, particularly in this aggressive model of intracranially-inoculated RML-scrapie. Studies are underway to assess the benefits of AdMSCs delivered intranasally or intracranially prior to disease onset in a mouse model of a human genetic prion disease.

We demonstrate the ability of AdMSCs to modulate astrogliosis through the relatively non-specific but therapeutically relevant delivery method of intranasal injection. The remarkable ability of these cells to migrate to the prion-infected brain, produce cytokines and growth factors, and to attenuate neurotoxic astrogliosis and restore microglia to a homeostatic, ramified phenotype, suggests an appeal for refinement of this therapeutic approach. A current avenue of interest is the utilization of extracellular vesicles (EVs) derived from mesenchymal stromal cells.[207,214] EVs are widely considered to be responsible for trafficking and delivering MSC-derived paracrine modulators. Their compact size allows them to more effectively cross the blood-brain barrier. EVs have a long half-life, and a cell-free therapy poses no threat of tumor development. MSC-derived EVs naturally contain unique arrays of neuromodulators, immune mediators, growth factors, and microRNAs that have been shown to inhibit aggregation of proteins such as amyloid-β and α-synuclein. Moreover, purified EVs can be modulated to contain specific cargo loads.[233,234] Further investigation is required to identify specific MSC-derived molecules that mediate astrogliosis, and to optimize stimulation or "priming" of MSCs to

promote optimal EV conditions to combat neurodegenerative diseases such as prion disease. The ideal treatment for prion disease would include a regulator of astrogliosis and inflammation, in combination with a therapeutic that can ameliorate PrP^{Sc} accumulation and restore neuronal health.

Table 3.1. Primer sequences for reverse transcriptase quantitative PCR

Gene	Forward primer	Reverse primer
TSG-6	GCTACAACCCACATGCAAAGGA	CCGTACTTGAGCCGAATGTGC
TGFβ1	CTTCAATACGTCAGACATTCGGG	GTAACGCCAGGAATTGTTGCT
VEGF	ACTTTCTGCTCTCTTGGGTGC	GCAGCCTGGGACCACTTG
FGF1	AAAGTGCGGGCGAAGTGTAT	CTCATTTGGTGTCTGCGAGC
IL1β	GCAGCAGCACATCAACAAG	CACGGGAAAGACACAGGTAG
CCL5	TTAAAAACCTGGATCGGAACCAA	TCGAGTGACAAACACGACTGC
TNFα	CCGATGGGTTGTACCTTGTC	AGATAGCAAATCGGCTGACG
C3	GAGCGAAGAGACCATCGTACT	TCTTTAGGAAGTCTTGCACAGTG
C1qa	AGAGAGGGGAGCCAGGAGC	CATTGCCAGGTTTGCCAGGG
NLRP3	CCTGGGGGACTTTGGAATCA	GACAACACGCGGATGTGAGA
Caspase-1	AACCACTCGTACACGTCTTGC	ATCCTCCAGCAGCAACTTCA
IL18	GACTCTTGCGTCAACTTCAAGG	GTTGTCTGATTCCAGGTCTCCA
CD16	TTTGGACACCCAGATGTTTCAG	GTCTTCCTTGAGCACCTGGATC
CD32	AATCCTGCCGTTCCTACTGATC	GTGTCACCGTGTCTTCCTTGAG
IL-6	CTGCAAGAGACTTCCATCCAG	AGTGGTATAGACAGGTCTGTTGG
CCL2	TTAAAAACCTGGATCGGAACCAA	GCATTAGCTTCAGATTTACGGGT
iNos	CCCTTCAATGGTTGGTACATGG	ACATTGATCTCCGTGACAGCC
NF-κB1	GTGGAGGCATGTTCGGTAGT	CCTGCGTTGGATTTCGTGAC
Arg-1	CGTAGACCCTGGGGAACACTAT	TCCATCACCTTGCCAATCCC
Igf-1	AAAGCAGCCCGCTCTATCC	CTTCTGAGTCTTGGGCATGTCA
β-actin	GCTGTGCTATGTTGCTCTAG	CGCTCGTTGCCAATAGTG

Table 3.2. DiD+ cells in brain regions after intranasal delivery

	Cortex	Hippocampus	Thalamus	Cerebellum
Mock-Labeled	0/2	0/2	0/2	0/2
DiD - 48 Hours	5/5	4/5	4/5	2/5
DiD – 7 Days	4/5	5/5	4/5	2/5

Supplemental Data

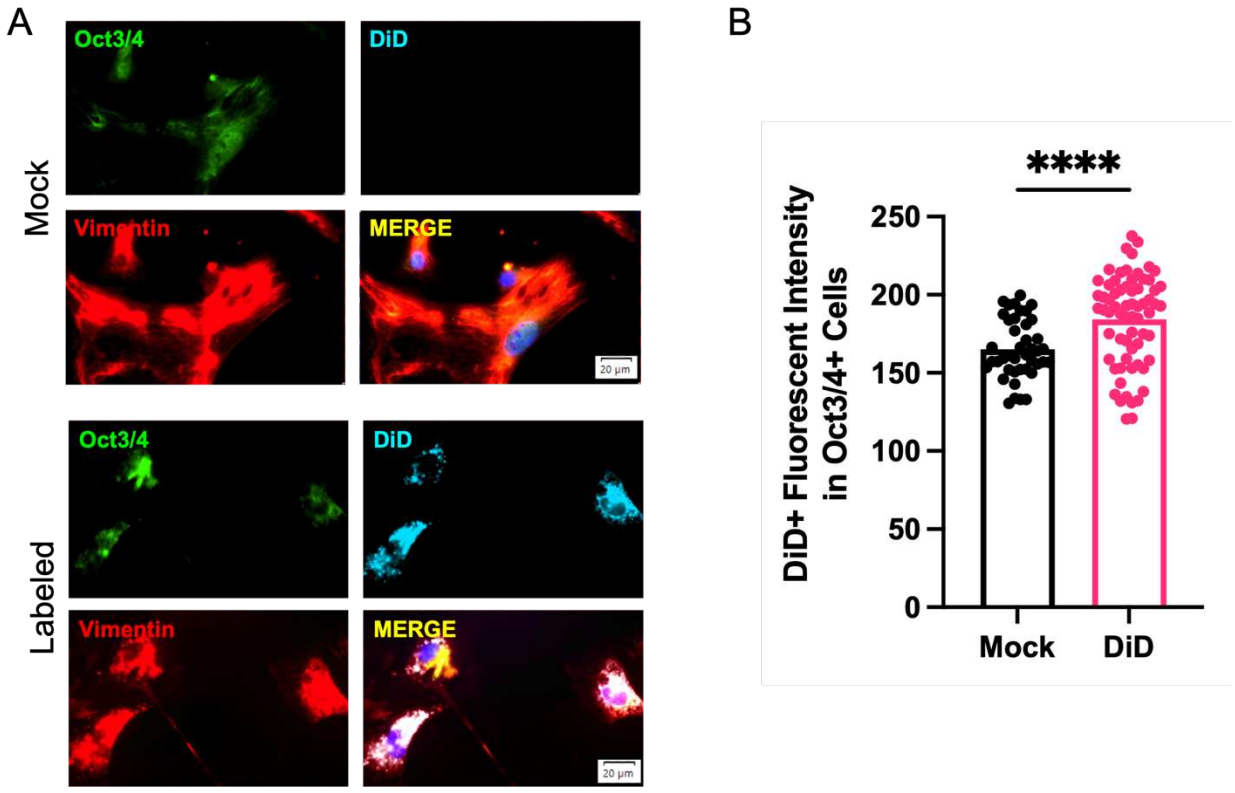

Supplemental Figure 3.1. AdMSCs can be labeled with DiD and stain positive for Oct3/4 and Vimentin in vitro and *in vivo*. (A) AdMSCs were labeled with DiD or mock (PBS) and incubated on chamber slides for 48 hours prior to staining with Oct3/4 and vimentin. (B) DiD fluorescence was measured in Oct3/4+ cells in the hippocampus and thalamus of mice that received intranasally delivered mock- or DiD-labeled AdMSCs (arbitrary units). T-test with Welch's corrections, ****p<0.0001, error bars = SEM.

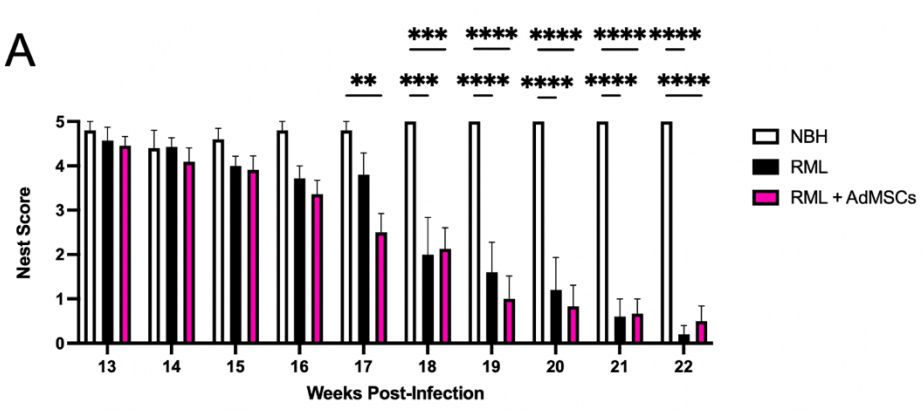
A
Nest Score
Weeks Post-Infection
NBH
RML
RML + AdMSCs

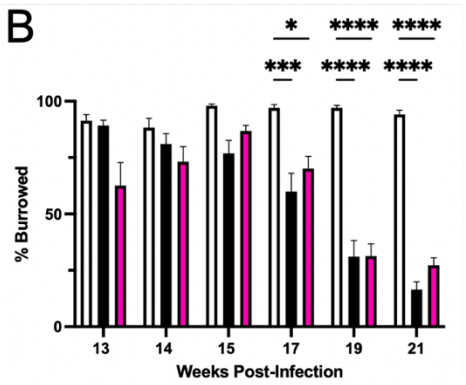
B
% Burrowed
Weeks Post-Infection

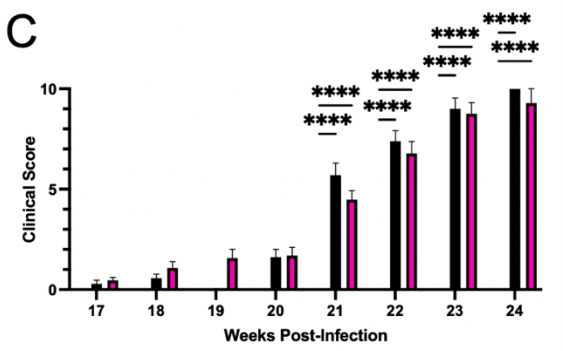
C
Clinical Score
Weeks Post-Infection

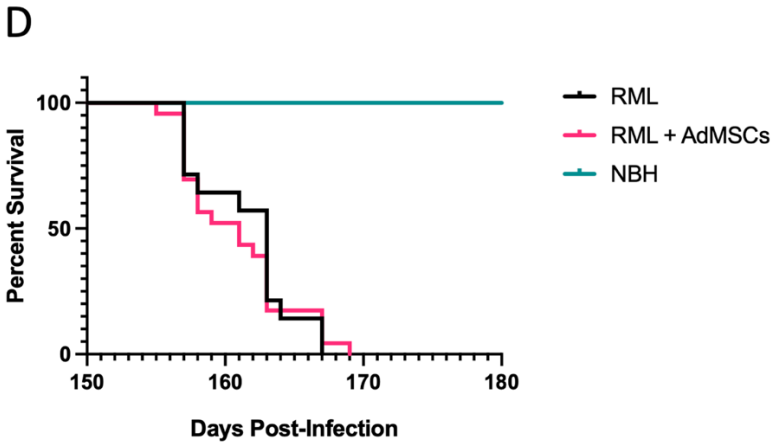
D
Percent Survival
Days Post-Infection
RML
RML + AdMSCs
NBH

Supplemental Figure 3.2. Intranasal delivery of AdMSCs did not affect behavioral, clinical signs or survival of prion-infected mice. (A) Mice were analyzed weekly for their ability to build nests and (B) bi-weekly for their ability to burrow beginning at 13 wpi. (C) Clinical scoring was performed weekly beginning at 17wpi. (D) Mice were euthanized after scoring a 10 or higher. Median survival was 163 days for both vehicle and AdMSC-treated animals. Survival curves were compared using a log-rank test. Behavioral and clinical signs were compared between groups using a Two-way ANOVA with post-hoc Tukey's test, *p<0.05, **p<0.01, ***p<0.001, ****p<0.0001, error bars = SEM.

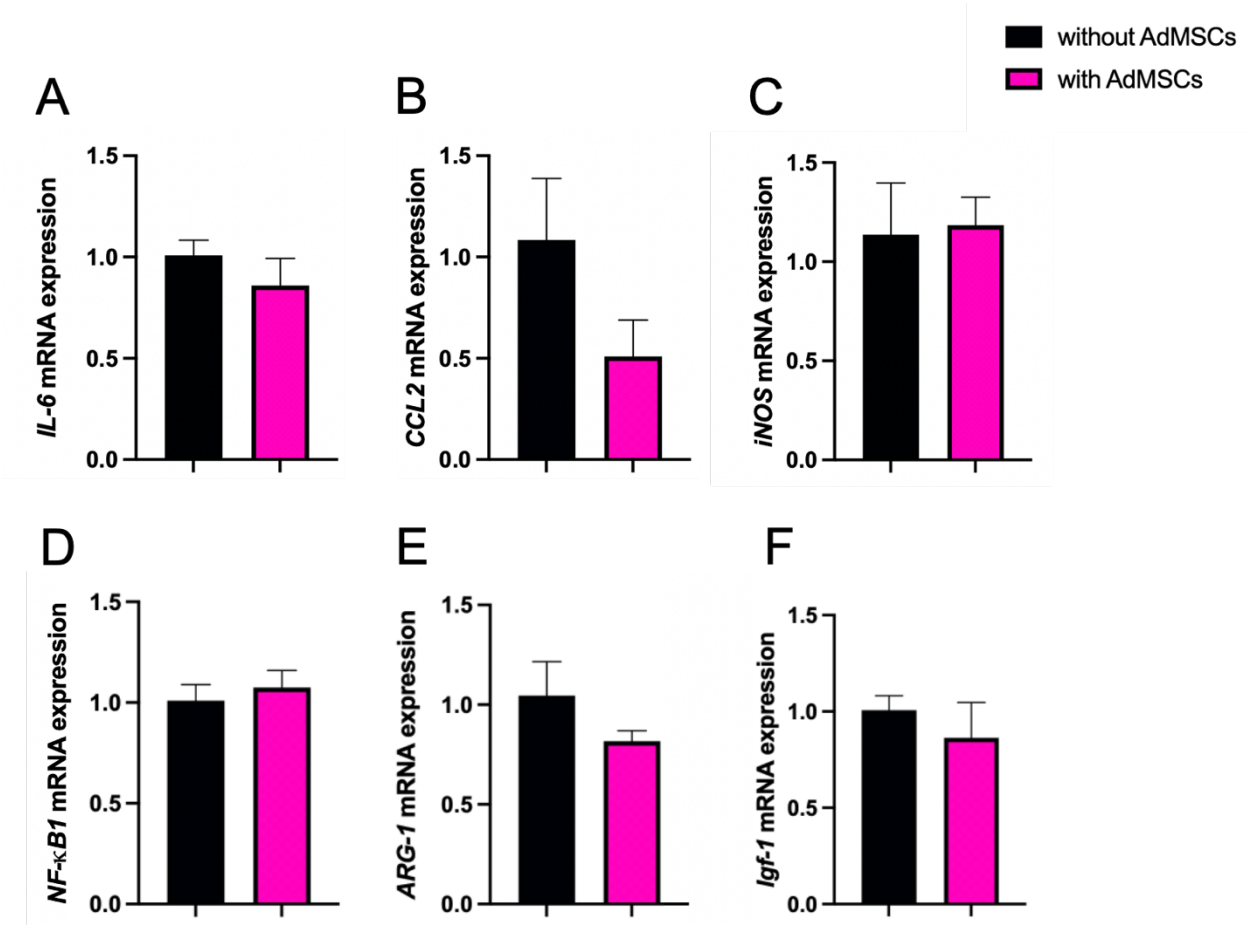

Supplemental Figure 3.3. AdMSC treatment does not induce changes in some inflammatory cytokine transcripts in the hippocampus at 16 weeks post infection (wpi). No changes were seen in hippocampal mRNA expression for (A) *IL6*, (B) *CCL2*, (C) *iNos*, (D) *NF-κB1*, (E) *Arg-1*, or (F) *Igf-1* with AdMSC treatment. Hippocampi were analyzed from 10 animals, 6 AdMSC-treated and 4 PBS-treated controls. T-test with Welch's corrections, *p<0.05, **p<0.01, error bars = SEM.

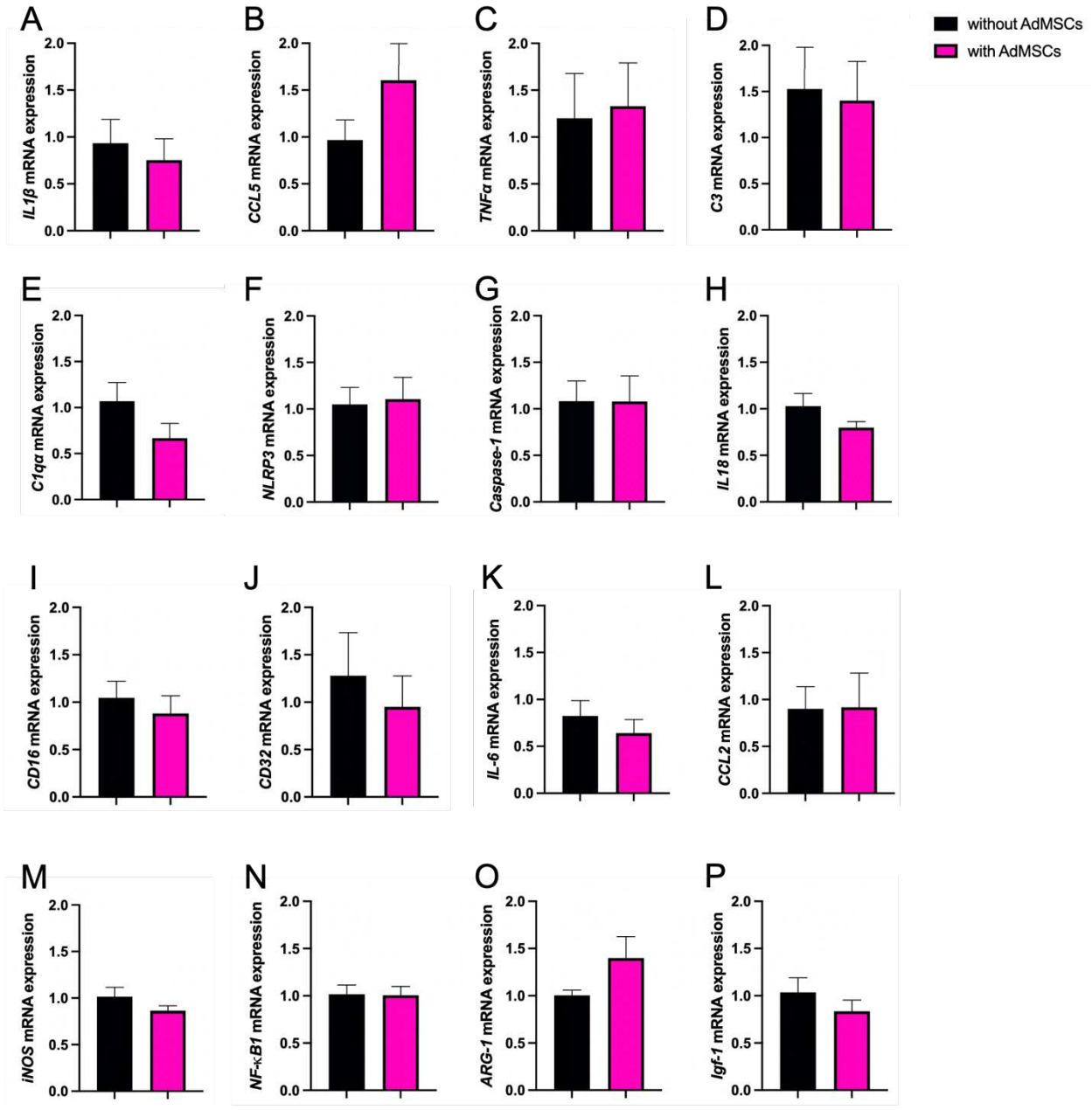

Supplemental Figure 3.4. AdMSC treatment has no effect on mRNA for inflammatory cytokine transcripts in the hippocampus at 18weeks post infection (wpi). Hippocampal mRNA expression did not change in animals treated with AdMSCs compared to controls for (A) *IL1β*, (B) *CCL5*, (C) *TNFα*, (D) *C3*, (E) *C1qa*, (F) *NLRP3*, (G) *Caspase-1*, (H) *IL18*, (I) *CD16*, (J) *CD32*, (K) *IL6*, (L) *CCL2*, (M) *iNos*, (N) *NF-κB1*, (O) *Arg-1*, or (P) *Igf-1.* Hippocampi were analyzed from 10 animals, 6 AdMSC-treated and 4 PBS-treated controls. T-test with Welch's corrections, $p<0.05$, error bars = SEM.

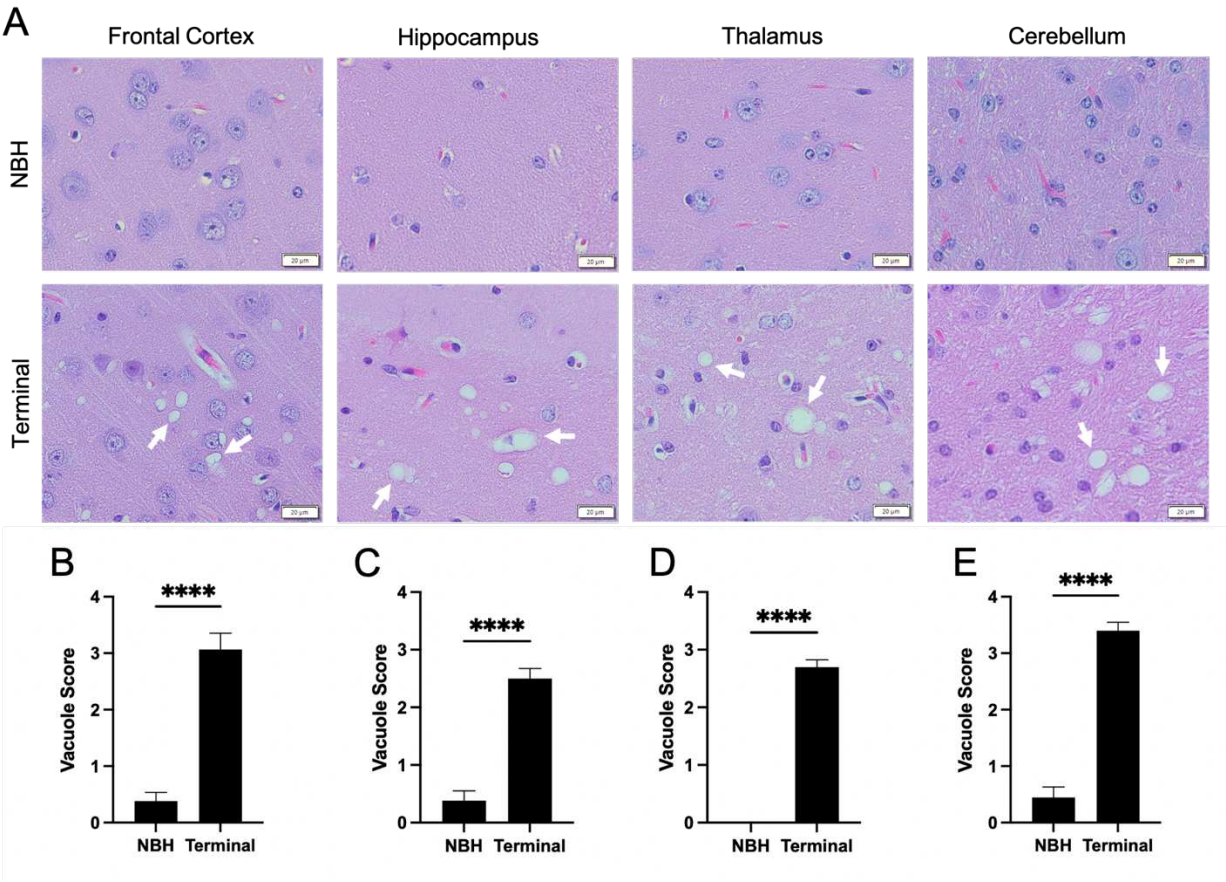

Supplemental Figure 3.5. Prion-infected mice show significant spongiosis throughout the brain at terminal stages. (A) H&E stained brains from NBH and terminal mice. Vacuoles in the (B) frontal cortex, (C) hippocampus, (D) thalamus and (E) cerebellum were scored on a scale of 0-5 based on size and number. An average of three scores for each brain region was calculated for each animal. Terminal mice had significantly more vacuoles in all brain regions compared to age-matched controls. H&E stained brains were analyzed from 7 NBH animals and 10 terminal animals. T-test with Welch's corrections, ****$p<0.0001$, error bars = SEM. 40x representative images, scale bar = 20 μm.

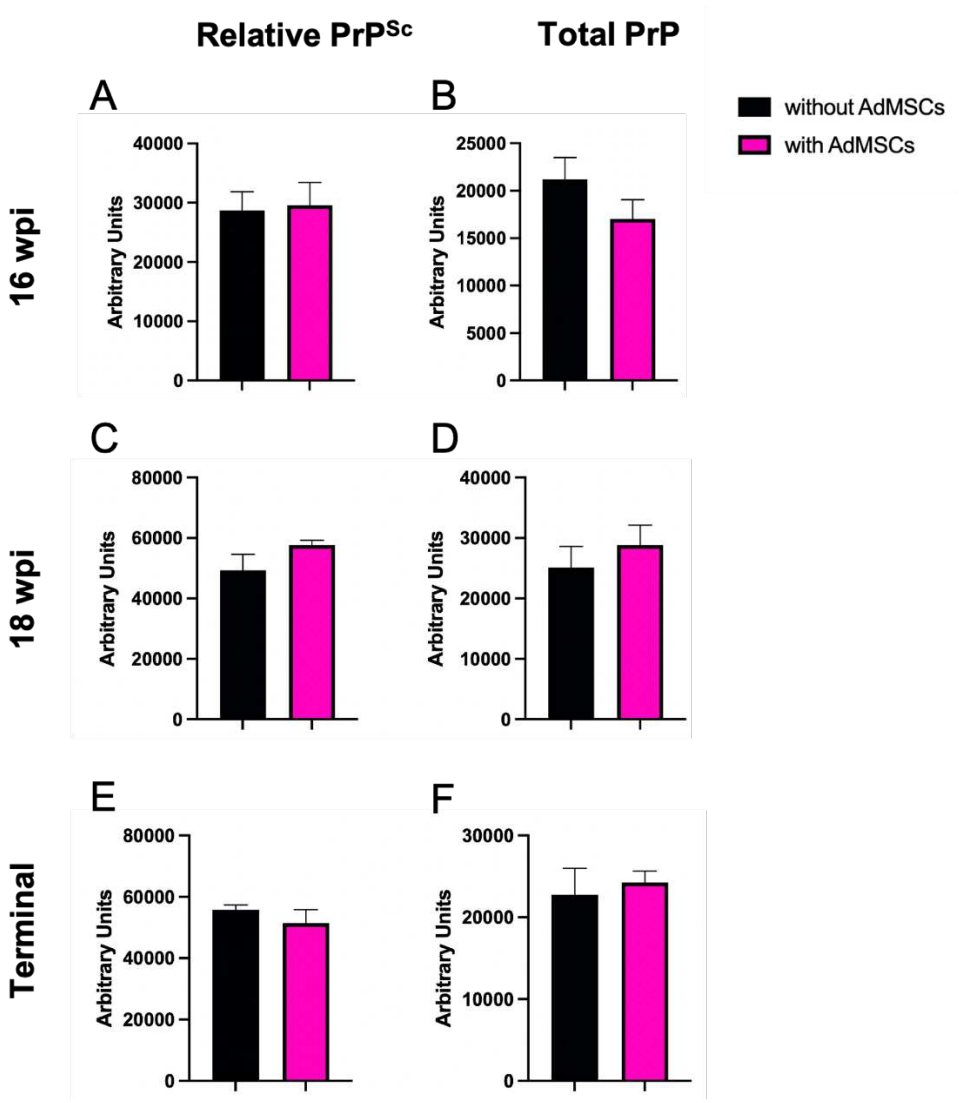

Supplemental Figure 3.6. AdMSC treatment does not induce detectable changes in PrP^{Sc}. Western blots were used to compare both PrP^{Sc} (PK-resistant PrP) and total PrP (not PK-treated) between vehicle and AdMSC-treated mice. At 16 wpi, no difference was detected between (A) PrP^{Sc} or (B) total PrP between treatment groups. At 18 wpi, no difference was detected between (C) PrP^{Sc} or (D) total PrP, and at terminal stages of disease, no difference was detected between (E) PrP^{Sc} or (F) total PrP between treatment groups. See Figure 5 for images of western blots. Brain homogenates were analyzed from 10 animals per timepoint, 6 AdMSC-treated and 4 PBS-treated controls (for terminal mice, 7 AdMSC-treated and 3 PBS-treated controls). T-test with Welch's corrections, $p<0.05$, error bars = SEM.

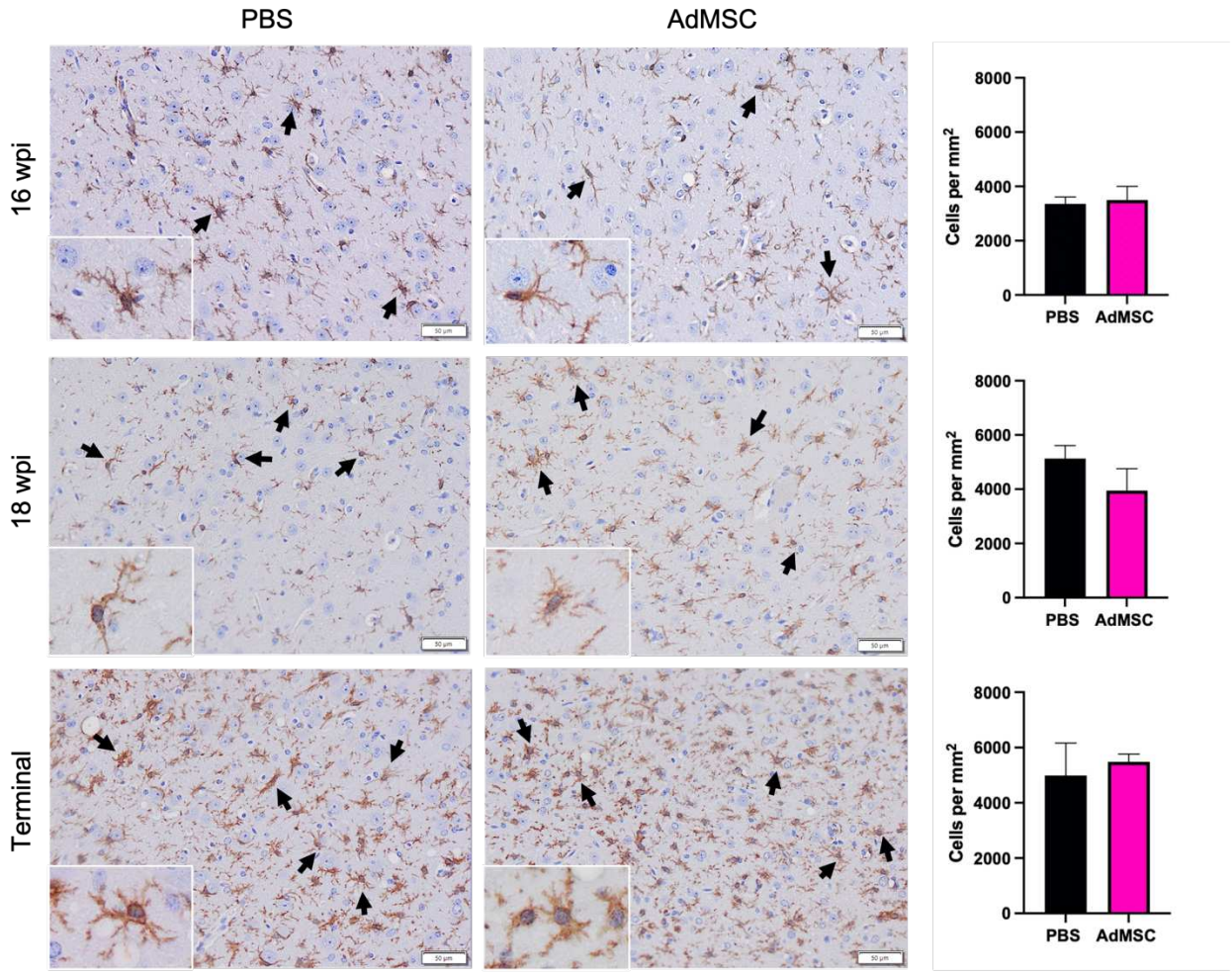

Supplemental Figure 3.7. AdMSC treatment does not change number of microglia in the thalamus. Counts of Iba1+ cells were performed in the thalamus. Thalamic microglia were analyzed from 10 animals per timepoint, 6 AdMSC-treated and 4 PBS-treated controls. T-test with Welch's corrections, error bars = SEM. IHC: 20x, scale bar = 50 μm.

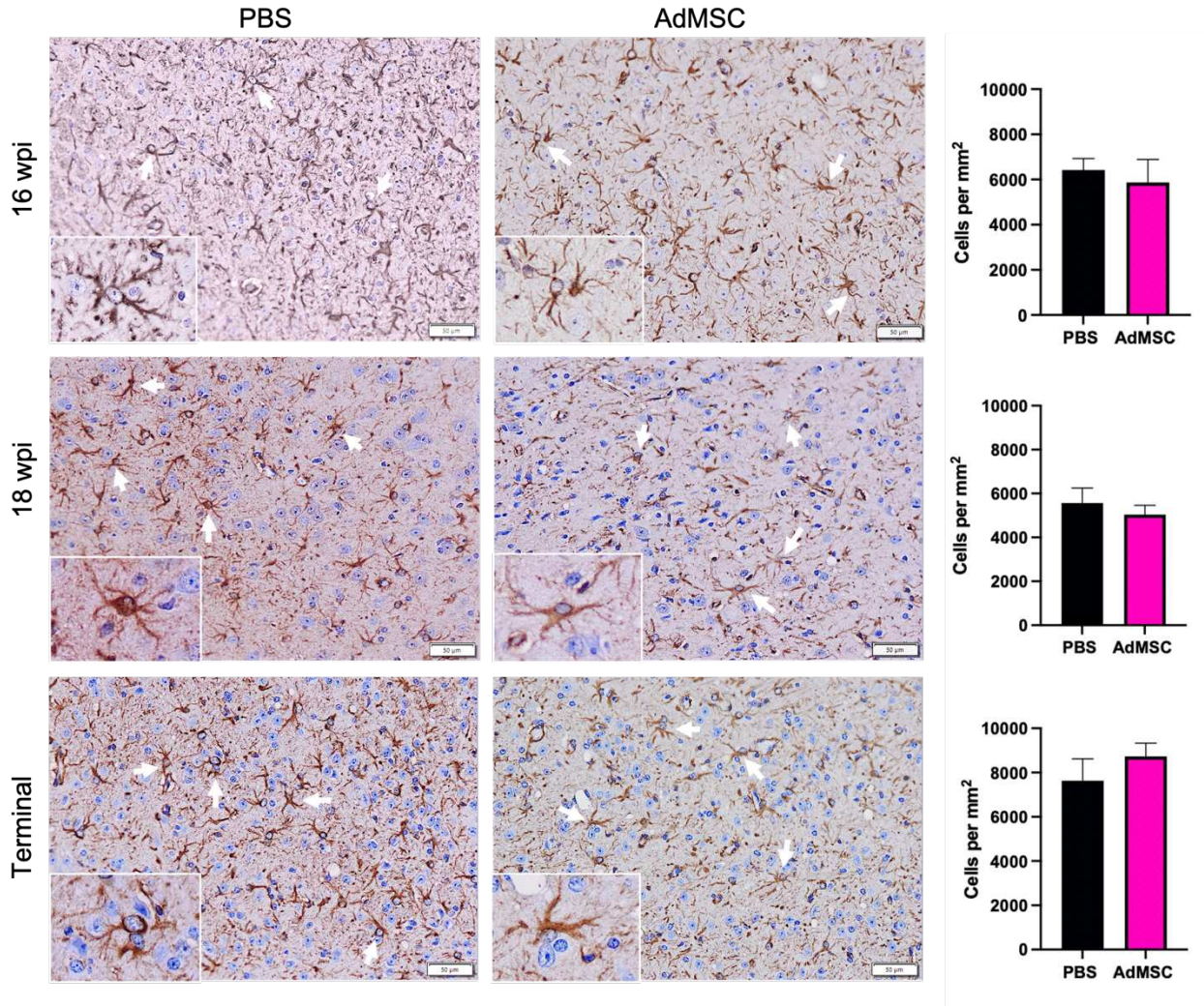

Supplemental Figure 3.8. AdMSC treatment does not change number of astrocytes in the thalamus. Counts of GFAP+ cells were performed in the thalamus. Thalamic astrocytes were analyzed from 10 animals per timepoint, 6 AdMSC-treated and 4 PBS-treated controls. T-test with Welch's corrections, error bars = SEM. IHC: 20x, scale bar = 50 µm.

Chapter 4:

Microglia-specific IKK and NF-κB signaling in a cellular model of prion infection

Summary

Prion diseases are a group of rare and fatal neurodegenerative diseases caused by the cellular prion protein, PrP^{C}, misfolding into the infectious form, PrP^{Sc}, which forms aggregates in the brain. This leads to activation of glial cells, inflammation, and irreversible neuronal loss. The role of glial cells in prion disease pathogenesis and neurotoxicity is poorly understood. Microglia can phagocytose PrP^{Sc}, leading to the release of inflammatory signaling molecules, which subsequently induce astrocyte reactivity. Animal models show highly upregulated inflammatory molecules that are a product of the Nuclear Factor-kappa B (NF-κB) signaling pathway, suggesting that this is a key regulator of inflammation in the prion-infected brain. The activation of the IKβ kinase complex (IKK) by cellular stress signals is critical for NF-κB-induced transcription of a huge variety of genes, including inflammatory cytokines and chemokines, enzymes, and genes involved in cell survival and autophagy. However, the contribution of microglia to NF-κB signaling in the prion-infected brain has not been evaluated. Here, we characterize a primary mixed glial cell model containing wild-type (WT) astrocytes and IKK knock-out (KO) microglia. We show that, upon infection with prions, NF-κB-related genes were significantly downregulated in mixed glial cultures containing IKK KO microglia. Despite this, we find glial conditioned media (GCM) from infected cultures containing IKK KO microglia (and wild-type astrocytes) to be equally neurotoxic to N2a neuroblastoma cells compared to GCM from WT cultures. PrP^{Sc} accumulation was found to be significantly

increased in mixed glia containing IKK KO microglia, suggesting that IKK signaling in microglia is critical for effective autophagy of prions.

Introduction

Prion diseases are rare, invariantly fatal neurodegenerative diseases characterized by the misfolding of the cellular prion protein, PrP^{C}, into the disease-associated PrP-scrapie, or PrP^{Sc}. The mechanism of the transformation of the alpha-helical PrP^{C} into the beta-sheet rich PrP^{Sc} is poorly understood, but can result from genetic mutation, infection with PrP^{Sc}, or occur sporadically. Prion diseases affect humans and a variety of mammalian species, with the aggregation of PrP^{Sc} resulting in neuroinflammation, followed by irreversible neuronal loss, associated behavioral and clinical signs similar to those seen in neurodegenerative diseases such as Alzheimer's disease, and, ultimately, death. [1-3,22,181]

The exact neurotoxic agent in prion disease is not fully understood, as expression of PrP is critical for cells to become infected and for neuronal loss,[36,38,39] but glial cells also play a distinct role in disease pathogenesis.[50,60,186] Neurons and astrocytes express the highest amount of PrP in the brain,[4] and therefore are easily infected with PrP^{Sc} and can traffic it between cells.[71] Microglia scavenge and phagocytose PrP^{Sc}, which results in a phenotypic change from scavenging and ramified to activated or amoeboid, often denoted as a shift from M2 to M1, or homeostatic microglia to disease-associated microglia (DAM).[69,75,82,128,186] This induces the secretion of factors such as pro-inflammatory cytokines and chemokines, which in turn can induce astrocytes to become reactive and in turn produce inflammatory and neurotoxic mediators.[45,49,79]

A key regulator of inflammation in the prion-infected brain is the Nuclear Factor-kappa B (NF-κB) pathway. In prion disease, toll-like receptors (TLRs) and nucleotide-binding oligomerization-domain protein-like receptors (NLRs, including NLRP3) bind to cytokines (particularly TNFα and IL1β), growth factors, damage-associated molecular patterns (DAMPs), and even PrP^{Sc} itself,[117,122,128,130] which activates the IKβ kinase complex (IKK); composed of the subunits IKKα, IKKβ and IKKγ. NF-κB is a complex that transcribes a DNA element called κB enhancer. Under normal conditions, NF-κB is inhibited through its binding to IκBα. When IKK is stimulated, it phosphorylates IκBα, causing it to dissociate from NF-κB. NF-κB translocates to the nucleus, binds to the κB enhancer, and transcribes a huge variety of genes. This includes many inflammatory cytokines and chemokines, enzymes, anti-apoptotic proteins, p62, other autophagy proteins, and proteins involved in the NLRP3 inflammasome.[111,112]

Animal models of prion disease show highly upregulated inflammatory molecules that are a product of this pathway, including TNF, IL1β, IL6, CCL2 and CCL5.[48,79,116,122] It's suggested that over 50% of genes upregulated in prion mouse models are associated with NF-κB.[79] BV2 and primary microglia models are shown to upregulate genes associated with NF- κB signaling upon exposure to purified prions.[122] Moreover, the NF- κB signaling pathway affects many pathways downstream, including Nod-Like Receptor family pyrin domain containing 3 (NLRP3) inflammasome signaling, and p62-induced autophagy.[111,113,114] However, few studies have assessed the role of NF-κB in prion disease, particularly the involvement of this pathway in microglia.

Animal models of prion disease that have a reduction or elimination of microglia have had varying effects on disease outcome,[75,87,89-92] depending on the time point in which the reduction occurs, but generally, microglia are found to be protective to the host, as disease worsens when

microglia are decreased or removed. Similarly, genetic manipulation to change the inflammatory state of astrocytes have not successfully extended the lives of mouse models.[49,92] Together, these findings suggest that inflammation from glial cells plays a critical role in host protection, but can become detrimental if left unchecked. Therefore, reduction, but not elimination, of glial-induced inflammation, may be a promising avenue for therapeutics.[93,123,160,177] To best develop therapeutics, further investigation is required to understand the involvement of specific inflammatory signaling pathways from astrocytes and microglia, and how they affect neuronal health in the prion-infected brain. Here, we investigate the role of microglia-specific NF-κB signaling and how it affects both prion-induced inflammation and protein aggregation in a cell-culture model of prion disease. We characterize mixed glia derived from mice with wild-type microglia, as well as those with microglia-specific knock-out (KO) of IKK,[235] which effectively knocks out NF-κB signaling in these cells. Infecting these cells with brain homogenates from terminal scrapie-infected prion mice results in changes in the inflammatory cytokine profile, neurotoxicity, phagocytosis of PrP^{Sc}, and autophagy.

Materials and Methods

Animal care and ethics statement

Cx3Cr1Cre-IKKflox mice (C57Bl/6 background) were kindly provided to us by Dr. Ronald Tjalkens.[236] All mice were bred and maintained at Lab Animal Resources, accredited by the Association for Assessment and Accreditation of Lab Animal Care International, in accordance with protocols approved by the Institutional Animal Care and Use Committee at Colorado State University.

Brain homogenates

CD-1 (Jackson Laboratory) mice were intracranially inoculated with 30ml of 1% Rocky Mountain Laboratories (RML) strains of mouse-adapted scrapie, or normal brain homogenate (NBH). Mice were monitored for weight loss and clinical signs of prion disease and euthanized after showing significant signs of terminal illness. Euthanasia was performed by deeply anaesthetization with isoflurane followed by decapitation. 20% brain homogenates were made in phosphate-buffered saline (PBS) using beads and a tissue homogenizer (Benchmark Bead Blaster 24) and stored at -80C. Brain homogenates were aliquoted and treated with UV light for 30 minutes to sterilize prior to using for cell culture.

Isolation and prion infection of mixed glia

Zero to two-day old C57Bl/6 or CX3CR1-IKKflox pups were euthanized and brains were extracted. Cerebellum, midbrain and hippocampus were removed and discarded, and the brains were placed in MEM/EBSS containing 2x penicillin/streptomycin/neomycin (PSN) (Sigma) on ice. Cortical tissue was used for mixed glial cultures, as described previously [123]. Media was removed and tissue was resuspended in prewarmed dissociation media (MEM/EBSS, 2x PSN and 1.5U/ml Dispase (Gibco)) and triturated with a Sigmacote (Sigma) coated glass pipet. The mixture was transferred to a beaker and stirred gently for 10 minutes, then tissue settled and supernatant was transferred to a tube on ice. DNase-I (4000U/ml, Roche) was added to dissociation media and tissue was stirred for 10 minutes. Extractions were repeated by adding fresh dissociation media (without DNase-I) 2 to 4 additional times, until only fibrous tissue remained in the beaker. The cell supernatant was centrifuged for 10 minutes at 1000 x g at 4C, media was aspirated from cell pellet and replaced with glial growth medium (MEM/EBSS, 10%

heat-inactivated FBS and 1% PSN). 10^6 mixed glial cells were plate in 10 cm dishes. Glial media was replaced after 24 hours and changed weekly. For in vitro prion infection, mixed glia were plated at 10^5 cells per well in 6-well plates and infected with 0.1% normal or RML brain homogenate once cells were ~80% confluent. Media was removed 72 hours later and cells were washed twice with PBS prior to fresh media being added to remove any residual brain homogenate. Supernatants (glial conditioned media) and protein, RNA, or cells were extracted from plates, as described below.

Viability Assay

At 7 days post-infection, glial conditioned media (GCM) was removed from mixed glia, centrifuged at 1000 x g for 5 minutes at 4°C to pellet cell debris, and transferred to a fresh tube that was stored at -80°C for viability assays. GCM were thawed in a waterbath at 37°C prior to use. N2a neuroblastoma cells were plated on black 96 well Nunc plates (Thermo Scientific) at 20,000 cells per well. 24 hours after plating, media was removed from N2a cells and replaced with GCM (8-12 replicate wells per treatment group). For each plate, fresh glial media was used as a control for live cells, and glial media containing 0.1% ethanol was used as a control for dead cells. N2as were incubated with GCM or control media for 48 hours. PrestoBlue Cell Viability Reagent (Thermo Fisher) was allowed to reach room temperature and diluted 1:10 with fresh glial media. Cells were washed gently with PBS and 50 µl PrestoBlue/media was added per well and incubated for 10 minutes at 37°C. Cells were analyzed using the FLUOstar Omega Plate Reader (BMG Labtech).

Detection of Apoptosis in N2a Cells

N2a cells were plated at 20,000 cells/well on glass coverslips in a 24-well plate. 24 hours later, media was removed and replaced with GCM, as described above. Cells were incubated for 48 hours at 37°C with GCM, then gently washed once with PBS. Caspase 3/7 - FITC (Thermo Scientific) and Annexin V - PE (Fisher Scientific) were combined following manufacturer's protocol in Annexin V binding buffer (BD) and incubated at room temperature in the dark for 30 minutes. Coverslips were immediately fixed with 2% paraformaldehyde for 10 minutes, washed once with binding buffer, and incubated in PBS with 10% normal donkey serum (NDS) for one hour in the dark at room temperature. Coverslips were incubated overnight at 4°C with MAP2 antibody (Cell Signaling, 1:100) in 5% NDS, washed twice with PBS, then incubated for one hour with donkey anti-rabbit Alexa Fluor 647 (1:250) at room temperature in the dark. Coverslips were washed twice with PBS, then incubated in Hoechst (ThermoFisher, 1:2000 dilution) for three minutes, then washed twice. Coverslips were removed from 24 well plates and mounted on glass slides with ProLong Gold Antifade media (ThermoFisher). Slides were covered from light and dried overnight at room temperature, then were kept at 4°C until imaging. Slides were imaged with an Olympus BX63 fluorescence microscope equipped with a motorized stage and Hamamatsu ORCA-flash 4.0 LT CCD camera and an Olympus Xline apochromat 20X (0.8 N.A.) air objective. The DAPI channel was used to identify areas containing approximately 10 N2a cells, and for each treatment 10 representative images were taken at 20x. Regions of interest (ROIs) were selected with Olympus cellSens software to identify MAP2+ N2a cells using adaptive thresholding, and then converted into individual ROIs. Mean gray intensity of Annexin V and Caspase3/7 was determined within each MAP2+ cell ROI. For each treatment, approximately 100 cells were analyzed.

Flow cytometry

Mixed glia at were washed and incubated with 3 ml of Cellstripper (Corning) for 15 min. Cells were scraped and pooled, then centrifuged for 5 min at 1000×*g* at 4C. Cells were resuspended in FACS buffer (1% heat inactivated FBS and 1 mM EDTA in sterile PBS) and centrifuged at 1000 x g. The cell pellet was resuspended in FACS buffer and aliquoted into 1.5 ml tubes. The cells were incubated for 1 hour in the dark at room temperature with following antibodies: anti-GLAST-PE (Miltenyi Biotec) and anti-CD11b-FITC (BD) at 1:50 dilution. Cells were centrifuged at 500×*g* for and washed with FACS buffer. Cells were transferred in 500 µl FACS buffer to library tubes on ice. 20,000 live cells per sample were analyzed using the CytekTM 4-laser Aurora Cytometer and data was processed in FlowJo, gating on intact cells, single cells, and PE/FITC-positive and PE/FITC-negative cells.

Immunoblotting

Cell lysates were isolated using the protein lysis buffer (50mM Tris, 150mM NaCl, 2mM EDTA, 1mM MgCl2, 100mM NaF, 10% glycerol, 1% Triton X-100, 1% Na deoxycholate, 0.1% SDS and 125mM sucrose) supplemented with Phos-STOP and protease inhibitors (Roche). A BCA Protein Assay kit (Thermo Scientific) was used to quantify protein concentration of lysates, and 500 µg protein was digested with 20 mg/ml proteinase K (PK) (Roche) for PrP^{Sc} blots for 1 hour at 37°C. Digestion was terminated with 2mM PMSF and lysates were spun at 40,000 x g for 1 hour at 4°C before being loaded on a gel. For PrP^{C} blots, 20 µg protein was used, and for all other blots 25 µg was used, with no PK digestion. Samples were run on a 4-20% acrylamide SDS page gels (BioRad) and transferred onto PVDF blotting paper (MilliPore). Blots for and LC3 were blocked and incubated with antibodies in 5% non-fat dried milk (Great Value). All other

blots were blocked and incubated with antibodies in 5% bovine serum albumin (Sigma-Aldrich). For PrP^{Sc} and PrP^{C} blots, primary antibody Bar-224 (Cayman Chemical Company) was used at 1:1,000 dilution. For LC3 and phospho-p62, primary antibodies (Cell Signaling) were used at 1:1000 dilution. HRP-conjugated secondary antibodies were used at a concentration of 1:5,000 (Vector Laboratories). Corresponding blots were incubated for 10 minutes in stripping buffer (1.5% glycine, 0.1% SDS, 1% Tween 20, in diH20, pH = 2.2), washed and reprobed for p62 (Cell Signaling). Loading control GAPDH was ran at a 1:10,000 dilution (MilliPore). The protein antibody complex was visualized using SuperSignal West Pico PLUS Chemiluminescent Substrate (Thermo Scientific) and visualized with the BioRad ChemiDoc MP. Quantification of average band intensity was performed using the "measure" function on ImageJ.

Scrapie Cell Assay

Protocol adapted from Bian et al. 2010 and is described in Hay et al 2022.[123,197] Briefly, primary mixed glial were infected with 0.1% RML or normal brain homogenate, as described above. 7 days later, cells were trypsinized and 50,000 cells were transferred to an ELISpot plate (Millipore). Plates were dried overnight and treated with cell lysis buffer (50 mM Tris-HCl, 150mM NaCl, 0.5% IGEPAL-CA630, 0.5% Sodium Deoxycholate in H2O pH= 7.6) containing 5ug/ml PK (Sigma Aldrich) and incubated for 90 min at 37°C on a shaker. The digestion was terminated with 2mM phenylmethylsulphonyl fluoride (PMSF, Thermo Fisher) at room temperature on a shaker for 20 minutes. Plates were incubated with 3M Guanidine Thiocyanate (Sigma Aldrich) in 10mM Tris-HCl (Sigma) (pH 8.0). Digestion was terminated and plates were washed thoroughly with PBS, then blocked with 5% Superblock (Pierce, Rockford, IL). Plates were incubated overnight with primary antibody Sha31 (Cayman Chemical Company), diluted

1:5000 in TBST (Tris-Buffered Saline with Triton-X) at 4°C. Plates were washed and incubated for 1 hour at room temperature with secondary antibody, AP-α-Mouse IgG (Southern Biotechnology Associates, Birmingham, AL), diluted 1: 5000 in TBST. Plates were washed thoroughly and dried overnight. NBT/BCIP tablet (Roche) in ultrapure water was added to plates and incubated in the dark for 30 minutes. Plates were washed and dried for at least one hour at 4C. Plates were scanned with a ImmunoSpot S6-V analyzer (Cellular Technology Ltd, Shaker Heights, OH), and determined spot numbers using ImmunoSpot5 software (Cellular Technology Ltd, Shaker Heights, OH).

Reverse transcriptase quantitative PCR analysis

RNA was extracted from 6-well dishes using cell scraping, QIAshredder and RNeasy extraction kits, in accordance with manufacturer's protocol, including a DNase digestion step with the RNase free DNase kit (Qiagen, Valencia, CA). Purity and concentration were determined using a ND-1000 spectrophotometer (NanoDrop Technologies, Wilmington, DE). Following isolation and purification, 25ng per sample of RNA was reverse transcribed using the iScript Reverse Transcriptase kit (BioRad, Hercules CA). cDNA was amplified within 24 hours of reverse transcription using iQ SYBR Green Supermix (BioRad, Hercules CA). For NF-κB panel, the RT^2 profiler PCR array for Mouse NF-κB Signaling Pathway (Qiagen) was used with Iq Sybr (Bio-Rad), following manufacturer's protocol. Plates were analyzed using the Bio-Rad CFX96 Real-Time System. Files were uploaded into RT^2 profiler PCR array analysis software for quality control and generation of heat maps and clustergram. Samples were normalized to 5 reference genes. For qPCR of specific genes, the corresponding validated primer sequences were used for each gene at 10mM. Plates were analyzed using the LightCycler 480 II (Roche). The

expression data was analyzed using the 2-ΔΔCT method and normalized to expression of reference genes *β-actin.* The fold difference was compared to control (C57 normal brain homogenate treated) samples [221]. All treatments were done in triplicate and cDNA was measured in triplicate. Data is a combination of three or four biological replicates. Validated primer sequences are listed in Table 4.1.

Table 4.1. Primer sequences for reverse transcriptase quantitative PCR

Gene	**Forward primer**	**Reverse primer**
IL1β	GCAGCAGCACATCAACAAG	CACGGGAAAGACACAGGTAG
TNFα	CCGATGGGTTGTACCTTGTC	AGATAGCAAATCGGCTGACG
NLRP3	CCTGGGGGACTTTGGAATCA	GACAACACGCGGATGTGAGA
Caspase-1	AACCACTCGTACACGTCTTGC	ATCCTCCAGCAGCAACTTCA
IL-6	CTGCAAGAGACTTCCATCCAG	AGTGGTATAGACAGGTCTGTTGG
CCL2	TTAAAAACCTGGATCGGAACCAA	GCATTAGCTTCAGATTTACGGGT
β-actin	GCTGTGCTATGTTGCTCTAG	CGCTCGTTGCCAATAGTG
IL18	GACTCTTGCGTCAACTTCAAGG	GTTGTCTGATTCCAGGTCTCCA
CCL5	TTAAAAACCTGGATCGGAACCAA	TCGAGTGACAAACACGACTGC
IL1α	AGACGGCTGAGTTTCAGTGAG	TCTGGGTTGGATGGTCTCTTC

Statistical analysis

For all analyses, outliers were identified and removed using a ROUT outlier test (Q=1%). Cleaned data was analyzed using a One-way ANOVA with Tukey's post-hoc analysis. All figures present mean +/- standard error of the mean (SEM). All data analysis and generation of graphs was done with Prism (v 9.1.0).

Results

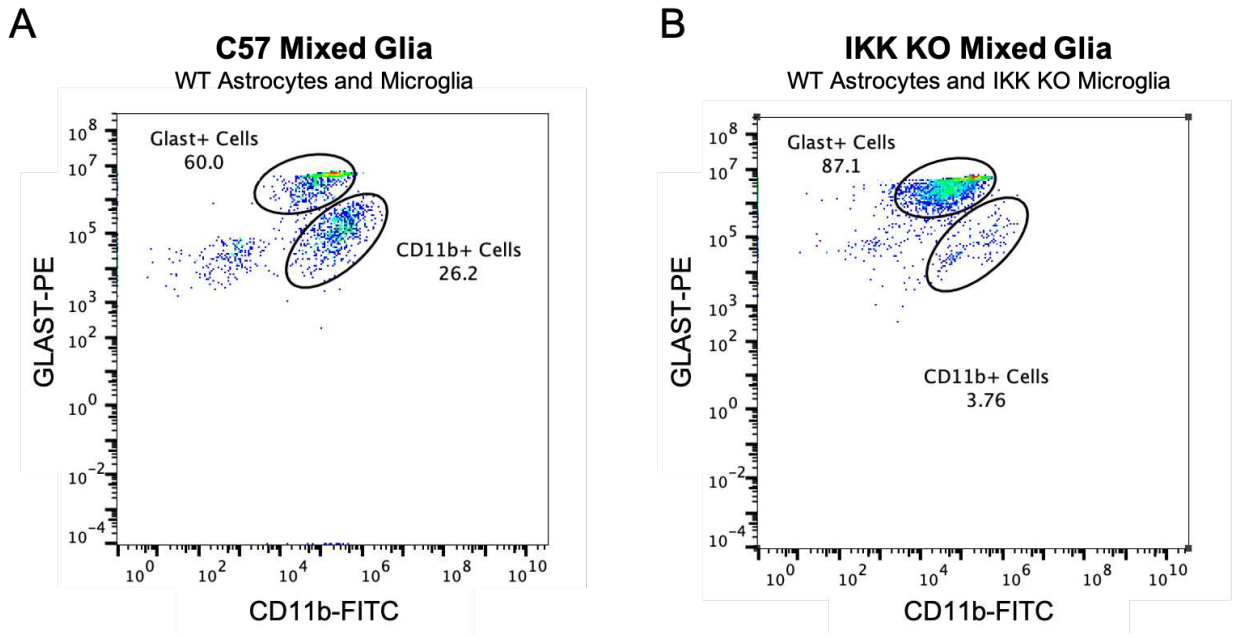

Figure 4.1. Significantly fewer microglia in mixed glial cultures containing IKK KO microglia. A) C57 mixed glia contain both astrocytes (GLAST+) and microglia (CD11b+). B) IKK KO mixed glia contain a greater number of astrocytes and fewer microglia, comparatively. Analysis of 20,000 cells per group.

Mixed glial cultures contain both astrocytes and microglia, but there are significantly fewer IKK KO microglia

Mixed glial cells on passage 1 from C57 (WT) or C57 with IKK KO microglia (IKK KO) were analyzed with flow cytometry to determine the relative number of astrocytes compared to microglia in these cultures. Cells were stained with an antibody for glutamate aspartate transporter (GLAST) and the microglia/macrophage marker CD11b. In the WT population, approximately 60% of cells were GLAST+ and about 26% were CD11b+, and about 14% did not stain positive for either marker. There were substantially more GLAST+ cells in the IKK KO glia, about 87%, but less than 4% CD11b+ cells, and only about 9% other cell types. This suggests that, although the IKK KO mixed glial cultures may be purer, they contain much fewer microglia than the WT cultures. This may suggest that knockout of IKK may impair microglia proliferation or survival.[235]

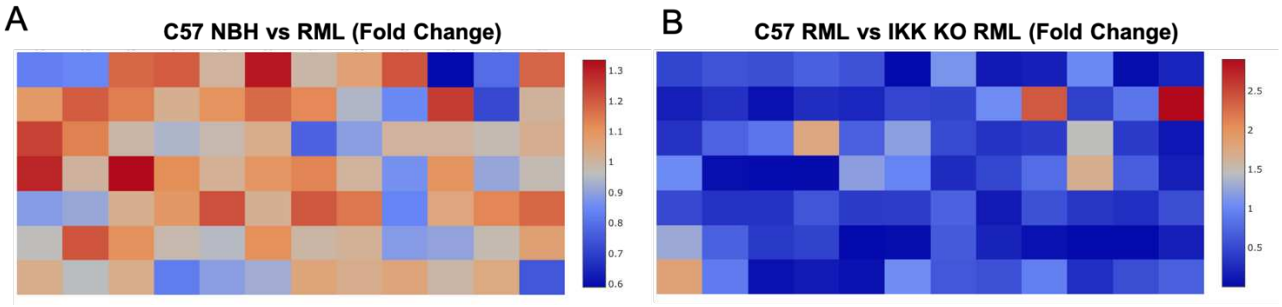

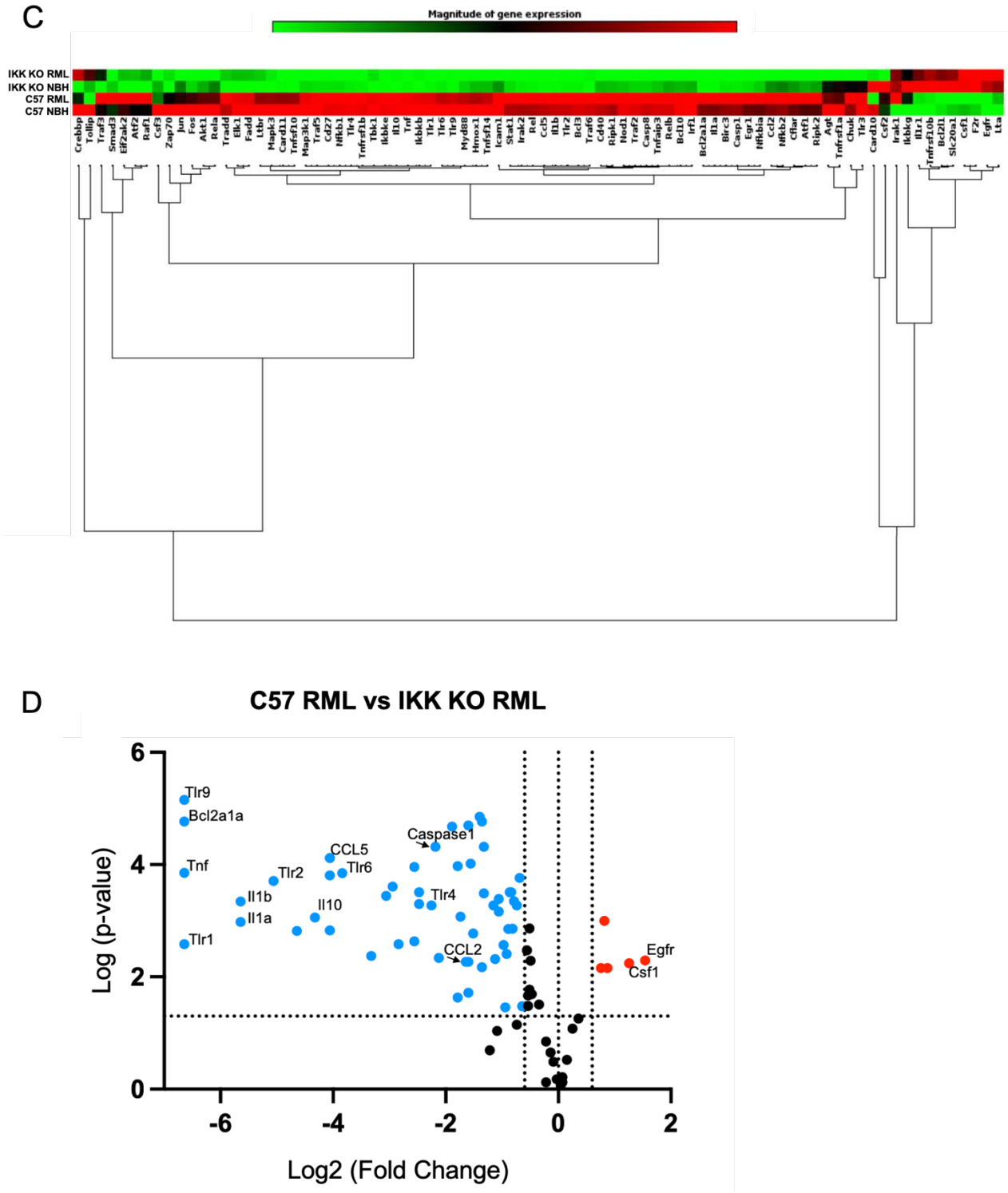

Figure 4.2. NF-κB-associated genes are significantly downregulated in infected mixed glial cultures containing IKK KO microglia. A) Heat map comparing NF-κB-related gene expression between mixed glia that were treated with normal brain homogenate (NBH) or RML-scrapie for 7 days shows a modest upregulation of genes in RML-infected glia. B) Heat map comparing RML-infected WT glia to infected microglia-specific IKK KO mixed glia shows a dramatic downregulation in most genes. C) Clustergram showing the maximum and minimum expression of all NF-

κB-related genes analyzed and how these genes cluster with one another. D) Volcano plot comparing NF-κB-related gene expression between RML-infected C57 to microglia-specific IKK KO mixed glia shows the majority of genes are downregulated in IKK KO cultures. X-axis intersections: fold change +/- 1.5. Y axis intersection: p-value < 0.05. Samples are composed of 3 pooled technical replicates, and 3 biological replicates for each group.

Prion infection induces a modest increase in NF-κB related genes, but knockout of IKK in microglia curtails this

Mixed glial cultures containing both astrocytes and microglia were treated with 0.1% NBH or RML brain homogenates for 7 days, as previously described. This is sufficient to induce infection and detectable PrP^{Sc} is newly synthesized, not from residual brain homogenate.[123] RNA was isolated from these cells and analyzed using a mouse NF-κB signaling pathway panel containing 84 genes of interest. A modest increase in NF-κB-related genes was observed in RML-infected C57 glia compared to NBH-treated C57 glia, with the largest fold-change being less than 1.4 (Figure 4.2A). This is consistent with our previous findings, which show a modest but significant increase in infected mixed glia in vitro (see also Figure 4.3).[123] The highest fold change was identified in the inflammatory cytokine IL1α (+1.34) and the anti-apoptotic gene Bcl2a1a (+1.31), and the lowest fold change was in the caspase recruitment domain CARD10 (-1.70), which is involved in mediating apoptosis and NF-κB activation.

A much larger difference in gene expression was observed between RML-infected C57 and microglia-specific IKK KO mixed glia, with the IKK KO glia showing a negative fold change of -1.5 or greater for 57 of the 84 genes analyzed (68%) (Figure 4.2B). The greatest fold changes were seen in toll-like receptor 9 (TLR9) (-193), and again in Bcl2a1a (-199). Few genes increased, but the largest increases were seen in epidermal growth factor receptor (Egfr) (+2.9) and macrophage colony-stimulating factor 1 (CSF1) (+2.4), which promotes microglia proliferation. Analysis of the gene expression of all four groups of cells using a clustergram (Figure 4.2C) demonstrates that the majority of NF-κB-related genes are downregulated in IKK

KO cultures compared to C57 cultures, regardless of NBH- or RML-treatment. However, a select group of genes is upregulated in IKK KO cultures, and these genes cluster with one another.

To best observe changes in gene expression between RML-infected C57 and IKK KO cultures, we opted to present this in a volcano plot and indicate specific genes that are highly increased or decreased, or have shown significance in other pathways involved in prion disease (Figure 4.2D). Of note, many inflammatory cytokines and chemokines are downregulated in IKK KO cultures (*TNFα*, *IL1α*, *IL1β*, *CCL2* and *CCL5*), as well as the anti-inflammatory cytokine IL10. Interestingly, the NLRP3-related gene *Caspase-1* is significantly decreased. Of note, many TLRs, including TLR1, TLR2, TLR4, TLR6 and TLR9, are all decreased in IKK KO cultures. A full list of genes with a significant fold change of + or – 1.5 is available in a table in Supplemental Figure 4.1.

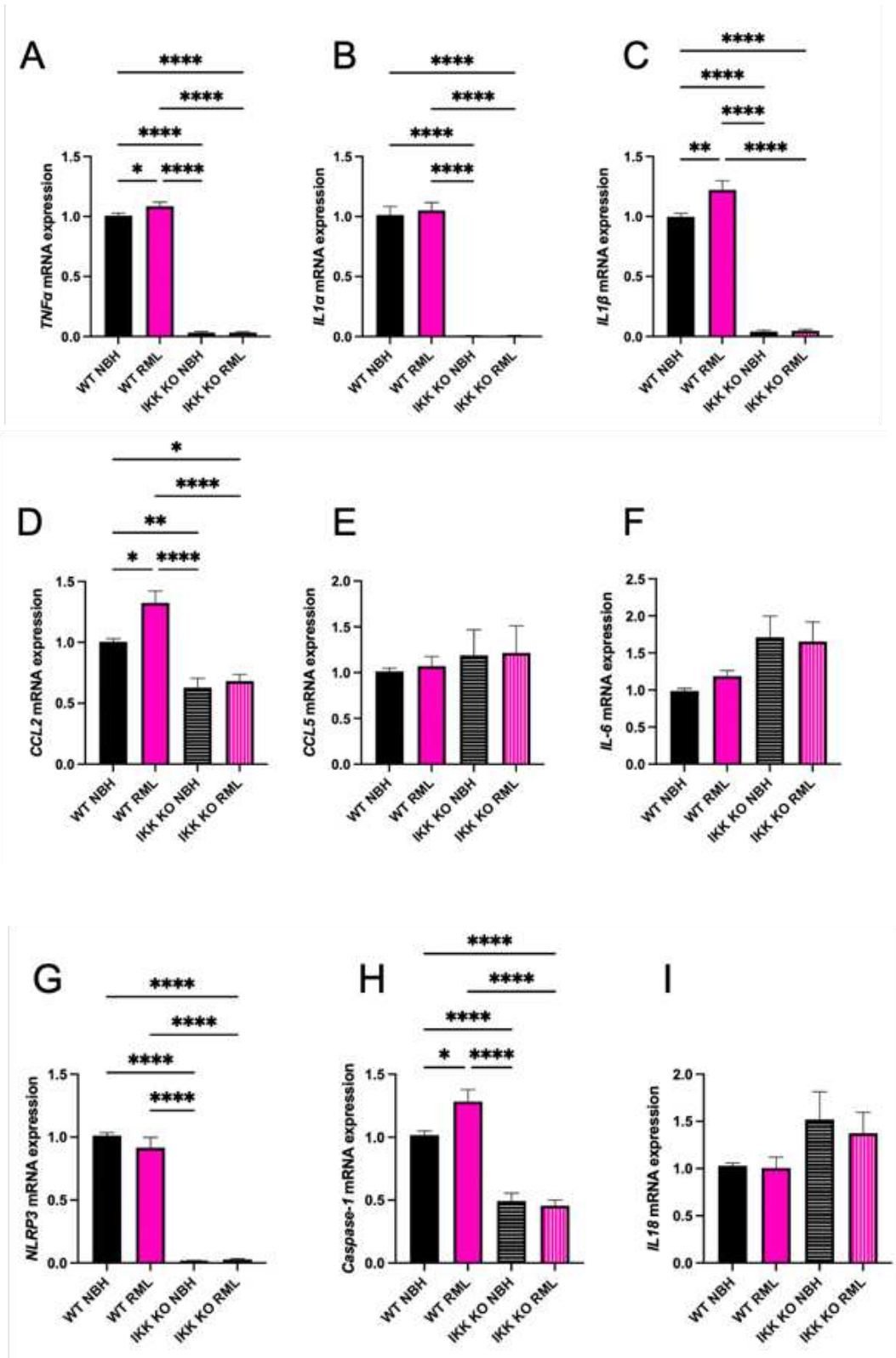

Figure 4.3. NF-κB and NLRP3-related genes are significantly downregulated in infected mixed glial cultures containing IKK KO microglia. C57 and microglia-specific IKK KO mixed glia were treated with NBH or infected

with RML brain homogenate for 7 days. mRNA expression of NF-κB-related cytokines and chemokines A) *TNFα*, B) *IL1α*, C) *IL1β*, D) *CCL2*, E) *CCL5* and F) *IL6* were analyzed, as were NLRP3-related genes G) *NLRP3*, H) *Caspase-1* and I) *IL18*. Analysis of 3-5 biological replicates, each with 3 technical replicates. One-way ANOVA and post-hoc Tukey test, error bars = SEM, *$p < 0.05$, **$p < 0.01$, ****$p < 0.0001$.

IKK KO in microglia significantly decreases many NF-κB and NLRP3 related genes in infected glia

We selected to analyze a few specific NF-κB-related inflammatory genes that are known to be upregulated in the prion-infected brain.[48,79,116] Additionally, we wanted to look at downstream effects on NLRP3-related genes. Mixed glia containing WT or microglia-specific IKK KO were treated for 7 days with NBH or RML-scrapie brain homogenates. RML infection modestly but significantly upregulated *TNFα*, *IL1β*, *CCL2* and *Caspase-1* in WT, but not IKK KO, mixed glia. A significant decrease was seen in the NF-κB-related genes *TNFα* (Figure 4.3A), *IL1α* (Figure 4.3B), *IL1β* (Figure 4.3C), and *CCL2* (Figure 4.3D) in both NBH-treated and RML-infected IKK KO cultures compared to RML-infected WT cultures ($p<0.0001$). No significant differences between WT and IKK KO cultures were observed for either NBH-treated or RML-infected groups for the NF-κB-related genes *CCL5* (Figure 4.3E) or *IL6* (Figure 4.3F). A significant decrease was also seen in genes that are downstream of the NF-κB pathway and are involved in the NLRP3 inflammasome related. *NLRP3* (Figure 4.3G) and *Caspase*-1 (Figure 4.3H) were both downregulated in IKK KO cultures compared to RML-infected WT cultures ($p<0.0001$), but no significant differences were observed for *IL18* (Figure 4.3I).

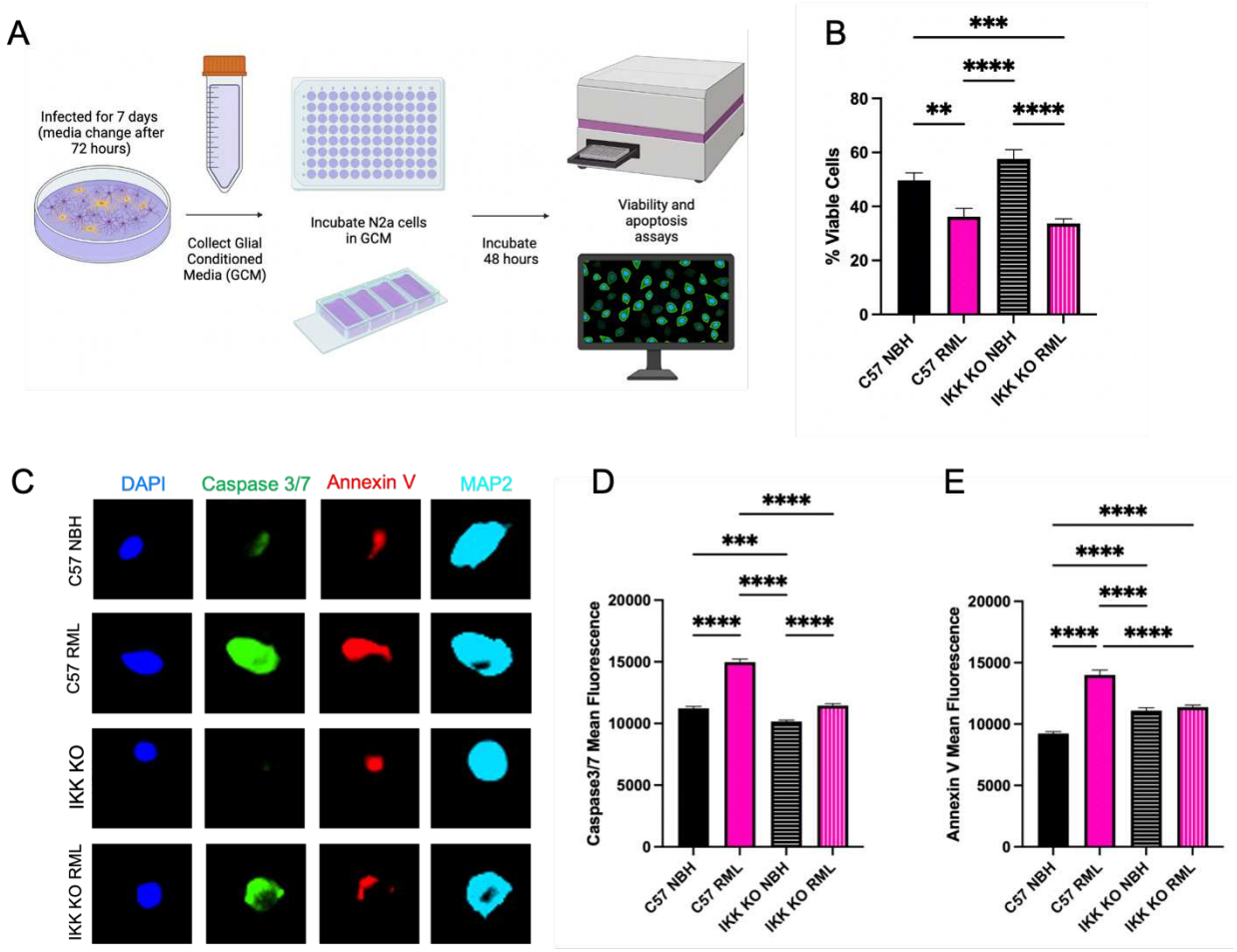

Figure 4.4. Decreased markers of apoptosis, but no overall changes in neurotoxicity between C57 and microglia-specific IKK KO mixed glia. A) Mixed glial cultures were treated for 7 days with NBH or RML homogenates. Glial conditioned media (GCM) was isolated and plated on N2as in 96-well plates and chamber slides for 48 hours. B) GCM-treated N2as were analyzed for percent viability using a Presto Blue cell viability assay. C) GCM-treated N2as that were incubated with the nuclei stain DAPI, apoptosis stain Caspase-3/7, cell viability stain Annexin V and neuronal-specific antibody MAP2 (representative images, 20x). Mean fluorescence of D) Caspase-3/7 and E) Annexin V were analyzed in MAP2+ N2as (arbitrary units). Presto Blue assay represents 3 biological replicates, each with 6-18 technical replicates. Caspase-3/7 and Annexin V assay represents one biological replicate, with approximately 100 technical replicates for each group. One-way ANOVA and post-hoc Tukey test, error bars = SEM, $*p < 0.05$, $**p < 0.01$, $***p < 0.001$, $****p < 0.0001$.

Glial conditioned media from infected glial cells decreases cell viability in N2a cells, even in the absence of NF-κB signaling from microglia

To determine the effects of factors secreted into the media by wild-type (WT) mixed glia compared to mixed glia with IKK KO microglia (hereafter referred to as IKK KO glia), glial

conditioned media (GCM) was harvested from NBH or RML-infected glia after 96-hour incubation. N2a neuroblastoma cells were incubated in GCM for 48 hours, then viability was measured with Presto Blue (Figure 4.4A). GCM from RML-infected WT glia had an average of 13.4% fewer viable cells ($p<0.01$), and RML-infected IKK KO glia had an average of 23.9% fewer viable cells ($p<0.0001$), compared to the NBH-treated controls (Figure 4.4B). However, there were no statistically significant differences in viability between WT and IKK KO GCM between NBH- or RML-infected cells. This suggests that, even in the absence of NF-κB signaling from microglia, these glial cells are still secreting neurotoxic factors.

To assess the involvement of apoptosis in neuronal death induced by GCM, N2a cells were incubated in GCM, as described above, and then stained for the neuronal marker MAP2, and the apoptosis markers Caspase-3/7 and Annexin V (representative images in Figure 4.4C). Significantly more Caspase-3/7 (Figure 4.4D) and Annexin V (Figure 4.4E) were observed in N2as treated with GCM from C57 RML-infected glia compared to C57 NBH-treated glia ($p<0.0001$). Likewise, significantly more Caspase-3/7 was observed in N2as treated with RML-infected IKK KO GCM compared to NBH-treated IKK KO GCM ($p<0.0001$). Interestingly, no significant differences were observed in Annexin V between these groups. Caspase-3/7 in N2as was significantly decreased for IKK KO NBH GCM compared to WT NBH GCM ($p<0.001$), and comparable to that of IKK KO RML GCM. Annexin V in N2as, however, was significantly higher for both IKK KO NBH and RML GCM compared to C57 NBH GCM ($p<0.0001$), but significantly lower compared to C57 RML GCM ($p<0.0001$). Together, these data suggest that GCM from microglia-specific IKK KO mixed glia is comparably neurotoxic in an N2a model, but that this may be through a cell death pathway other than apoptosis.

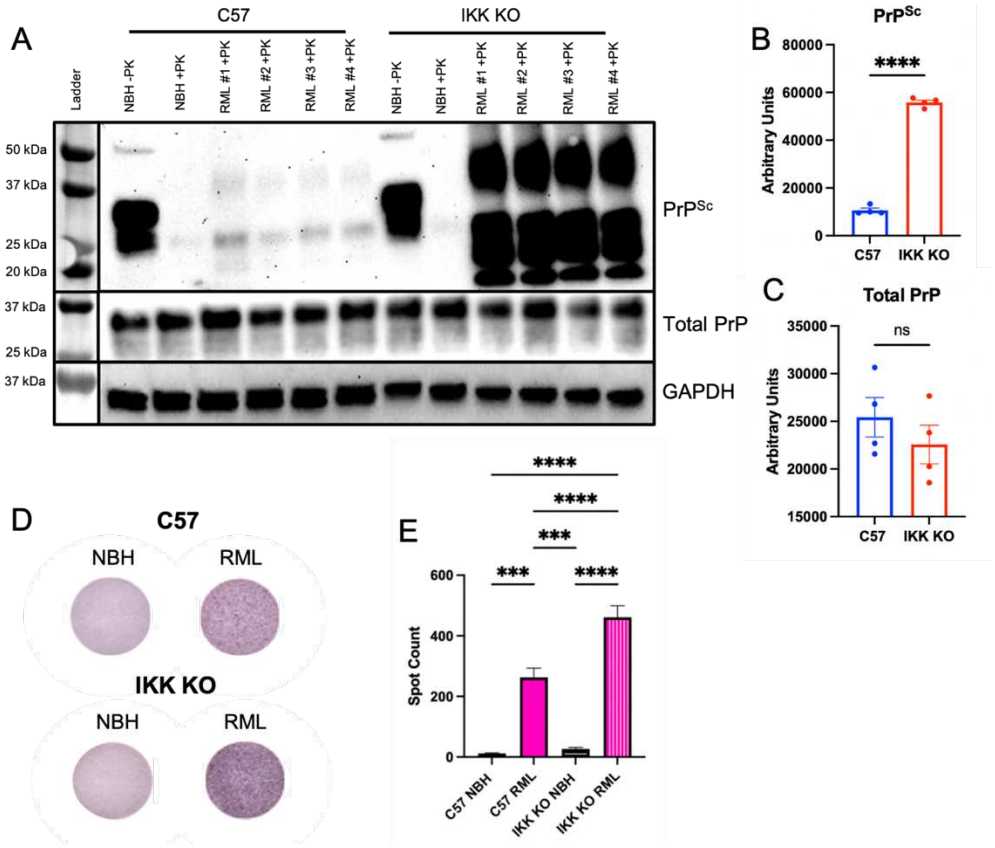

Figure 4.5. Mixed glial cultures containing IKK KO microglia have increased PrP^{Sc}. C57 and microglia-specific IKK KO mixed glia were treated with NBH or RML for 7 days. A) Cell lysates were analyzed for PrP^{Sc}, total PrP and GAPDH (loading control) via western blot (representative of two biological replicates). B) Quantification of PrP^{Sc}. C) Quantification of total PrP. D) PrP^{Sc} spot counts were analyzed via a scrapie cell assay (representative images). E) Quantification of PrP^{Sc} spots, 3 experiments combined, each with 5-25 technical replicates. One-way ANOVA and post-hoc Tukey test, error bars = SEM, ***$p < 0.001$, ****$p < 0.0001$, ns = not significant.

PrP^{Sc} is significantly increased in mixed glial cultures containing IKK KO microglia

C57 and microglia-specific IKK KO mixed glial cultures were infected with RML or treated with NBH for 7 days, as described above. Cell lysates were analyzed via western blot to determine relative amounts of PK-resistant PrP (PrP^{Sc}) and total PrP (not digested with PK) (Figure 4.5A). Analysis of band intensity shows that PrP^{Sc} is significantly higher in RML-infected glia containing IKK KO microglia ($p<0.0001$) (Figure 4.5B), but that there are no significant changes in total PrP (Figure 4.5C) between these groups. Cells that were infected for 7 days were trypsinized and transferred to EliSPOT plates where they were lysed and PK-

digested and stained for PrP. Spots, representative of PrP^{Sc} aggregates, were significantly higher in RML-infected C57 mixed glia and IKK KO mixed glia compared to NBH controls (representative images in Figure 4.5D) ($p<0.001$; $p<0.0001$, respectively, Figure 4.5E). Microglia-specific IKK KO mixed glia that were RML infected showed significantly more PrP^{Sc} compared to their C57 counterpart ($p<0.0001$). Together, these data indicate that mixed glial cultures containing IKK KO microglia have substantially higher PrP^{Sc} accumulation compared to WT mixed glial cultures.

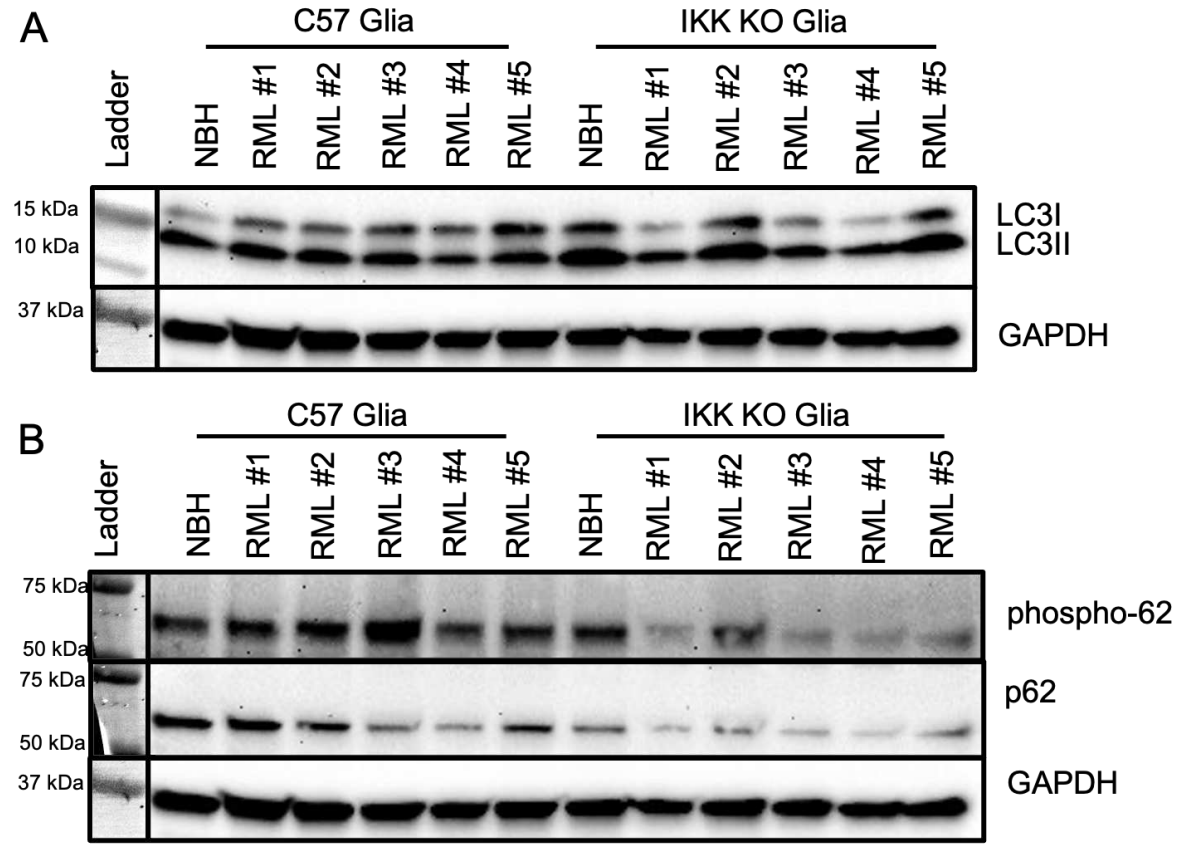

Figure 4.6. Decreased markers of autophagy in microglia-specific IKK KO mixed glial cultures. Cell lysates from 7-day NBH-treated or RML-infected C57 or microglia-specific IKK KO mixed glia were analyzed for the autophagy markers A) LC3-I and II, B) phosphor-p62 and p62. Representative of two biological replicates.

Infected mixed glia with IKK KO microglia show changes in markers of autophagy

C57 and microglia-specific IKK KO mixed glial cultures were infected with RML or treated with NBH for 7 days, as described above. To better understand why PrP^{Sc} is significantly increased in the IKK KO mixed glial cultures (Figure 4.5), cell lysates were analyzed via western blot to identify changes in markers of autophagy. Both pathways are important for PrP^{Sc} clearance and have been shown to be dysregulated in prion disease.[64,142,152] Comparing LC3-I and II is a reliable indicator of autophagosome formation, as LC3-I is the cytoplasmic form of the protein, and is recruited by p62 to the autophagosome and converted into LC3-II. Therefore, similar levels of both proteins suggests normal autophagy, but decreased LC3-I and increased LC3-II suggests that autophagy is increased.[142] LC3-I appears decreased in some samples of IKK KO infected glia compared to C57 infected glia, suggesting that autophagy may be increased in these cells (Figure 4.6A). p62 is produced by both the NF-κB pathway and the Nrf2 oxidative stress pathway.[145] It becomes phosphorylated as it forms the autophagosome alongside LC3II. Increased phospho-p62 is therefore a marker of increased autophagy.[140] However, both phospho-p62 and p62 appear decreased ($p<0.063$ and $p<0.058$, trending toward significant, data not shown) in IKK KO infected glia compared to C57 infected glia (Figure 4.6B), suggesting that total p62 may be decreased in these cells. Together, these data suggest a decrease in autophagy in infected microglia-specific IKK KO mixed glial cultures, as autophagy may be dysregulated due to an overall decrease in p62.

Discussion

Microglia are potent regulators of prion infection and are involved in host protection through inflammatory signaling, communication with astrocytes, phagocytosis and degradation of PrP^{Sc}.[57,89-92] Many genes involved in the NF-κB signaling pathway are highly upregulated in animal models with prion disease,[48,84,116] suggesting that this pathway is a critical innate immune response to prion infection. To date, no studies have analyzed the role of microglia-specific NF-κB signaling. A study from Julius et al. in 2008 knocked IKK out of cells in the CNS with neuroectodermal lineage – namely neurons, oligodendrocytes, and astrocytes. They failed to see any changes in disease time-course, PrP^{Sc} accumulation or astrogliosis, and concluded that NF-κB does not play a significant role in prion-induced inflammatory signaling. [119] Another study directly knocked out the subunits of NF-κB, once again in cells derived from the neuroectoderm. This group saw a decrease in survival in these mice upon prion inoculation, and increased apoptosis.[113] Both of these studies failed to account for microglia, which are derived from the mesoderm[120] and known to be critical regulators of NF-κB-related inflammation in prion and other diseases.[45,49,79,92] Here, we utilize a primary cell model that contains wild-type astrocytes and IKK KO microglia[235] to characterize the role of microglia-specific NF-κB signaling in an in vitro model of prion disease.

Cx3Cr1Cre express Cre recombinase under the *Cx3cr1* promoter in the mononuclear phagocyte system, and were combined with floxed IKKβ mice[235] to generate mice with IKK knockout (KO) specific to mononuclear phagocytes (macrophages, monocytes and microglia). As macrophages and monocytes are rarely found in the brain, even in prion disease,[79] these cells are effectively microglia-specific IKK KO. In an innate immune response, IKK is critical for NF-

κB translocation to the nucleus for transcription,[111,112] making these cells effectively NF-κB KO. All other brain cells derived from these mice have functional IKK and NF-κB signaling. We will henceforth refer to the microglia-specific IKK KO cells, which contain wild-type (WT) astrocytes, as IKK KO.

We first characterized these cells by comparing the relative percentages of astrocytes and microglia between C57 (WT) and microglia-specific IKK KO mixed glia through flow cytometry. We found that although IKK KO cultures had fewer cell types other than astrocytes and microglia, they also had substantially less microglia compared to WT cultures (~4% compared to 26%) (Figure 4.1). It has been shown previously that IKK is important for cell survival and proliferation, and IKK KO has been shown to be embryonically lethal in some animal models.[235] As NF-κB is a potent regulator of apoptosis and contributes to the upregulation of anti-apoptotic genes, knocking it out of cells may be detrimental to their survival. Indeed, IKK KO cells expressed significantly less of the anti-apoptotic gene Bcl2a1a (Figure 4.2) and significantly more Tnfrsf10b, also known as Death Receptor 5, and a potent regulator of apoptosis (Supplemental Table 4.1).

It has been established that even a small number of microglia can greatly impact a cell culture system, especially in modulation of astrocytes.[121] There is significant cross-talk between astrocytes and microglia, as astrocytes remain relatively unresponsive to environment changes in the absence of microglia-derived signaling, [45,46] and microglia rely heavily on astrocytes to promote their proliferation.[237] Astrocytes highly express CSF1, which, alongside IL34, which is expressed by neurons, binds to colony stimulating factor 1 receptor (CSF1R) on microglia to promote their proliferation and survival.[237] Interestingly, one of the few upregulated genes in the IKK KO cultures was CSF1 (Figure 4.2), suggesting that astrocytes in these cultures are

producing increased CSF1 to promote microglial survival. CSF1 is highly upregulated in the brain in response to inflammatory-inducing signals such as LPS.[238]

Nearly 70% of the 84 NF-κB-related genes analyzed were downregulated in RML-scrapie-infected IKK KO glia compared to RML-infected WT glia (Figure 4.2) (Supplemental Table 4.1 for complete list). Of these genes, many were inflammatory cytokines and chemokines known to be upregulated in the prion-infected brain.[48,79,116] Some of these cytokines, including TNFα, IL1α and IL1β, are known to be predominantly produced by microglia and influence the state of astrocyte reactivity.[45,49] Others, namely the cytokine CCL2, is known to be produced by astrocytes and promotes an M1 phenotype in microglia.[51] This suggests that in the absence of microglia-specific NF-κB signaling, signaling from astrocytes is also decreased, as they are not being fully activated by microglia.

To further interrogate the influence of microglia-specific IKK KO on specific genes of interest, we performed qPCR analysis on three to five sets of RML-infected primary mixed glia, each isolated from a separate set of mouse pups (Figure 4.3). We performed this analysis multiple times due to drastically different responses in some genes. *TNFα*, *IL1α* and *IL1β* were consistently downregulated in IKK KO glia, as were the NLRP3-related genes *NLRP3* and *Caspase-1*. This suggests that these genes are predominantly upregulated by NF-κB and the majority are produced by microglia. We also saw an overall downregulation in *CCL2*, although this was less robust than the other genes. As this chemokine is produced mainly by astrocytes,[51] it is likely still being expressed in the absence of microglia NF-κB signaling. Due to their known involvement in NF-κB signaling and/or prion pathogenesis, we additionally looked at expression of *CCL5* and *IL6*, as well as the NLRP3-related gene *IL18*. We saw a large variation in expression of these genes with each set of glia analyzed, showing both significant

downregulation and, intriguingly, significant upregulation. This suggests that there may be compensatory signaling pathways from astrocytes, microglia, or both, that are contributing to inflammation in these cells. However, unlike many of the other genes, no significant changes were seen between the WT glia treated with normal brain homogenate (NBH) or RML, suggesting that this inflammation is not induced by prions.

Another set of genes that are significantly downregulated in these cells are TLRs, particularly TLR1, TLR2, TLR4, TLR6 and TLR9, all of which are highly expressed in microglia. This decrease in TLR expression is consistent with a decrease in microglial numbers, and also likely contributes to an overall decrease in inflammatory molecules, [238] as signaling is dysregulated in the absence of sufficient TLRs. TLR3 is very slightly downregulated, but this TLR is highly expressed in astrocytes, along with low-level expression of TLR1, TLR4, TLR5 and TLR9.[239] Interestingly, microglia have been shown to be critical for TLR4 signaling in astrocytes, and important for optimal signaling through TLR2 and TLR3.[240] This may contribute to overall downregulation of astrocyte-specific signaling in cultures containing IKK KO microglia, as there are much fewer microglia present to prime the astrocytes. TLR4 is one of the best studied TLRs, as its stimulation by signals such as LPS induce NF-κB inflammation in microglia,[112,238] which is critical to elicit an astrocyte response.[240] In prion mouse models, TLR1-9 are all upregulated in the brain at terminal stages of disease.[238] TLR2 and TLR4 signaling are important for sensing DAMPs and has been shown to be implicated in prion disease, as knocking out either of these receptors in mice accelerates disease.[223,241]

Microglia-induced inflammation is often cited as an inducer of neuronal cell death, either directly or indirectly.[45,46,49,56,92,127,128] Therefore, it was surprising that glial conditioned media (GCM) from infected WT and IKK KO microglia showed similarly neurotoxicity. Incubating

N2a neuroblastoma cells with GCM from C57 RML-infected glia induced significantly more cell death and apoptotic markers than GCM from C57 NBH-treated glia (Figure 4.4). A similar trend was seen in GCM from IKK KO RML-infected glia compared to IKK KO NBH-treated glia. However, there were no differences in cell viability between GCM from C57 or IKK KO RML-infected glia, nor NBH controls. Both the early apoptotic marker Caspase-3/7 and overall viability were decreased in GCM from RML-infected cells, although Annexin V, a marker of early cell death, remained unchanged. Interestingly, Caspase-3/7 was decreased for GCM from IKK KO glia compared to GCM from C57 RML-infected glia. Annexin V was also decreased in GCM from IKK KO glia compared to GCM from C57 RML-infected glia, but is significantly higher for all IKK KO groups compared to GCM from C57 NBH-treated glia. Caspase-3/7 is a distinct marker of apoptosis signaling, and its decrease in these cells suggests that GCM from IKK KO mixed glia is not significantly contributing to neuronal apoptosis. However, the increase in Annexin V suggests that cell death is still occurring, as this dye binds to phosphotidylserine (PS) residues that are unexposed in a healthy cell, but become exposed on the outside of the cell membrane during the early stages of cell death.[156] This stain, although generally a marker of apoptosis, can also bind to PS residues in necrotic cells.[242] It appears that incubating N2as with GCM from microglia-specific IKK KO RML-infected glia does not rescue neurotoxicity when compared to GCM from C57 RML-infected glia. This suggests that there is something being secreted by the mixed glia in the microglia-specific IKK KO cultures that is still inducing non-apoptotic neuronal cell death. The absence of functional microglia may not be protecting neurons from toxic signals from astrocytes. Moreover, this observation may be limited to in vitro analysis. Microglia-specific IKK KO was shown to be protective against kainic acid-induced hippocampal neuronal cell death *in vivo*.[243] Microglial NF-κB signaling contributed to

death of motor neurons in a mouse model of ALS.[244] However, prion diseases present unique pathogenesis to other neurodegenerative diseases. Further investigation both in vitro and *in vivo* is required to understand the role of microglia-specific IKK KO on neurotoxicity in prion disease.

The first indicator that cellular responses to misfolded proteins might be impaired in the cell cultures containing IKK KO microglia was the huge accumulation of PrP^{Sc} in these cells, identified with both western blot and scrapie cell assay (Figure 4.5). Accumulation of misfolded proteins is commonly associated with dysregulation of autophagy and lysosomal function. Rescue of either of these pathways has been shown to improve life expectancy and clinical pathology in prion-infected mice.[144,153,245]

Misfolded proteins are first identified and ubiquitinated by chaperone proteins, leading to the binding and sequestering of these aggregates by p62, a protein that is upregulated by both NF-κB and the Keap1-Nrf2 oxidative stress pathway.[140,145] Cytosolic LC3-I binds to phosphatidylethanolamine on newly synthesized autophagosomes, forming LC3-II and binding to p62 to engulf the p62-polyubiquitin-protein complex. This autophagosome complex is then degraded by the lysosome.[145] Ratios of LC3-I and LC3-II are a common indicator of early autophagy, as LC3-II increase demonstrates the development of the autophagosome, but buildup of this protein alongside p62 may indicate that autophagy or lysosomal function is being impaired, which is also seen in prion disease.[140,143,153] We observed some decrease in LC3-I and increase in LC3-II for some samples from our IKK KO RML-infected mixed glial cultures, while ratios remain relatively consistent in C57 RML-infected cultures, suggesting that there may be increased autophagosome development, or a decrease in late endosomal development, in IKK KO cells (Figure 4.6). However, we see a decrease in both phosphorylated and unphosphorylated

p62, suggesting that this protein may have decreased expression. This would hinder autophagosome maturation and inhibit protein degradation by the lysosome. Although p62 can still be produced by the Keap1-Nrf2 oxidative stress pathway, a decrease in NF-κB signaling in IKK KO microglia may have contributed to an overall decrease in p62 expression, leading to impairments in autophagy, causing increased buildup of PrP^{Sc} in cultures containing IKK KO microglia. Moreover, signals that activate the IKK complex have been shown to initiate autophagy even in the absence of downstream NF-κB signaling, suggesting that knockout of IKK leads impaired autophagy regardless of NF-κB-induced p62 signaling.[114]

Further characterization of this model is necessary to understand how microglia-specific IKK KO affects overall NF-κB signaling, as well as downstream effects such as the involvement of other inflammatory pathways, namely autophagy, and neuronal cell death. Although we see profound differences in each of these responses to prion infection, it is difficult to tease out whether this is due to the role IKK plays, or the overall decrease in microglia in response to IKK KO. *In vivo* studies are the obvious next step to begin to answer these questions. Understanding the involvement of IKK and NF-κB signaling in microglia may help uncover both biomarkers and therapeutic targets for prion diseases.

Supplemental Data

Supplemental Table 4.1. NF-κB-related genes with significant fold change comparing RML-infected microglia-specific IKK KO to C57 mixed glia

Gene Symbol	Fold Δ	p Value		Gene Symbol	Fold Δ	p Value
Atf1	-1.82	0.000312		*Mapk3*	-1.97	0.002692
Bcl10	-1.72	0.000448		*Myd88*	-3.05	0.005395
Bcl2a1a	-199.00	0.000017		*Nfkb1*	-3.05	0.000020
Bcl3	-8.19	0.000360		*Nfkb2*	-1.66	0.000535
Birc3	-5.58	0.000312		*Nfkbia*	-2.54	0.006722
Card11	-27.81	0.001518		*Nod1*	-2.48	0.000048
Casp1	-4.60	0.000048		*Rel*	-7.50	0.000248
Casp8	-5.65	0.000505		*Rela*	-1.76	0.001384
Ccl2	-3.14	0.005412		*Relb*	-2.83	0.001681
Ccl5	-16.46	0.000076		*Ripk1*	-3.30	0.000846
Cd27	-3.51	0.023269		*Ripk2*	-1.88	0.003934
Cd40	-4.43	0.004571		*Stat1*	-2.63	0.000014
Cflar	-2.07	0.000412		*Tbk1*	-2.24	0.000532
Chuk	-2.15	0.004812		*Tlr1*	-188.38	0.002608
Csf1	2.39	0.005718		*Tlr2*	-28.98	0.000196
Egfr	2.91	0.005073		*Tlr3*	-1.56	0.033222
Egr1	-3.07	0.019219		*Tlr4*	-4.74	0.000531
F2r	1.76	0.001001		*Tlr6*	-14.74	0.000142
Fos	-1.94	0.035054		*Tlr9*	-193.02	0.000007
Hmox1	-2.96	0.000096		*Tnf*	-153.33	0.000141
Icam1	-2.54	0.000017		*Tnfaip3*	-5.75	0.002321
Ikbkb	-2.51	0.000324		*Tnfrsf1b*	-15.64	0.000156
Ikbke	-10.17	0.004238		*Tnfsf10*	-7.13	0.002627
Il10	-21.46	0.000871		*Tnfsf10b*	1.83	0.006976
Il1a	-57.43	0.001057		*Tnfsf14*	-15.85	0.001487
Il1b	-46.23	0.000453		*Tradd*	-1.60	0.000172
Irak2	-3.67	0.000021		*Traf2*	-1.79	0.000312
Irf1	-2.09	0.000685		*Traf5*	-3.39	0.000106
Lta	1.69	0.006960		*Traf6*	-1.86	0.001397
Map3k1	-5.83	0.000110				

Chapter 5:

Summary and Future Directions

This work highlights the importance of microglia, astrocytes, and the cross-talk between the two in the prion-infected brain. Prion diseases remain untreatable and invariably fatal, despite numerous efforts to develop therapeutics. Antibodies and small molecules that specifically target PrP^{Sc} have been unsuccessful or shown strain specificity.[157,159] Research has uncovered a huge number of cellular pathways that are dysregulated by PrP^{Sc} aggregation, but unfortunately developing drugs to target some of these pathways has had toxic side effects in animal models or clinical trials.[151,157] There is an urgent need for safe, effective therapeutics for human prion diseases, to treat individuals with sporadic disease, help those whose families are plagued with genetic disease, and alleviate any threats of an outbreak if chronic wasting disease crosses the species barrier into humans.[28,246]

Although further works is required to optimize them as a therapeutic for prion disease, we propose mesenchymal stromal cells (MSCs) as a promising candidate to decrease astrocyte reactivity, polarize microglia toward a homeostatic phenotype, and reduce overall inflammation in the prion-infected brain. Adipose-derived MSCs (AdMSCs) have the potential to be taken from a patient, can be easily isolated and expanded in culture, and be delivered autologously to said patient.[178] Although we have focused on intranasal delivery, which is a common method used,[167,220,247] other studies have used intracranial delivery and intravenous delivery and showed effective MSC trafficking to the brain.[160,177,210] These are both routes that should be considered for further investigation - particularly intracranial delivery. Despite being less therapeutically applicable, it may be the best "proof-of-principle" to assess the benefits of AdMSCs against

prion disease. The greatest disappointment we encountered was that in our animal model, AdMSCs were unable to attenuate neurodegeneration, which resulted in no improvement in behavior or increase in survival time. This may be due not to the ineffectiveness of AdMSCs in promoting neuronal health, but due to only a small number of them reaching the site of neurodegeneration, not enough to combat the effects of PrP^{Sc} aggregation at late timepoints in disease. Therefore, utilization of a more direct delivery method for AdMSCs will be best to evaluate their efficacy in either direct or indirect intervention against prion-induced neurodegeneration.

A second focus of further investigation is into the factors that are secreted by AdMSCs that directly benefit the prion-infected brain. It is very unlikely that this is just a singular factor. We were intrigued by TSG-6, which is secreted by AdMSCs upon stimulation with both cytokines and prion-infected brain homogenates,[123] and has been shown to attenuate NF-κB signaling in glia and polarize microglia to an M2 phenotype.[161,163,203] To assess the role of TSG-6 in decreasing inflammation in BV2 cells, we used small interfering RNA (siRNA) to knock down TSG-6 in AdMSCs (Figure 5.1A-B) and co-cultured them with RML-treated BV2 microglia (Figure 5.1C-E). We saw a decrease in inflammatory markers *IL1β* and *IL6*, and an increase in the M2 microglia marker *Arg-1* when co-cultured with AdMSCs for 24 hours. However, there seemed to be no changes between wild-type (WT) and TSG-6 siRNA knockdown AdMSCs. Although this experiment should be repeated, it suggests that TSG-6 alone is not the main contributing factor to AdMSC-induced protection against inflammation, and these cells likely contain a variety of beneficial small molecules.

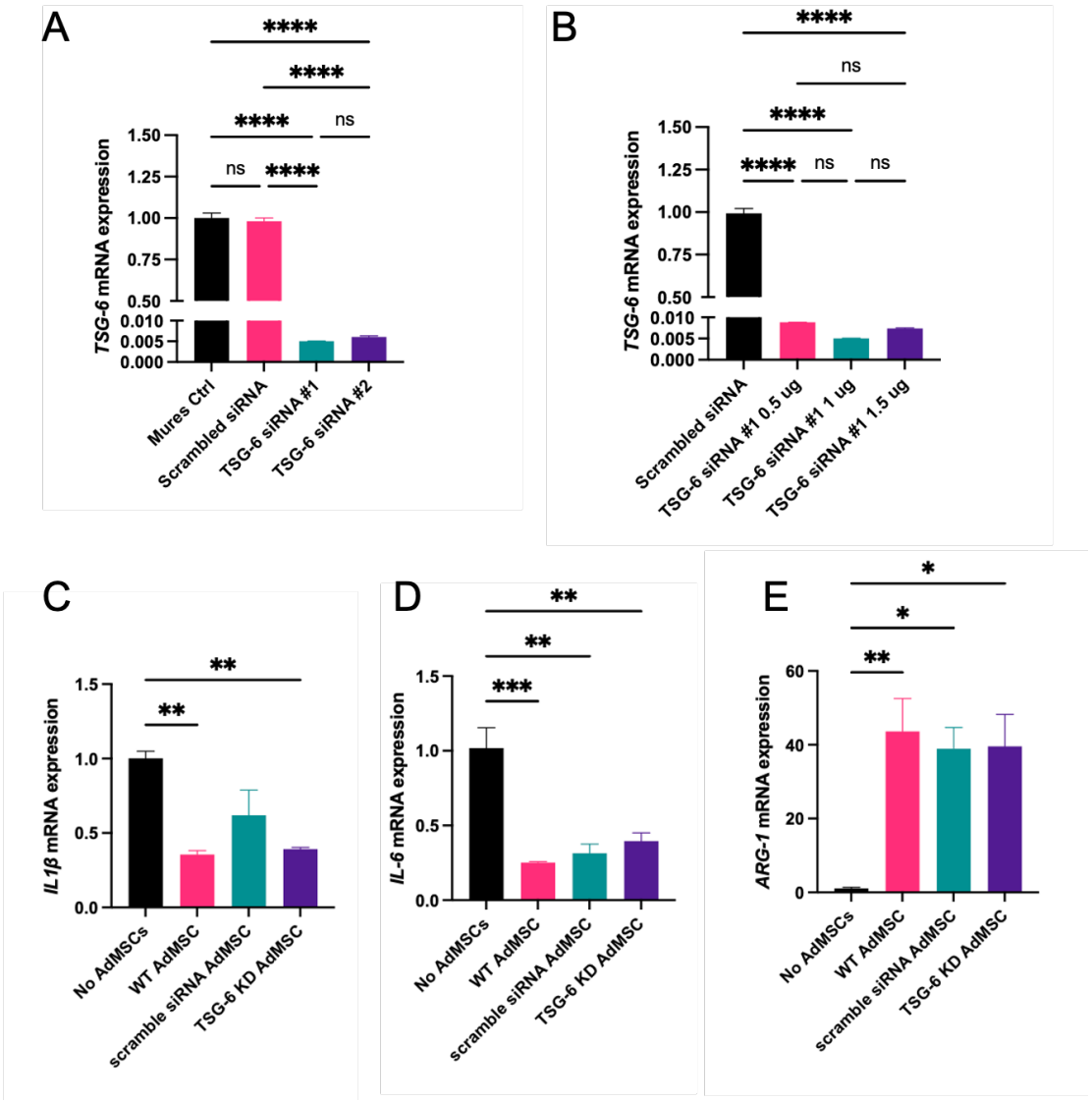

Figure 5.1. SiRNA knock-down of TSG-6 has no effect on AdMSC attenuation of BV2 inflammation. A) Two siRNA sequences were tested to knock-down TSG-6 in AdMSCs for 48 hours, using Mures as a delivery method. B) Various amounts of siRNA #1 were tested to knock-down TSG-6 in AdMSCs for 48 hours. 1µg siRNA #1 was used to knock-down TSG-6 in AdMSCs for 48 hours in cell-culture plate inserts. After 24 hours, AdMSC inserts were placed on RML-scrapie-treated BV2 cells and co-cultured for the additional 24 hours. RNA was isolated and analyzed for C) *IL1β*, D) IL6 and E) Arg-1. One biological replicate each with three technical replicates. Normalized to *βactin*. One-way ANOVA and post-hoc Tukey test, error bars = SEM, * $p< 0.05$, ** $p< 0.01$, *** $p< 0.001$, **** $p< 0.0001$, ns = not significant.

It has been well established that the therapeutic properties of MSCs are not from their stem-cell-like properties and ability to differentiate to a variety of cell types, but from their propensity to migrate and interact with a variety of cell types through paracrine signaling. This

has been attributed not to the cells themselves, but through the extracellular vesicles (EVs) that they secrete.[174,211,212,234] EVs generally refers to exosomes, microvesicles, and apoptotic bodies. MSC-derived EVs (MSC-EVs) have been shown to contain neurotrophic factors that contribute to neural cell proliferation and differentiation, and growth factors such as VEGF and FGF that promote angiogenesis, stimulating growth of blood vessels to improve neuronal survival.[233,234] Of course, MSC-EVs contain a plethora of anti-inflammatory cytokines and chemokines that can act upon glial cells to reprogram them to a protective phenotype.[233] MicroRNAs contained in EVs have demonstrated the ability to increase endothelial cell proliferation, improving blood brain barrier (BBB) integrity.[248] They also can contain enzymes such as nephrilysin, which is potent in degrading amyloid-β in Alzheimer's disease models.[249]

Like the cells they are derived from, MSC-EVs express surface markers and membrane-binding proteins such as CD29 and CD44, allowing for them to be selected for, characterized, and, most importantly, interact with cells of interest. They can remain in the brain longer than the cells they are derived from, and there is no concern that they will undergo aging or form tumors, or elicit a significant immune response.[234] In fact, multiple clinical trials are underway for using EVs to treat amyotrophic lateral sclerosis and multiple sclerosis.[234] Moreover, EVs from AdMSCs, due to their smaller size, may more easily migrate to the brain and cross the BBB, which may address the aforementioned problem of ensuring that the therapeutic is reaching the brain.

A final pitch for the use of MSC-derived EVs for the treatment of prion disease is their potential to be modulated. As we have shown, stimulating MSCs with cytokines or prion-infected brain homogenates promotes their production of anti-inflammatory molecules and growth factors. "Priming" these cells can be taken a step further, by loading these EVs with

specific cargo to be delivered to the brain region of interest. This was elegantly demonstrated recently by Peng et al. in a mouse model of Parkinson's disease. They developed MSC-derived exosomes that, when delivered intranasally, specifically migrated to sites of increased reactive oxygen species - to dopaminergic neurons in the substantia nigra. These exosomes were loaded with curcumin, which decreased α-synuclein aggregates and neurotoxicity, and increased dopamine production. Additionally, these exosomes downregulated a variety of inflammatory cytokines and disease-associated microglia.[214]

How could we utilize this therapeutic strategy to specifically target PrP^{Sc} and related neurotoxicity and neuroinflammation? Based on the work I present in this dissertation, my suggestion would be two-fold: 1) stimulate AdMSCs to produce EVs containing increased immunomodulating molecules and growth factors to target glial inflammation,[123] and 2) load these EVs with drugs to promote PrP^{Sc} degradation, such as rapamycin to induce autophagy.[144,250]

A caveat to developing therapeutics for prion diseases is that diagnoses for these diseases often come too late for treatments to be effective. This isn't the case for genetic prion diseases, however, as these can be screened for. Therefore, a current direction we are taking to assess AdMSCs as a treatment for prion diseases is using animal models of genetic prion disease. We are currently exploring the therapeutic potential of intracranially-delivered AdMSCs into a mouse model of Gerstmann-Straussler-Scheinker Syndrome (GSS), a disease characterized by a single point mutation, P102L, (P101L in mice) in the prion protein. This mutation leads to spontaneous PrP^{Sc} development. In a mouse model, this induces major PrP^{Sc} aggregation in the cerebellum, which leads to motor dysfunction and ataxia, and eventually death.[251,252] We are working to characterize the inflammatory and glial profile, as well as neuronal function using

electrophysiology, over the course of aging in this mouse model. Additionally, we are using stereotaxic injections to deliver TNFα-stimulated AdMSCs into the cerebellum of GSS mice. These mice live approximately 24 weeks before they die of naturally-accumulated PrP^{Sc}. We have delivered $2x10^5$ stimulated AdMSCs to the left cerebellar hemisphere of mice at 12 weeks, 16 weeks, and 18 weeks, and euthanized them at 16 weeks, 18 weeks, and 22 weeks, respectively. Currently, cerebellar mRNA has only been analyzed for the mice that received AdMSCs at 12 weeks (and were euthanized at 16 weeks) (Figure 5.2).

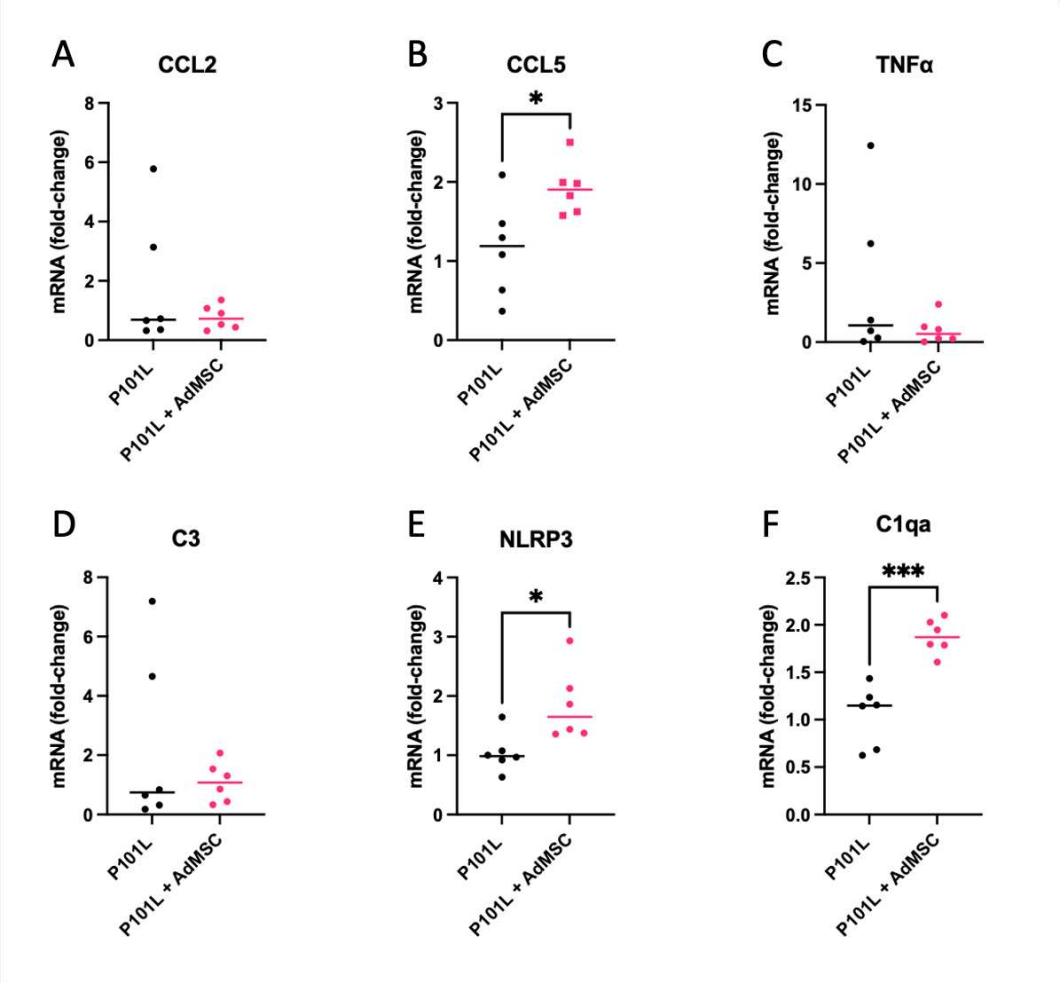

Figure 5.2. mRNA profile of 16-week-old GSS P101L mice after intra-cerebellar AdMSC delivery at 12 weeks. Animals received either PBS or $2x10^5$ TNFα-stimulated AdMSCs through stereotaxic delivery to the left hippocampus at 12 weeks of age. Cerebellar mRNA was analyzed for A) *CCL2*, B) *CCL5*, C) *TNFα*, D) *C3*, E) *NLRP3* and F) *C1qa*. Five or six biological replicates each with three technical replicates. Normalized to *βactin*. Unpaired T-test, error bars = SEM, * $p< 0.05$, *** $p< 0.001$.

Unexpectedly, treatment with AdMSCs actually increased markers of inflammation. Further analysis with different time points for treatment is necessary to assess if this treatment is beneficial or detrimental to this model of GSS. Additionally, the effect on astrocytes, microglia, and most importantly neurons, need to be further assessed in these animals.

In addition to introducing AdMSCs as a therapeutic for glial-induced inflammation in prion disease, this work also highlights the importance of IKK and NF-κB signaling in microglia in prion pathogenesis. We have shown that an in vitro model of prion-infected mixed glia shows significantly decreased NF-κB-related genes in cultures containing IKK KO microglia. However, these cultures have increased PrP^{Sc} accumulation and lowered markers of autophagy. Interestingly, these cultures contain significantly fewer microglia compared to WT cultures. Are the effects we are seeing the result of IKK KO in microglia, a reduction of microglia as a whole, or a combination of both? Both increased inflammation and impaired autophagy have been shown to be detrimental in prion animal models.[49,92,144] Which of the two of these factors is most important for survival? The best way to answer this is, of course, by observing this *in vivo*. We have inoculated both WT and microglia-specific IKK KO mice with RML mouse-adapted scrapie. Over the next few months, we will be performing behavioral assays and checking them for signs of clinical disease. After euthanasia, we will assess the brains for PrP^{Sc} accumulation and markers of autophagy, hippocampal mRNA expression of NF-κB and NLRP3-related genes, and astrocyte and microglia number and morphology. Additionally, we will assess neuronal health between these mice by counting pyknotic neurons in the CA1 region of the hippocampus, and evaluate the relative amount of vacuoles throughout the brain. Ultimately, we hope to thoroughly characterize the role of IKK and NF-κB signaling in microglia, and determine if this would be an effective therapeutic target for prion disease.

References

1 Gajdusek, D. C. Transmissible and non-transmissible amyloidoses: autocatalytic post-translational conversion of host precursor proteins to beta-pleated sheet configurations. *J Neuroimmunol* **20**, 95-110 (1988). https://doi.org:10.1016/0165-5728(88)90140-3

2 Diack, A. B. *et al.* Insights into Mechanisms of Chronic Neurodegeneration. *Int J Mol Sci* **17** (2016). https://doi.org:10.3390/ijms17010082

3 Kretzschmar, H. & Tatzelt, J. Prion disease: a tale of folds and strains. *Brain Pathol* **23**, 321-332 (2013). https://doi.org:10.1111/bpa.12045

4 Moser, M., Colello, R. J., Pott, U. & Oesch, B. Developmental expression of the prion protein gene in glial cells. *Neuron* **14**, 509-517 (1995). https://doi.org:10.1016/0896-6273(95)90307-0

5 Lakkaraju, A. K. K. *et al.* Loss of PIKfyve drives the spongiform degeneration in prion diseases. *EMBO Mol Med* **13**, e14714 (2021). https://doi.org:10.15252/emmm.202114714

6 Cheng, C. J. & Daggett, V. Molecular dynamics simulations capture the misfolding of the bovine prion protein at acidic pH. *Biomolecules* **4**, 181-201 (2014). https://doi.org:10.3390/biom4010181

7 Puoti, G. *et al.* Sporadic human prion diseases: molecular insights and diagnosis. *Lancet Neurol* **11**, 618-628 (2012). https://doi.org:10.1016/S1474-4422(12)70063-7

8 O'Sullivan, D. B. *et al.* NMR characterization of the pH 4 beta-intermediate of the prion protein: the N-terminal half of the protein remains unstructured and retains a high degree of flexibility. *Biochem J* **401**, 533-540 (2007). https://doi.org:10.1042/BJ20060668

9 Huang, P., Lian, F., Wen, Y., Guo, C. & Lin, D. Prion protein oligomer and its neurotoxicity. *Acta Biochim Biophys Sin (Shanghai)* **45**, 442-451 (2013). https://doi.org:10.1093/abbs/gmt037

10 Salahuddin, P., Fatima, M. T., Abdelhameed, A. S., Nusrat, S. & Khan, R. H. Structure of amyloid oligomers and their mechanisms of toxicities: Targeting amyloid oligomers using novel therapeutic approaches. *Eur J Med Chem* **114**, 41-58 (2016). https://doi.org:10.1016/j.ejmech.2016.02.065

11 Forloni, G. *et al.* Neurotoxicity of a prion protein fragment. *Nature* **362**, 543-546 (1993). https://doi.org:10.1038/362543a0

12 Yu, Z. *et al.* Unique Properties of the Rabbit Prion Protein Oligomer. *PLoS One* **11**, e0160874 (2016). https://doi.org:10.1371/journal.pone.0160874

13 Liberski, P. P. Kuru: a journey back in time from papua new Guinea to the neanderthals' extinction. *Pathogens* **2**, 472-505 (2013). https://doi.org:10.3390/pathogens2030472

14 Mathiason, C. K. Scrapie, CWD, and Transmissible Mink Encephalopathy. *Prog Mol Biol Transl Sci* **150**, 267-292 (2017). https://doi.org:10.1016/bs.pmbts.2017.07.009

15 Wickner, R. B. Scrapie in ancient China? *Science* **309**, 874 (2005). https://doi.org:10.1126/science.309.5736.874b

16 Prevention, C. f. D. C. a. Chronic Wasting Disease (CWD): Occurance. (2023).

17 Huang, W. J., Chen, W. W. & Zhang, X. Prions mediated neurodegenerative disorders. *Eur Rev Med Pharmacol Sci* **19**, 4028-4034 (2015).

18 Asante, E. A. *et al.* A naturally occurring variant of the human prion protein completely prevents prion disease. *Nature* **522**, 478-481 (2015). https://doi.org:10.1038/nature14510

19 Collinge, J. *et al.* Kuru in the 21st century--an acquired human prion disease with very long incubation periods. *Lancet* **367**, 2068-2074 (2006). https://doi.org:10.1016/S0140-6736(06)68930-7
20 Zhou, S., Shi, D., Liu, X., Liu, H. & Yao, X. Protective V127 prion variant prevents prion disease by interrupting the formation of dimer and fibril from molecular dynamics simulations. *Sci Rep* **6**, 21804 (2016). https://doi.org:10.1038/srep21804
21 Mead, S. *et al.* A novel protective prion protein variant that colocalizes with kuru exposure. *N Engl J Med* **361**, 2056-2065 (2009). https://doi.org:10.1056/NEJMoa0809716
22 Prusiner, S. B. Novel proteinaceous infectious particles cause scrapie. *Science* **216**, 136-144 (1982). https://doi.org:10.1126/science.6801762
23 Health, N. I. o. Creutzfeldt-Jakob Disease. (2023).
24 Prevention, C. f. D. C. a. Creutzfeldt-Jakob Disease, Classic (CJD). (2021).
25 Kobayashi, A., Kitamoto, T. & Mizusawa, H. Iatrogenic Creutzfeldt-Jakob disease. *Handb Clin Neurol* **153**, 207-218 (2018). https://doi.org:10.1016/B978-0-444-63945-5.00012-X
26 Brandel, J. P. & Knight, R. Variant Creutzfeldt-Jakob disease. *Handb Clin Neurol* **153**, 191-205 (2018). https://doi.org:10.1016/B978-0-444-63945-5.00011-8
27 Hannaoui, S. *et al.* Transmission of cervid prions to humanized mice demonstrates the zoonotic potential of CWD. *Acta Neuropathol* **144**, 767-784 (2022). https://doi.org:10.1007/s00401-022-02482-9
28 Race, B. *et al.* Chronic wasting disease agents in nonhuman primates. *Emerg Infect Dis* **20**, 833-837 (2014). https://doi.org:10.3201/eid2005.130778
29 Joseph Wiedemer, Y. S. C., An Cao and Ibrahim Mustafa. A Unique Presentation of Creutzfeldt-Jakob Disease in a Patient Consuming Deer Antler Velvet. *American Journal of Infectious Diseases* **17**, 43-48 (2021).
30 Wagner, K. *et al.* Tissue-specific biochemical differences between chronic wasting disease prions isolated from free-ranging white-tailed deer (Odocoileus virginianus). *J Biol Chem* **298**, 101834 (2022). https://doi.org:10.1016/j.jbc.2022.101834
31 Carta, M. & Aguzzi, A. Molecular foundations of prion strain diversity. *Curr Opin Neurobiol* **72**, 22-31 (2022). https://doi.org:10.1016/j.conb.2021.07.010
32 Bartz, J. C. Prion Strain Diversity. *Cold Spring Harb Perspect Med* **6** (2016). https://doi.org:10.1101/cshperspect.a024349
33 Cobb, N. J. & Surewicz, W. K. Prion diseases and their biochemical mechanisms. *Biochemistry* **48**, 2574-2585 (2009). https://doi.org:10.1021/bi900108v
34 Legname, G. Elucidating the function of the prion protein. *PLoS Pathog* **13**, e1006458 (2017). https://doi.org:10.1371/journal.ppat.1006458
35 Bueler, H. *et al.* Normal development and behaviour of mice lacking the neuronal cell-surface PrP protein. *Nature* **356**, 577-582 (1992). https://doi.org:10.1038/356577a0
36 Bueler, H. *et al.* Mice devoid of PrP are resistant to scrapie. *Cell* **73**, 1339-1347 (1993). https://doi.org:10.1016/0092-8674(93)90360-3
37 Manson, J. C. *et al.* 129/Ola mice carrying a null mutation in PrP that abolishes mRNA production are developmentally normal. *Mol Neurobiol* **8**, 121-127 (1994). https://doi.org:10.1007/BF02780662
38 Lakkaraju, A. K. K. *et al.* Glial activation in prion diseases is selectively triggered by neuronal PrP(Sc). *Brain Pathol* **32**, e13056 (2022). https://doi.org:10.1111/bpa.13056

39 Mallucci, G. *et al.* Depleting neuronal PrP in prion infection prevents disease and reverses spongiosis. *Science* **302**, 871-874 (2003). https://doi.org:10.1126/science.1090187
40 von Bartheld, C. S., Bahney, J. & Herculano-Houzel, S. The search for true numbers of neurons and glial cells in the human brain: A review of 150 years of cell counting. *J Comp Neurol* **524**, 3865-3895 (2016). https://doi.org:10.1002/cne.24040
41 Prinz, M. *et al.* Intrinsic resistance of oligodendrocytes to prion infection. *J Neurosci* **24**, 5974-5981 (2004). https://doi.org:10.1523/JNEUROSCI.0122-04.2004
42 Liu, L. R., Liu, J. C., Bao, J. S., Bai, Q. Q. & Wang, G. Q. Interaction of Microglia and Astrocytes in the Neurovascular Unit. *Front Immunol* **11**, 1024 (2020). https://doi.org:10.3389/fimmu.2020.01024
43 Simmons, M. L. & Murphy, S. Induction of nitric oxide synthase in glial cells. *J Neurochem* **59**, 897-905 (1992). https://doi.org:10.1111/j.1471-4159.1992.tb08328.x
44 Hansson, E. & Ronnback, L. Glial neuronal signaling in the central nervous system. *FASEB J* **17**, 341-348 (2003). https://doi.org:10.1096/fj.02-0429rev
45 Liddelow, S. A. *et al.* Neurotoxic reactive astrocytes are induced by activated microglia. *Nature* **541**, 481-487 (2017). https://doi.org:10.1038/nature21029
46 Chen, S. H. *et al.* Microglial regulation of immunological and neuroprotective functions of astroglia. *Glia* **63**, 118-131 (2015). https://doi.org:10.1002/glia.22738
47 Liddelow, S. A. & Barres, B. A. Reactive Astrocytes: Production, Function, and Therapeutic Potential. *Immunity* **46**, 957-967 (2017). https://doi.org:10.1016/j.immuni.2017.06.006
48 Carroll, J. A. *et al.* Prion Strain Differences in Accumulation of PrPSc on Neurons and Glia Are Associated with Similar Expression Profiles of Neuroinflammatory Genes: Comparison of Three Prion Strains. *PLoS Pathog* **12**, e1005551 (2016). https://doi.org:10.1371/journal.ppat.1005551
49 Hartmann, K. *et al.* Complement 3(+)-astrocytes are highly abundant in prion diseases, but their abolishment led to an accelerated disease course and early dysregulation of microglia. *Acta Neuropathol Commun* **7**, 83 (2019). https://doi.org:10.1186/s40478-019-0735-1
50 Carroll, J. A., Race, B., Williams, K., Striebel, J. & Chesebro, B. RNA-seq and network analysis reveal unique glial gene expression signatures during prion infection. *Mol Brain* **13**, 71 (2020). https://doi.org:10.1186/s13041-020-00610-8
51 He, M. *et al.* Astrocyte-Derived CCL2 is Associated with M1 Activation and Recruitment of Cultured Microglial Cells. *Cell Physiol Biochem* **38**, 859-870 (2016). https://doi.org:10.1159/000443040
52 Jurga, A. M., Paleczna, M. & Kuter, K. Z. Overview of General and Discriminating Markers of Differential Microglia Phenotypes. *Front Cell Neurosci* **14**, 198 (2020). https://doi.org:10.3389/fncel.2020.00198
53 Sansing, L. H. *et al.* Toll-like receptor 4 contributes to poor outcome after intracerebral hemorrhage. *Ann Neurol* **70**, 646-656 (2011). https://doi.org:10.1002/ana.22528
54 Tang, Y. & Le, W. Differential Roles of M1 and M2 Microglia in Neurodegenerative Diseases. *Mol Neurobiol* **53**, 1181-1194 (2016). https://doi.org:10.1007/s12035-014-9070-5
55 Soulet, D. & Rivest, S. Microglia. *Curr Biol* **18**, R506-508 (2008). https://doi.org:10.1016/j.cub.2008.04.047

56 Chhor, V. *et al.* Characterization of phenotype markers and neuronotoxic potential of polarised primary microglia in vitro. *Brain Behav Immun* **32**, 70-85 (2013). https://doi.org:10.1016/j.bbi.2013.02.005
57 Shi, F. *et al.* Inhibition of phagocytosis reduced the classical activation of BV2 microglia induced by amyloidogenic fragments of beta-amyloid and prion proteins. *Acta Biochim Biophys Sin (Shanghai)* **45**, 973-978 (2013). https://doi.org:10.1093/abbs/gmt101
58 Tribouillard-Tanvier, D. *et al.* Early cytokine elevation, PrPres deposition, and gliosis in mouse scrapie: no effect on disease by deletion of cytokine genes IL-12p40 and IL-12p35. *J Virol* **86**, 10377-10383 (2012). https://doi.org:10.1128/JVI.01340-12
59 Manuelidis, L., Tesin, D. M., Sklaviadis, T. & Manuelidis, E. E. Astrocyte gene expression in Creutzfeldt-Jakob disease. *Proc Natl Acad Sci U S A* **84**, 5937-5941 (1987). https://doi.org:10.1073/pnas.84.16.5937
60 Scheckel, C., Imeri, M., Schwarz, P. & Aguzzi, A. Ribosomal profiling during prion disease uncovers progressive translational derangement in glia but not in neurons. *Elife* **9** (2020). https://doi.org:10.7554/eLife.62911
61 Beekes, M. *et al.* Late increase of serum S100 beta protein levels in hamsters after oral or intraperitoneal infection with scrapie. *J Infect Dis* **180**, 518-520 (1999). https://doi.org:10.1086/314907
62 Otto, M. *et al.* Diagnosis of Creutzfeldt-Jakob disease by measurement of S100 protein in serum: prospective case-control study. *BMJ* **316**, 577-582 (1998). https://doi.org:10.1136/bmj.316.7131.577
63 Coulthart, M. B. *et al.* Diagnostic accuracy of cerebrospinal fluid protein markers for sporadic Creutzfeldt-Jakob disease in Canada: a 6-year prospective study. *BMC Neurol* **11**, 133 (2011). https://doi.org:10.1186/1471-2377-11-133
64 Smith, H. L. *et al.* Astrocyte Unfolded Protein Response Induces a Specific Reactivity State that Causes Non-Cell-Autonomous Neuronal Degeneration. *Neuron* **105**, 855-866 e855 (2020). https://doi.org:10.1016/j.neuron.2019.12.014
65 Lee, S., Jha, M. K. & Suk, K. Lipocalin-2 in the Inflammatory Activation of Brain Astrocytes. *Crit Rev Immunol* **35**, 77-84 (2015). https://doi.org:10.1615/critrevimmunol.2015012127
66 Guttenplan, K. A. *et al.* Neurotoxic reactive astrocytes induce cell death via saturated lipids. *Nature* **599**, 102-107 (2021). https://doi.org:10.1038/s41586-021-03960-y
67 Kushwaha, R., Sinha, A., Makarava, N., Molesworth, K. & Baskakov, I. V. Non-cell autonomous astrocyte-mediated neuronal toxicity in prion diseases. *Acta Neuropathol Commun* **9**, 22 (2021). https://doi.org:10.1186/s40478-021-01123-8
68 Pankiewicz, J. E. *et al.* Absence of Apolipoprotein E is associated with exacerbation of prion pathology and promotes microglial neurodegenerative phenotype. *Acta Neuropathol Commun* **9**, 157 (2021). https://doi.org:10.1186/s40478-021-01261-z
69 Wang, Y. *et al.* Loss of Homeostatic Microglia Signature in Prion Diseases. *Cells* **11** (2022). https://doi.org:10.3390/cells11192948
70 Satoh, J. *et al.* TMEM119 marks a subset of microglia in the human brain. *Neuropathology* **36**, 39-49 (2016). https://doi.org:10.1111/neup.12235
71 Victoria, G. S., Arkhipenko, A., Zhu, S., Syan, S. & Zurzolo, C. Astrocyte-to-neuron intercellular prion transfer is mediated by cell-cell contact. *Sci Rep* **6**, 20762 (2016). https://doi.org:10.1038/srep20762

72 Sandberg, M. K. *et al.* Prion neuropathology follows the accumulation of alternate prion protein isoforms after infective titre has peaked. *Nat Commun* **5**, 4347 (2014). https://doi.org:10.1038/ncomms5347
73 Makarava, N., Chang, J. C., Kushwaha, R. & Baskakov, I. V. Region-Specific Response of Astrocytes to Prion Infection. *Front Neurosci* **13**, 1048 (2019). https://doi.org:10.3389/fnins.2019.01048
74 Zeisel, A. *et al.* Molecular Architecture of the Mouse Nervous System. *Cell* **174**, 999-1014 e1022 (2018). https://doi.org:10.1016/j.cell.2018.06.021
75 Gomez-Nicola, D., Fransen, N. L., Suzzi, S. & Perry, V. H. Regulation of microglial proliferation during chronic neurodegeneration. *J Neurosci* **33**, 2481-2493 (2013). https://doi.org:10.1523/JNEUROSCI.4440-12.2013
76 Giese, A. *et al.* Role of microglia in neuronal cell death in prion disease. *Brain Pathol* **8**, 449-457 (1998). https://doi.org:10.1111/j.1750-3639.1998.tb00167.x
77 Baker, C. A., Martin, D. & Manuelidis, L. Microglia from Creutzfeldt-Jakob disease-infected brains are infectious and show specific mRNA activation profiles. *J Virol* **76**, 10905-10913 (2002). https://doi.org:10.1128/jvi.76.21.10905-10913.2002
78 Priller, J. *et al.* Early and rapid engraftment of bone marrow-derived microglia in scrapie. *J Neurosci* **26**, 11753-11762 (2006). https://doi.org:10.1523/JNEUROSCI.2275-06.2006
79 Carroll, J. A. & Chesebro, B. Neuroinflammation, Microglia, and Cell-Association during Prion Disease. *Viruses* **11** (2019). https://doi.org:10.3390/v11010065
80 Hughes, M. M., Field, R. H., Perry, V. H., Murray, C. L. & Cunningham, C. Microglia in the degenerating brain are capable of phagocytosis of beads and of apoptotic cells, but do not efficiently remove PrPSc, even upon LPS stimulation. *Glia* **58**, 2017-2030 (2010). https://doi.org:10.1002/glia.21070
81 Hong, S. *et al.* Complement and microglia mediate early synapse loss in Alzheimer mouse models. *Science* **352**, 712-716 (2016). https://doi.org:10.1126/science.aad8373
82 Garcao, P., Oliveira, C. R. & Agostinho, P. Comparative study of microglia activation induced by amyloid-beta and prion peptides: role in neurodegeneration. *J Neurosci Res* **84**, 182-193 (2006). https://doi.org:10.1002/jnr.20870
83 Thackray, A. M., McKenzie, A. N., Klein, M. A., Lauder, A. & Bujdoso, R. Accelerated prion disease in the absence of interleukin-10. *J Virol* **78**, 13697-13707 (2004). https://doi.org:10.1128/JVI.78.24.13697-13707.2004
84 Carroll, J. A., Striebel, J. F., Race, B., Phillips, K. & Chesebro, B. Prion infection of mouse brain reveals multiple new upregulated genes involved in neuroinflammation or signal transduction. *J Virol* **89**, 2388-2404 (2015). https://doi.org:10.1128/JVI.02952-14
85 Shi, F. *et al.* Prion protein participates in the regulation of classical and alternative activation of BV2 microglia. *J Neurochem* **124**, 168-174 (2013). https://doi.org:10.1111/jnc.12053
86 Ding, T. *et al.* Cellular prion protein participates in the regulation of inflammatory response and apoptosis in BV2 microglia during infection with Mycobacterium bovis. *J Mol Neurosci* **51**, 118-126 (2013). https://doi.org:10.1007/s12031-013-9962-2
87 Race, B. *et al.* Microglia have limited influence on early prion pathogenesis, clearance, or replication. *PLoS One* **17**, e0276850 (2022). https://doi.org:10.1371/journal.pone.0276850
88 Veremeyko, T., Yung, A. W. Y., Dukhinova, M., Strekalova, T. & Ponomarev, E. D. The Role of Neuronal Factors in the Epigenetic Reprogramming of Microglia in the Normal

and Diseased Central Nervous System. *Front Cell Neurosci* **13**, 453 (2019). https://doi.org:10.3389/fncel.2019.00453
89 De Lucia, C. *et al.* Microglia regulate hippocampal neurogenesis during chronic neurodegeneration. *Brain Behav Immun* **55**, 179-190 (2016). https://doi.org:10.1016/j.bbi.2015.11.001
90 Zhu, C. *et al.* A neuroprotective role for microglia in prion diseases. *J Exp Med* **213**, 1047-1059 (2016). https://doi.org:10.1084/jem.20151000
91 Carroll, J. A., Race, B., Williams, K., Striebel, J. & Chesebro, B. Microglia Are Critical in Host Defense against Prion Disease. *J Virol* **92** (2018). https://doi.org:10.1128/JVI.00549-18
92 Bradford, B. M., McGuire, L. I., Hume, D. A., Pridans, C. & Mabbott, N. A. Microglia deficiency accelerates prion disease but does not enhance prion accumulation in the brain. *Glia* **70**, 2169-2187 (2022). https://doi.org:10.1002/glia.24244
93 de Melo, A. *et al.* The role of microglia in prion diseases and possible therapeutic targets: a literature review. *Prion* **15**, 191-206 (2021). https://doi.org:10.1080/19336896.2021.1991771
94 Benilova, I. *et al.* Highly infectious prions are not directly neurotoxic. *Proc Natl Acad Sci U S A* **117**, 23815-23822 (2020). https://doi.org:10.1073/pnas.2007406117
95 Sandberg, M. K., Al-Doujaily, H., Sharps, B., Clarke, A. R. & Collinge, J. Prion propagation and toxicity in vivo occur in two distinct mechanistic phases. *Nature* **470**, 540-542 (2011). https://doi.org:10.1038/nature09768
96 Giese, A., Groschup, M. H., Hess, B. & Kretzschmar, H. A. Neuronal cell death in scrapie-infected mice is due to apoptosis. *Brain Pathol* **5**, 213-221 (1995). https://doi.org:10.1111/j.1750-3639.1995.tb00597.x
97 Groveman, B. R., Smith, A., Williams, K. & Haigh, C. L. Cerebral organoids as a new model for prion disease. *PLoS Pathog* **17**, e1009747 (2021). https://doi.org:10.1371/journal.ppat.1009747
98 Le, N. T. T., Wu, B. & Harris, D. A. Prion neurotoxicity. *Brain Pathol* **29**, 263-277 (2019). https://doi.org:10.1111/bpa.12694
99 Tanaka, M. *et al.* Comparison of abnormal isoform of prion protein in prion-infected cell lines and primary-cultured neurons by PrPSc-specific immunostaining. *J Gen Virol* **97**, 2030-2042 (2016). https://doi.org:10.1099/jgv.0.000514
100 Hannaoui, S. *et al.* Prion propagation and toxicity occur in vitro with two-phase kinetics specific to strain and neuronal type. *J Virol* **87**, 2535-2548 (2013). https://doi.org:10.1128/JVI.03082-12
101 Suzuki, A., Yamasaki, T., Hasebe, R. & Horiuchi, M. Enhancement of binding avidity by bivalent binding enables PrPSc-specific detection by anti-PrP monoclonal antibody 132. *PLoS One* **14**, e0217944 (2019). https://doi.org:10.1371/journal.pone.0217944
102 Chesebro, B. *et al.* Fatal transmissible amyloid encephalopathy: a new type of prion disease associated with lack of prion protein membrane anchoring. *PLoS Pathog* **6**, e1000800 (2010). https://doi.org:10.1371/journal.ppat.1000800
103 Race, B., Phillips, K., Meade-White, K., Striebel, J. & Chesebro, B. Increased infectivity of anchorless mouse scrapie prions in transgenic mice overexpressing human prion protein. *J Virol* **89**, 6022-6032 (2015). https://doi.org:10.1128/JVI.00362-15
104 Fang, C. *et al.* Prions activate a p38 MAPK synaptotoxic signaling pathway. *PLoS Pathog* **14**, e1007283 (2018). https://doi.org:10.1371/journal.ppat.1007283

105 Goniotaki, D. *et al.* Inhibition of group-I metabotropic glutamate receptors protects against prion toxicity. *PLoS Pathog* **13**, e1006733 (2017). https://doi.org:10.1371/journal.ppat.1006733
106 Shmerling, D. *et al.* Expression of amino-terminally truncated PrP in the mouse leading to ataxia and specific cerebellar lesions. *Cell* **93**, 203-214 (1998). https://doi.org:10.1016/s0092-8674(00)81572-x
107 Li, A. *et al.* Neonatal lethality in transgenic mice expressing prion protein with a deletion of residues 105-125. *EMBO J* **26**, 548-558 (2007). https://doi.org:10.1038/sj.emboj.7601507
108 Biasini, E. *et al.* A mutant prion protein sensitizes neurons to glutamate-induced excitotoxicity. *J Neurosci* **33**, 2408-2418 (2013). https://doi.org:10.1523/JNEUROSCI.3406-12.2013
109 Solomon, I. H. *et al.* An N-terminal polybasic domain and cell surface localization are required for mutant prion protein toxicity. *J Biol Chem* **286**, 14724-14736 (2011). https://doi.org:10.1074/jbc.M110.214973
110 Nuvolone, M., Sorce, S., Schwarz, P. & Aguzzi, A. Prion pathogenesis in the absence of NLRP3/ASC inflammasomes. *PLoS One* **10**, e0117208 (2015). https://doi.org:10.1371/journal.pone.0117208
111 Wardyn, J. D., Ponsford, A. H. & Sanderson, C. M. Dissecting molecular cross-talk between Nrf2 and NF-kappaB response pathways. *Biochem Soc Trans* **43**, 621-626 (2015). https://doi.org:10.1042/BST20150014
112 Liu, T., Zhang, L., Joo, D. & Sun, S. C. NF-kappaB signaling in inflammation. *Signal Transduct Target Ther* **2**, 17023- (2017). https://doi.org:10.1038/sigtrans.2017.23
113 Bourteele, S. *et al.* Alteration of NF-kappaB activity leads to mitochondrial apoptosis after infection with pathological prion protein. *Cell Microbiol* **9**, 2202-2217 (2007). https://doi.org:10.1111/j.1462-5822.2007.00950.x
114 Criollo, A. *et al.* The IKK complex contributes to the induction of autophagy. *EMBO J* **29**, 619-631 (2010). https://doi.org:10.1038/emboj.2009.364
115 Mattson, M. P., Culmsee, C., Yu, Z. & Camandola, S. Roles of nuclear factor kappaB in neuronal survival and plasticity. *J Neurochem* **74**, 443-456 (2000). https://doi.org:10.1046/j.1471-4159.2000.740443.x
116 Kim, J. I. *et al.* Expression of cytokine genes and increased nuclear factor-kappa B activity in the brains of scrapie-infected mice. *Brain Res Mol Brain Res* **73**, 17-27 (1999). https://doi.org:10.1016/s0169-328x(99)00229-6
117 Fabrizi, C. *et al.* The stimulation of inducible nitric-oxide synthase by the prion protein fragment 106--126 in human microglia is tumor necrosis factor-alpha-dependent and involves p38 mitogen-activated protein kinase. *J Biol Chem* **276**, 25692-25696 (2001). https://doi.org:10.1074/jbc.M100133200
118 Kim, T. K. *et al.* Core transcriptional regulatory circuits in prion diseases. *Mol Brain* **13**, 10 (2020). https://doi.org:10.1186/s13041-020-0551-3
119 Julius, C. *et al.* Prion propagation in mice lacking central nervous system NF-kappaB signalling. *J Gen Virol* **89**, 1545-1550 (2008). https://doi.org:10.1099/vir.0.83622-0
120 Chan, W. Y., Kohsaka, S. & Rezaie, P. The origin and cell lineage of microglia: new concepts. *Brain Res Rev* **53**, 344-354 (2007). https://doi.org:10.1016/j.brainresrev.2006.11.002

121 Saura, J. Microglial cells in astroglial cultures: a cautionary note. *J Neuroinflammation* **4**, 26 (2007). https://doi.org:10.1186/1742-2094-4-26
122 Srivastava, S. *et al.* Inflammatory response of microglia to prions is controlled by sialylation of PrP(Sc). *Sci Rep* **8**, 11326 (2018). https://doi.org:10.1038/s41598-018-29720-z
123 Hay, A. J. D., Murphy, T. J., Popichak, K. A., Zabel, M. D. & Moreno, J. A. Adipose-derived mesenchymal stromal cells decrease prion-induced glial inflammation in vitro. *Sci Rep* **12**, 22567 (2022). https://doi.org:10.1038/s41598-022-26628-7
124 Wu, G. R. *et al.* Prion protein is required for tumor necrosis factor alpha (TNFalpha)-triggered nuclear factor kappaB (NF-kappaB) signaling and cytokine production. *J Biol Chem* **292**, 18747-18759 (2017). https://doi.org:10.1074/jbc.M117.787283
125 Afonina, I. S., Zhong, Z., Karin, M. & Beyaert, R. Limiting inflammation-the negative regulation of NF-kappaB and the NLRP3 inflammasome. *Nat Immunol* **18**, 861-869 (2017). https://doi.org:10.1038/ni.3772
126 Blevins, H. M., Xu, Y., Biby, S. & Zhang, S. The NLRP3 Inflammasome Pathway: A Review of Mechanisms and Inhibitors for the Treatment of Inflammatory Diseases. *Front Aging Neurosci* **14**, 879021 (2022). https://doi.org:10.3389/fnagi.2022.879021
127 Shi, F. *et al.* Inhibition of phagocytosis and lysosomal acidification suppresses neurotoxic prion peptide-induced NALP3 inflammasome activation in BV2 microglia. *J Neuroimmunol* **260**, 121-125 (2013). https://doi.org:10.1016/j.jneuroim.2013.04.016
128 Shi, F. *et al.* The NALP3 inflammasome is involved in neurotoxic prion peptide-induced microglial activation. *J Neuroinflammation* **9**, 73 (2012). https://doi.org:10.1186/1742-2094-9-73
129 Hafner-Bratkovic, I., Bencina, M., Fitzgerald, K. A., Golenbock, D. & Jerala, R. NLRP3 inflammasome activation in macrophage cell lines by prion protein fibrils as the source of IL-1beta and neuronal toxicity. *Cell Mol Life Sci* **69**, 4215-4228 (2012). https://doi.org:10.1007/s00018-012-1140-0
130 Lai, M. *et al.* The NLRP3-Caspase 1 Inflammasome Negatively Regulates Autophagy via TLR4-TRIF in Prion Peptide-Infected Microglia. *Front Aging Neurosci* **10**, 116 (2018). https://doi.org:10.3389/fnagi.2018.00116
131 Guentchev, M. *et al.* Oxidative damage to nucleic acids in human prion disease. *Neurobiol Dis* **9**, 275-281 (2002). https://doi.org:10.1006/nbdi.2002.0477
132 Van Everbroeck, B. *et al.* Extracellular protein deposition correlates with glial activation and oxidative stress in Creutzfeldt-Jakob and Alzheimer's disease. *Acta Neuropathol* **108**, 194-200 (2004). https://doi.org:10.1007/s00401-004-0879-2
133 Yun, S. W., Gerlach, M., Riederer, P. & Klein, M. A. Oxidative stress in the brain at early preclinical stages of mouse scrapie. *Exp Neurol* **201**, 90-98 (2006). https://doi.org:10.1016/j.expneurol.2006.03.025
134 Jalland, C. M. *et al.* Accelerated clinical course of prion disease in mice compromised in repair of oxidative DNA damage. *Free Radic Biol Med* **68**, 1-7 (2014). https://doi.org:10.1016/j.freeradbiomed.2013.11.013
135 Shah, S. Z. A. *et al.* p62-Keap1-NRF2-ARE Pathway: A Contentious Player for Selective Targeting of Autophagy, Oxidative Stress and Mitochondrial Dysfunction in Prion Diseases. *Front Mol Neurosci* **11**, 310 (2018). https://doi.org:10.3389/fnmol.2018.00310
136 Sorce, S. *et al.* The role of the NADPH oxidase NOX2 in prion pathogenesis. *PLoS Pathog* **10**, e1004531 (2014). https://doi.org:10.1371/journal.ppat.1004531

137 Mikiko Suzuki, A. O., Nadine Keleku-Lukwete, and Masayuki Yamamoto. Overview of redox regulation by Keap1–Nrf2 system in toxicology and cancer. *Current Opinions in Toxicology*, 29-36 (2016).
138 Deriziotis, P. *et al.* Misfolded PrP impairs the UPS by interaction with the 20S proteasome and inhibition of substrate entry. *EMBO J* **30**, 3065-3077 (2011). https://doi.org:10.1038/emboj.2011.224
139 Lin, Z., Zhao, D. & Yang, L. Interaction between misfolded PrP and the ubiquitin-proteasome system in prion-mediated neurodegeneration. *Acta Biochim Biophys Sin (Shanghai)* **45**, 477-484 (2013). https://doi.org:10.1093/abbs/gmt020
140 Ma, S., Attarwala, I. Y. & Xie, X. Q. SQSTM1/p62: A Potential Target for Neurodegenerative Disease. *ACS Chem Neurosci* **10**, 2094-2114 (2019). https://doi.org:10.1021/acschemneuro.8b00516
141 Yoshinori Katsuragi, Y. I. a. M. K. Regulation of the Keap1–Nrf2 pathway by p62/SQSTM1. *Current Opinions in Toxicology*, 54-61 (2016).
142 Homma, T. *et al.* Increased expression of p62/SQSTM1 in prion diseases and its association with pathogenic prion protein. *Sci Rep* **4**, 4504 (2014). https://doi.org:10.1038/srep04504
143 Cortes, C. J. *et al.* Early Delivery of Misfolded PrP from ER to Lysosomes by Autophagy. *Int J Cell Biol* **2013**, 560421 (2013). https://doi.org:10.1155/2013/560421
144 Cortes, C. J., Qin, K., Cook, J., Solanki, A. & Mastrianni, J. A. Rapamycin delays disease onset and prevents PrP plaque deposition in a mouse model of Gerstmann-Straussler-Scheinker disease. *J Neurosci* **32**, 12396-12405 (2012). https://doi.org:10.1523/JNEUROSCI.6189-11.2012
145 Chen, Y. *et al.* p62/SQSTM1, a Central but Unexploited Target: Advances in Its Physiological/Pathogenic Functions and Small Molecular Modulators. *J Med Chem* **63**, 10135-10157 (2020). https://doi.org:10.1021/acs.jmedchem.9b02038
146 Li, J. *et al.* PINK1-parkin-mediated neuronal mitophagy deficiency in prion disease. *Cell Death Dis* **13**, 162 (2022). https://doi.org:10.1038/s41419-022-04613-2
147 Ponia, S. S. *et al.* Mitophagy antagonism by ZIKV reveals Ajuba as a regulator of PINK1 signaling, PKR-dependent inflammation, and viral invasion of tissues. *Cell Rep* **37**, 109888 (2021). https://doi.org:10.1016/j.celrep.2021.109888
148 Sliter, D. A. *et al.* Parkin and PINK1 mitigate STING-induced inflammation. *Nature* **561**, 258-262 (2018). https://doi.org:10.1038/s41586-018-0448-9
149 Hotamisligil, G. S. & Davis, R. J. Cell Signaling and Stress Responses. *Cold Spring Harb Perspect Biol* **8** (2016). https://doi.org:10.1101/cshperspect.a006072
150 Moreno, J. A. *et al.* Sustained translational repression by eIF2alpha-P mediates prion neurodegeneration. *Nature* **485**, 507-511 (2012). https://doi.org:10.1038/nature11058
151 Moreno, J. A. *et al.* Oral treatment targeting the unfolded protein response prevents neurodegeneration and clinical disease in prion-infected mice. *Sci Transl Med* **5**, 206ra138 (2013). https://doi.org:10.1126/scitranslmed.3006767
152 Tanaka, M., Yamasaki, T., Hasebe, R., Suzuki, A. & Horiuchi, M. Enhanced phosphorylation of PERK in primary cultured neurons as an autonomous neuronal response to prion infection. *PLoS One* **15**, e0234147 (2020). https://doi.org:10.1371/journal.pone.0234147

153 Shim, S. Y., Karri, S., Law, S., Schatzl, H. M. & Gilch, S. Prion infection impairs lysosomal degradation capacity by interfering with rab7 membrane attachment in neuronal cells. *Sci Rep* **6**, 21658 (2016). https://doi.org:10.1038/srep21658
154 Bertheloot, D., Latz, E. & Franklin, B. S. Necroptosis, pyroptosis and apoptosis: an intricate game of cell death. *Cell Mol Immunol* **18**, 1106-1121 (2021). https://doi.org:10.1038/s41423-020-00630-3
155 Duprez, L., Wirawan, E., Vanden Berghe, T. & Vandenabeele, P. Major cell death pathways at a glance. *Microbes Infect* **11**, 1050-1062 (2009). https://doi.org:10.1016/j.micinf.2009.08.013
156 van Engeland, M., Kuijpers, H. J., Ramaekers, F. C., Reutelingsperger, C. P. & Schutte, B. Plasma membrane alterations and cytoskeletal changes in apoptosis. *Exp Cell Res* **235**, 421-430 (1997). https://doi.org:10.1006/excr.1997.3738
157 Shim, K. H., Sharma, N. & An, S. S. A. Prion therapeutics: Lessons from the past. *Prion* **16**, 265-294 (2022). https://doi.org:10.1080/19336896.2022.2153551
158 Vallabh, S. M. *et al.* Therapeutic Trial of anle138b in Mouse Models of Genetic Prion Disease. *J Virol* **97**, e0167222 (2023). https://doi.org:10.1128/jvi.01672-22
159 Giles, K. *et al.* Different 2-Aminothiazole Therapeutics Produce Distinct Patterns of Scrapie Prion Neuropathology in Mouse Brains. *J Pharmacol Exp Ther* **355**, 2-12 (2015). https://doi.org:10.1124/jpet.115.224659
160 Shan, Z. *et al.* Therapeutic effect of autologous compact bone-derived mesenchymal stem cell transplantation on prion disease. *J Gen Virol* **98**, 2615-2627 (2017). https://doi.org:10.1099/jgv.0.000907
161 Tang, B. *et al.* Tumor Necrosis Factor-stimulated Gene-6 (TSG-6) Secreted by BMSCs Regulates Activated Astrocytes by Inhibiting NF-kappaB Signaling Pathway to Ameliorate Blood Brain Barrier Damage After Intracerebral Hemorrhage. *Neurochem Res* **46**, 2387-2402 (2021). https://doi.org:10.1007/s11064-021-03375-1
162 Liu, X. *et al.* Bone marrow mesenchymal stem cell-derived exosomes attenuate cerebral ischemia-reperfusion injury-induced neuroinflammation and pyroptosis by modulating microglia M1/M2 phenotypes. *Exp Neurol* **341**, 113700 (2021). https://doi.org:10.1016/j.expneurol.2021.113700
163 Yang, H. *et al.* Anti-inflammatory protein TSG-6 secreted by bone marrow mesenchymal stem cells attenuates neuropathic pain by inhibiting the TLR2/MyD88/NF-kappaB signaling pathway in spinal microglia. *J Neuroinflammation* **17**, 154 (2020). https://doi.org:10.1186/s12974-020-1731-x
164 Angeloni, C., Gatti, M., Prata, C., Hrelia, S. & Maraldi, T. Role of Mesenchymal Stem Cells in Counteracting Oxidative Stress-Related Neurodegeneration. *Int J Mol Sci* **21** (2020). https://doi.org:10.3390/ijms21093299
165 Friedenstein, A. J., Chailakhyan, R. K., Latsinik, N. V., Panasyuk, A. F. & Keiliss-Borok, I. V. Stromal cells responsible for transferring the microenvironment of the hemopoietic tissues. Cloning in vitro and retransplantation in vivo. *Transplantation* **17**, 331-340 (1974). https://doi.org:10.1097/00007890-197404000-00001
166 Li, M., Chen, H. & Zhu, M. Mesenchymal stem cells for regenerative medicine in central nervous system. *Front Neurosci* **16**, 1068114 (2022). https://doi.org:10.3389/fnins.2022.1068114
167 Danielyan, L. *et al.* Intranasal delivery of bone marrow-derived mesenchymal stem cells, macrophages, and microglia to the brain in mouse models of Alzheimer's and Parkinson's

disease. *Cell Transplant* **23 Suppl 1**, S123-139 (2014). https://doi.org:10.3727/096368914X684970

168 Hu, J. & Wang, X. Alzheimer's Disease: From Pathogenesis to Mesenchymal Stem Cell Therapy - Bridging the Missing Link. *Front Cell Neurosci* **15**, 811852 (2021). https://doi.org:10.3389/fncel.2021.811852

169 Song, C. H., Honmou, O., Furuoka, H. & Horiuchi, M. Identification of chemoattractive factors involved in the migration of bone marrow-derived mesenchymal stem cells to brain lesions caused by prions. *J Virol* **85**, 11069-11078 (2011). https://doi.org:10.1128/JVI.05318-11

170 Hemeda, H. *et al.* Interferon-gamma and tumor necrosis factor-alpha differentially affect cytokine expression and migration properties of mesenchymal stem cells. *Stem Cells Dev* **19**, 693-706 (2010). https://doi.org:10.1089/scd.2009.0365

171 Mukhamedshina, Y. O., Gracheva, O. A., Mukhutdinova, D. M., Chelyshev, Y. A. & Rizvanov, A. A. Mesenchymal stem cells and the neuronal microenvironment in the area of spinal cord injury. *Neural Regen Res* **14**, 227-237 (2019). https://doi.org:10.4103/1673-5374.244778

172 Fu, X. *et al.* Mesenchymal Stem Cell Migration and Tissue Repair. *Cells* **8** (2019). https://doi.org:10.3390/cells8080784

173 Lee, H. J. *et al.* Human umbilical cord blood-derived mesenchymal stem cells improve neuropathology and cognitive impairment in an Alzheimer's disease mouse model through modulation of neuroinflammation. *Neurobiol Aging* **33**, 588-602 (2012). https://doi.org:10.1016/j.neurobiolaging.2010.03.024

174 Santamaria, G. *et al.* Intranasal delivery of mesenchymal stem cell secretome repairs the brain of Alzheimer's mice. *Cell Death Differ* **28**, 203-218 (2021). https://doi.org:10.1038/s41418-020-0592-2

175 Shin, J. Y. & Lee, P. H. Mesenchymal stem cells modulate misfolded alpha-synuclein in parkinsonian disorders: A multitarget disease-modifying strategy. *Stem Cell Res* **47**, 101908 (2020). https://doi.org:10.1016/j.scr.2020.101908

176 Chen, Y., Shen, J., Ke, K. & Gu, X. Clinical potential and current progress of mesenchymal stem cells for Parkinson's disease: a systematic review. *Neurol Sci* **41**, 1051-1061 (2020). https://doi.org:10.1007/s10072-020-04240-9

177 Song, C. H. *et al.* Effect of transplantation of bone marrow-derived mesenchymal stem cells on mice infected with prions. *J Virol* **83**, 5918-5927 (2009). https://doi.org:10.1128/JVI.00165-09

178 Fernandez, O. *et al.* Adipose-derived mesenchymal stem cells (AdMSC) for the treatment of secondary-progressive multiple sclerosis: A triple blinded, placebo controlled, randomized phase I/II safety and feasibility study. *PLoS One* **13**, e0195891 (2018). https://doi.org:10.1371/journal.pone.0195891

179 Prusiner, S. B. Prions. *Proc Natl Acad Sci U S A* **95**, 13363-13383 (1998). https://doi.org:10.1073/pnas.95.23.13363

180 Kretzschmar, H. A., Prusiner, S. B., Stowring, L. E. & DeArmond, S. J. Scrapie prion proteins are synthesized in neurons. *Am J Pathol* **122**, 1-5 (1986).

181 Come, J. H., Fraser, P. E. & Lansbury, P. T., Jr. A kinetic model for amyloid formation in the prion diseases: importance of seeding. *Proc Natl Acad Sci U S A* **90**, 5959-5963 (1993). https://doi.org:10.1073/pnas.90.13.5959

182 Collinge, J. & Clarke, A. R. A general model of prion strains and their pathogenicity. *Science* **318**, 930-936 (2007). https://doi.org:10.1126/science.1138718
183 Muhleisen, H., Gehrmann, J. & Meyermann, R. Reactive microglia in Creutzfeldt-Jakob disease. *Neuropathol Appl Neurobiol* **21**, 505-517 (1995). https://doi.org:10.1111/j.1365-2990.1995.tb01097.x
184 Mallucci, G. R. Prion neurodegeneration: starts and stops at the synapse. *Prion* **3**, 195-201 (2009). https://doi.org:10.4161/pri.3.4.9981
185 Giovannoni, F. & Quintana, F. J. The Role of Astrocytes in CNS Inflammation. *Trends Immunol* **41**, 805-819 (2020). https://doi.org:10.1016/j.it.2020.07.007
186 Sorce, S. *et al.* Genome-wide transcriptomics identifies an early preclinical signature of prion infection. *PLoS Pathog* **16**, e1008653 (2020). https://doi.org:10.1371/journal.ppat.1008653
187 Mazini, L., Rochette, L., Amine, M. & Malka, G. Regenerative Capacity of Adipose Derived Stem Cells (ADSCs), Comparison with Mesenchymal Stem Cells (MSCs). *Int J Mol Sci* **20** (2019). https://doi.org:10.3390/ijms20102523
188 Sheikh, A. M. *et al.* Mesenchymal stem cell transplantation modulates neuroinflammation in focal cerebral ischemia: contribution of fractalkine and IL-5. *Neurobiol Dis* **41**, 717-724 (2011). https://doi.org:10.1016/j.nbd.2010.12.009
189 Kyurkchiev, D. *et al.* Secretion of immunoregulatory cytokines by mesenchymal stem cells. *World J Stem Cells* **6**, 552-570 (2014). https://doi.org:10.4252/wjsc.v6.i5.552
190 Teixeira, F. G. *et al.* Impact of the Secretome of Human Mesenchymal Stem Cells on Brain Structure and Animal Behavior in a Rat Model of Parkinson's Disease. *Stem Cells Transl Med* **6**, 634-646 (2017). https://doi.org:10.5966/sctm.2016-0071
191 Chen, D. *et al.* Therapeutic effects of intranigral transplantation of mesenchymal stem cells in rat models of Parkinson's disease. *J Neurosci Res* **95**, 907-917 (2017). https://doi.org:10.1002/jnr.23879
192 Bian, J., Kang, H. E. & Telling, G. C. Quinacrine promotes replication and conformational mutation of chronic wasting disease prions. *Proc Natl Acad Sci U S A* **111**, 6028-6033 (2014). https://doi.org:10.1073/pnas.1322377111
193 Reimann, R. R. *et al.* Differential Toxicity of Antibodies to the Prion Protein. *PLoS Pathog* **12**, e1005401 (2016). https://doi.org:10.1371/journal.ppat.1005401
194 Nazor Friberg, K. *et al.* Intracerebral Infusion of Antisense Oligonucleotides Into Prion-infected Mice. *Mol Ther Nucleic Acids* **1**, e9 (2012). https://doi.org:10.1038/mtna.2011.6
195 Kirkley, K. S., Popichak, K. A., Afzali, M. F., Legare, M. E. & Tjalkens, R. B. Microglia amplify inflammatory activation of astrocytes in manganese neurotoxicity. *J Neuroinflammation* **14**, 99 (2017). https://doi.org:10.1186/s12974-017-0871-0
196 Popichak, K. A., Afzali, M. F., Kirkley, K. S. & Tjalkens, R. B. Glial-neuronal signaling mechanisms underlying the neuroinflammatory effects of manganese. *J Neuroinflammation* **15**, 324 (2018). https://doi.org:10.1186/s12974-018-1349-4
197 Bian, J. *et al.* Cell-based quantification of chronic wasting disease prions. *J Virol* **84**, 8322-8326 (2010). https://doi.org:10.1128/JVI.00633-10
198 Chow, L., Johnson, V., Coy, J., Regan, D. & Dow, S. Mechanisms of Immune Suppression Utilized by Canine Adipose and Bone Marrow-Derived Mesenchymal Stem Cells. *Stem Cells Dev* **26**, 374-389 (2017). https://doi.org:10.1089/scd.2016.0207

199 English, K., Barry, F. P., Field-Corbett, C. P. & Mahon, B. P. IFN-gamma and TNF-alpha differentially regulate immunomodulation by murine mesenchymal stem cells. *Immunol Lett* **110**, 91-100 (2007). https://doi.org:10.1016/j.imlet.2007.04.001
200 Xiao, Q. *et al.* TNF-alpha increases bone marrow mesenchymal stem cell migration to ischemic tissues. *Cell Biochem Biophys* **62**, 409-414 (2012). https://doi.org:10.1007/s12013-011-9317-y
201 Yu, Y. *et al.* Hypoxia and low-dose inflammatory stimulus synergistically enhance bone marrow mesenchymal stem cell migration. *Cell Prolif* **50** (2017). https://doi.org:10.1111/cpr.12309
202 Bisht, K., Sharma, K. & Tremblay, M. E. Chronic stress as a risk factor for Alzheimer's disease: Roles of microglia-mediated synaptic remodeling, inflammation, and oxidative stress. *Neurobiol Stress* **9**, 9-21 (2018). https://doi.org:10.1016/j.ynstr.2018.05.003
203 Liu, Y. *et al.* Mesenchymal stem cells enhance microglia M2 polarization and attenuate neuroinflammation through TSG-6. *Brain Res* **1724**, 146422 (2019). https://doi.org:10.1016/j.brainres.2019.146422
204 Mabbott, N. A., Bruce, M. E., Botto, M., Walport, M. J. & Pepys, M. B. Temporary depletion of complement component C3 or genetic deficiency of C1q significantly delays onset of scrapie. *Nat Med* **7**, 485-487 (2001). https://doi.org:10.1038/86562
205 Chow, L. *et al.* Antibacterial activity of human mesenchymal stem cells mediated directly by constitutively secreted factors and indirectly by activation of innate immune effector cells. *Stem Cells Transl Med* **9**, 235-249 (2020). https://doi.org:10.1002/sctm.19-0092
206 Liu, F. *et al.* MSC-secreted TGF-beta regulates lipopolysaccharide-stimulated macrophage M2-like polarization via the Akt/FoxO1 pathway. *Stem Cell Res Ther* **10**, 345 (2019). https://doi.org:10.1186/s13287-019-1447-y
207 Liu, W. *et al.* Exosome-shuttled miR-216a-5p from hypoxic preconditioned mesenchymal stem cells repair traumatic spinal cord injury by shifting microglial M1/M2 polarization. *J Neuroinflammation* **17**, 47 (2020). https://doi.org:10.1186/s12974-020-1726-7
208 Bourgognon, J. M. *et al.* Inhibition of neuroinflammatory nitric oxide signaling suppresses glycation and prevents neuronal dysfunction in mouse prion disease. *Proc Natl Acad Sci U S A* **118** (2021). https://doi.org:10.1073/pnas.2009579118
209 Katsuda, T., Kosaka, N., Takeshita, F. & Ochiya, T. The therapeutic potential of mesenchymal stem cell-derived extracellular vesicles. *Proteomics* **13**, 1637-1653 (2013). https://doi.org:10.1002/pmic.201200373
210 Harach, T. *et al.* Administrations of human adult ischemia-tolerant mesenchymal stem cells and factors reduce amyloid beta pathology in a mouse model of Alzheimer's disease. *Neurobiol Aging* **51**, 83-96 (2017). https://doi.org:10.1016/j.neurobiolaging.2016.11.009
211 Ding, M. *et al.* Exosomes Isolated From Human Umbilical Cord Mesenchymal Stem Cells Alleviate Neuroinflammation and Reduce Amyloid-Beta Deposition by Modulating Microglial Activation in Alzheimer's Disease. *Neurochem Res* **43**, 2165-2177 (2018). https://doi.org:10.1007/s11064-018-2641-5
212 Harrell, C. R., Jovicic, N., Djonov, V., Arsenijevic, N. & Volarevic, V. Mesenchymal Stem Cell-Derived Exosomes and Other Extracellular Vesicles as New Remedies in the Therapy of Inflammatory Diseases. *Cells* **8** (2019). https://doi.org:10.3390/cells8121605
213 Sanchez-Castillo, A. I. *et al.* Switching Roles: Beneficial Effects of Adipose Tissue-Derived Mesenchymal Stem Cells on Microglia and Their Implication in

Neurodegenerative Diseases. *Biomolecules* **12** (2022). https://doi.org:10.3390/biom12020219
214 Peng, H. *et al.* Intranasal Administration of Self-Oriented Nanocarriers Based on Therapeutic Exosomes for Synergistic Treatment of Parkinson's Disease. *ACS Nano* **16**, 869-884 (2022). https://doi.org:10.1021/acsnano.1c08473
215 Nuvolone, M. *et al.* Strictly co-isogenic C57BL/6J-Prnp-/- mice: A rigorous resource for prion science. *J Exp Med* **213**, 313-327 (2016). https://doi.org:10.1084/jem.20151610
216 Fraser, H. & Dickinson, A. G. The sequential development of the brain lesion of scrapie in three strains of mice. *J Comp Pathol* **78**, 301-311 (1968). https://doi.org:10.1016/0021-9975(68)90006-6
217 Scott, M. R. *et al.* Propagation of prion strains through specific conformers of the prion protein. *J Virol* **71**, 9032-9044 (1997). https://doi.org:10.1128/JVI.71.12.9032-9044.1997
218 Sun, J. L. *et al.* Novel Prion Strain as Cause of Chronic Wasting Disease in a Moose, Finland. *Emerg Infect Dis* **29**, 323-332 (2023). https://doi.org:10.3201/eid2902.220882
219 Garrovo, C. *et al.* In vivo tracking of murine adipose tissue-derived multipotent adult stem cells and ex vivo cross-validation. *Int J Mol Imaging* **2013**, 426961 (2013). https://doi.org:10.1155/2013/426961
220 Donega, V. *et al.* Intranasal administration of human MSC for ischemic brain injury in the mouse: in vitro and in vivo neuroregenerative functions. *PLoS One* **9**, e112339 (2014). https://doi.org:10.1371/journal.pone.0112339
221 Livak, K. J. & Schmittgen, T. D. Analysis of relative gene expression data using real-time quantitative PCR and the 2(-Delta Delta C(T)) Method. *Methods* **25**, 402-408 (2001). https://doi.org:10.1006/meth.2001.1262
222 Hass, R. & Otte, A. Mesenchymal stem cells as all-round supporters in a normal and neoplastic microenvironment. *Cell Commun Signal* **10**, 26 (2012). https://doi.org:10.1186/1478-811X-10-26
223 Carroll, J. A., Race, B., Williams, K. & Chesebro, B. Toll-like receptor 2 confers partial neuroprotection during prion disease. *PLoS One* **13**, e0208559 (2018). https://doi.org:10.1371/journal.pone.0208559
224 Petito, C. K. *et al.* DNA fragmentation follows delayed neuronal death in CA1 neurons exposed to transient global ischemia in the rat. *J Cereb Blood Flow Metab* **17**, 967-976 (1997). https://doi.org:10.1097/00004647-199709000-00006
225 Majer, A. *et al.* Early mechanisms of pathobiology are revealed by transcriptional temporal dynamics in hippocampal CA1 neurons of prion infected mice. *PLoS Pathog* **8**, e1003002 (2012). https://doi.org:10.1371/journal.ppat.1003002
226 Boche, D., Cunningham, C., Docagne, F., Scott, H. & Perry, V. H. TGFbeta1 regulates the inflammatory response during chronic neurodegeneration. *Neurobiol Dis* **22**, 638-650 (2006). https://doi.org:10.1016/j.nbd.2006.01.004
227 Xu, Z. *et al.* Vascular endothelial growth factor is neuroprotective against ischemic brain injury by inhibiting scavenger receptor A expression on microglia. *J Neurochem* **142**, 700-709 (2017). https://doi.org:10.1111/jnc.14108
228 Dordoe, C. *et al.* Non-mitogenic fibroblast growth factor 1 protects against ischemic stroke by regulating microglia/macrophage polarization through Nrf2 and NF-kappaB pathways. *Neuropharmacology* **212**, 109064 (2022). https://doi.org:10.1016/j.neuropharm.2022.109064

229 Qin, Q. *et al.* Ectoderm-derived frontal bone mesenchymal stem cells promote traumatic brain injury recovery by alleviating neuroinflammation and glutamate excitotoxicity partially via FGF1. *Stem Cell Res Ther* **13**, 341 (2022). https://doi.org:10.1186/s13287-022-03032-6

230 Sigurdson, C. J., Bartz, J. C. & Glatzel, M. Cellular and Molecular Mechanisms of Prion Disease. *Annu Rev Pathol* **14**, 497-516 (2019). https://doi.org:10.1146/annurev-pathmechdis-012418-013109

231 Nimmerjahn, A., Kirchhoff, F. & Helmchen, F. Resting microglial cells are highly dynamic surveillants of brain parenchyma in vivo. *Science* **308**, 1314-1318 (2005). https://doi.org:10.1126/science.1110647

232 Dihne, M., Block, F., Korr, H. & Topper, R. Time course of glial proliferation and glial apoptosis following excitotoxic CNS injury. *Brain Res* **902**, 178-189 (2001). https://doi.org:10.1016/s0006-8993(01)02378-2

233 Rezaie, J., Nejati, V., Mahmoodi, M. & Ahmadi, M. Mesenchymal stem cells derived extracellular vesicles: A promising nanomedicine for drug delivery system. *Biochem Pharmacol* **203**, 115167 (2022). https://doi.org:10.1016/j.bcp.2022.115167

234 Yari, H. *et al.* Emerging role of mesenchymal stromal cells (MSCs)-derived exosome in neurodegeneration-associated conditions: a groundbreaking cell-free approach. *Stem Cell Res Ther* **13**, 423 (2022). https://doi.org:10.1186/s13287-022-03122-5

235 Li, Z. W., Omori, S. A., Labuda, T., Karin, M. & Rickert, R. C. IKK beta is required for peripheral B cell survival and proliferation. *J Immunol* **170**, 4630-4637 (2003). https://doi.org:10.4049/jimmunol.170.9.4630

236 Rocha, S. M. *et al.* Microglia-specific knock-out of NF-kappaB/IKK2 increases the accumulation of misfolded alpha-synuclein through the inhibition of p62/sequestosome-1-dependent autophagy in the rotenone model of Parkinson's disease. *Glia* (2023). https://doi.org:10.1002/glia.24385

237 Easley-Neal, C., Foreman, O., Sharma, N., Zarrin, A. A. & Weimer, R. M. CSF1R Ligands IL-34 and CSF1 Are Differentially Required for Microglia Development and Maintenance in White and Gray Matter Brain Regions. *Front Immunol* **10**, 2199 (2019). https://doi.org:10.3389/fimmu.2019.02199

238 Carroll, J. A., Race, B., Williams, K., Striebel, J. F. & Chesebro, B. Innate immune responses after stimulation with Toll-like receptor agonists in ex vivo microglial cultures and an in vivo model using mice with reduced microglia. *J Neuroinflammation* **18**, 194 (2021). https://doi.org:10.1186/s12974-021-02240-w

239 Jack, C. S. *et al.* TLR signaling tailors innate immune responses in human microglia and astrocytes. *J Immunol* **175**, 4320-4330 (2005). https://doi.org:10.4049/jimmunol.175.7.4320

240 Holm, T. H., Draeby, D. & Owens, T. Microglia are required for astroglial Toll-like receptor 4 response and for optimal TLR2 and TLR3 response. *Glia* **60**, 630-638 (2012). https://doi.org:10.1002/glia.22296

241 Spinner, D. S. *et al.* Accelerated prion disease pathogenesis in Toll-like receptor 4 signaling-mutant mice. *J Virol* **82**, 10701-10708 (2008). https://doi.org:10.1128/JVI.00522-08

242 Crowley, L. C., Marfell, B. J., Scott, A. P. & Waterhouse, N. J. Quantitation of Apoptosis and Necrosis by Annexin V Binding, Propidium Iodide Uptake, and Flow Cytometry. *Cold Spring Harb Protoc* **2016** (2016). https://doi.org:10.1101/pdb.prot087288

243 Cho, I. H. *et al.* Role of microglial IKKbeta in kainic acid-induced hippocampal neuronal cell death. *Brain* **131**, 3019-3033 (2008). https://doi.org:10.1093/brain/awn230
244 Frakes, A. E. *et al.* Microglia induce motor neuron death via the classical NF-kappaB pathway in amyotrophic lateral sclerosis. *Neuron* **81**, 1009-1023 (2014). https://doi.org:10.1016/j.neuron.2014.01.013
245 Xu, Y. *et al.* Overexpression of p62/SQSTM1 promotes the degradations of abnormally accumulated PrP mutants in cytoplasm and relieves the associated cytotoxicities via autophagy-lysosome-dependent way. *Med Microbiol Immunol* **203**, 73-84 (2014). https://doi.org:10.1007/s00430-013-0316-z
246 Hannaoui, S. *et al.* Transmission of cervid prions to humanized mice demonstrates the zoonotic potential of CWD. *Acta Neuropathologica* **144**, 767-784 (2022). https://doi.org:10.1007/s00401-022-02482-9
247 Shahror, R. A., Wu, C. C., Chiang, Y. H. & Chen, K. Y. Tracking Superparamagnetic Iron Oxide-labeled Mesenchymal Stem Cells using MRI after Intranasal Delivery in a Traumatic Brain Injury Murine Model. *J Vis Exp* (2019). https://doi.org:10.3791/60450
248 Pan, Q. *et al.* miR-132-3p priming enhances the effects of mesenchymal stromal cell-derived exosomes on ameliorating brain ischemic injury. *Stem Cell Res Ther* **11**, 260 (2020). https://doi.org:10.1186/s13287-020-01761-0
249 Katsuda, T. *et al.* Human adipose tissue-derived mesenchymal stem cells secrete functional neprilysin-bound exosomes. *Sci Rep* **3**, 1197 (2013). https://doi.org:10.1038/srep01197
250 Li, H. *et al.* Development of rapamycin-encapsulated exosome-mimetic nanoparticles-in-PLGA microspheres for treatment of hemangiomas. *Biomed Pharmacother* **148**, 112737 (2022). https://doi.org:10.1016/j.biopha.2022.112737
251 Nazor, K. E. *et al.* Immunodetection of disease-associated mutant PrP, which accelerates disease in GSS transgenic mice. *EMBO J* **24**, 2472-2480 (2005). https://doi.org:10.1038/sj.emboj.7600717
252 Nazor, K. E., Seward, T. & Telling, G. C. Motor behavioral and neuropathological deficits in mice deficient for normal prion protein expression. *Biochim Biophys Acta* **1772**, 645-653 (2007). https://doi.org:10.1016/j.bbadis.2007.04.004